Interaction of the *fac*-$[M(CO)_3]^+$ (M = ^{99}Tc, Re) Core with DNA Bases and Amino Acids

Dissertation

zur

Erlangung der naturwissenschaftlichen Doktorwürde

(Dr. Sc. Nat.)

vorgelegt der

Mathematisch-naturwissenschaftlichen Fakultät

der

Universität Zürich

von

Fabio Zobi

aus Italien

Promotionskomitee

Prof. Dr. Roger Alberto (Vorsitz)

Prof. Dr. Paul J. Dyson

Zürich 2005

Acknowledgments

First and foremost my gratitude goes to my supervisor, Prof. Dr. Roger Alberto, for his support and patience throughout the duration of this project. His comments have been invaluable and his guidance indispensable for the successful completion of this study.

Thanks also go to all the colleagues and friends who have joined or left the research group since January 2002 for their daily help here at the Inorganic Chemistry Institute.

I am particularly obliged to Dr. Helmut W. Schmalle and Dr. Bernhard Spingler for X-ray data collection and processing; to Dr. Jae Kyoung Pak for suggestions regarding organic synthesis; to Dr. Stefan Mundwiler and Dr. Susan Kunze for their help with analytical high performance liquid chromatography; to Dr. Olivier Blacque for theoretical calculations and to Prof. Dr. Roland Sigel and Dr. Pascal Häfliger for his assistance with biochemical experiments. I am also thankful to Dr. Thomas Fox and Dr. Paul Schmutz for NMR data collection and processing.

Table of Contents

Synopsis **4**

Zusammenfassung **5**

Introduction **6**

I.1 General Remarks 6

I.2 The Elements Technetium and Rhenium 6

I.3 Chemistry of the Elements 8

I.4 Chemistry of the *fac*-$[M(CO)_3]^+$ Core (M = Tc, Re) 9

I.5 Chemo- and Radiotherapeutic Agents in Cancer Research 11

I.6 Scope and Purpose of This Study 12

Chapter 1. Interaction of $[M(H_2O)_3(CO)_3]^+$ Complex (M = Re, ^{99}Tc) with Guanine. Comparison with Leading Anticancer Drug Cisplatin **15**

1.1 Results 18

1.2 Discussion 29

1.3 Conclusions 36

Chapter 2. Guanine and Plasmid DNA Binding of Mono- and Trinuclear $[Re(CO)_3]^+$ Complexes with Amino Acid Ligands **41**

2.1 Results and Discussion 44

2.2 Conclusion 57

Chapter 3. Interaction of $[Re(H_2O)_3(CO)_3]^+$ Complex (1) with d(GpG) and d(CpGpG) **61**

3.1 Results and Discussion 63

3.2 Conclusion 74

Chapter 4. Vitamin B12 as a Shuttle for Rhenium Complexes **77**

4.1 Results and Discussion 79

4.2 Conclusion 82

Chapter 5. Novel Nucleoside-Mimicking Complexes Based on the *fac*-$[Re(CO)_3]^+$ Moiety: Structure, Reactivity and Solution Behaviour of $[Re(CO)_3(Ser)(7\text{-MeG})]$, $[Re(CO)_3(Ser)(3\text{-pic})]$ and $[Re(CO)_3(Ser)(Ade)]$ **85**

5.1 Results and Discussion 86

5.2 Conclusion 108

Chapter 6. Cytotoxicity of Re^I Complexes **110**

6.1 Results and Discussion 110

6.2 Conclusion 116

Chapter 7. Binding of 9-Methylguanine to [*cis*-Ru(2,2'-bipyridine)$_2$]$^{2+}$ **118**

7.1 Results and Discussion 118
7.2 Conclusion 121
Conclusions and Outlook **123**
Experimental Section **125**
Materials and Methods 125
Synthesis of Compounds 127
Summary **136**
Crystallography Section. **139**
Curriculum Vitae **156**

Synopsis

This study is focused on the interaction of the metal ions technetium (Tc) and rhenium (Re) with amino acids and DNA bases, in particular with guanine. It is shown in this thesis that two guanine bases can coordinate to a Re^{I} or a Tc^{I} centre yielding reasonably stable complexes with slow on and off rates, the on rates being comparable to an active form of cisplatin. For the first time x-ray structures of a Tc- and Re-complexes with two purine bases bound *cis* to the metal center are presented. Theoretical and ^{1}H NMR studies indicate that the two guanines can freely rotate about the Re-N7(9) bond.

Rhenium forms stable adducts with d(GpG) and d(CpGpG) via coordination of the N7 atom of guanine residues as corroborated by the pH-dependence studies of the H8 resonances at pH values near 2. The $[Re(CO)_3]^+$ moiety displays a principally similar reactivity pattern with plasmid DNA as e.g. cisplatin. It alters the tertiary structure of □X174 DNA by altering the electrophoretic mobility of the open circular and the supercoiled form of plasmid DNA. The induced changes involve most likely covalent binding to two bases as found for cisplatin.

The *fac*-$[Re(CO)_3]^+$ core can be derivatized with the amino acid serine and the appropriate nitrogenous base to yield nucleoside mimicking complexes. These compounds show an interesting solution behavior and are remarkably stable in Human Serum (HS). The amino acid complexes of Re can be bridged by CN^- in B12 to yield robust complexes comprising the central structural feature [Co-CN-Re]. Certain Re complexes show high antiproliferative activity toward B16 F1 mouse melanoma cells.

Zusammenfassung

Diese Arbeit befasst sich mit der Wechselwirkung von Technetium- und Rheniumionen mit Aminosäuren und Nukleobasen, insbesondere mit Guanin. Es wird gezeigt, dass zwei Guaninbasen an ein Re^{I}- oder ein Tc^{I}-Metallzentrum koordinieren können und recht stabile Komplexe bilden mit langsamen Geschwindigkeitskonstanten für die Hinreaction, die ähnlich den Werten von Cisplatin in seiner aktivierten Form sind. Zum ersten Mal werden Kristallstrukturen von Tc- und Re-Komplexen mit zwei cis-gebunden Purinbasen präsentiert. Theoretische Studien und NMR-Messungen zeigen, dass die beiden Guanine frei um die Re-$N^{7(9)}$-Bindung rotieren können.

Rhenium bildet stabile Addukte mit d(GpG) and d(CpGpG) durch Koordination der N^{7}-Atome der Guanineinheiten, was durch pH-abhängige Studien der H^{8}-Resonanzen bestätigt wurde. Die $[Re(CO)_3]^{+}$-Einheit zeigt ein vornehmlich gleiches Reaktionsverhalten mit Plasmid-DNS wie z.B. Cisplatin. Sie verändert die Tertiärstruktur von ΦX174-DNS, was sich veränderter elektrophoretischer Mobilitäten von Plasmid-DNS in der entspannt zirkularen und in der Superhelixform zeigt. Diese Änderungen beinhalten höchstwahrscheinlich die kovalente Bindung zweier Basen, wie es bei Cisplatin gefunden wird.

Die *fac*-$[Re(CO)_3]^{+}$-Einheit kann mit der Aminosäure Serin und mit den passenden Stickstoffbasen derivatisiert werden, um Nukleosid-imitierende Komplexe zu bilden. Diese Substanzen zeigen in Lösung ein interessantes Verhalten und sind in Humanserum erstaunlich stabil. Die Aminosäurekomplexe von Rhenium können über CN^{-} mit B_{12} verbrückt werden, um stabile Komplexe mit der zentralen Einheit [Co-CN-Re] zu bilden. Einige Rheniumkomplexe zeigen hohe antiproliferative Aktivität gegen B16 F1-Mausmelanomzellen.

Introduction

I.1 General Remarks

This study is focused on the interaction of the metal ions technetium (Tc) and rhenium (Re) with amino acids and DNA bases, in particular with guanine. The thesis is structured in chapters with each chapter dealing with a specific issue of the study. Although every section is presented in a format resembling that of a scientific publication, with a results and discussion section following an introduction to the topic, the subject matters dealt within each chapter are intimately related to one another. These are presented in a consecutive logical manner that I hope will help the reader to better appreciate the scope and purpose of this study. All experimental details are given at the end of this work.

I.2 The Elements Technetium and Rhenium

I.2.1 Technetium

Technetium (from Gr. *technetos*: artificial, element 43) was predicted on the basis of the periodic table, and was erroneously reported as having been discovered in 1925, at which time it was named masurium.[1] The element was actually discovered by Perrier and Segre in Italy in 1937.[2, 3] It was also found in a sample of molybdenum sent by E. Lawrence that was bombarded by deuterons in the Berkeley cyclotron. Technetium was the first element to be produced artificially. Since its discovery, searches for the element in terrestrial material have been made. Finally in 1962, technetium-99 was isolated and identified in African pitchblende (a uranium rich ore) in extremely minute quantities as a spontaneous fission product of uranium-238 by B.T. Kenna and P.K. Kuroda.[4, 5] Technetium has been found in the spectrum of red giant S-, M-, and N-type stars, and its presence in stellar matter is leading to new theories of the production of heavy elements in the stars.[6, 7]

Technetium is a silvery-grey metal that tarnishes slowly in moist air. The common oxidation states of technetium are +7, +5, and +4. Under oxidizing conditions technetium (VII) will exist as the pertechnetate ion, TcO_4^-. The chemistry of technetium is similar to that of rhenium. Technetium dissolves in nitric acid, aqua regia, and concentrated sulphuric acid, but is not soluble in hydrochloric acid of any strength. The element is a remarkable corrosion inhibitor for steel. The metal is an excellent superconductor at 11K and below.

Twenty-two isotopes of technetium with masses ranging from 90 to 111 are reported. All the isotopes of technetium are radioactive. It is one of two elements with Z < 83 that have no stable isotopes; the other element is promethium (Z = 61). Technetium has three long-lived radioactive isotopes: ^{97}Tc ($t_{½}$ =2.6 x 10^6 yr), ^{98}Tc ($t_{½}$ = 4.2 x 10^6 yr) and ^{99}Tc ($t_{½}$ = 2.1 x 10^5 yr). ^{95m}Tc ("m" stands for meta state) ($t_{½}$ = 61 d) is used in tracer work. However, the most useful isotope of technetium is ^{99m}Tc ($t_{½}$ = 6.01 h). Technetium-99m in some chemical form is used in more than 85% of the diagnostic scans done each year in hospitals. The nuclear properties of ^{99m}Tc are virtually ideal for diagnostic imaging.[8] Technetium-99m emits a 140 keV γ-ray with 89% abundance which is close to optimum for imaging with gamma cameras found in most hospitals. Its 6 h half-life is sufficiently long to synthesize the ^{99m}Tc-labeled radiopharmaceuticals, assay them for purity, inject them into the patient and perform the imaging studies yet short enough to minimize the radiation dose to the patient. Because ^{99}Tc is produced as a fission product from the fission of uranium in nuclear reactors, large quantities have been produced over the years.

I.2.2 Rhenium

Rhenium, first detected by Noddack, Tacke, and Berg in 1925 in the X-ray spectra of certain mineral concentrates,[1] was the last of the stable elements to be discovered. It is among the least abundant both in the crust of the earth and in the solar system. There are no sufficiently elevated concentrations anywhere in nature to permit economic extraction as the primary commodity, and the only commercial source is as a by-product of the molybdenum industry. When molybdenite is roasted in air to molybdenum trioxide, volatile dirhenium heptoxide passes into the effluent gases and flue dusts and may be recovered by wet scrubbing or leaching with water. Rhenium is then isolated from the aqueous extracts either by selective adsorption as ReO_4^- on an anion exchanger or by solvent extraction, and it is finally precipitated as NH_4ReO_4 or Re_2S_7.

Rhenium, of atomic number 75 and atomic weight 186.2, belongs to group VII of the periodic table. It occurs naturally as a mixture of two isotopes, ^{185}Re (37.40%) and ^{187}Re (62.60%).[9] The heavier isotope is a weak β-emitter, and the daughter ^{187}Os is present in all rhenium-bearing rocks.[10] The end-point energy of the emitted β-particles (2.62 % ± 0.09 keV) is the lowest recorded for β-decay and is even lower than the difference in the atomic binding energies of Re and Os (ca. 13.8 keV).[11, 12] The measured half-life for decay to continuum states, (6.6 % ± 1.3) x 10^{10} yr, is longer than the total half-life, (4.3 % ± 0.5) X 10^{10} yr, estimated from ^{187}Re/^{187}Os ratios in geologically dated molybdenltes.[13]

On all counts, rhenium is an exceptionally rare element. A careful search in the Fraunhofer spectrum of the sun was negative, putting an upper limit of not more than 0.5 atom per 10^{12} H.[14] Concentrations in iron meteorites (0.0023-4.4 ppm based on the analysis of 70 specimens) are an order of magnitude less than those of osmium and iridium,[15] and the mean osmium to rhenium ratio in chondritic meteorites is 11.4 % ± 1.3.[16] A sample of 32 chondrites representing all classes was found to contain 0.0311-0.0804 ppm corresponding to 0.025-0.076 atom of Re per 10^6 silicon.[16] The atomic abundance in the Orgueil meteorite, a Type I carbonaceous chondrite generally considered most nearly representative of the composition of primitive solar dust, is 0.052 (Si = 10^6), almost equal to the mean in all chondrites (0.053).[16] The abundance of rhenium in the solar system is usually taken as 0.055 and, together with that of Tb, Tm, Lu, and Ta, is the lowest among the stable elements.[17]

The earth's crust is essentially depleted in rhenium. On the basis of analyses on 14 igneous and metamorphic rocks, the crustal abundance has been estimated at 0.5 % ± 0.3 ppb.[18] The element is highly dispersed within the crust, and elevated concentrations normally occur only in molybdenites.[19] A strong geochemical association with molybdenum persists through all stages of magmatic crystallization, and rhenium is finally incorporated as an isomorphous solid solution of ReS_2 in MoS_2.[19] A large number of molybdenites have been analyzed and the rhenium content has been found to vary over very wide limits from <0.1 ppm to >2000 ppm (0.2%).[19] Of the many factors that influence the ratio of Re to Mo, one seems to be well established: molybdenites with the highest content of rhenium (ca. 0.1 %) tend to be associated with copper in multi-mineral accretions.[19]

I.3 Chemistry of the Elements[20]

Technetium and rhenium are known to exists in formal oxidation states ranging from –I (d^8) to VII (d^0). They form a large variety of complexes with coordination numbers ranging from 4 to 9 encompassing virtually all known geometries. Oxo complexes of the elements can broadly be assigned to three major types: 5- or 6-coordinate species with a MO^{3+} core, 6-coordinate species with linear $O=M=O^+$ core and species based on the linear $O=M-O-M=O^{4+}$ core to which ligands are attached to form an octahedron around each metal. Both metals form strong triple bonds to nitrogen in oxidation states V and VI with $M\equiv N^{2+}$ and $M\equiv N^{3+}$ cores in octahedral geometry.

M_2O_7 and MO_4^- oxides of both metals are well known as well as M_2S_7 sulfides which are obtained from H_2S saturated solutions of MO_4^- in the presence of HCl. The pertechnetate and the

perrhenate ions (MO_4^-) dominate the aqueous chemistry of both elements. Both anions are tetrahedral and numerous salts are known. Interestingly TcO_4^- (but not ReO_4^-) shows catalytic activity and it is a remarkable corrosion inhibitor for iron and steel. Only three binary halides of Tc are known, TcF_6, TcF_5 and $TcCl_4$ while a relatively large number of halides are known for Re. Among the most interesting are ReF_7, the only known heptafluoride other than IF_7 and Re_2Cl_{10} which shows in the crystal structure magnetic interaction but no actual Re-Re bond. Oxohalides, on the other hand, are fairly numerous and occur for oxidation states +5, +6 and +7.

Both elements have a tendency to form M-M multiple metal bonds although several major differences in their chemistry exist. For example, trinuclear clusters of Re are very important but unknown for Tc. Re forms many Re_2^{6+} complexes with Re-Re quadruple bonds, whereas Tc prefers Tc_2^{5+} and Tc_4^{4+} complexes with lower bond order. Incidentally, the $[Re_2Cl_8]^{2-}$ ion was the first stable chemical entity shown to posses a quadruple bond. Finally Tc forms Tc_6 and Tc_8 prismatic clusters within which there are three or four Tc≡Tc units whereas Re forms rectangular Re_4 clusters with two Re≡Re bonds. Other important complexes of Tc and Re are nitrene species, hydrido and dihydrogen complexes and organometallic compounds among which the carbonyl species are among the most significant and will be discussed in more details in the following section.

I.4 Chemistry of the *fac*-$[M(CO)_3]^+$ Core (M = Tc, Re)

The syntheses of carbonyl complexes $[Re_2(CO)_{10}]$ and $[Tc_2(CO)_{10}]$ are traditionally performed in autoclaves. $[NEt_4][ReBr_3(CO)_3]$ is prepared from $[Re_2(CO)_{10}]$ by bromination to $[ReBr(CO)_5]$ and substitution of two COs with $[NEt_4]Br$.[21] Originally the complexes were prepared in organic solvents. Reduction of Tc(VII) and/or Re(VII) to Tc(I) or Re(I) under concomitant coordination of three COs could be achieved by bubbling of CO through a THF solution of the permetallates in the presence of BH_3THF and Cl^-. This resulted in the reduction of the metal center and coordination of at least three CO ligands.[22, 23]

Under these conditions different complexes in the +1 valency were found as products when varying the reaction conditions. When X^- (X = Cl, Br) is present in the reaction mixture, $[M_2(\mu\text{-}X)_3(CO)_6]$ forms quantitatively (M = Tc, Re). Addition of excess $[NEt_4]X$ lead to cleavage and formation of the final product $[TcX_3(CO)_3]^{2-}$ or $[ReX_3(CO)_3]^{2-}$. In the complete absence of X^-, the mixed hydrido-carbonyl complexes $[TcH(CO)_4]_3$ and $[Tc_3H_4(CO)_9]^-$ form together in almost 100%

yield. Addition of NaOH in methanol and subsequent acidification leads $[TcX_3(CO)_3]^{2-}$ (or $[ReX_3(CO)_3]^{2-}$).[22, 23]

For many years the synthesis of carbonyl complexes in water was practically unknown, since there was no need to develop such an approach. Nowadays carbonylation of Tc can be archived via the so-called boranocarbonates, originally described by Malone and Parry in 1967.[24, 25] Alberto found that $K_2H_3BCO_2$, prepared continuously from commercially available H_3BTHF solutions and reacted in situ with an alcoholic solution of potassium hydroxide, combines the possibility of in situ CO formation and reducing properties. $[^{99m}Tc(OH_2)_3(CO)_3]^+$ can now be prepared in water in a one-pot synthesis without the necessity of an additional reducing agent or of gaseous CO. In fact, a small amount of $K_2H_3BCO_2$ dissolved in a few ml of aqueous $[^{99m}TcO_4]^-$ gives $[^{99m}Tc(OH_2)_3(CO)_3]^+$ in yields of >98% after 10 min at 90 °C.[26]

When $[TcX_3(CO)_3]^{2-}$ or $[ReX_3(CO)_3]^{2-}$ are dissolved in water, the halides are readily substituted by H_2O and very high halide concentration is required to get small amounts of mono-halide substituted species. Thus, $[TcX_3(CO)_3]^{2-}$ and $[ReX_3(CO)_3]^{2-}$ transform completely to the corresponding aqua-ions $[M(OH_2)_3(CO)_3]^+$ (M = Re, **1**; M = ^{99}Tc, **2**). Three coordination sites are occupied by very tightly bound CO ligands, whereas the remaining sites are occupied by three labilized water ligands. Like most aqua-ions, **1** and **2** act as Bronstedt acids, and can also be expected to exhibit this characteristic. However, mono-cationic species are in general not very acidic and the pKa values are usually higher than 8. Deprotonation of coordinated water ligands leads temporarily to terminal hydroxo complexes which subsequently tend to oligo- or polymerize by formation of μ-OH or μ-O species.

The *fac*-$[M(CO)_3]^+$ moiety is very stable in water and $[M(S)_3(CO)_3]^+$ complexes (S = monodentate solvent molecule) exchange specifically the labile solvent ligands (i.e. H_2O). This represents a major advantage over the vast majority of Tc(I) or Re(I) compounds, where the low valency is stabilized by pH independent ligands (i.e. phosphanes) which can hardly be substituted by other incoming chelators. The M(I) center possesses a d^6 electronic configuration in an octahedral field. In general, such complexes are known to be kinetically inert.

Complexes **1** and **2** bind a large variety of ligands. Aliphatic amines as isolated ligand groups coordinate only weakly to **1** or **2**. Carboxylate groups and other anions showed similar features. Thioether groups coordinate very slowly, but their complexes are of extremely high (kinetic)

stability. On the other hand, aromatic amines show fast complexation and very high thermodynamic or kinetic stability. The combination of an aromatic and an aliphatic amine and even more with an additional carboxylic acid, are among the best ligands in aqueous solutions for **1** and **2**.

I.5 Chemo- and Radiotherapeutic Agents in Cancer Research

The use of inorganic and organometallic complexes in cancer imaging and therapy is an ongoing active field of research. Virtually almost all transition metals from group 3 to 12 and elements of group 13 are investigated for such purposes.[27] Complexes of Sc and Y are used in cancer imaging and therapy. Metallocenes of Ti, V, Nb and Mo are effective against different type of cancer cell lines including cisplatin resistant cell lines.[27] Organometallic complexes of Tc and Re are amongst the most widely used radiopharmaceuticals.[8, 28] Arene as well as amine and imine complexes of Ru and Os show remarkable antitumor activity.[27, 29] μ-caboxylato dirhodium compounds also show antitumor properties by inhibiting DNA replication and protein synthesis.[27] β-emitting radionuclides of Cu, Ag are used as therapeutic radiopharmaceuticals,[28] In is commonly used in cancer imaging while Ga compound show activity against soft tissue tumors.[27]

The anticancer drug cisplatin, however, remains the most effective inorganic compound for treatment of a variety of tumors. While the mechanism of action is not entirely understood, there is consensus in the community that binding of the drug to DNA is critical for its antitumor activity. A large body of evidence indicates a preference of the drug for DNA sequences containing two or more adjacent guanosine nucleosides. The bifunctional binding of cisplatin to purine bases occurs preferentially at GpG, ApG and GpNpG (where N = any nucleoside) sequences and these account all together for ≈ 90% of all cisplatin/DNA binding modes. Monofunctional adducts account for the remaining 10 %.

NMR and X-ray investigations have been carried out in the last twenty years to elucidate the structural feature of this interaction. Bifunctional binding to purines determines the loss of stacking in coordinated bases and leads to bending of the double helix associated to some extent with unwinding.[30] These DNA modifications contribute to a cascade of events, including transcription inhibition and repair shielding of cisplatin-DNA cross-links which ultimately result in cell death.[30]

One of the major disadvantages of cisplatin is its severe toxic side effects. The drug is unspecific in its interaction with DNA and virtually any base can be platinated. Furthermore many cancers

develop resistance to the drug.[27] Also, the coordination sphere of the metal ion cannot be derivatized with targeting agents as the molecules thus obtained lose their activity. Therefore, much interest remains in synthesizing metal complexes capable to bind to DNA bases in a fashion similar to cisplatin but do not present the disadvantages listed above.

I.6 Scope and Purpose of This Study

It is well known that by combining radiotherapy and chemotherapy, important therapeutic advantages can be obtained to cure cancer.[31] In cancer treatment it is therefore desirable to employ compounds that might function mechanistically as cisplatin derivatives, causing intrastrand linkages of DNA, in combination with an inherent radioactivity of the metal center. Such a class of compounds would act to inhibit DNA transcription while delivering a highly localized radiation dose in the target tumor tissues. At the same time the molecules may also be precisely localized in the body.

In current clinical practice radionuclides that decay by β-particle emission are most extensively used for radiopharmaceutical applications (see section I.5). ^{186}Re and ^{188}Re are two such radionuclides that are used as FDA approved drugs as cytotoxic therapeutic agents in human medicine. Mono-nuclear octahedral $^{186}Re^{I}$ and/or $^{188}Re^{I}$ complex may combine the inherent radioactivity of the metal center with the mechanistic properties of cisplatin resulting in a novel class of compounds which may be defined as “chemo-radiotherapeutic agents”.

This study therefore attempts to answer the following questions:

1. Can a rhenium and/or technetium tricarbonyl core interact with DNA in a fashion similar to cisplatin? Whereby interaction with DNA in a fashion similar to cisplatin is meant the binding of two nucleobases in *cis* position around the metal core.
2. If so, what are the differences?
3. Can a rhenium-based DNA targeting radiopharmaceutical with chemotoxic properties be designed?

The following chapters will describe the interaction of the *fac*-$[M(CO)_3]^+$ core (M = ^{99}Tc, Re) with guanine bases (untethered, Chapter 1) or as part of an olygonucleotide sequence (Chapter 3). The reactivity pattern of the above mentioned core with plasmid DNA will be illustrated and compared to that of cisplatin (Chapter 2). It will also be shown how the tricarbonyl core can be

protected with amino acids (Chapter 2 and 5) and it will be shown the reactions of the compounds thus obtained with biologically relevant molecules like Vitamin B12 (Chapter 4) or derivatized DNA bases (Chapter 5). Finally the cytotoxicity of compounds presented (Chapter 6) will be described. The last chapter of this study (Chapter 7) is dedicated to the metal ion Ru in the +2 oxidation state and there the first structurally characterized complex of Ru with two DNA bases covalently bound to the metal center will be presented.

I.7 References

(1) Berg, O.; Tacke, I. *Naturwissensch.* **1925**, *13*, 571-574.

(2) Perrier, C.; Segre, E. *J. Chem. Phys*. **1937**, *5*, 712-716.

(3) Perrier, C.; Segre, E. *Nature* **1937**, *140*, 193-194.

(4) Kenna, B. T.; Kuroda, P. K. *J. Inorg. Nucl. Chem.* **1964**, *26*, 493-499.

(5) Kenna, B. T.; Kuroda, P. K. *J. Inorg. Nucl. Chem.* **1961**, *23*, 142-144.

(6) Kipper, T. A.; Kipper, M. A. *Soviet Astronomy Letters* **1984**, *10*, 363-365.

(7) Cosner, K. R.; Despain, K. H.; Truran, J. W. *Astrophysical Journal* **1984**, *283*, 313-315.

(8) Jurisson, S. S.; Lydon, J. D. *Chem. Rev.* **1999**, *99*, 2205-2218.

(9) Riley, G. H. *J. Sci. Instrum.* **1967**, *44*, 769-770.

(10) Esenov, E.; Egizbaev, K.E.; Kalinin, S. K.; Fain, E. E. *Geokhimiya* **1970**, 610-612.

(11) Brodzins, R.l.; Conway, D. C. *Phys. Rev. B* **1965**, *138*, 1368-1369.

(12) Huster, E.; Verbeek, H. *Z. Phys.* **1967**, *203*, 435.

(13) Herr, W.; Hoffmeister, W. *Helv. Phys. Acta* **1962**, *35*, 320.

(14) Swensson, J. W. *Solar Phys.* **1970**, *13*, 25.

(15) Fouche, K. F.; Smales, A. A. *Chem. Geol.* **1966**, *1*, 329.

(16) Morgan, J. W.; Lovering, J. F. *Geochim.Cosmochim. Acta* **1967**, *31*, 1893.

(17) Cameron, A. G. W. in "*Origin and Distribution of the Elements*", Ahrens, L. H., Ed., Pergamon Press, Oxford, **1968**, p. 125.

(18) Morgan, J. W.; Lovering, J. F. *Earth Planet. Sci. Lett.* **1967**, *3*, 219.

(19) Morris, D. F. C.; Short, E. L. in *"Handbook of Geochemistry"*, Wedepohl, K. H., Ed., Springer-Verlag, Heidelberg, **1969**, Vol. 2.

(20) Cotton, F. A.; Wilkinson, G.; Murillo, C. A.; Bochmann, M. in *"Advanced Inorganic Chemistry"*, 6th Ed., Wiley-Interscience, New York, **1999**, p. 974-1000.

(21) Abel, E. W.; Butler, I. S.; Ganorkar, M. C.; Jenkins, C. R.; Stiddard, M. H. *Inorganic Chemistry* **1966**, *5*, 25-27.

(22) Alberto, R.; Schibli, R.; Egli, A.; Schubiger, P. A.; Herrmann, W. A.; Artus, G.; Abram, U.; Kaden, T. A. *J. Organomet. Chem.* **1995**, *493*, 119-127.

(23) Alberto, R.; Schibli, R.; Schubiger, P. A.; Abram, U.; Kaden, T. A. *Polyhedron* **1996**, *15*, 1079-1089.

(24) Malone, L. J.; Parry, R. W. *Inorg. Chem.* **1967**, *6*, 817-822.

(25) Malone, L. J.; Manley, M. R. *Inorg. Chem.* **1967**, *6*, 2260-2262.

(26) Alberto, R.; Ortner, K.; Wheatley, N.; Schibli, R.; Schubiger, A. P. *J. Am. Chem. Soc.* **2001**, *123*, 3135-3136.

(27) Clarke, M. J.; Zhu, F. C.; Frasca, D. R. *Chem. Rev.* **1999**, *99*, 2511-2533.

(28) Volkert, W. A.; Hoffman, T. J. *Chem. Rev.* **1999**, *99*, 2269-2292.

(29) Guo, Z. J.; Sadler, P. J. *Angew. Chem. In. Ed.* **1999**, *38*, 1513-1531.

(30) Sherman, S. E.; Lippard, S. J. *Chem. Rev.* **1987**, *87*, 1153-1181.

(31) See for example: (a) Fischer, B.; Benzina, S.; Ganansia-Leymarie, V.; Denis, J.; Bergerat, J. P.; Dufour, P.; Gueulette, J.: Bischoff, P. *Can. J. Physiol. Pharmacol.* **2004**, *82*, 140-145. (b) Ennis, R. D. *Curr. Oncol. Rep.* **2004**, *6*, 230-236.

Chapter 1. Interaction of $[M(H_2O)_3(CO)_3]^+$ Complex (M = Re, ^{99}Tc) with Guanine. Comparison with Leading Anticancer Drug Cisplatin

It is now generally accepted that the cytotoxicity of the leading anticancer drug cisplatin is due to the formation of 1,2-intrastrand adducts between the N7 atoms of two adjacent guanine residues in DNA.[1] The products of this interaction are d(GpG) cross-links and less frequently d(ApG). Not only are these adducts been observed both in vitro and in vivo, but clinically inactive compounds fail to form such cross-links.[1a]

Early structure-activity relationship studies indicated that for any *cis*-PtA_2X_2 analogue of cisplatin (A_2 is two amines or a bidentate amine ligand and X is an anionic leaving group) the carrier amine ligand had to have at least one proton for the drug to retain its anticancer activity.[2] This observation, along with the realization that d(GpG) can assume different conformations around the metal core,[3] led to the hypothesis that hydrogen bonding interactions between bound G ligands and the carrier amine of the drug were important for the stabilization of the DNA distortion induced by the intrastrand lesion.[3a, 4] By using the so called "retro models", Marzilli, Natile and coworkers have later demonstrated that the guanine O6 H-bonding to carrier amine ligand hydrogen is not important for the bases to assume a particular orientation around the metal center and they hypothesized that the small size of the NH group rather than its hydrogen-bonding ability is important for the anticancer activity of the drug.[5]

In the area of new drug design, much interest remains in synthesizing metal complexes capable to bind to DNA bases in a fashion similar to cisplatin. It also remains of fundamental interests to understand the factors driving the formation of different head-to-head (HH) and head-to-tail (HT) conformers *cis*-bis-metal adducts of nucleobases. Understanding the factors driving the formation of different HH and HT conformers is of particular importance for *cis*-PtA_2{d(GpG)} complexes. In fact, one principal hypothesis originally advanced by Lippard to explain the activity of the drug, suggests that the HH form in the intrastrand lesion is recognized by a damage recognition protein (Figure 1.1) whose binding prevents DNA repair, allowing the cisplatin adduct to persist long enough to activate apoptosis.[6] Marzilli suggested that the HT form in the interstrand lesion causes weaker binding of the damage recognition protein making this lesion a better substrate for repair.[7] Therefore, according to this hypothesis, the formation of a HT conformer results in lower cytotoxicity of the drug.

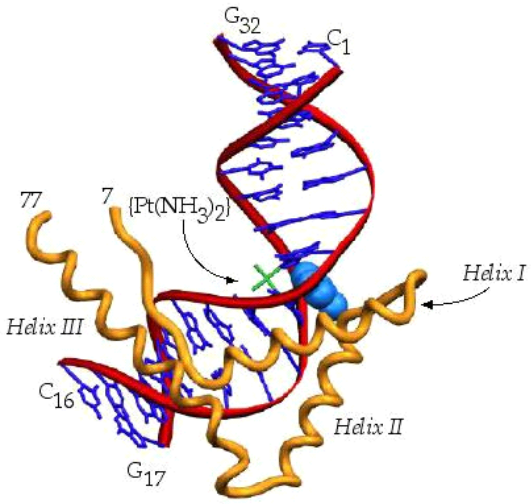

Figure 1.1. Crystal structure of high mobility group (HMG) domain proteins that bind to platinated DNA.[1a]

Mononuclear and dinuclear tricarbonyl rhenium(I) complexes of the type $[ReBr(CO)_3(Ph_2PCH_2)_2NR]$ and $[Re_2(\mu\text{-}OR)_3(CO)_6]$ have recently been described to efficiently suppress the growth of solid and suspended tumor cell lines.[2] Substitution of the alkoxide or hydroxide ligands and coordination to N7 in purine bases in a fashion similar to cisplatin was anticipated to be a possible mode of action for some of these complexes.[2a]

Work on novel $[M(OH_2)_3(CO)_3]^+$ (M= ^{99m}Tc , ^{188}Re) based radiopharmaceuticals, has shown that the d^6 "*fac*-$[M(CO)_3]^+$" moiety binds a wide variety of mono- and multidentate ligands to yield highly robust complexes. Aromatic amines in particular are potent ligands, and there exist a rhenium structure with a single N7 bound 9-ethylguanine.[3] Hence, it is likely that $[M(OH_2)_3(CO)_3]^+$ would also bind to two bases, isolated or in DNA despite the octahedral geometry and therefore exhibit potential cytostatic properties based on a mechanism comparable to cisplatin. To assess this possibility the basic coordination chemistry of $[Re(OH_2)_3(CO)_3]^+$ (**1**) and $[^{99}Tc(OH_2)_3(CO)_3]^+$ (**2**) with, guanosine (G) and 2-deoxyguanosine (2dG) was studied.

New DNA-targeting chemotoxic agents based on a metal or metal fragment of octahedral geometry, which results exclusively in the formation of a HT conformer when bound to two purine bases, might be expected, for the reasons mentioned above, as being of low efficacy. It is, therefore, important to understand the factors determining the orientation of purine bases when coordinated to the $[M(CO)_3]^+$ core, and more generally to a metal of octahedral geometry. Reedijk and others, in

fact, have pointed out that the carbonyl oxygen of coordinated guanine becomes sterically demanding in octahedral complexes. Therefore, steric hindrance between O(6) in guanine ligands and the CO ligands might force the two bases in a HT orientation in rhenium tricarbonyl complexes.[10]

To this end, the interaction of **1** and **2** with 9-methylguanine (9-MeG) and 7-methylguanine (7-MeG, Figure 1.2) was studied. The first of the two ligands was chosen as the simplest N(9) derivatized guanine, while 7-MeG was chosen because metal binding to N(9) does not impose steric hindrance.

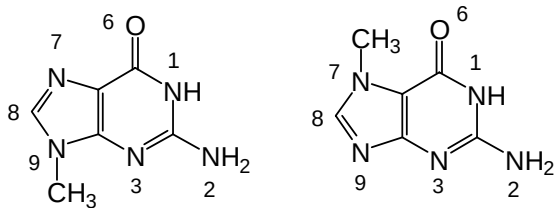

9-MeG **7-MeG**

Figure 1.2. Structure of 9-MeG and 7-MeG with numbering of relevant atoms.

In this chapter the first x-ray structures of technetium and rhenium complexes bound to two guanines via the N7 atoms together with kinetic and thermodynamic data of the interaction of **1** and **2** with G and 2dG is presented. The comparison of these data with those of $[Pt(NH_3)_2(H_2O)_2]^{2+}$, implies that **1** or **2** are potential cytotoxic agents affecting DNA like cisplatin. Structural evidence points to the fact that, as in the Pt case, two guanine ligands can adopt several conformations in an octahedral $[(CO)_3Re(purine)_2X]$ complex (X = H_2O, Br). The results suggest that neither hydrogen bonding interactions nor steric factors are important in determining the orientation of the ligands. The apparent intramolecular hydrogen bonding interactions one observes in the solid state structures result from the intrinsic conformation assumed by the ligands when bound to $[Re(CO)_3]^+$ core. The presence of HH and HT conformers in complexes with either 9-MeG or 7-MeG points to the fact that the steric hindrance imposed by the carbonyl oxygen of coordinated guanine is not a driving force for the preference of one conformation over the other.

Taken together, the results presented in this chapter suggest that complexes with ^{99m}Tc or ^{188}Re could be used as novel radiodiagnostic or -therapeutic agents.

1.1 Results

1.1.1 Interaction of 1 and 2 with G and 2dG

The reaction of **1** with 2 eq. of G, or 2dG in CH_3OH or in a CH_3OH/H_2O mixture (Scheme 1.1) can conveniently be monitored by ^1H NMR spectroscopy or HPLC. The mono- and the bis-purine base substituted complexes $[Re(S)_2(G)(CO)_3]^+$ (**3a**, S = solvent molecule), $[Re(S)(G)_2(CO)_3]^+$ (**3**) and $[Re(S)_2(2dG)(CO)_3]^+$ (**4a**), $[Re(S)(2dG)_2(CO)_3]^+$ (**4**) formed stepwise. This was also observed in the formation of $[^{99}Tc(S)(G)_2(CO)_3]^+$ (**5**). The Re and the ^{99}Tc complexes could be obtained as analytically pure white microcrystalline solids although the formation of the bis-substituted complexes **3**, **4** and **5** is not complete at a 1:2 stoichiometry. This is evident from ^1H NMR experiments performed in D_2O where by mixing **1** or **2** with 2 eq. of G or 2dG an equilibrium similar to the one depicted in Scheme 1.1 is reached and in the aromatic region of the spectrum the mono- and the bis-purine base substituted complexes are distinguished (Figure 1.3). No exchange-NOE signal could be detected between the H8 protons of coordinated guanosines in complexes **3** to **5**.

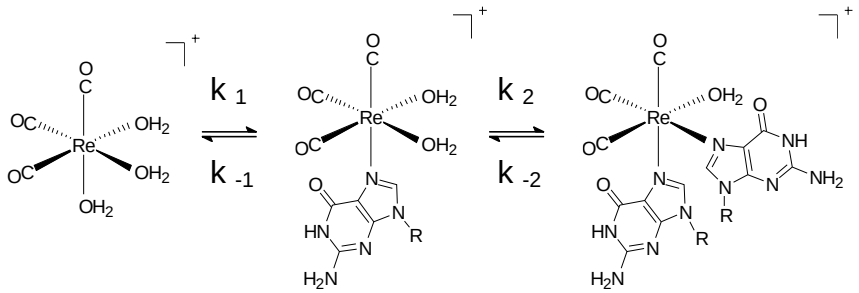

Scheme 1.1. Formation of mono- and the bis-purine base substituted complexes of **1**.

Although in H_2O and CH_3OH one single stereoisomer is found, this is not the case in aprotic solvents. The existence of distinct stereoisomers in other solvents such as DMSO parallels the chemistry of **1** and cisplatin. Dissolving (**4**)Br (prepared from aqueous methanol) in DMSO-d^6 shows initially one single species as indicated by a single set of two sharp H8 signals for the independent guanosines. Within days however three different isomers are in stable equilibrium and they do not exhibit any cross-peaks between the H8 protons of coordinated purines (2D exchange-NOESY, Figure 1.4). This indicates that in the single species the two H8's are separated by more than 3 Å.

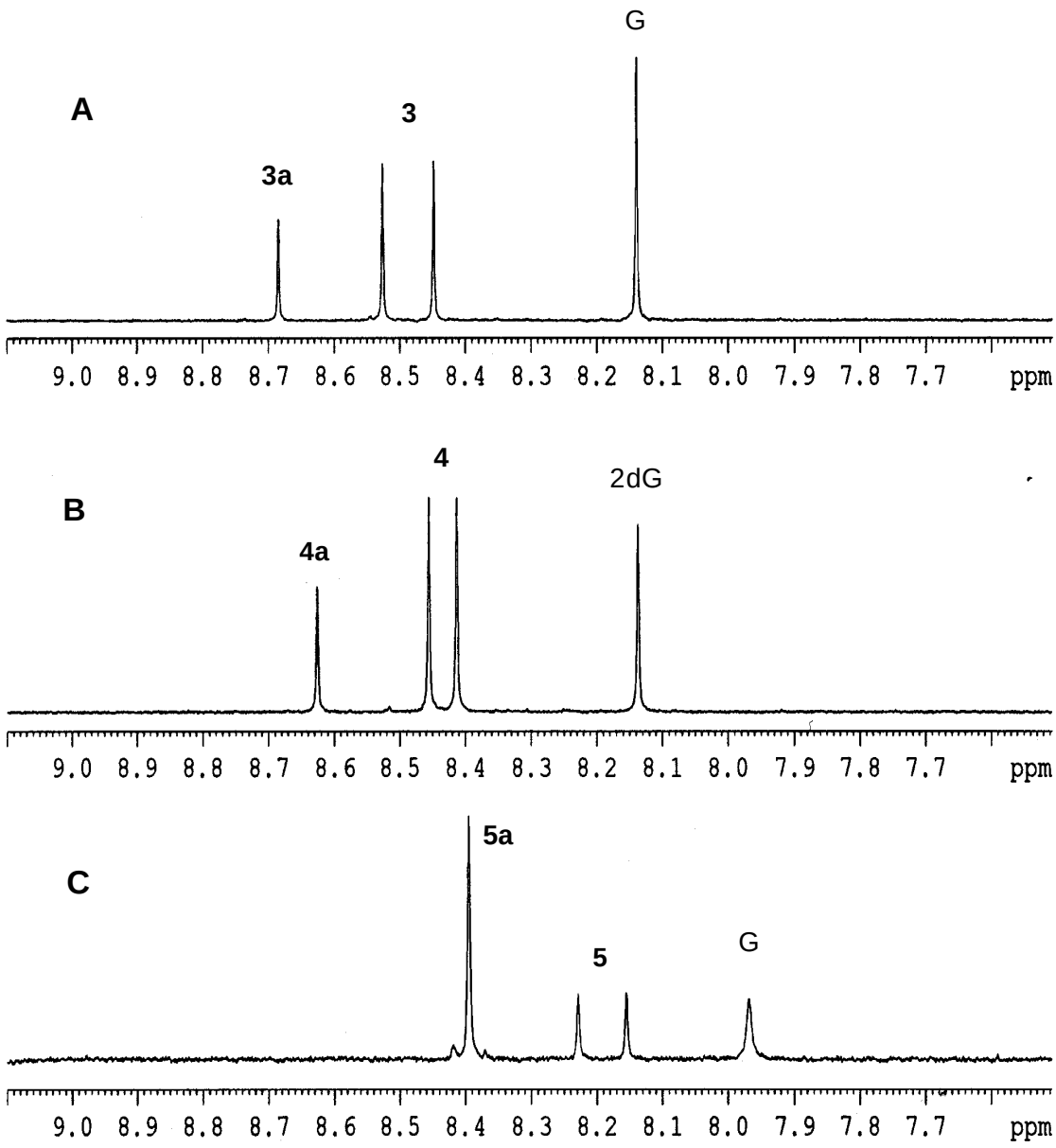

Figure 1.3. NMR spectrum (12h, 310K, D_2O, 7.5-9.1 ppm) of A: **1** plus 2eq. of G; B: **1** plus 2eq. of 2dG; C: **2** plus 2eq. of G.

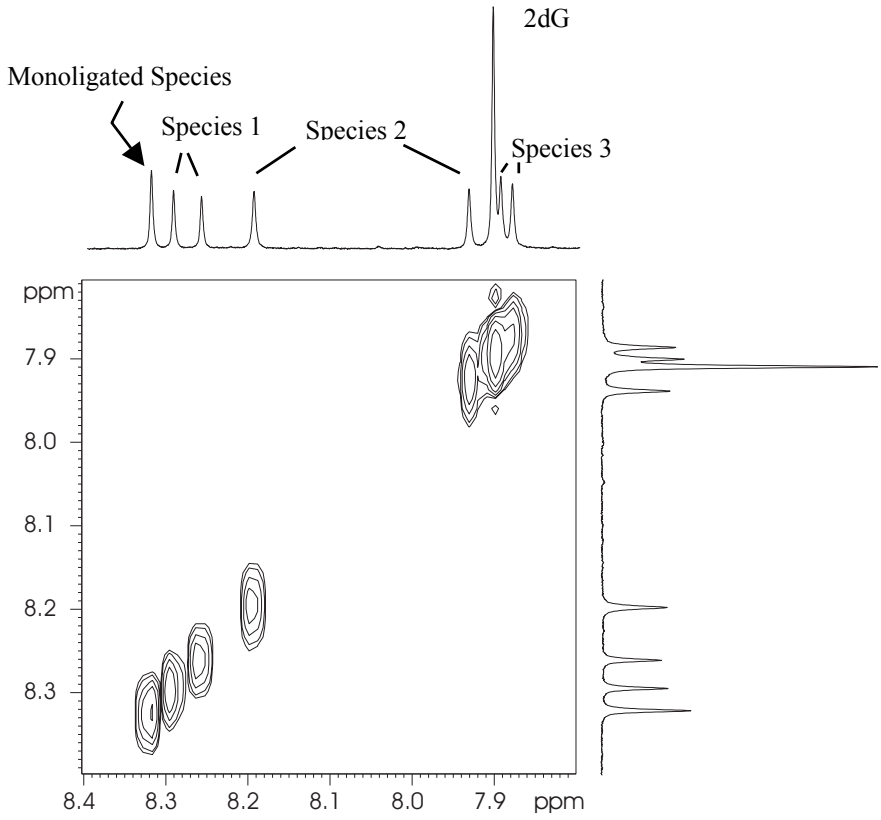

Figure 1.4. 2D exchange-NOESY ^{1}H NMR spectrum (DMSO-d^{6}, 25 ^{o}C, 7.8-8.4 ppm) of aged solution of (**4)**Br.

The rates of substitution and the stability constants K_1 and K_2 of the purine bases G and 2dG are important for comparing the behaviour of **1** with cisplatin. The species distribution at equilibrium, measured by ^{1}H-NMR, allowed an estimation of the stability constants according to Scheme 1.1. The values are 1.04 x 10^3 ± 0.46 M^{-1} (K_1) and 4.31 x 10^2 ± 0.45 M^{-1} (K_2) for G and 1.92 x 10^3 ± 0.98 M^{-1} (K_1) and 4.48 x 10^2 ± 0.31 M^{-1} (K_2) for 2dG. The rate of formation k_1 of $[M(OH_2)_2(G)(CO)_3]^+$ was determined under pseudo first order conditions by monitoring the growth of the monoligated species with ^{1}H NMR in D_2O. The rates of decomposition k_{-2} for **3** and **4** were received from the decrease of the corresponding ^{1}H signals in water considering the back and forward reaction according to literature.[12] From K_1, K_2, k_1, and k_{-2} the remaining k_{-1} and k_2 could be calculated (Table 1.1).

Although the conditions for the determination of the rate constants for Re^{I}-G differ slightly from those of Pt^{II} it is obvious that they are in the same order of magnitude. k_1 is larger for Re than for Pt, but the reverse is true for k_2. This might reflect the sterically more demanding octahedral Re complex. Binding of G to the Tc complex is about 5 times faster in k_1, a behaviour that is expected going one group higher in the periodic table. Comparison of stability constants K_1 and K_2 is difficult since platination of a base can be considered irreversible.

Rate constants exclusively refer to the interaction of Re and ^{99}Tc with N7 in G or 2dG. Although the nucleosides offer multiple binding sites, the metals coordinate selectively to N7 and no evidence for coordination to *i.e.* carbonyl oxygen, or to the ribose was seen. Steric hindrance from the sugar excludes binding to N3 and direct binding of a metal to the exocyclic $C2NH_2$ group has never been observed under physiological conditions.[14]

Table 1.1. Rate constants for the formation of the 1:1 ($k_1/10^{-2}$ $M^{-1}s^{-1}$) and 1:2 ($k_2/10^{-2}$ $M^{-1}s^{-1}$) complexes between *cis*-$[Pt(NH_3)_2(H_2O)_2]^{2+}$ or $[M(H_2O)_3(CO)_3]^{+}$ (M = Re, ^{99}Tc) with G and 2dG.

Complex	Base	k_1	k_2	T (K)
$[Pt(NH_3)_2(OH_2)_2]^{2+}$ [a]	G	23.7 ± 0.3	15.8 ± 0.2	298.2
$[Re(OH_2)_3(CO)_3]^{+}$ [b]	G	28.5 ± 1.6	4.40 ± 0.27	310.2
$[Re(OH_2)_3(CO)_3]^{+}$ [b]	2dG	14.5 ± 2.2	6.01 ± 0.15	298.2
$[^{99}Tc(OH_2)_3(CO)_3]^{+}$ [b]	G	104.1 ± 9.3		298.2

[a] = Unbuffered aqueous solution: pH = 3.85-4.15.[13] [b] = Unbuffered aqueous solution.

1.1.2 $[ReBr(BzIm)_2(CO)_3]$ Complex

In order to gain further insights on the possible orientation of G and 2dG in complexes **3** and **4**, $[ReBr(BzIm)_2(CO)_3]$ (**6**) was initially synthesized. In this compound, obtained from the reaction of **1** with 2 eq. of BzIm, the aromatic ligand is intended as a simple model purine. As in the case of the μ-oxo bridged $Re_2O_3Cl_4(Me_3BzIm)_4$ and the $RuX_2(dmso\text{-}S)_{2-n}(CO)_n(L)_2$ (X = Cl, Br ; L = BzIm,

Me_3BzIm) complexes, the two *cis* BzIm ligands in **6** are in a HH arrangement. All Re-L distances (where L = coordinated atom of ligand) fall within ranges of expected values found in Re^{I} compounds. No pronounced asymmetry between Re-N7-C5 and Re-N7-C8 bond angles (see Figure 1.5) was found. Unsymmetrical angles are common in all Co^{III}, Ru^{II} and Re^{I} complexes with Me_3BzIm, where Metal-N-C8 bond angles are consistently more acute than Metal-N-C5 angles: Metal-N-C8 angles range 119.2(2)–124.8(4)^{o}, Metal-N-C5 angles range 129.5(3)–135.9(2)^{o}.

As mentioned in the previous section, in D_2O and DMSO-d^6 no exchange-NOE signal could be detected between the H8 protons of coordinated guanosines in complexes **3** to **5**. This indicates that the two protons are separated by a distance greater than 3 Å. In **6** the corresponding hydrogens are separated by 3.75 Å. The H8-H8 distance in **6** was measured as a function of the BzIm ligand rotation with respect to other BzIm-N/Re/Br/*cis*-CO's plane and the results are shown in Figure 1.5. It is predicted that an exchange-NOE signal between H8 protons would be detected if the two N-donor heterocyclic ligands in **6** were in a HT conformation. These results tentatively point toward a HH arrangement of the coordinated bases in complexes **3**, **4** and **5**. If this assignment is correct then the difference in H8 chemical shifts in the species formed following equilibration of **4** in DMSO-d^6 is due to a slight different average mutual tilt between the two HH ligands.

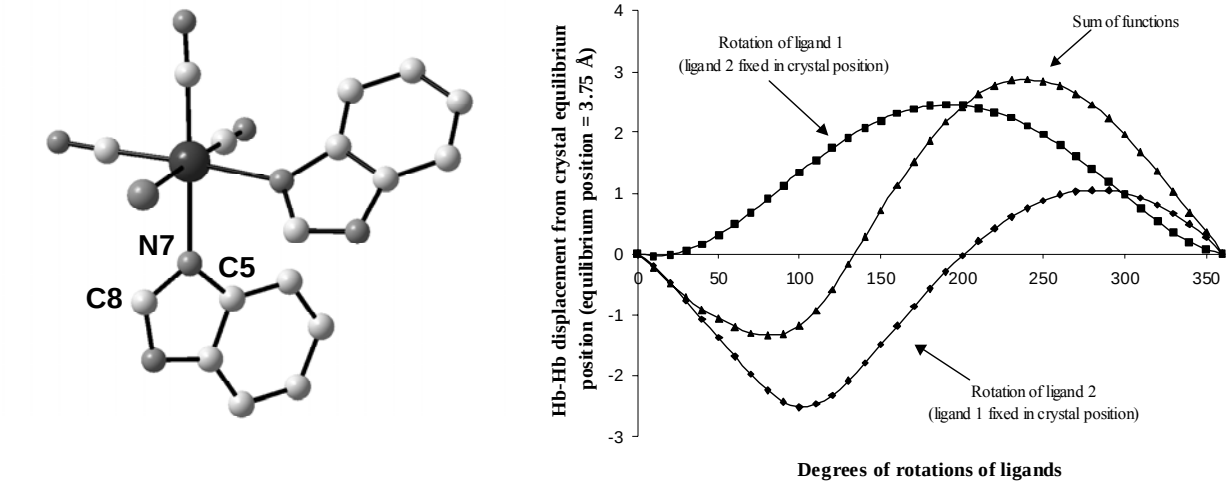

Figure 1.5. X-ray structure of **6** (left) and H8-H8 displacement from crystal equilibrium position as a function of ligand rotation around the Re-N bond (right).

1.1.3 Interaction of 1 and 2 with 9-MeG and 7-MeG

Synthetic Aspects. Reaction of **1** and **2** with 2 eq. of 9-MeG or 7-MeG in CH_3OH or in a CH_3OH/H_2O mixture can be conveniently monitored by ^1H NMR and HPLC analysis. Both the mono- and bis-ligated species are observed, and in fact, reaction of the $[Re(CO)_3]^+$ fragment with guanine bases lead to the equilibrium depicted in Scheme 1.1. As is the case with G and 2dG, complexes $[Re(CH_3OH)(9\text{-MeG})_2(CO)_3]^+$ (**7**), $[^{99}Tc(CH_3OH)(9\text{-MeG})_2(CO)_3]^+$ (**8**) and $[Re(CH_3OH)(7\text{-MeG})_2(CO)_3]^+$ (**9**) formed stepwise. The reaction in the presence of water gave the corresponding complexes i.e. $[Re(OH_2)(9\text{-MeG})_2(CO)_3]^+$ (**10**), $[^{99}Tc(H_2O)(9\text{-MeG})_2(CO)_3]^+$ (**11**) and $[Re(H_2O)(7\text{-MeG})_2(CO)_3]^+$ (**12**). Although the reaction did not go to completion at a 1: 2 stoichiometry, compounds **7**, **8**, **10** and **12** could be obtained as analytically pure, white microcrystalline solids when a slight excess of the corresponding base was utilized. No appreciable difference in the HPLC chromatograms was found if the reaction was carried out in water or a methanol/water mixture. Oriskovich had originally shown that the above mentioned fragment can bind a single 9-ethylguanine (9-EtG) via the N7 atom after displacement of a labile CH_3CN to yield a stable complex, where the remaining two coordination sites were occupied by bipyridine.[21] In this case, coordination of purine ligands occurred via displacement of the weakly bound water and/or methanol molecules.

X-ray Crystallography. Crystal data and experiment details are listed in the crystallography section while selected geometrical parameters are listed in Table 1.2. Crystals suitable for X-ray analysis were obtained in one of two ways. Slow solvent evaporation of a methanol/water solution gave crystals of the HH conformer of complex **10** (**10HH**) and the HT conformer of complex **12** (**12HT**), while vapor diffusion of pentane into a methanolic solution gave crystals of the HH conformer of complex **12** (**12HH**) and of the HT conformer of complexes **7** (**7HT**), **8** (**8HT**) and **10** (**10HT**). In all but one case, a solvent molecule is found occupying the sixth coordination site with exception of **12HH**, where a bromide is found. All relevant bonds and angles (Table 2) are in good agreement with the structure reported by Oriskovich et al.[21]

Table 1.2. Selected Bond Distances (Å) and Angles (deg.) of Complexes **7HT**-**12HH**.[a]

	7HT	**8HT**[b]	**10HT**	**10HH**	**12HT**[c]	**12HH**[c]	Re(9-EtG)[d]
Distances							
Re-N(7)	2.185(4)	2.190(3)	2.203(4)	2.212(13)	2.213(3)	2.215(10)	2.220(10)
Re-N(17)	2.193(5)	2.204(3)	2.193(4)	2.186(13)	2.184(4)	2.198(10)	
Re-C(21)	1.914(5)	1.897(4)	1.922(7)	1.880(17)	1.931(4)	1.916(18)	1.875(17)
Re-C(22)	1.922(6)	1.918(4)	1.918(5)	1.916(15)	1.911(4)	1.891(15)	1.896(15)
Re-C(23)	1.925(5)	1.919(4)	1.959(6)	1.881(16)	1.893(4)	1.901(19)	1.919(14)
Re-O(1)	2.163(4)	2.177(3)	2.168(4)	2.167(11)	2.184(3)		
Re-Br(1)						2.599(2)	
Angles							
N(7)-Re-N(17)	85.12(16)	86.05(11)	83.05(16)	82.0(4)	86.46(13)	84.8(4)	
N(7)-Re-C(21)	95.5(2)	95.21(15)	96.7(2)	173.8(5)	178.08(15)	177.2(5)	176.1(6)
N(7)-Re-C(22)	93.9(2)	176.17(14)	92.4(2)	95.4(5)	92.78(16)	93.3(5)	93.8(5)
N(7)-Re-C(23)	175.2(2)	93.30(15)	172.3(2)	96.9(5)	92.76(16)	92.1(5)	97.8(5)
N(17)-Re-C(21)	96.2(2)	95.72(14)	91.6(2)	93.8(5)	92.37(17)	93.1(6)	
N(17)-Re-C(22)	175.4(2)	91.25(14)	175.0(2)	177.0(5)	176.91(16)	92.8(5)	
N(17)-Re-C(23)	91.5(2)	176.35(15)	97.5(2)	94.4(5)	92.15(17)	175.6(5)	
O(1)-Re-N(7)	81.71(17)	82.62(12)	83.30(17)	81.9(4)	85.95(12)		
O(1)-Re-N(17)	80.27(18)	81.02(12)	81.64(16)	88.0(4)	84.04(13)		
Br(1)-Re-N(7)						83.3(3)	
Br(1)-Re-N(17)						84.5(3)	
C(21)-Re-C(22)	88.3(2)	87.91(17)	86.8(3)	88.7(6)	88.3(2)	88.6(6)	87.0(7)
C(21)-Re-C(23)	88.3(3)	87.75(17)	91.0(3)	87.9(6)	88.8(2)	89.9(6)	87.3(7)
C(22)-Re-C(23)	89.2(3)	89.22(17)	87.3(2)	87.5(6)	90.9(2)	90.5(6)	89.4(6)

[a] C(21), C(22), C(23) refer to carbonyl groups. [b] **8HT** values refer to ^{99}Tc. [c] For complexes **12HH** and **12HT** N(7) and N(17) refer to N(9) and N(19) respectively, that is to the N atoms bound to Re. [d] See reference 21.

The crystal structure of the cations **7HT** and **8HT** are given in Figure 1.6. In these complexes the two 9-MeG bases are in HT orientation which is the most common solid-state conformation of cis-bis(ligand) complexes of purines with Pt^{II}, Co^{III}, Cu^{II} and Zn^{II}.[8] In both complexes one of the 9-MeG ligands is stabilized by a hydrogen bond between the carbonyl oxygen (O16 in Figure 1.6) and a proton of the coordinated CH_3OH molecule. In both complexes the guanines coordinate through N7 only while the carbonyl oxygens (O6 and O16) are not involved in coordination as encountered with other metals.[7] In both species the O6 carbonyl group of one guanine bisects the plane between two CO ligands with average O6-CO oxygen distances of 3.2 Å.

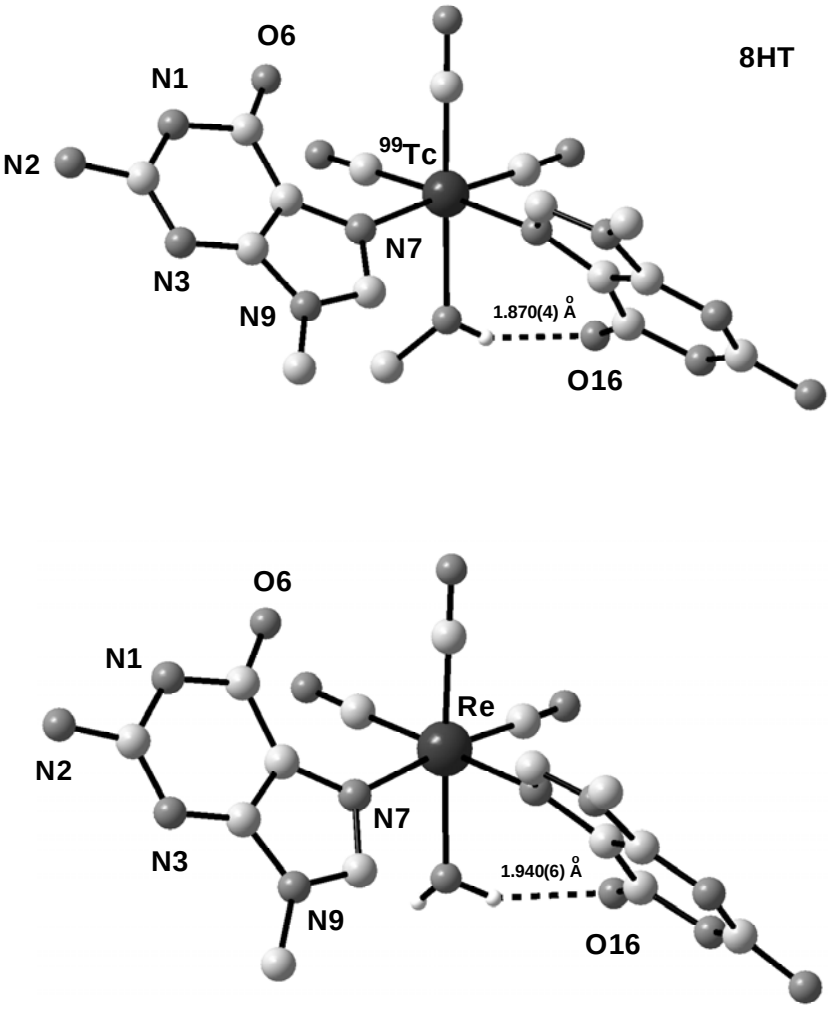

Figure 1.6. X-ray structures of cations **7HT** (top) and **8HT** (bottom).

Replacing CH_3OH by H_2O affords a better model of the complexes in aqueous solution. X-ray quality crystals of **10HT** were obtained from **7** in water. The crystal structure of the cation **10HT** is given in Figure 1.7. Although water offers a second proton, no reorientation of the bases took place and the structural features resemble closely those of **7HT** and **8HT** with no additional hydrogen bond being formed. In this complex also the two 9-MeG bases are in HT orientation with one base stabilized by a hydrogen bond between the carbonyl oxygen (O16 in Figure 1.7) and a proton of the coordinated H_2O molecule.

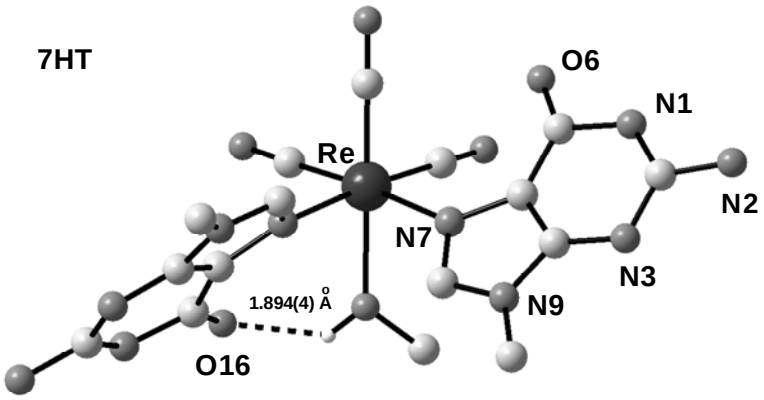

Figure 1.7. X-ray structure of cation **10HT**.

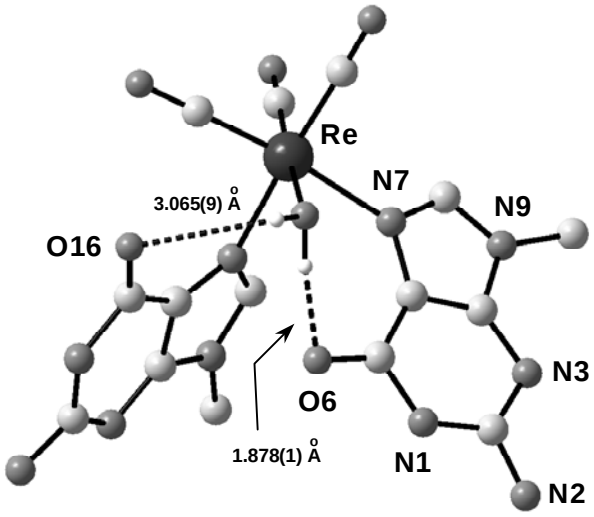

Figure 1.8. X-ray structure of cation **10HH**.

In complex **10HH** (see Figure 1.8), the same bases are found in a HH orientation. Both carbonyl oxygens can now participate in hydrogen bonding with the coordinated water molecule; however, only O6 shows a significant interaction (coordinated water-H-O6 bond = 1.878(1) Å; coordinated water-H-O16 bond = 3.065(9) Å, see Figure 1.8). It is also interesting to note that in crystal

structures of *cis*-$[(NH_3)_2Pt(9\text{-}EtG)_2](X)_2$ (X = Cl^-, ½ SO_4^{2-} or ½ $Pt(CN)_4^{2-}$) where the two bases are found in a HH conformation, only a single intramolecular hydrogen bond is formed between O6 and a NH_3 group.[22]

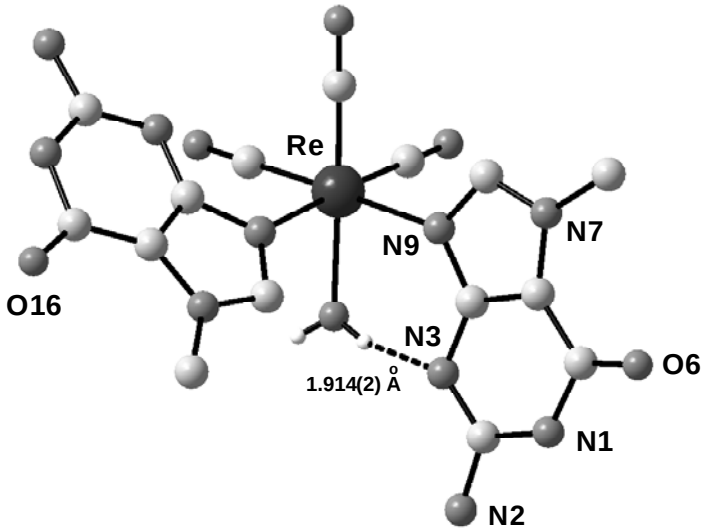

Figure 1.9. X-ray structure of cation **12HT**.

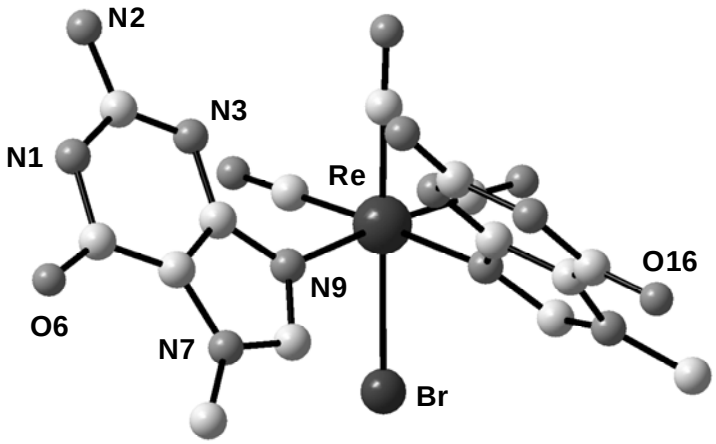

Figure 1.10. X-ray structure of **12HH**.

Complexes with 7-MeG also exhibit both HH and HT orientation of the bases. The crystal structure of the cation **12HT** given in Figure 1.9. The structural features of this complex resemble those of **10HT**. In this case the two purines are in a HT orientation with one base stabilized by a hydrogen bond between N3 and the a proton of the coordinated H_2O molecule (coordinated water-

H-N3 bond = 1.914(2) Å, see Figure 1.9). Complex **12HH** is the only complex bearing a bromide at the sixth coordination site. The crystal structure of this molecule is given in Figure 1.10. Interestingly the two bases were found in a HH orientation.

NMR Studies. ^{1}H NMR spectra of **10** and **12** are easily interpreted since in D_2O only two resonances are found, one in the aromatic region, while the other in the 3-4 ppm region, with a relative intensity of 1:3. These signals correspond to the aromatic H8 proton and to the methyl group covalently bound to the N9 or N7 atom. Figure 1.11 shows the aromatic region of ^{1}H NMR spectra obtained when crystals of (**10HT**)ClO_4 and of (**10HH**)Br are dissolved in D_2O. The single major peak resonating at 8.09 ppm corresponds to the bis-ligated species, while the two smaller signals flanking it, at 8.33 and 7.81 ppm, correspond to the mono-ligated species and to free 9-MeG, respectively. With time, the intensity of the small signals increases while the signal of **10HT** (and/or **10HH**) decreases, correspondingly, until the equilibrium depicted in Scheme 1.1 is reached. When crystals of (**12HT**)ClO_4 and **12HH** are dissolved in D_2O, a similar spectrum and a similar behavior is observed.

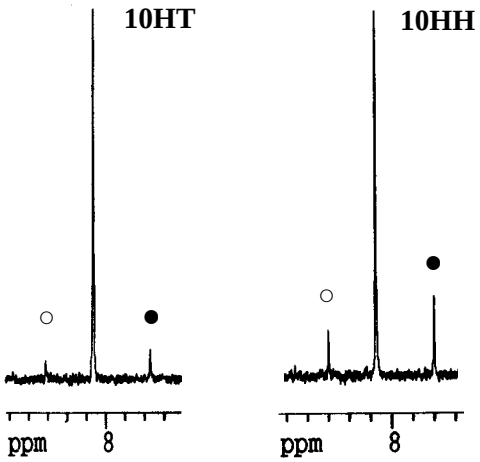

Figure 1.11. ^{1}H NMR spectrum (7.7-8.5 ppm) of **10HT** (left) and **10HH** in D_2O (298 K). The open circle (○) indicates the mono-bound species, the filled circle (●) free 9-MeG.

Raman Spectroscopy. Raman spectra of crystals of (**10HT**)ClO_4, (**10HH**)Br and of 9-MeG are shown in Figure 1.12. The spectra were recorded and compared in order to see if the intermolecular base stacking observed in the solid state structure of (**10HH**)Br (Figure 1.13B) would give rise to a

Raman hypochromic effect.[23] All spectra show highly characteristic guanine vibrational modes around 1580, 1500 and 1370 cm^{-1}. In addition, spectra of (**10HT**)ClO_4 and (**10HH**)Br show characteristic carbonyl ligand bands around 2030-1890 cm^{-1}. No appreciable decrease in signal intensity of the guanine bands was found in the spectrum of (**10HH**)Br. In this latter spectrum, the bands at around 1580 and 1370 cm^{-1} are actually found to have a higher relative intensity to the carbonyl ligand bands when compared to the spectrum of (**10HT**)ClO_4. The spectra reported bear a resemblance to those of HH conformers of 9-EtG adducts of cisplatin.[22] As in this later case, it is likely that since the intermolecular base stacking does not exceed the dimer level in (**10HH**)Br, it cannot cause a large enough hypochromic effect to reduce the intensity of the guanine bands.

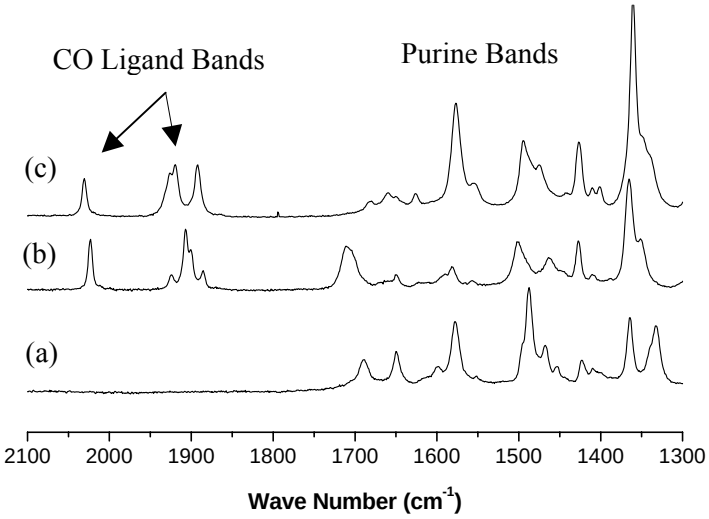

Figure 1.12. Solid state Raman spectra (2100-1300 cm^{-1}) of 9-MeG (a), (**10HT**)ClO_4 (b) and (**10HH**)Br (c).

1.2 Discussion

Crystal Packing. Packing diagrams of the four structures are given in Figure 1.13. Complex **10HT** (Figure 1.13A) shows alternating metal complexes separated along the x-axis by the perchlorate counter ions (on average Re-Cl > 6 Å). The packing is stabilized by extensive hydrogen bonding interactions involving the complex, the counter ion and the water molecules (see Hydrogen Bonding subsection). No evidence of base-base π-stacking interactions was found in this case. Complex **10HH** (Figure 1.13B) shows π-stacking of one coordinated purine involving the six member ring of the bases which are separated on average by 3.8 Å. The bases participating in π-

stacking are oriented in an antiparallel fashion. In complex **12HT** (Figure 1.13C) both bases participate in π-stacking interactions however one couple of bases shows only partial overlap. The other two bases are fully eclipsed and are oriented in an antiparallel fashion so as to maximize dipole-dipole interactions. In this latter case the mean average base-base separation is 3.8 Å. The packing diagram of complex **12HH** (Figure 1.13D) shows two cavities along the (001) projection. The larger of the two cavities is occupied by disordered pentane molecules while the smaller one by water molecules. Solvent molecules are however not shown in Figure 1.13D for clarity.

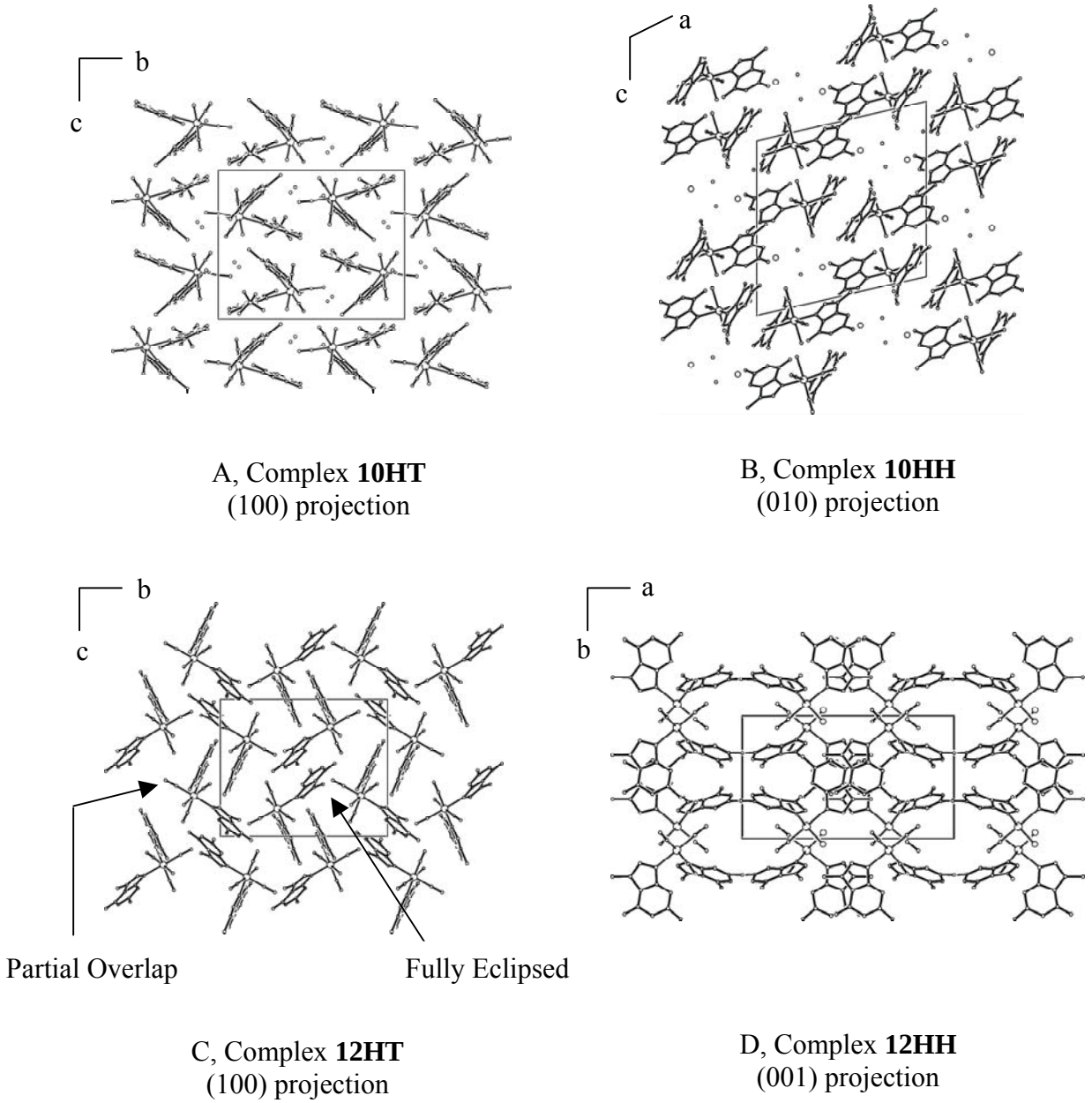

A, Complex **10HT**
(100) projection

B, Complex **10HH**
(010) projection

C, Complex **12HT**
(100) projection

D, Complex **12HH**
(001) projection

Figure 1.13. Perspective views of the crystal packing of structures comprising cations **10HT-12HH** generated by PLUTON.[44] Solvent molecules and counter ion are not shown in C and D for clarity.

No evidence of base-base π-stacking interactions was found and the overlap involving the six member ring visible in the figure is only apparent as the rings are separated by a distance greater than 7.5 Å.

Base Geometry and Conformation. Extensive studies on *cis*-PtA_2{d(GpG)} and simpler *cis*-PtA_2G_2 adducts have now established that the two bases can assume a HH and a HT conformation around the metal core.[24-35] Solid state structural data indicate that base tilt (or cant) can have two different directions, right-handed (R) and left-handed (L).[24, 31-35] Furthermore, HT isomers can be divided into two groups differing in the degree of canting. ΔHTR and ΛTHL isomers show less tilted bases while ΛHTR and ΔTHL isomers show more tilted bases.[5b-c, 36-38] In discussing the Re structures presented in this study it is used the same nomenclature employed to describe the HT and HH isomers of Pt compounds.

In all Re structures the two bases show right-hand canting. The two HT isomers of 7- and 9-MeG are of ΛHTR subgroup. This form is, to our knowledge, never been observed in the solid state structure of a metal fragment bound to two nucleotides. For *cis*-PtA_2G_2 models where G = nucleoside and nucleotide, for example, the ΔHTR form is observed exclusively in the solid state.[25-28, 39] A high degree of canting allowing the ΛHTR form is found only when G is not a 5'-nucleotide or when the base is part of an oligonucleotide.[22, 29, 31-34, 40-41] Therefore, structures **10HT** and **12HT** represent the first examples of ΛHTR forms of a metal fragment bound to two nucleotides. The ΛHTR form is unfavoured by electronic (dipole-dipole) interactions. It is now established that G(dipole)-G(dipole) interactions favour the less tilted HT atropisomer as this orientation of the bases places the H8 end of the dipole closer to the negative six-member ring of the *cis*-G base than in the more tilted form.[3, 5, 36-38] This feature stabilizes the ΔHTR form and it is one of the reasons for the exclusive crystallization of this form when the two bases are nucleotides. In structures **10HT** and **12HT** this is not the case and the ΛHTR form is observed.

Dihedral Angles. The base-base (B/B') and the base-coordination plane (B/CP) dihedral angles are useful parameters for comparing structural features of metal complexes of purines. B/B' is the angle formed by the intersection of the planes that pass through the two bases in a *cis* arrangement while B/CP is the angle formed by the intersection of the plane that passes through one of the bases and the plane defined by Re, the two N atoms of the bases coordinated to it and two C atoms trans to them. The B/B' angle is calculated according to the method outlined by Orbell, Marzilli and Kistenmacher by confining one of the two bases to the plane of the paper so that the N→Re vector

points leftward and the second base projects outward toward the viewer.[42] Relevant conformational parameters and dihedral angles are given in Table 1.3.

Table 1.3. Conformational Parameters of Complexes **10HT**-**12HH**.

	Dihedral angles (deg.)[a]			∟ N_B-Re-$N_{B'}$	
X-Ray Structure	B/B'	B/CP	B'/CP	(deg.)	Base canting
10HT	66	48	50	83.06(17)	ΛHTR
10HH	57	51	46	81.9(4)	HHR
12HT	75	38	78	86.45(13)	ΛHTR
12HH	62	48	47	84.8(4)	HHR
Optimized Geometry					
A	84	51	61	86.4	
B	86	64	53	89.1	
C	84	30	79	86.3	
D	81	71	86	87.4	

[a] See text for definitions.

The average B/B' angle of the Re complexes is 65° smaller than the average B/B' angle reported for *cis*-bis nucleotide complexes of Pt where the angle is generally greater than 70°.[22, 25, 30, 39] B/CP angles are small (near 50°) for all complexes except **12HT** where one of the bases shows a rather large B/CP angle of 78° while the other base a very small angle of 38°. Orbell *et al.* found that it was possible in some case to rationalize a large (near 90°) or a small B/CP dihedral angle in terms of intramolecular effects. They found, for example, that interligand hydrogen bonding tends to favour a small B/CP angle, while repulsive interligand steric factors tend to favour a large B/CP angle.[40] All Re complexes with the exception of **12HH**, show a strong (on average 1.91 ± 0.03 Å) intramolecular hydrogen bond between one base and the coordinated water molecule and show no intramolecular hydrogen bonding between coordinated purines. Complex **12HT**, however, is the only complex in which both bases participate in π-stacking interactions and neither of them shows base-base intermolecular hydrogen bonding. In this case, therefore, intermolecular rather than intramolecular effects can rationalize the B/CP angles. Intermolecular base-base hydrogen bonding tends to favour a small B/CP angle, while π-stacking interactions tend to favour a large B/CP angle.

Hydrogen Bonding. All structures have extensive hydrogen-bonding interactions between the guanines and the counter ions and the water molecules present in the crystals. Complete tables of these interactions are given in Supporting Information. Solvent molecule-guanine hydrogen-bonding involves mainly the $N(2)H_2$ and O6 groups of the bases. Although the Re complexes are generally well separated (on average in the four structures Re-Re > 8 Å), some intercomplex interactions occur. All structures with exception of **12HT**, shows base-base intermolecular hydrogen bonding. These interactions are shown in Figure 1.14. Complex **10HT** (Figure 1.14A) shows the unusual base-pairing scheme involving N2 and N3 (N2H-N3 bond 2.184(4) Å) which has been observed previously in the HT structure of the Pt-acyclovir complex.[31] The intermolecular base-base hydrogen bonding scheme of complex **10HH** (Figure 1.14B) involves, on the other hand, the carbonyl O6 atom and $N2H_2$ and N1H with distances of 2.353(7) and 1.972(1) Å respectively. To our knowledge this type of intermolecular interaction has never been reported in *cis*-bis purine metal complexes. Complex **12HH** shows the most unusual intermolecular base-base hydrogen bonding pair of the three structures. The hydrogen bonding scheme of complex **12HH** (Figure 1.14C) involves the carbonyl O6 atom and the H8 proton (2.445(2) Å). This type of interaction can be explained in electronic terms. As it is the case with other metals, the binding by N7 to Re^{I} leads to donation of electron density from the base imidazole ring to the metal. This interaction makes the H8 proton, already electron deficient and bearing a partial positive charge,[43] even more positive and therefore likely to participate in hydrogen bonding.

Theoretical Calculations. In order to obtain further information about the relative orientation of the coordinated purine ligands, the minima of the total energy surface corresponding to both HH and HT conformations of complexes $[Re(9\text{-MeG})_2(H_2O)(CO_3)]^+$ and $[Re(7\text{-MeG})_2(H_2O)(CO_3)]^+$ have been first fully optimized by aid of DFT calculations.[16] The most stable conformations found for both complexes exhibit a HH orientation while the HT conformers lie +5.8 and +6.9 kcal/mol higher in energy for complexes with 9-MeG and 7-MeG, respectively (Figure 1.15). The calculated values for the base-base (B/B') and the base-coordination plane (B/CP) dihedral angles defining the orientations of the purine ligands in the optimized conformers are in a reasonable agreement with those observed in the corresponding crystal structures (Table 1.3). However, it is well established that in the gas phase (DFT calculations level), the lowest energy structure maximizes the hydrogen bonding between ligands whereas in condensed phase systems, the hydrogen bonding will most likely be with surrounding solvent molecules. Thus, one can assume that the calculated energetic preference for the HH conformers is due to the fact that the two ligands in a HH orientation are well suited to make two intramolecular hydrogen bonds with the coordinated water, whereas the bases in

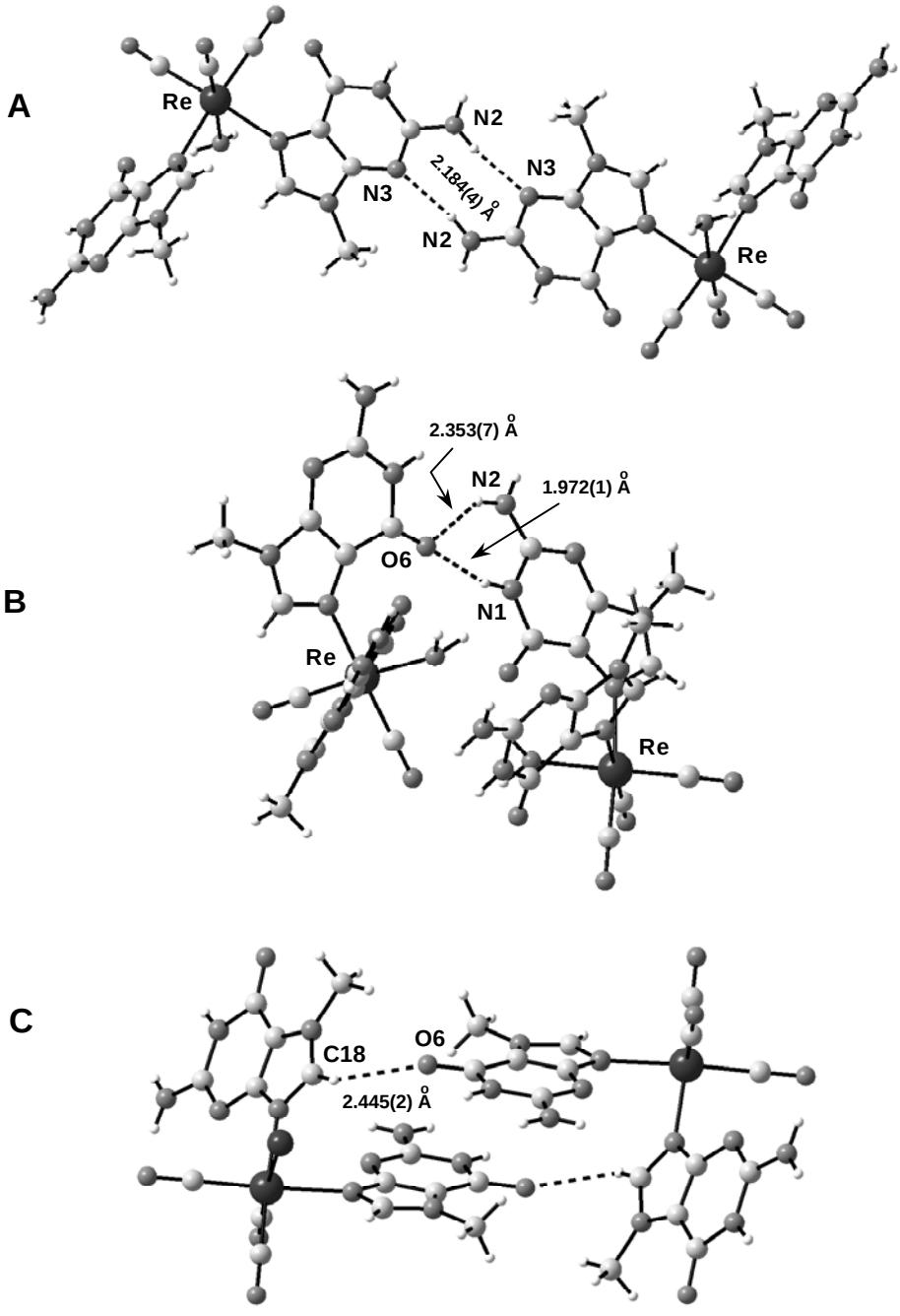

Figure 1.14. Intermolecular base-base hydrogen bonding in complexes **10HT** (A), **10HH** (B) and **12HH** (C).

a HT orientation can support only one such interaction. Consequently, further calculations were performed in which a free water molecule was added in the vicinity of the coordinated water molecule, in order to allow only one guanine ligand to interact with the coordinated water in both conformers. The most stable conformations found for both complexes now exhibit HT orientations: the HH conformers are higher in energy by +5.3 and +4.2 kcal/mol for complexes with 9-MeG and 7-MeG, respectively (See Figure 1.16). Furthermore, linear transit calculations simulating the rotation of one ligand around the Re-N bond in both cases of the *cis*-bis-guanine complex with 9-MeG and 7-MeG show that the energetic barriers ΔE rise approximately to 8.7 and 6.5 kcal/mol, respectively (the non-coordinated water molecule being still involved in the calculation). Finally, from our DFT calculations, one can conclude that in solution free rotation of the guanine ligands occurs, leading to relative orientations of the ligands in the solid state mainly governed by intra- or inter-molecular interactions.

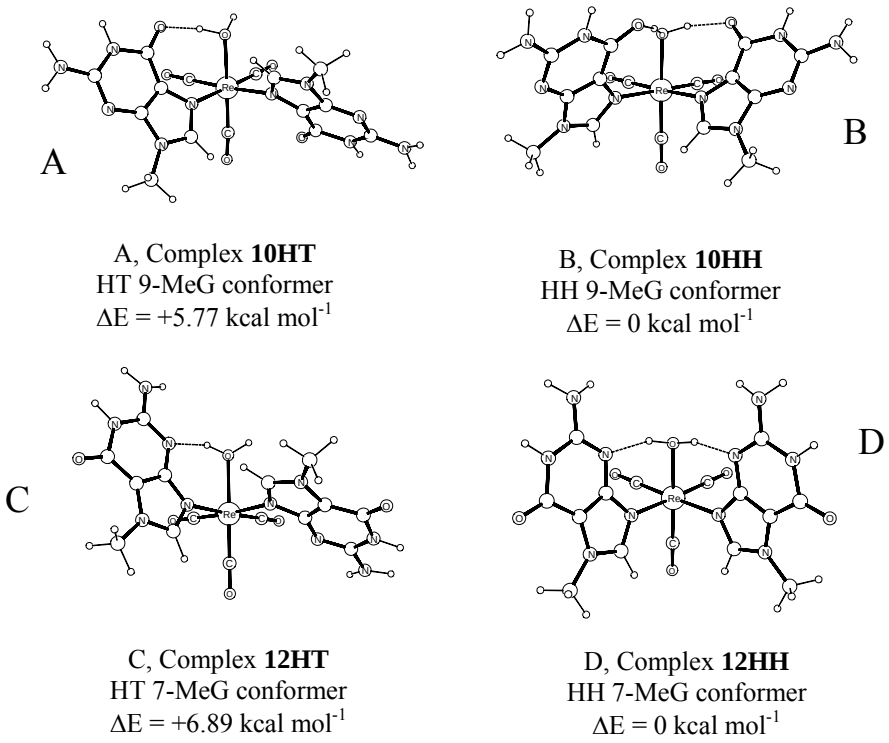

A, Complex **10HT**
HT 9-MeG conformer
$\Delta E = +5.77$ kcal mol^{-1}

B, Complex **10HH**
HH 9-MeG conformer
$\Delta E = 0$ kcal mol^{-1}

C, Complex **12HT**
HT 7-MeG conformer
$\Delta E = +6.89$ kcal mol^{-1}

D, Complex **12HH**
HH 7-MeG conformer
$\Delta E = 0$ kcal mol^{-1}

Figure 1.15. Optimized geometries and relative energies (ΔE) of HH and HT conformers of complexes **10HT-12HH** (A-D).

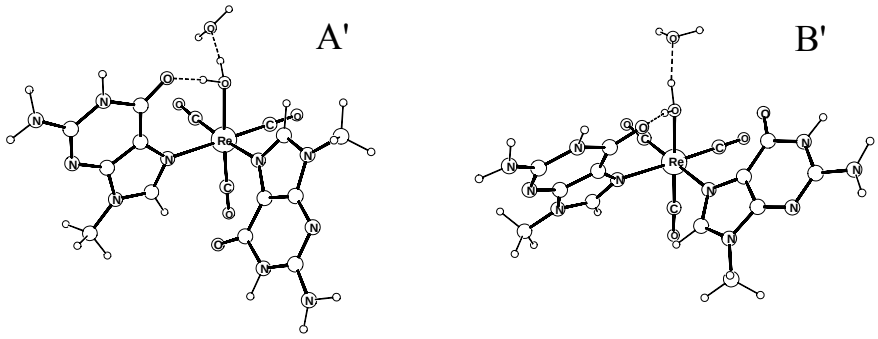

A', Complex **10HT**
HT 9-MeG conformer
$\Delta E = 0.00$ kcal mol^{-1}

B', Complex **10HH**
HH 9-MeG conformer
$\Delta E = +5.30$ kcal mol^{-1}

Figure 1.16. Optimized geometries and relative energies (ΔE) of complexes **10HT**•H_2O (A') and **10HH**•H_2O (B').

1.3 Conclusions

It was shown in this chapter that two guanine bases can coordinate to a Re^I or a Tc^I centre yielding reasonably stable complexes with slow on and off rates, the on rates being comparable to an active form of cisplatin. The first x-ray structure of a Tc-complex with purine bases was presented. They are in a HT orientation in the solid-state. Guanine ligands can assume both a HH and a HT conformation in an octahedral complex around the Re^I tricarbonyl core. The structural evidence presented clearly shows the two conformations. Although it is clear that intermolecular packing forces are responsible for the exclusive crystallization of one form, the ^{1}H NMR evidence indicates that these two forms are present in solution in equilibrium. Because conformer intercoversion is fast on the NMR time scale, it is impossible to use NMR methods to distinguish among the forms present in solution. This is the same "dynamic motion problem" present in most cisplatin adducts of untethered guanines.[3, 5]

The presence of a single H8 resonance in the ^{1}H NMR spectrum of **10HT** and **10HH** indicates that the two guanines can freely rotate about the Re-N7(9) bond. This implies that no steric hindrance is imposed by the O6 carbonyl oxygen. The presence of HH and HT conformers in complexes with either 9-MeG or 7-MeG in the solid state and in solution delineates the fact that

intramolecular hydrogen bonding and steric hindrance imposed by the carbonyl oxygen of coordinated guanines are not driving forces for the preference of one or the other conformation. DFT calculations confirmed the expected free rotation of the guanine ligands in solution leading to relative orientations of the ligands, because of small energy differences between conformers and relatively low energetic barriers leading from one conformer to the other.

1.4 References

(1) (a) Jamieson, E. R.; Lippard, S. J. *Chem. Rev.* **1999**, *99*, 2467-2498. (b) Spingler, B.; Whittington, D. A.; Lippard, S. J. *Inorg. Chem.* **2001**, *40*, 5596-5602. (c) Takahara, P. M.; Frederick, C. A.; Lippard, S. J. *J. Am. Chem. Soc.* **1996**, *118*, 12309-12321. (d) Gelasco, A.; Lippard, S. J. *Biochemistry* **1998**, *37*, 9230-9239.

(2) Wong, H. C.; Intini, F. P.; Natile, G.; Marzilli, L. G. *Inorg. Chem.* **1999**, *38*, 1006-1014.

(3) (a) Xu, Y.; Natile, G.; Intini, F. P.; Marzilli, L. G. *J. Am. Chem. Soc.* **1990**, *112*, 8177-8179. (b) Ano, S. O.; Intini, F. P.; Natile, G.; Marzilli, L. G. *J. Am. Chem. Soc.* **1997**, *119*, 8570-8571. (c) Ano, S. O.; Intini, F. P.; Natile, G.; Marzilli, L. G. *J. Am. Chem. Soc.* **1998**, *120*, 12017-12022. (d) Marzilli, L. G.; Ano, S. O.; Intini, F. P.; Natile, G. *J. Am. Chem. Soc.* **1999**, *121*, 9133-9142.

(4) (a) Hambley, T. W. *Inorg. Chem.* **1991**, *30*, 937-942. (b) Vickery, K.; Bonin, A. M.; Fenton, R. R.; O'Mara, S.; Russell, P. J.; Webster, L. K.; Hambley, T. W. *J. Med. Chem.* **1993**, *36*, 3663-3668. (c) Fenton, R. R.; Easdale, W. J.; Er, H. M.; O'Mara, S. M.; McKeage, M. J.; Russell, P. J.; Hambley, T. W. *J. Med. Chem.* **1997**, *40*, 1090-1098. (d) Rezler, E. M.; Fenton, R. R.; Easdale, W. J.; McKeage, M. J.; Russell, P. J.; Hambley, T. W. *J. Med. Chem.* **1997**, *40*, 3508-3515. (e) Hambley, T. W. *Coord. Chem. Rev.* **1997**, *166*, 181-223. (f) Guo, Z.; Sadler, P. J.; Zang, E. *J. Chem. Soc., Chem. Commun.* **1997**, 27-28.

(5) (a) Sullivan, S. T.; Ciccarese, A.; Fanizzi, F. P.; Marzilli, L. G. *J. Am. Chem. Soc.* **2001**, *123*, 9345-9355. (b) Williams, K. M.; Scarcia, T.; Natile, G.; Marzilli, L. G. *Inorg. Chem.* **2001**, *40*, 445-454. (c) Saad, J. S.; Scarcia, T.; Natile, G.; Marzilli, L. G. *Inorg. Chem.* **2002**, *41*, 4923-4935.

(6) Pil, P.; Lippard, S. J. *Science* **1992**, *256*, 234-237.

(7) Sullivan, S. T.; Ciccarese, A.; Fanizzi, F. P.; Marzilli, L. G. *Inorg. Chem.* **2000**, *39*, 836-842.

(8) (a) Yan, Y.-K.; Cho, S. E.; Shaffer, K. A.; Rowell, J. E.; Barnes, B. J.; Hall, I. H. *Pharmazie* **2000**, *55*, 307-313. (b) Zhang, J.; Vittal, J. J.; Henderson, W.; Wheaton, J. R.; Hall, I. H.; Hor, T. S. A. Yan, Y.-K. *J. Organomet. Chem.* **2002**, *650*, 123-132.

(9) Zobi, F.; Spingler, B.; Fox, T.; Alberto, R. *Inorg. Chem.* **2003**, *42*, 2818-2820.

(10) Van Vliet, P. M.; Haasnoot, J. G.; Reedijk, J. *Inorg. Chem.* **1994**, *33*, 1934-1939.

(11) (a) Alberto, R; Egli, A; Abram, U; Hegetschweiler, K; Gramlich, V; Schubiger, P. A. *J. Chem. Soc., Dalton Trans.* **1994**, *19*, 2815-20. (b) Alberto, R; Schibli, R; Egli, A; Schubiger, P. A.; Herrmann, W. A.; Artus, G.; Abram, U.; Kaden, T. A. *J. Organomet. Chem.* **1995**, *493*, 119-27.

(12) CELL, *2.92*, 1999 ed.; STOE & Cie, GmbH: Darmstadt, Germany, 1999.

(13) Sheldrick, G. M. *Acta Crystallogr. Sect. A* **1990**, *46*, 467-473.

(14) Altomare, A.; Burla, M. C.; Camalli, M.; Cascarano, G. L.; Giacovazzo, C.; Guagliardi, A.; Moliterni, A. G. G.; Polidori, G.; Spagna, R. *J. Appl. Crystallogr.* **1999**, *32*, 115-119.

(15) Sheldrick, G. M. *SHELXL-97*; University of Göttigen: Göttigen, Germany, 1997.

(16) TURBOMOLE, Program package for ab initio electronic structure calculations, Theoretical Chemistry, University of Karlsruhe, Germany, http://www.turbomole.com. (a) Ahlrichs, R.; Bär, M.; Häser, M.; Horn, H.; Kölmel, C. *Chem. Phys. Letters* **1989**, *162*, 165-169. (b) Treutler, O.; Ahlrichs, R. *J. Chem. Phys.* **1995**, *102*, 346-354. (c) von Arnim, M.; Ahlrichs, R. *J. Comp. Chem.* **1998**, *19*, 1746-1757.

(17) Vosko, S. H.; Wilk, L.; Nusair, M. *Can. J. Phys.* **1980**, *58*, 1200-1211.

(18) Becke, A. D. *Phys. Rev. A* **1988**, *38*, 3098-3100.

(19) (a) Perdew, J. P. *Phys. Rev. B* **1986**, *33*, 8822-8824. (b) Perdew, J. P. *Phys. Rev. B* **1986**, *34*, 7406. (c) Eichkorn, K.; Treutler, O.; Öhm, H.; Häser, M.; Ahlrichs, R. *Chem. Phys. Letters* **1995**, *240*, 283-290. (d) Eichkorn, K.; Treutler, O.; Öhm, H.; Häser, M.; Ahlrichs, R. *Chem. Phys. Letters* **1995**, *242*, 652. (e) Eichkorn, K.; Weigand, F.; Treutler, O.; Ahlrichs, R. *Theor. Chem. Acc.* **1997**, *97*, 119-124.

(20) (a) Schäfer, A.; Huber, C.; Ahlrichs, R. *J. Chem. Phys.* **1994**, *100*, 5829-5835. (b) Schäfer, A.; Huber, C.; Ahlrichs, R. *J. Chem. Phys.* **1992**, *97*, 2571-2577.

(21) Oriskovich, T. A.; White, P. S., Thorp, H. H. *Inorg. Chem.* **1995**, *34*, 1629-1631.

(22) Schölhorn, H.; Raudaschl-Sieber, G.; Müller, G.; Thewalt, U.; Lippert, B. *J. Am. Chem. Soc.* **1985**, *107*, 5932-5937.

(23) (a) Tomlinson, B. L.; Peticolas, W. L. *J. Chem. Phys.* **1970**, *52*, 2154-2156. (b) Tinoco, I. Jr. *J. Am. Chem. Soc.* **1960**, *82*, 4785-4790. (c) Rhodes, W. *J. Am. Chem. Soc.* **1961**, *83*, 3609-3617.

(24) Kozelka, J.; Fouchet, M.-H.; Chottard, J.-C. *Eur. J. Biochem.***1992**, *205*, 895-906.

(25) Cramer, R. E.; Dahlstrom, P. L.; Seu, M. J. T.; Norton, T.; Kashiwagi, M. *Inorg. Chem.* **1980**, *19*, 148-154.

(26) Marzilli, L. G.; Chalilpoyil, P.; Chiang, C. C.; Kistenmacher, T. J. *J. Am. Chem. Soc.* **1980**, *102*, 2480-2482.

(27) Kistenmacher, T. J.; Chiang, C. C.; Chalilpoyil, P.; Marzilli, L. G. *J. Am. Chem. Soc.* **1979**, *101*, 1143-1148.

(28) Barnham, K. J.; Bauer, C. J.; Djuran, M. I.; Mazid, M. A.; Rau, T.; Sadler, P. J. *Inorg. Chem.* **1995**, *34*, 2826-2832.

(29) Lippert, B.; Raudaschl, G.; Lock, C. J. L.; Pilon, P. *Inorg. Chim. Acta* **1984**, *93*, 43-50.

(30) Longato, B.; Bandoli, G.; Trovò, G.; Marasciulo, E.; Valle, G. *Inorg. Chem.* **1995**, *34*, 1745-1750.

(31) Grabner, S.; Plavec, J.; Bukovec, N.; Di Leo, D. ; Cini, R. ; Natile, G.; *J. Chem. Soc. Dalton Trans.* **1998**, *9*, 1447-1451.

(32) Cini, R.; Grabner, S.; Bukovec, N.; Cesarino, L.; Natile, G. *Eur. J. Inorg. Chem.* **2000**, *7*, 1601-1607.

(33) Sindellari, L.; Schölhorn, H.; Thewalt, U.; Raudaschl-Sieber, G.; Lippert, B. *Inorg. Chim. Acta* **1990**, *168*, 27-32.

(34) Sinur, A.; Grabner, S. *Acta Crystallogr., Sect. C* **1995**, *51*, 1769-1772.

(35) Grehl, M ; Krebs, B. *Inorg. Chem.* **1994**, *33*, 3877-3885.

(36) Marzilli, L. G.; Intini, F. P.; Kiser, D.; Wong, H. C.; Ano, S. O.; Marzilli, P. A.; Natile, G. *Inorg. Chem.* **1998**, *37*, 6898-6905.

(37) Ano, S. O.; Intini, F. P.; Natile, G.; Marzilli, L. G. *Inorg. Chem.* **1999**, *38*, 2989-2999.

(38) Saad, J. S.; Scarcia, T.; Shinozuka, K.; Natile, G.; Marzilli, L. G. *Inorg. Chem.* **2002**, *41*, 546-557.

(39) Gellert, R. W.; Bau, R. *J. Am. Chem. Soc.* **1975**, *97*, 7379-7380.

(40) Orbell, J. D.; Wilkowski, K.; De Castro, B.; Marzilli, L. G.; Kistenmacher, T. J. *Inorg. Chem.* **1982**, *21*, 813-821.

(41) Admiraal, G.; Van der Veer, J. L.; De Graff, R. A. G.; Den Hartog, J. H. J.; Reedijk, J. *J. Am. Chem. Soc.* **1987**, *109*, 592-594.

(42) Orbell, J. D.; Marzilli, L. G.; Kistenmacher, T. J. *J. Am. Chem. Soc.* **1981**, *103*, 5126-5133.

(43) Marzilli, L. G.; Marzilli, P. A.; Alessio, E. *Pure Appl. Chem.* **1998**, *70*, 961-968.

(44) Spek, A. L. *Acta Crystallogr., Sect. A* **1990**, *46*, 34.

Chapter 2. Guanine and Plasmid DNA Binding of Mono- and Trinuclear $[Re(CO)_3]^+$ Complexes with Amino Acid Ligands

In the last decades metal-based antitumor drugs have been playing an important role as therapeutic agents in antiblastic chemotherapy. Cisplatin remains the most effective metal-based drug used in clinics but other nonphysiological and physiological transition metal ions have received much attention. Among the metal ions studied for their therapeutic potential the octahedral geometry is often encountered. Ruthenium (II) and (III) compounds, for example, have raised great interest and complexes of the type $[trans\text{-}RuCl_4(X)(X')]^+$ (X = imidazole, indazole; X' = Me_2SO, indazole) have already entered phase I clinical trials.[1] Although the mode of actions of these complexes is not yet well understood, there is evidence for DNA as a likely target, similar to the well established platinum drugs.[2-19] Dinuclear rhodium acetate $[Rh_2(\mu\text{-}(O_2CCH_3)_4)(H_2O)_2]$, and related complexes have shown good antitumor activity as well[20] and structural studies suggest that their activity may be analogous to that of cisplatin by binding adjacent purines on DNA.[21-24]

As mentioned in the previous chapter, recent studies have reported that a number of different compounds all based on the *fac*-$[Re(CO)_3]^+$ core show cytotoxic properties. Studies on L1210 lymphoid leukemia and other cell lines indicated that Re^I alkoxo/hydroxo carbonyl complexes were effective in inhibiting DNA synthesis via the inhibition of dihydrofolate reductase and other enzymes for purine and pyrimidine pathways. Interaction with DNA, however, was not ruled out and it was anticipated that the compounds may bind to the nitrogenous bases after displacement of the alkoxide or hydroxide ligands.[25] Similarly the cytotoxicity of Re^I carbonyl 2-(dimethylamino)ethoxide complexes may involve binding to DNA bases or side-chains or amino acid residues in peptides[26] while phosphine-derivatized amine complexes seem unlikely alkylating agents.[27]

In chapter 1 it has been shown that the $[M(CO)_3]^+$ moiety (M = Re, ^{99}Tc) can bind two guanine bases in a *cis* fashion,[28] and X-ray crystallography confirmed that the two bases can assume both a head-to-head (HH) and a head-to-tail (HT) conformation around the Re core.[29] It was also demonstrated that the two bases can freely rotate about the Re-N7 bond and that neither intramolecular hydrogen bonding nor steric hindrance imposed by the carbonyl oxygen of coordinated guanines are driving forces for the preference of one or the other conformation in the octahedral complex.[29]

In order to understand if the cytotoxicity exhibited by some *fac*-$[Re(CO)_3]^+$ core based complexes is due to an alkylating event which may result in the formation of inter- or intrastrand links between DNA bases in a mode of action analogous to cisplatin, the interaction of a series of rhenium tricarbonyl complexes (Figure 2.1) with ΦX174 plasmid DNA has been studied. For these studies four new complexes were prepared and fully characterized. Three of these are based on the amino acids L-proline (Pro) and N,N-dimethylglycine (DMGly, **13**, **14**, and **15** in Figure 2.1) and are rare examples of structurally characterized molecules in which an amino acid is bound to the above mentioned core.

The amino acids were chosen as a kind of protecting group for the rhenium $[Re(CO)_3]^+$ core as in human serum (HS) $[Re(H_2O)_3(CO)_3]^+$ (**1**, see Figure 2.1) interacts unspecifically with potential coordination sites in serum proteins and is therefore not available at high concentration. Amino acids seem good candidates for protecting groups for the rhenium $[Re(CO)_3]^+$ core for two main reasons. First, depending on the choice of the amino acid, they afford robust bi- or tridentate protecting groups for the metal core. Second, since amino acids are not foreign to biological systems, once displaced from the metal core, which can then be thought as activated, they will not give rise to toxic side effects but they will simply be recycled in the biochemical pathways.

It will be shown in this chapter that reaction of **1** with the amino acids Pro and DMGly gives complexes with the unusual trimeric structures **13** and **14** (see Figure 2.1) and that specific complexes influence the tertiary structure of ΦX174 DNA by altering the electrophoretic mobility of the open circular and the supercoiled form of plasmid DNA. The induced changes involve covalent binding to two bases rather than simple electrostatic interaction.

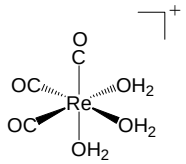

$[Re(H_2O)_3(CO)_3]^+$ (**1**)

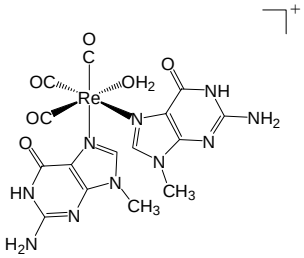

$[Re(H_2O)(9\text{-}MeG)_2(CO)_3]^+$ (**10**)

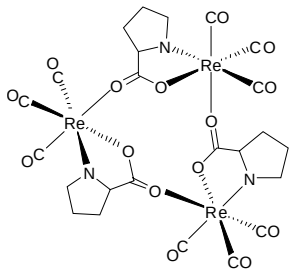

$[Re(Pro)(CO)_3]_3$ (**13**)

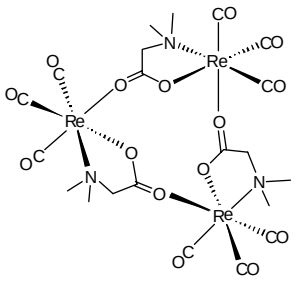

$[Re(DMGly)(CO)_3]_3$ (**14**)

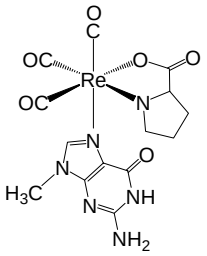

$[Re(Pro)(9\text{-}MeG)(CO)_3]$ (**15**)

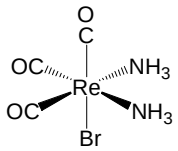

$[ReBr(NH_3)_2(CO)_3]$ (**16**)

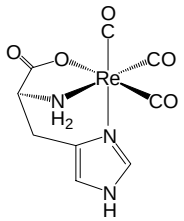

$[Re(His)(CO)_3]$ (**18**)

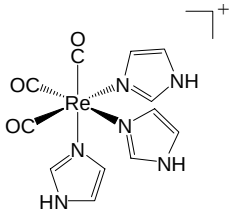

$[Re(Im)_3(CO)_3]^+$ (**19**)

Figure 2.1. Rhenium complexes investigated in this chapter.

2.1 Results and Discussion

Synthetic Aspects. In this section the preparation of complexes **13-16** is discussed in more details and the reasons behind the choice of specific ligands are elucidated. As mentioned earlier, $[Re(H_2O)_3(CO)_3]^+$ (**1**) is readily trapped in human serum (HS) by the serum proteins and it is not easily released. The $[Re(CO)_3]^+$ moiety must, therefore, be protected by ligands that, on one hand, prevent its interaction with serum proteins and are on the other hand labile enough to be displaced and to allow the Re core to bind to bases in DNA.

The two NH_3 groups in $[ReBr(NH_3)_2(CO)_3]$ (**16**) were intended to serve the function of the *cis*-labile exchangeable chloride ligands encountered in cisplatin and other transition-metal complexes tested for anti-tumor activity. Contrary to the latter, where the function is usually fulfilled by halides, the NH_3 ligand was chosen to confer an overall neutral charge to the complex. Behrens and Pässler first prepared and studied the $[ReCl(NH_3)_2(CO)_3]$ complex by reacting $[ReCl(CO)_5]$ in a benzene/liquid ammonia mixture under controlled pressure.[37] It was found that the bromide analog can be obtained by a much simpler route by reacting $[ReBr(CO)_5]$ in a NH_3 saturated benzene solution heated to 60 ^{0}C. Complex **16** thus obtained is soluble in polar organic solvents. In a water/methanol mixture (1:1), however, **16** hydrolyzes to give **1** with rate constants of about $3.8 \pm 0.9 \times 10^{-3}$ s^{-1} (k_1) and $2.0 \pm 0.5 \times 10^{-4}$ s^{-1} (k_2) as determined by HPLC methods.

The NH_3 ligand is too labile to serve a as protecting group for the $[Re(CO)_3]^+$ core. We therefore focused our attention on amino acids. Amino acids without coordinating side chain afford bidentate protecting groups for the Re core. The interaction of organometallic complexes with amino acids and peptides, actually pioneered bioorganometallic chemistry,[38-40] and has again received much attention in recent years.[41] Reaction of **1** with the amino acids L-proline (Pro) and N,N-dimethylglycine (DMGly) yields trinuclear complexes of the type $[Re(L)(CO)_3]_3$ (L = Pro, **13**; L = DMGly, **14**). The reaction goes to completion within a few hours in a methanol/water mixture (9:1) and in the presence of a slight excess of amino acids required to neutralize the proton released upon coordination of the carboxylate group. Proline was first chosen because secondary amines are weaker coordinating and easier to replace.

In order to investigate whether $[Re(Pro)(CO)_3]_3$ (**13**) binds to DNA bases its interaction with 9-methylguanine (9-MeG) was studied. Complex **13** reacts with 9-MeG in a methanol/water mixture to give $[Re(Pro)(9\text{-MeG})(CO)_3]$ (**15**) in good yield as the only product even if excess nucleobase is

used. Obviously proline, forming a stable five-membered ring upon coordination, is still a good bidentate ligand/protecting group for the $[Re(CO)_3]^+$ core and cannot easily be displaced by free guanine or incorporated though bidentate binding into DNA. Thus, since **13** has a single available coordination site for DNA binding, the complex is unlikely to be able to form *cis*-bis intra- or interstrand adducts with the nitrogen in purine or pyrimidine bases. Under the same condition other DNA bases show little or no reaction with **13**.

Since Pro seemed to be too inert to be displaced from the metal core by DNA bases, the reaction of **1** with N,N-dimethylglycine (DMGly) was investigated. DMGly, containing a tertiary amine, should be even less strongly coordinating than the secondary amine in Pro. The extra CH_3 group on the amine should give a more labile ligand due to steric hindrance. Reaction of **1** with the DMGly also yields a trinuclear complex, $[Re(DMGly)(CO)_3]_3$ (**14**). It is noteworthy to mention that **13** and **14** are obtained as trimeric species in the solid state. In aqueous solution however, ^1H NMR and ESI-MS evidence suggests that the corresponding monomeric species $[Re(L)(H_2O)(CO)_3]$ (L = amino acid) are also present. These related equilibria have not been investigated in detail as it is beyond the scope of this study. In the schemes therefore presented the trinuclear rather than the mononuclear species is always shown.

In a water/methanol mixture, (50 ^oC) **14** reacts with an excess of 9-MeG stepwise. In our HPLC gradient complex **14** has a retention time (rt) of 15.5 min (see Figure 2.2). After 1h a second peak is observed with rt of 18.5 min. HPLC-MS chromatography indicates that this species is $[Re(DMGly)(9\text{-}MeG)(CO)_3]$ (**17**). After a further 1h a third peak appears at 17.5 min which was identified as $[Re(9\text{-}MeG)_2(H_2O)(CO)_3]^+$ (**10**). The reaction proceeds further until a fourth peak is seen at 16.5 min and an equilibrium is reached. This final species was identified by HPLC-MS as $[Re(9\text{-}MeG)(H_2O)_2(CO)_3]^+$ (**10a**, see Figure 2.2).

As anticipated, the conversion of **14** to complex **10** implies that DMGly can be displaced due to increased steric hindrance from the Re coordination sphere in favour of 9-MeG. In fact, as described in more details later, the Re-N(1) and Re-O(1) bond lengths in **14** are 0.06 and 0.04 Å respectively longer than in **13** and the N(1)-Re-O(1) bite angle is about 0.7^o more acute in **14** (see x-ray crystallography subsection 2.2.2). These differences lead to a weakening of the Re-N/O bonds and consequently to an increased reactivity of **14** inducing excess 9-MeG to displace DMGly.

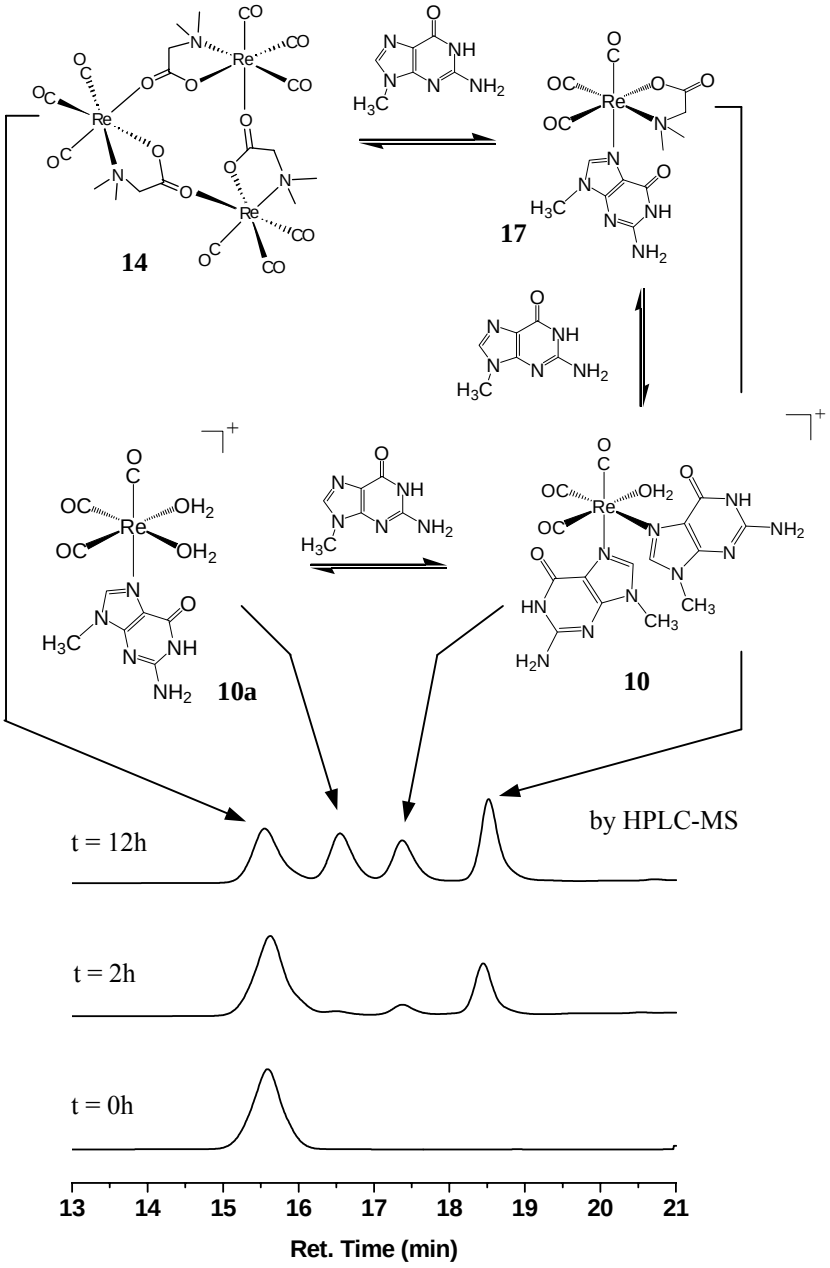

Figure 2.2. HPLC chromatogram of the reaction of **14** with excess 9-MeG and equilibrium scheme.

The results suggest that **14** might be a good candidate for a model Re pro-drug. While a ligand like DMGly protects the $[Re(CO)_3]^+$ core from reacting with coordinating sites in blood proteins the steric hindrance imposed on one (or both) of the coordinated atoms renders the ligand weak enough

to be displaced by stronger (even monodentate) ligands such as guanine. Indeed, in human serum little or no reaction of **14** with serum proteins was seen during a 12h incubation period at 37 °C.

X-ray Crystallography. Crystal data and experiment details are listed in the crystallography section. The crystal structure of compound **16** is shown in Figure 2.3. The structure consists of discrete molecules separated by van der Waals distances with short contacts occurring exclusively between Br, carbonyl oxygens and protons of NH_3 (on average NH-Br = 2.940(5) Å, NH-OC = 2.605(7) Å). The molecule crystallizes in the orthorhombic space group Pnma with Br, Re and C2O laying on a mirror plane at x, ¾, z. The geometry around rhenium is octahedral with Re-N1 distance of 2.240(6) Å which is comparable to the average Re-NH_2R distances (2.238 Å) in the bidentate en of the related $[Re(en\text{-}N,N')(en\text{-}N)(CO)_3]^+$ (en = ethylenediamine) complex and significantly longer than the average distance in the monodentate en.[42]

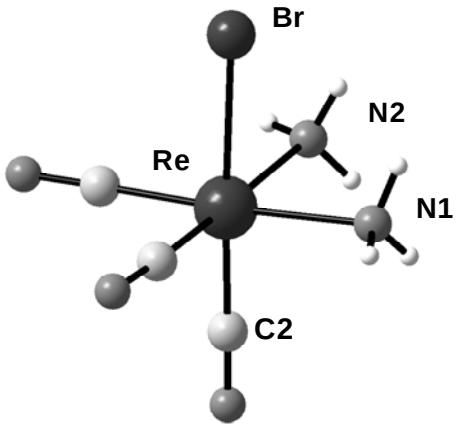

Figure 2.3. Crystal structure of $[ReBr(NH_3)_2(CO)_3]$ (**16**). Selected bond distances (Å) and angles (deg) are the following: Re-N1 2.240(6), Re-Br 2.6604(14); N1-Re-Br 84.65(17), N1-Re-N2 81.4(3).

Figure 2.4 and Figure 2.5 depict the molecular structure in the crystal of complexes **13** and **14**. Both molecules are macrocyclic trimers in which the rhenium atoms are bridged by the carbonyl oxygen of the amino acid ligand with the metal atoms being 5.43 Å apart from each other. In **13** the three Re atoms are related to each other by a three-fold rotation axis while in **14** there is no symmetry element that relates the three metal atoms. In both structures the rhenium is bonded in a distorted octahedral geometry with N-Re-O bite angles of 75-79^o. All bond lengths are in good

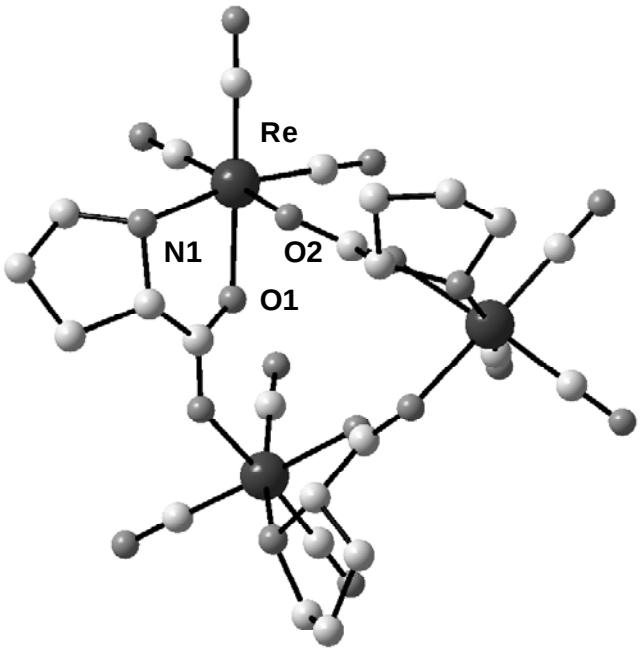

Figure 2.4. Crystal structure of $[Re(Pro)(CO)_3]_3$ (**13**). Selected bond distances (Å) and angles (deg) are the following: Re-N1 2.205(5), Re-O1 2.138(4), Re-O2 2.195(4); N1-Re-O1 75.69(17), N1-Re-O2 76.93(17), O1-Re-O2 83.29(17).

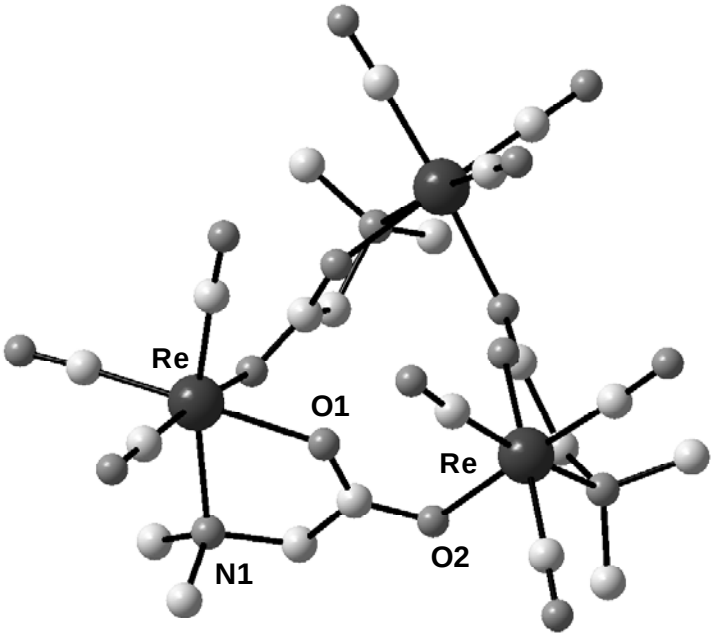

Figure 2.5. Crystal structure of $[Re(DMGly)(CO)_3]_3$ (**14**). Selected bond distances (Å) and angles (deg) are the following: Re-O1 2.172(8), Re-N1 2.260(10), Re-O2 2.189(8); O1-Re-N1 75.0(4).

agreement with the structure of [Re(His)$(CO)_3$] (**18**, see Figure 2.1). Complexes **13** and **14** are rare examples of structurally characterized molecules in which an amino acid is bound to the $[Re(CO)_3]^+$ core and to our knowledge they represent the first example a macrocyclic trimer of the $[Re(CO)_3]^+$ core not involving a μ-type bridge.

These unusual Re trinuclear complexes are closely related to a family of chiral-at-metal trimers of general formula $[\{(\eta^n\text{-ring})M(L)\}_3](BF_4)_3$ (where M = Ru, Os, Rh, Ir; L = amino acid) which result from the reaction of $[(\eta^n\text{-ring})MCl(L)]$ with $AgBF_4$.[41] In these cationic complexes the aminocarboxylate ligand also acts as a tridentate bridging group where, as in **13** and **14**, the nitrogen atom and one the carboxylic oxygen atoms are bonded to a metal center forming a five-membered metallacycle and the remaining oxygen coordinates to a second neighboured metal center. The structures of **13** and **14** also resemble the self-assembled ruthenium macrocyclic ionophores with high affinity and selectivity for Li^+ and Na^+ recently described by Severin.[43-44] The twelve atoms forming the central macrocyclic cavity in **13** and **14** are shown in Figure 2.6 along with mean average distances.

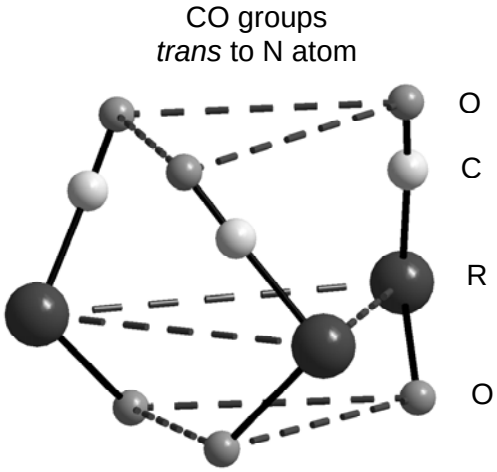

	Compound **13**	Compound **14**
Avg. CO-OC	4.36 Å	4.48 Å
Avg. Re-Re	5.43 Å	5.43 Å
Avg. O-O	4.10 Å	4.11 Å

Figure 2.6. The twelve atoms forming the central macrocyclic cavity in **13** and **14**. Mean average distances are shown to the right.

The average O-O distance (where O = bridging carboxyl oxygen of the amino acid) is about 1 Å longer than the average O-O distance of Severin's inophores. Compounds **13** and **14** might therefore be selective for larger cations like K^+ and/or Rb^+ although a high thermodynamic stability is not expected.

The molecular structure of **15** is shown in Figure 2.7. The complex crystallizes in the monoclinic space group $P2_1$ with three independent molecules in the unit cell. In the crystal the molecules show an extensive network of intermolecular hydrogen-bonding interactions between the guanines and the amino acids. Two types of such interactions are shown in Figure 2.8. The proton bound to N1 and one of the protons of the extracyclic $N2H_2$ group always form a hydrogen bond with the oxygens O1 and O2, respectively, of the carboxylate group of the coordinated proline. The average mean distances for these interactions are N1H-O1 = 2.068(6) Å and N2H-O2 = 1.992(3) Å.

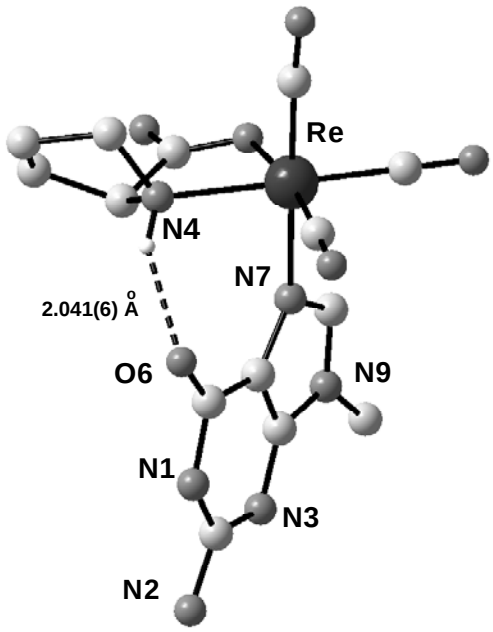

Figure 2.7. Crystal structure of [Re(Pro)(9-MeG)$(CO)_3$] (**15**). Selected bond distances (Å) and angles (deg) are the following: Re-O1 2.163(4), Re-N7 2.208(4), Re-N4 2.216(4); O1-Re-N7 81.58(15), O1-Re-N4 75.95(15), N7-Re-N4 83.29(15).

The second proton of the $N2H_2$ group forms one of three unique hydrogen bonds: either with the carboxylic oxygen O2 of an adjacent complex (Figure 2.8A, on average N2H'-O2 = 2.064(4) Å), or with N3 (Figure 2.8B, on average N2H'-N3 = 2.116(3) Å) or finally with the oxygen of a solvent

methanol molecule (on average N2H'-$OHCH_3$ = 2.170(7) Å). The geometry is octahedral with all bond distances and angles falling within expected values. Finally, the position of the guanine in the crystal state is stabilized by an intramolecular hydrogen bond (on average 2.041(6) Å) between the proline N4H proton and the carbonyl oxygen O6 of the base.

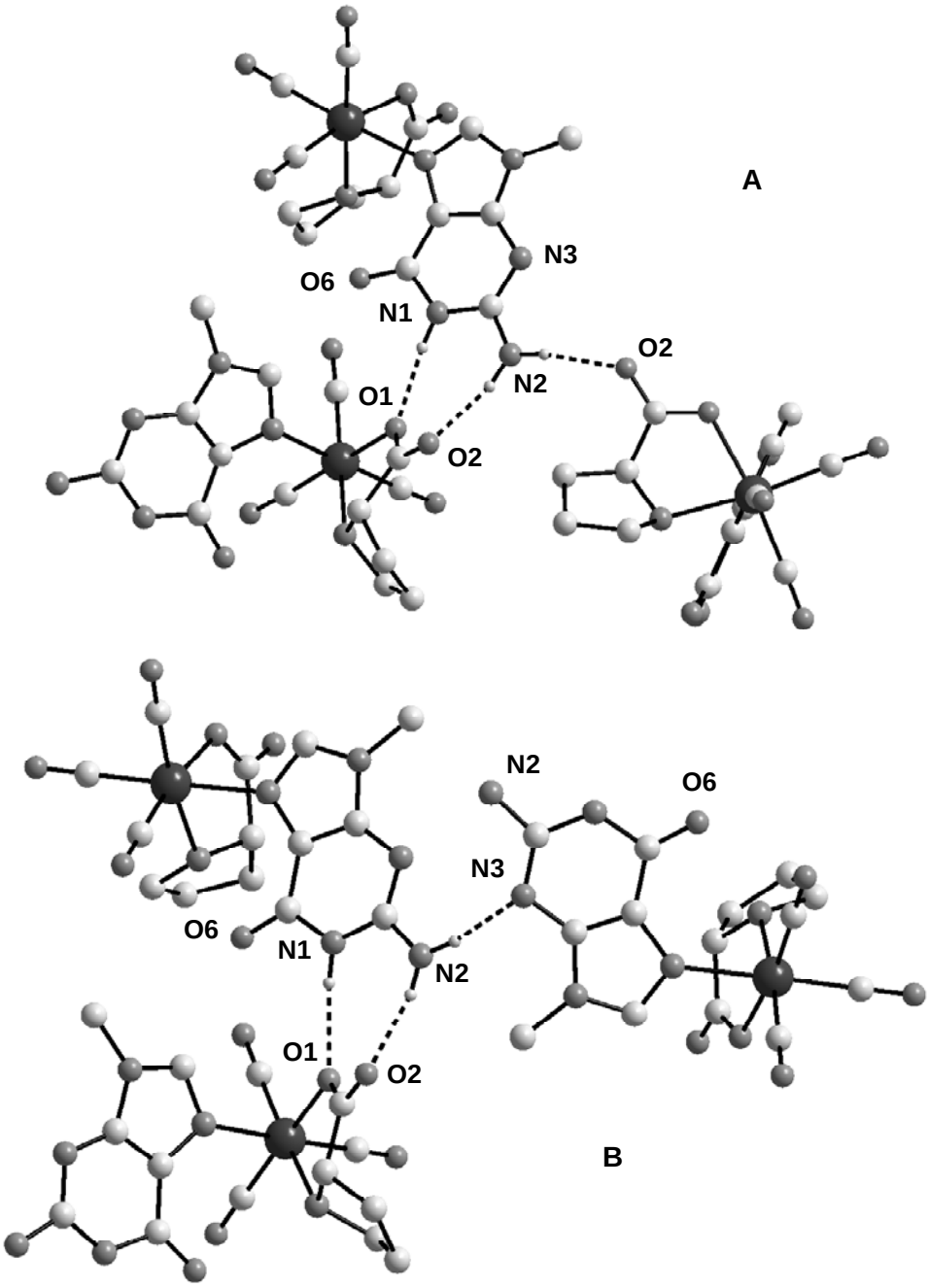

Figure 2.8. Two types of intermolecular hydrogen-bonding interactions in the crystal of **15**. Labels are as in Figure 2.7. Solvent methanol molecules are not shown for clarity.

Conformational Change of ΦX174 DNA Induced by Re^{I} Complex Binding. Gel mobility shift assays demonstrate the conformational changes in macromolecules. The study of metal-DNA binding and of the changes induced by metal complexes on the tertiary structure of DNA by this technique is now well established. Different Pt and Ru complexes, for example, cause unwinding of supercoiled (sc) or winding of open circular (oc) plasmid DNA.[45-58] These structural changes can be observed on the gel matrix. Unwinding of sc plasmid DNA for example causes relaxation of the DNA molecule and, consequently, the frictional force between DNA and the gel matrix during electrophoresis increases. Thus, the band corresponding to the DNA-metal adduct moves relatively slower than the one of native sc DNA. The opposite is true if a metal complex causes winding of oc plasmid DNA. In this case winding of oc DNA renders the molecule more compact, the frictional force is reduced and the band of the corresponding DNA-metal adduct moves relatively faster.

The analysis of the binding and of the influence of compounds shown in Figure 2.1 on the tertiary structure of DNA was determined by their ability to alter the electrophoretic mobility of the open circular and supercoiled form ΦX174 DNA. Figure 2.9A shows the mobility of native ΦX174 plasmid DNA and plasmid DNA (abbreviated as pDNA) incubated with compound **1**. Clearly, increasing the r_b value (r_b = metal/base pair ratio) for the incubation of DNA with **1** induces a gradual increase in mobility of the oc form. Increase in mobility starts at r_b = 0.18 (lane 5) and progresses until at r_b = 18 (lane 7) when a high degree of DNA mobility is reached. At a r_b = 180 (lane 8) the band disappears from the gel.

The same effect is observed when ΦX174 pDNA is incubated with cisplatin. Figure 2.9B shows the mobility of native ΦX174 pDNA and pDNA incubated with compound **1** and cisplatin under the same conditions. The influence on the tertiary structure and mobility of DNA produced by the two compounds is similar although the analogous effect as induced by **1** can be obtained already with a 10 times lower concentration of cisplatin. At r_b = 0.018 (lane 2), in fact, **1** causes no change in the mobility of DNA as indicated by the presence of both the oc and the sc forms of the plasmid as in reference lanes 1 and 8. At r_b = 0.018 (lane 5), however, cisplatin induces a shift similar to the one caused by **1** at r_b = 0.18 (lane 3). The same is true if comparing lanes 4 and 6 where r_b values are 1.8 and 0.18 for **1** and cisplatin respectively. At higher cisplatin concentration (r_b = 1.8, lane 7) the band disappears from the gel as previously noted.[47, 56]

It is well established that Pt binding to pDNA causes winding of the oc form and unwinding of the sc form.[45-55] The same effect is known to occur with other metal ions like Ru when covalent

binding to N7 in G and noncovalent, hydrophobic interactions take place.[53, 56-58] It is therefore likely that the shift in mobility of ΦX174 pDNA caused by Re is due to similar molecular events taking place as with Pt and Ru. Since in almost all our experiments both oc and sc forms are present at the same time, binding of Re to DNA results in a concerted unwinding of the sc form together with winding of the oc form. These events result in an equilibrium tertiary DNA structure which is revealed by a single band on the gel.

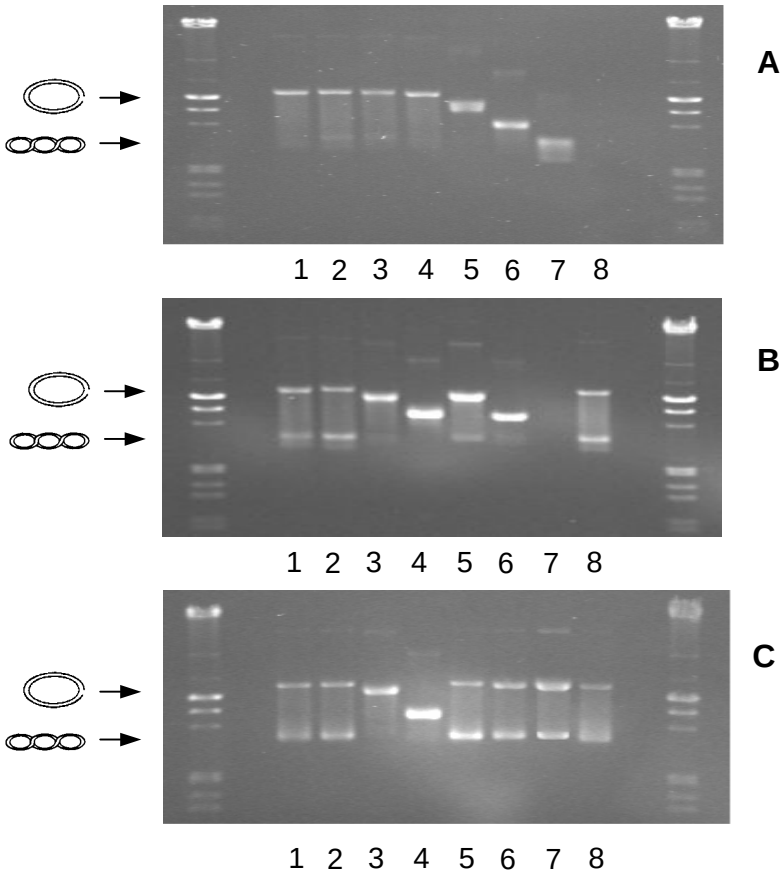

Figure 2.9. (A) Electrophoresis in 0.75% agarose gel of ΦX174 DNA (5 nM, batch 1) incubated with various concentrations of **1**. Lane 1 reference ΦX174 DNA. Lanes 2 to 7 ΦX174 DNA plus **1**. r_b levels for lanes 2-8: (2) 0.00018; (3) 0.0018; (4) 0.018; (5) 0.18; (6) 1.8; (7) 18; (8) 180. (B) Electrophoresis in 0.75% agarose gel of ΦX174 DNA (5 nM, batch 2) incubated with various concentrations of **1** (lanes 2-4) and cisplatin (lanes 5-7). Lanes 1 and 8 reference ΦX174 DNA. r_b levels for lanes 2-7: (2, 5) 0.018; (3, 6) 0.18; (4, 7) 1.8. (C) Electrophoresis in 0.75% agarose gel of ΦX174 DNA (5 nM, batch 2) incubated with various concentrations of **1** (lanes 2-4) and **19** (lanes 5-7). Lanes 1 and 8 reference ΦX174 DNA. r_b levels for lanes 2-7: (2, 5) 0.018; (3, 6) 0.18; (4, 7) 1.8.

In order to evaluate whether these changes are due to electrostatic rather than to a covalent interaction, ΦX174 pDNA was incubated with **1** and **19** ($[Re(Im)_3(CO)_3]^+$, Figure 2.1) under the same conditions (Figure 2.9C). The high kinetic stability of complex **19**[32] rules out possible ligand exchange and inner sphere coordination to DNA. Any eventually observed change of the tertiary structure of the plasmid can therefore not be attributed to coordination to one of the nucleobases. However, while **1** induced the shift in mobility (lanes 2-4), complex **19** has no effect at all (lanes 5-7, see Figure 2.9C) indicating that metal binding to DNA is responsible for the observed changes rather than simple electrostatic interactions.

The question now arises whether the structural changes induced by compound **1** are due to the binding of $[Re(CO)_3]^+$ to one or two DNA bases. To answer this question **1**, **10**, **13**, and **18** (Figure 2.1) were subjected to the same study and incubated with pDNA. Compounds **1** and **10** have two coordination sites allowing the formation of *cis*-bis adducts of guanine, whereas **13** has only one such site as demonstrated with compound **15** and is therefore not able to form *cis*-bis intra- or interstrand adducts with the purine bases. Compound **18**, finally, is inert towards ligand substitution[31] and it has no available coordination sites. Figure 2.10 shows the mobility of ΦX174 pDNA with and without incubation with compound **1**, **10**, **13**, and **18** under the same conditions. As expected complex **1** (lanes 2-4) and complex **10** (lanes 5-7) induce the increase in mobility of plasmid DNA while complexes **13** (lanes 8-10) and **18** (lanes 1-13) do not. These results imply that two available coordination sites are necessary to induce the DNA shift in mobility. Consequently the shift in mobility is most likely due to binding of the $[Re(CO)_3]^+$ core to two DNA bases.

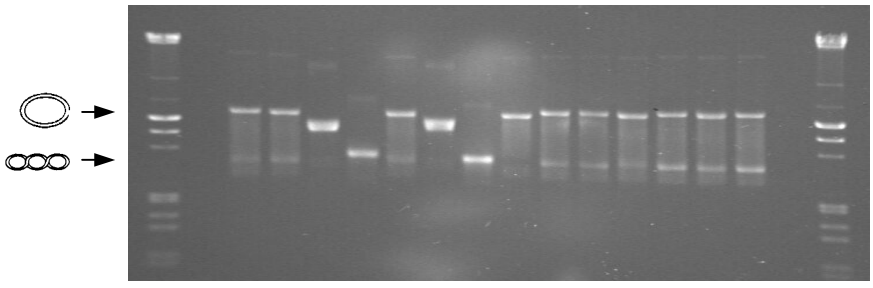

Figure 2.10. Electrophoresis in 0.75% agarose gel of ΦX174 DNA (5 nM, batch 2) incubated with various concentrations of **1** (lanes 2-4), **10** (lanes 5-7), **13** (lanes 8-10), **18** (lanes 11-13). Lanes 1 and 14 reference ΦX174 DNA. r_b levels for lanes 2-13: (2, 5, 8, 11) 0.018; (3, 6, 9, 12) 0.18; (4, 7, 10, 13) 1.8.

Furthermore, when analyzing the binding and the influence of compounds **14** on the tertiary structure of ΦX174 DNA effects analogous to those induced by **1** and **10** were observed (Figure 2.11). As discussed before (Figure 2.2) the reaction of **14** with excess 9-MeG establishes an equilibrium with species **10** and **10a**, indicating that DMGly is displaced from the rhenium coordination sphere in favor of the base (see Figure 2.2). The shift in mobility induced by **14** is visible at r_b values of 0.13 (lane 7), 0.36 (lane 9), 3.6 (lane 10), 0.54 (lane 12) and 5.4 (lane 13). These results further suggest that the shift in mobility of ΦX174 pDNA is due to binding of rhenium to two DNA bases following, in this case, displacement of DMGly.

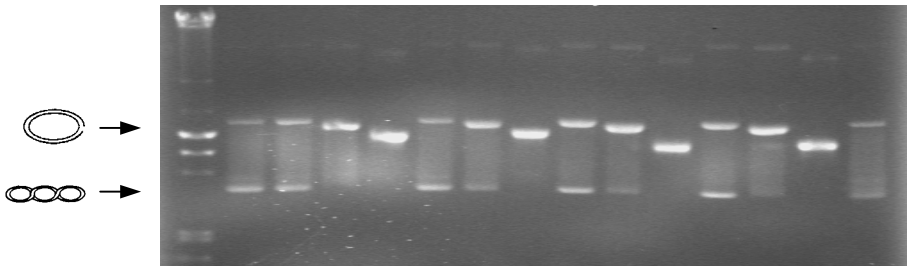

Figure 2.11. Electrophoresis in 0.75% agarose gel of ΦX174 DNA (5 nM, batch 2) incubated with various concentrations of **1** (lanes 2-4) and **14** (lanes 5-13). Lanes 1 and 14 reference ΦX174 DNA. r_b levels for lanes 2-13: (2, 5) 0.013; (3, 6) 0.13; (4, 7) 1.3; (8) 0.036; (9) 0.36; (10) 3.6; (11) 0.054; (12) 0.54; (13) 5.4.

The interaction of Re with DNA may also involve binding to the phosphate backbone. However, Re binding to the bases is most likely the molecular event. Interaction between Re and phosphate oxygen of phosphate containing model ligands has never been observed in our studies. Since two available coordination sites on the metal are the prerequisite to induce changes in the tertiary structure of plasmid DNA, bidentate binding to the phosphate backbone would give rise to a rather strained four-member ring not obviously affecting the tertiary structure, while interaction with the bases can be easily rationalized on the base of our previous results.

The stability of the Re-DNA adduct is an important factor for using such Re-complexes as DNA binding agents in cancer therapy. One principal hypothesis, originally advanced by Lippard to explain the activity of cisplatin, suggests that the HH form in the intrastrand lesion is recognized by

a damage recognition protein whose binding prevents DNA repair. The cisplatin adduct persists then long enough to activate apoptosis.[59] If this hypothesis is correct, a relatively stable Re-DNA adduct is required to activate the same cellular response.

Figure 2.12A shows the mobility of native ΦX174 pDNA incubated with compound **1** and compound **16** while Figure 2.12B shows the same samples after a further 22h incubation period in the presence of 6 eq. of histidine. As expected, compound **16** induces the same mobility shift of DNA as **1** (Figure 2.12A). When the adducts thus formed are challenged with histidine (Figure 2.12B) no appreciable changes in lanes 2, 3 (r_b = 0.018 and 0.18, compound **1**), 5 and 6 (r_b = 0.018 and 0.18, compound **16**) was found. Lanes 4 and 7 (r_b = 1.8, compound **1** and **16** respectively) however, show a remarkable decrease in mobility when compared to the same lanes in Figure 2.12A. This effect is most likely due to trapping of unspecifically bound Re (e.g. weakly bound to adenine). The Re-DNA adduct formed, however, is clearly stable.

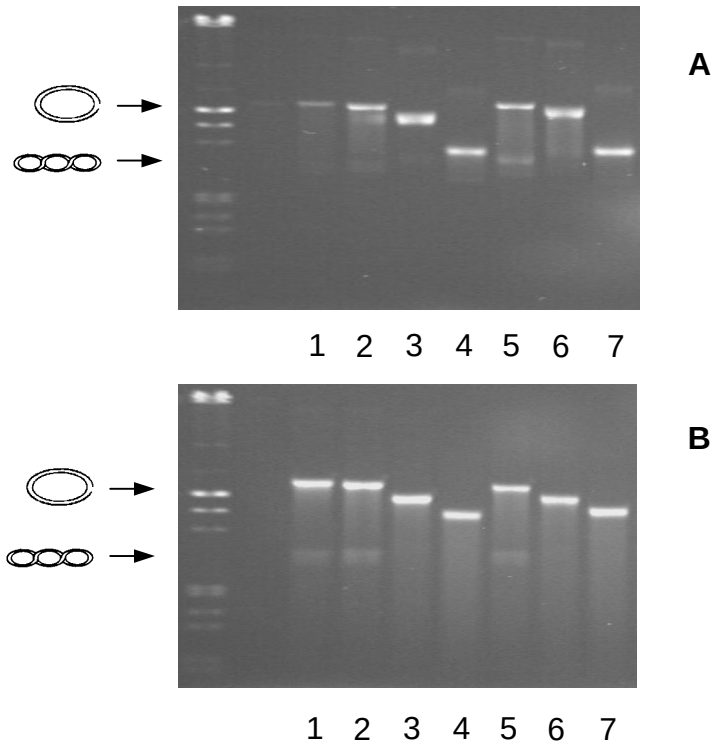

Figure 2.12. (A) Electrophoresis in 0.75% agarose gel of ΦX174 DNA (5 nM, batch 1) incubated with various concentrations of **1** (lanes 2-4) and **16** (lanes 5-7). (B) Electrophoresis in 0.75% agarose gel of same solutions of (A) challenged with histidine for 22 h. Lane 1 reference ΦX174 DNA. r_b levels for lanes 2-7: (2, 5) 0.018; (3, 6) 0.18; (4, 7) 1.8.

2.2 Conclusion

It was shown in this chapter that the $[Re(CO)_3]^+$ moiety displays a principally similar reactivity pattern with pDNA as e.g. cisplatin. It binds selectively to two free guanines, implying a possible interaction with adjacent guanines in DNA as well. To protect the Re center in plasma from unwanted coordination (trapping) to serum proteins coligands such as proline or N,N-dimethylglycine were used yielding Re complexes in the form of pro-drugs. DMGly in particular can be replaced by coordination to N7 of guanine. The complexes with proline are too stable in this respect but both complexes do not cross react with human serum.

If the coligands are labile enough the corresponding complexes such as $[Re(DMGly)(CO)_3]_3$ influence the tertiary structure of ΦX174 DNA by altering the electrophoretic mobility of the open circular and the supercoiled form of plasmid DNA. The induced changes involve most likely covalent binding to two bases as found for cisplatin. Although less potent, the presented model complexes depict the in vitro reactivity characteristics as required for therapeutic agents. They might therefore serve as future inorganic medicinal drugs provided that they are able to accumulate to a sufficient extent in the cell and in the nucleus in particular. Cell uptake and cytotoxicity studies will be presented in chapter 5.

2.3 References

(1) Sava, G.; Gagliardi, R.; Bergamo, A.; Alessio, E.; Mestroni, G. *Anticancer Res.* **1999**, *19*, 969-972.

(2) Barton, J. K.; Lolis, E.; *J. Am. Chem. Soc.* **1985**, *107*, 708-709.

(3) Grover, N.; Gupta, N.; Thorp, H. H. *J. Am. Chem. Soc.* **1992**, *114*, 3390-3393.

(4) Frasca, D.; Ciampa, J.; Emerson, J.; Umans, R. S.; Clarke, M. J. *Met.-Based Drugs* **1996**, *3*, 197-209.

(5) Clarke, M. J.; Jansen, B.; Marx, K. A.; Kruger, R. *Inorg. Chim. Acta* **1986**, *124*, 13-28.

(6) McNamara, M.; Clarke, M. J. *Inorg. Chim. Acta* **1992**, *195*, 175-185.

(7) Novakova, O.; Kasparkova, J.; Vrana, O.; van Vliet, P.; M. Reedijk, J.; Brabec, V. *Biochem.* **1995**, *34*, 12369-12378.

(8) van Vliet, P. M.; Toekimin, S. M. S.; Haasnoot, J. G.; Reedijk, J.; Novakova, O.; Vrana, O.; Brabec, V. *Inorg. Chim Acta* **1995**, *231*, 57-64.

(9) Pacor, S.; Sava, G.; Ceschia, V.; Bregant, F.; Mestroni, G.; Alessio, E. *Chem. Biol. Interact.* **1991**, *78*, 223-234.

(10) Cauci, S.; Viglino, P.; Esposito, G.; Quadrifoglio, F. *J. Inorg. Biochem.* **1991**, *43*, 739-751.

(11) Esposito, G.; Cauci, S.; Fogolari, F.; Alessio, E.; Scocchi, M.; Quadrifoglio, F.; Viglino, P. *Biochem.* **1992**, *31*, 7094-7103.

(12) Loseto, F.; Alessio, E.; Mestroni, G.; Lacidogna, G.; Nassi, A.; Giordano, D.; Cosuccia, M. *Anticancer Res.* **1991**, *11*, 1549-1553.

(13) Hotze, A. C. G.; Broekhuisen, M. E. T.; Velders, A. H.; van der Schilden, K.; Haasnoot, J. G.; Reedijk, J. *Eur. J. Inorg. Chem.* **2002**, 369-376.

(14) Hotze, A. C. G.; Bacac, M.; Velders, A. H.; Jansen, B. A. J.; Kooijman, H. Spek, A. L.; Haasnoot, J. G.; Reedijk, J. *J. Med. Chem.* **2003**, *46*, 1743-1750.

(15) Hotze, A. C. G.; Velders, A. H.; Ugozzoli, F.; Biagini-Cingi, M.; Manotti-Lanfredi, A. M.; Haasnoot, J. G.; Reedijk, J. *Inorg. Chem.* **2000**, *39*, 3838-3844.

(16) Chen, H. M.; Parkinson, J. A.; Parsons, S.; Coxall, R. A.; Gould, R. O.; Sadler, P. J. *J. Am. Chem. Soc.* **2002**, *124*, 3064-3082.

(17) Chen, H. M.; Parkinson, J. A.; Morris, R. E.; Sadler, P. J. *J. Am. Chem. Soc.* **2003**, *125*, 173-186.

(18) Novakova, O.; Chen, H. M.; Vrana, O.; Rodger, A.; Sadler, P. J.; Brabec, V. *Biochem.* **2003**, *42*, 11544-11554.

(19) Morris, R. E.; Aird, R. E.; Murdoch, P. D.; Chen, H. M.; Cummings, J.; Hughes, N. D.; Parsons, S.; Parkin, A.; Boyd, G.; Jodrell, D. I.; Sadler, P. J. *J. Med. Chem.* **2001**, *44*, 3616-3621.

(20) Bear, J. L.; Yao, C. L.; Liu, L. M.; Capdevielle, F. J.; Korp, J. D.; Albright, T. A.; Kang, S. K.; Kadish, K. M. *Inorg. Chem.* **1989**, *28*, 1254-1262.

(21) Rubin, J. R.; Haromy, T. P.; Sundaralingam, M.; *Acta Cryst. Sect. C* **1991**, *47*, 1712-1714.

(22) Crawford, C. A.; Day, E. F.; Saharan, V. P.; Folting, K.; Huffman, J. C.; Dunbar, K. R.; Christou, G. *Chem. Commun.* **1996**, 1113-1114.

(23) Chifotides, H. T.; Koshlap, K. M.; Perez, L. M.; Dunbar, K. R. *J. Am. Chem. Soc.* **2003**, *125*, 10703-10713.

(24) Chifotides, H. T.; Koshlap, K. M.; Perez, L. M.; Dunbar, K. R. *J. Am. Chem. Soc.* **2003**, *125*, 10714-10724.

(25) Yan, Y. K.; Cho, S. E.; Shaffer, K. A.; Rowell, J. E.; Barnes, B. J.; Hall, I. H. *Pharmazie* **2000**, *55*, 307-313.

(26) Wang, W. W.; Yan, Y. K.; Hor, T. S. A.; Vittal, J. J.; Wheaton, J. R.; Hall, I. H. *Polyhedron* **2002**, *21*, 1991-1999.

(27) Zhang, J. Y.; Vittal, J. J.; Henderson, W.; Wheaton, J. R.; Hall, I. H.; Hor, T. S. A.; Yan, Y. K. *J. Organomet. Chem.* **2002**, *650*, 123-132.

(28) Zobi, F.; Spingler, B.; Fox, T.; Alberto, R. *Inorg. Chem.* **2003**, *42*, 2818-2820.

(29) Zobi, F.; Blacque, O.; Schmalle, H. W.; Spingler, B.; Alberto, R. *Inorg. Chem.* **2004**, *43*, 2087-2096.

(30) Alberto, R.; Egli, A.; Abram, U.; Hegetschweiler, K.; Gramlich, V.; Schubiger P. A., *J. Chem. Soc. Dalton Trans.* **1994**, 2815-2820.

(31) Schibli, R.; La Bella, R.; Alberto, R.; Garcia-Garayoa, E.; Ortner, K.; Abram, U.; Schubiger, P. A. *Bioconjugate Chem.* **2000**, *11*, 345-351.

(32) Alberto, R.; Schibli, R.; Waibel, R.; Abram, U.; Schubiger, A. P. *Coord. Chem. Rev.* **1999**, *192*, 901-919.

(33) CELL, *2.87 5*, **1998** ed.; STOE & Cie, GmbH: Darmstadt, Germany, **1998**.

(34) G. M. Sheldrick, *Acta Cryst. Sect. A* **1990**, *46*, 467-473

(35) A. Altomare, M. C. Burla, M. Camalli, G. L. Cascarano, C. Giacovazzo, A. Guagliardi, A. G. G. Moliterni, G. Polidori, R. Spagna, *J. Appl. Cryst.* **1999**, *32*, 115-119.

(36) G. M. Sheldrick, *SHELX-97*; University of Göttigen: Göttigen, Germany, **1997**

(37) Behrens, H.; Passler, P. *Zeit. Anorg. Allg. Chemie* **1969**, *365*, 128-136.

(38) Kramer, R.; Maurus, M.; Bergs, R.; Polborn, K.; Sunkel, K.; Wagner, B.; Beck, W. *Chem. Ber.-Recueil* **1993**, *126*, 1969-1980.

(39) Severin, K.; Bergs, R.; Beck, W. *Angew. Chem. Internat. Ed.* **1998**, *37*, 1635-1654.

(40) Beck, W.; Severin, K.; *Chem. Uns. Zeit* **2002**, *36*, 356-365.

(41) Carmona, D.; Lamata, M. P.; Oro, L. A. *Eur. J. Inorg. Chem.* **2002**, 2239-2251.

(42) Lindner, E.; Trad, S.; Hoehne, S. *Chem. Ber.* **1980**, *113*, 639-649.

(43) Piotrowski, H.; Polborn, K.; Hilt, G.; Severin, K. *J. Am. Chem. Soc.* **2001**, *123*, 2699-2700.

(44) Grote, Z.; Lehaire, M. L.; Scopelliti, R.; Severin, K. *J. Am. Chem. Soc.* **2003**, *125*, 13638-13639.

(45) Cohen, G. L.; Ledner, J. A.; Bauer, W. R.; Ushay, H. M.; Caravana, C.; Lippard, S. J. *J. Am. Chem. Soc.* **1980**, *102*, 2487-2488.

(46) Howegrant, M.; Wu, K. C.; Bauer, W. R.; Lippard, S. J. *Biochem.* **1976**, *15*, 4339-4346.

(47) Bauer, W. R.; Gonias, S. L.; Kam, S. K.; Wu, K. C.; Lippard, S. J. *Biochem.* **1978**, *17*, 1060-1068.

(48) Ushay, H. M.; Tullius, T. D.; Lippard, S. J. *Biochem.* **1981**, *20*, 3744-3748.

(49) Herman, T. S.; Teicher, B. A.; Chan, V.; Collins, L. S.; Kaufmann, M. E.; Loh, C. *Cancer Res.* **1988**, *48*, 2335-2341.

(50) Keck, M. V.; Lippard, S. J. *J. Am. Chem. Soc.* **1992**, *114*, 3386-3390.

(51) Navarroranninger, C.; Lopezsolera, I.; Perez, J. M.; Rodriguez, J.; Garciaruano, J. L.; Raithby, P. R.; Masaguer, J. R.; Alonso, C. *J. Med. Chem.* **1993**, *36*, 3795-3801.

(52) NavarroRanninger, C.; LopezSolera, I.; Gonzalez, V. M.; Perez, J. M.; AlvarezValdes, A.; Martin, A.; Raithby, P. R.; Masaguer, J. R.; Alonso, C. *Inorg. Chem.* **1996**, *35*, 5181-5187.

(53) Milkevitch, M.; Storrie, H.; Brauns, E.; Brewer, K. J.; Shirley, B. W. *Inorg. Chem.* **1997**, *36*, 4534-4538.

(54) Buning, H.; Altman, J.; Beck, W.; Zorbas, H. *Biochem.* **1997**, *36*, 11408-11418.

(55) Perez, J. M.; Lopez-Solera, I.; Montero, E. I.; Brana, M. F.; Alonso, C.; Robinson, S. P.; Navarro-Ranninger, C. *J. Med. Chem.* **1999**, *42*, 5482-5486.

(56) Chan, H. L.; Liu, H. C.; Tzeng, B. L. C.; You, Y. S. Y.; Peng, S. M.; Yang, M. S.; Che, C. M. *Inorg. Chem.* **2002**, *41*, 3161-3171.

(57) Williams, R. L.; Toft, H. N.; Winkel, B.; Brewer, K. J. *Inorg. Chem.* **2003**, *42*, 4394-4400.

(58) Novakova, O.; Chen, H. M.; Vrana, O.; Rodger, A.; Sadler, P. J.; Brabec, V. *Biochem.* **2003**, *42*, 11544-11554.

(59) Pil, P. M.; Lippard, S. J. *Science* **1992**, *256*, 234-237.

(60) Arion, V. B.; Reisner, E.; Fremuth, M.; Jakupec, M. A.; Keppler, B. K.; Kukushkin, V. Y.; Pombeiro, A. J. L.*Inorg. Chem.* **2003**, *42*, 6024-6031.

Chapter 3. Interaction of $[Re(H_2O)_3(CO)_3]^+$ Complex (1) with d(GpG) and d(CpGpG)

NMR and X-ray investigations have been carried out in the last twenty years to elucidate the structural feature of the interaction of the anticancer drug cisplatin with DNA bases. Bifunctional binding to purines determines the loss of stacking in coordinated bases and leads to bending of the double helix associated to some extent with unwinding. These DNA modifications contribute to a cascade of events, including transcription inhibition and repair shielding of cisplatin-DNA cross-links which ultimately result in cell death.[1-3]

Insights into the nature of the GpG platinum adducts emerged from the X-ray structure determination of $(NH_3)_2Pt\{d(pGpG)\}$ (see Figure 3.1) followed by those of longer oligonucleotides.[4-9] To our knowledge this structure remains to date the only structure of a metal fragment bound to GG. For other transition metals of interest in cancer therapy, among which Ru and Rh play a predominant role, the structure of the d(GpG) adducts has been determined only in solution via NMR studies.

Cauci and coworkers have demonstrated that the antitumor octahedral *trans*-$RuCl_2(DMSO)_4$ complex forms with d(GpG) a stable compound characterized by covalent bifunctional binding to N7.[10] Via NMR and molecular modeling studies they showed that the guanine bases in the Ru-d(GpG) adduct are in a head-to-head (HH) orientation. Their model shows structural features similar to the those exhibited by the corresponding platinum adduct demonstrating that such a way of interacting with DNA is not exclusive to Pt or to metals with square planar geometry, as originally suggested by Lippard, but might be a common feature of transition metals with two available *cis* position for covalent binding.[10]

More recently, Chifotides, Dunbar and coworkers have presented a binding study of the d(pGpG) fragment with antitumor tetrakis(μ-carboxylato)dirhodium(II,II) compounds.[11-13] They have shown that the interaction of the dirhodium units with d(pGpG) yields an adduct in which both metal-metal bonded rhodium centers are capable of engaging in *cis* binding to GG intrastrand sites by establishing *N7/O6* bridges that span the Rh-Rh bond. In their model the guanine residues are also found in a left-handed HH arrangement.

In solution *cis*-$[Pt(NH_3)_2\{d(GpG)\}]$, the simplest cross-link model, has only one set of ^1H NMR signals. This observation has been taken to imply that this cross-link model favours the HH

conformer, which undergoes slow Pt-N7 bond rotation. The phosphate backbone of the dinucleotide is thought to stabilize an HH arrangement, thereby rendering an HT form less favourable. By using the so called "retro models", Marzilli, Natile and their coworkers have later demonstrated that at least four different conformers of comparable stability exist of *cis*-$[Pt(N_2)_2\{d(GpG)\}]$ (where N = derivatized amine), three HH conformers and one HT adduct.[14-24]

In the previous chapters it was demonstrated that the *fac*-$[Re(CO)_3]^+$ core binds two guanine bases yielding reasonably stable complexes. It was shown that the guanine ligands can assume both a HH and a HT conformation around the metal center and that the two bases can freely rotate about the Re-N7 bond. It was also shown that the $[Re(CO)_3]^+$ moiety displays a principally similar reactivity pattern with plasmid DNA as e.g. cisplatin implying a possible interaction with adjacent guanines in DNA as well.

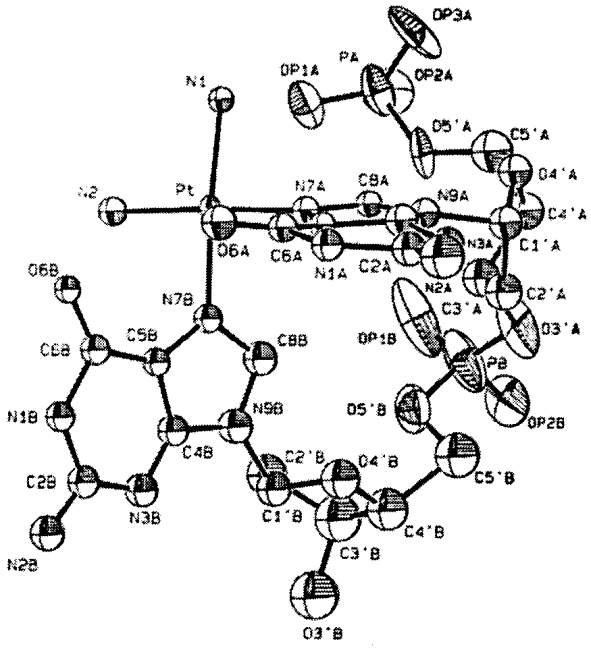

Figure 3.1. Molecular structure of *cis*-$[Pt(NH_3)_2\{d(pGpG)\}]$.[5]

In this chapter the interaction of **1** with d(GpG) and d(CpGpG) is described. The reactions of **1** with these DNA fragments, studied in solution via NMR and other spectroscopic methods, yield stable adducts in which the metal center binds to the guanine residues via N7. In the case where the DNA fragment is d(GpG), two major products form in the reaction with **1**. These are assigned to a HH and a HT species based on NMR evidence and ring current shift calculations. On the other hand, a single major product is found in the reaction of **1** with d(CpGpG).

3.1 Results and Discussion

Interaction of 1 with d(GpG). The reaction of **1** with 1 eq. of d(GpG) in D_2O was monitored by ^1H NMR spectroscopy. At 37 ^oC the addition of **1** to a solution of d(GpG) causes the immediate appearance in the spectrum of six peaks in the 8.5-8.7 ppm region. With time the resonances due to the H8 signals of free d(GpG) decrease in intensity, two new sets of sharp well separated peaks of the non equivalent H8 protons appear between 7.7 and 8.2 ppm while the original peaks in the 8.5-8.7 ppm region remain relatively constant with respect to the total H8 signal intensity. Figure 3.1 shows the aromatic region (7.7-8.7 ppm) at the end of the reaction of **1** with d(GpG) (≈ 18h incubation).

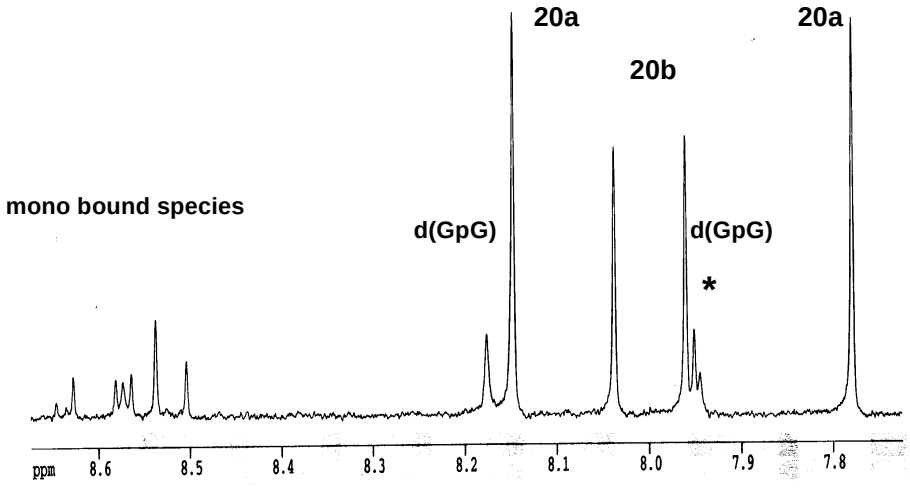

Figure 3.1. ^1H NMR spectrum (D_2O, 37 ^oC, 7.7-8.7 ppm) obtained after ≈ 18h incubation of **1** with 1eq d(GpG). The star indicates an unreactive impurity present in the sample.

The peaks in the 8.5-8.7 ppm are assigned to mono bound Re-d(GpG) species. In Chapter 1 it was shown that in mono bound species of the type $[Re(B)(H_2O)_2(CO)_3]^+$ (where B = 9/7-MeG, G or 2dG) the H8 signal is shifted downfield by about 0.55 ppm with respect to the free base. This occurs because binding by N7 to Re^I leads to donation of electron density from the base imidazole ring to the metal. This interaction makes the H8 proton, already electron deficient and bearing a partial positive charge, even more positive (i.e. electron deficient) causing a downfield shift of the resonance associated with the proton. Coordination of a second nucleoside to $[Re(B)(H_2O)_2(CO)_3]^+$, however, results in a relative upfield shift of the same resonance. This is most likely due to ring current effects of the nucleobases which shield to some extent the proton from the external magnetic field of the probe.

The two sets of peaks between 7.7 and 8.2 ppm are consequently assigned to bis bound Re-d(GpG) species (**20a** and **20b**). The two guanine bases bind to Re through N7, a fact corroborated by the pH independence of the H8 resonances at pH values near 2 (Figure 3.2). In fact all chemical shifts of the H8 are unaffected by lowering the pH below 4, contrary to what is expected for a free guanine N7. On the other hand resonances assigned to mono bound Re-d(GpG) species suffer a progressive downfield shift as the pH is lowered below 4.

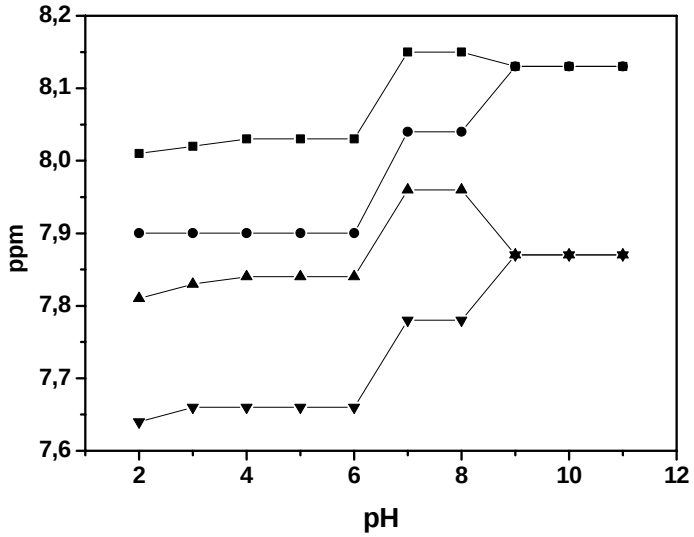

Figure 3.2. pH dependence of the H8 ^{1}H NMR resonances of bis bound Re-d(GpG) adducts.

At alkaline pH (pH > 8) a single set of peaks is observed. CD spectroscopy and MS analysis indicate that at pH > 8, **1** dissociates from d(GpG). The CD profile of a solution of d(GpG) shows minima at 235 and 283 nm and a maximum at 258 nm (Figure 3.3, spectrum a). After the addition of 1 eq. of **1**, in the same profile maxima are detected at 254 and 292 nm with a minimum present at 274 nm (Figure 3.3, spectrum b). The CD spectrum of the alkaline NMR solution described above shows features closely resembling those of free d(GpG).

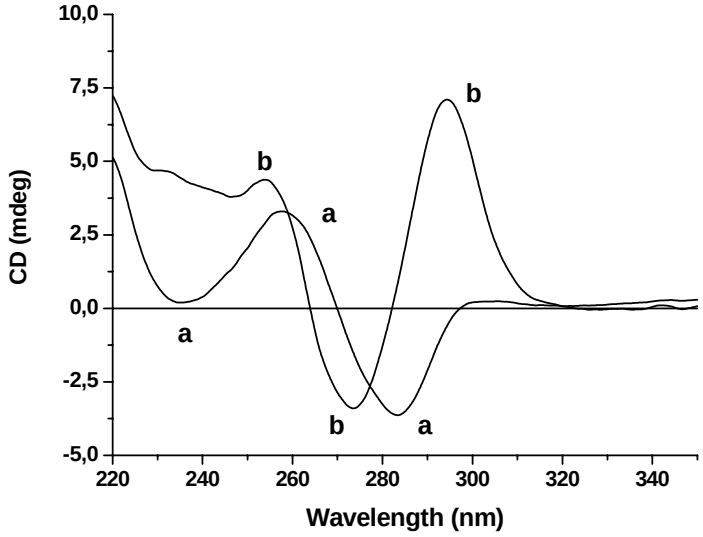

Figure 3.3. CD profile (H_2O, 37 ^oC) of a 0.1 mM solution of d(GpG) (a) and of the same solution after the addition of 1 eq. of **1** (b, 24h incubation).

Furthermore, at pH 7, MS analysis of the products formed in situ in the NMR tube shows a single peak with a clear Re_1 pattern at 866.6 *m/z* corresponding to $[Re(d(GpG))(CO)_3]^+$ (see Figure 3.4). However, when the pH is raised above 8 the peak can no longer be detected. Metal dissociation from d(GpG) at alkaline pH appears to be a unique behaviour of the $[Re(CO)_3]^+$ core as to our knowledge the same has never been described for d(GpG) complexes of Pt, Ru or Rh.

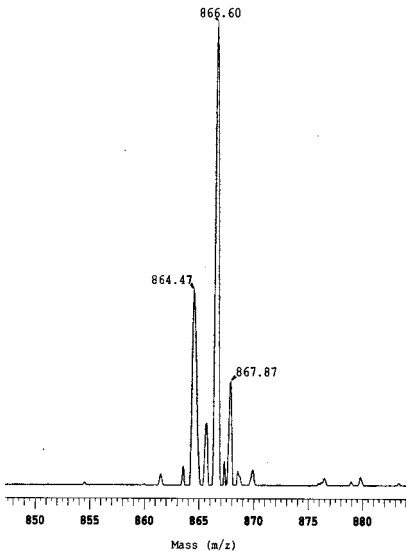

Figure 3.4. MS spectrum (845-888 *m/z*) of a d(GpG) solution incubated (H_2O, 37 ^oC, 12h) with **1**.

Binding of **1** to the guanine residues causes a downfield shift of about 0.3 ppm of the ^{31}P resonances of free d(GpG) (Figure 3.5). Such a downfield shift of the ^{31}P signal with respect to free d(GpG) is common for Pt and Rh metal macrochelates of this DNA fragment.[11-13, 25-27] A down field shift of the main ^{31}P signal in DNA usually indicates an increase in the unwinding angle characterized by changes in the R-O-P-O-R torsion angles.

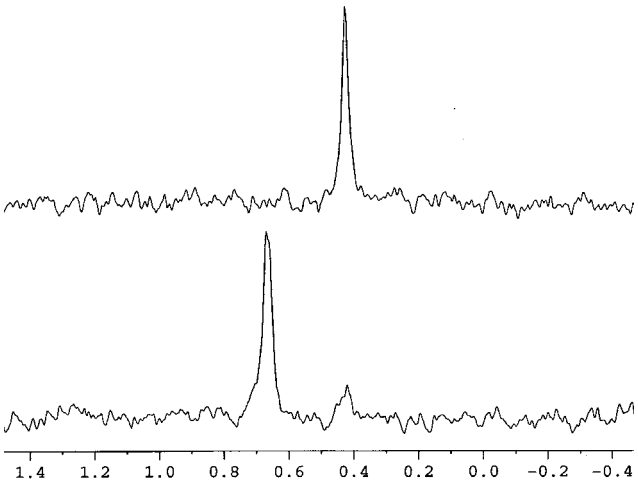

Figure 3.4. ^{31}P NMR spectrum of d(GpG) (top) and of a 1:1 mixture of **1** : d(GpG) incubated in D_2O, 37 ^{o}C, ≈ 18h (bottom).

A strong NOE cross-peak was detected between H8 and H1 of 3'G of **20a**, suggesting a *syn* orientation of 3'G (Figure 3.5). On the other hand, no exchange-NOE signal could be detected between the H8 protons of coordinated guanosines in the **20a** and **20b**. This indicates that the two protons are separated by a distance greater than 3 Å.

Based on these observations a model structure of **20a** was calculated. The structure presented in Figure 3.6 does not represent the exact solution structure of **20a**. Calculation were performed in order to determine the relative orientation of the two bases (i.e. HT vs. HH orientation). The H8-H1 distance of 3'G of **20a** was fixed to 2.8 Å and two different conformations of the molecule were calculated, one in which the two guanine residues were in a HT orientation and the other in which the bases were in a HH orientation. The HH model placed the two H8 protons in close proximity to each other (H8-H8 distance < 3 Å). In this orientation a NOE cross-peak is expected between the two hydrogen atoms in disagreement with the experimental results. In the HT model, on the other hand, the two H8 protons are separated by a distance of 3.9 Å. In this case no exchange-NOE signal

is expected and the relative orientation of the guanine residues in **20a** is assigned to a HT orientation.

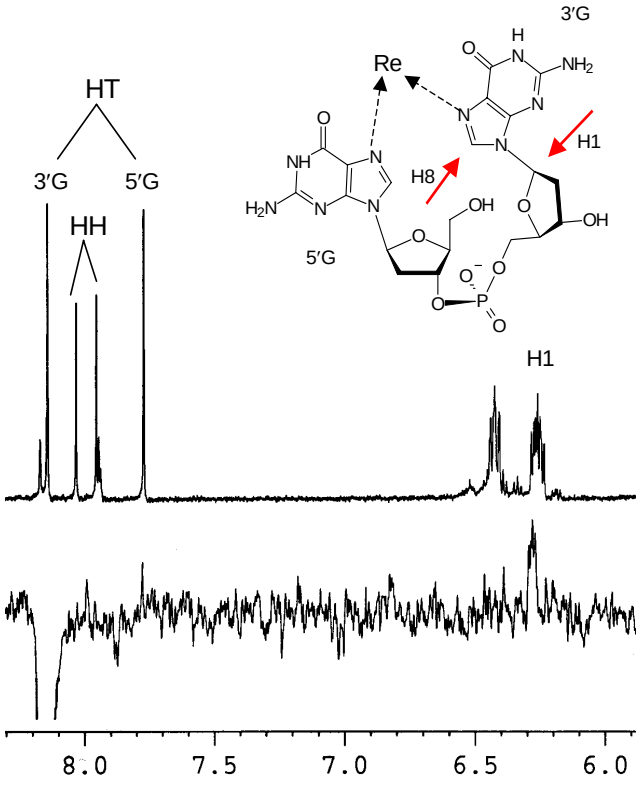

Figure 3.5. Expanded NOESY spectrum (8.3-5.9 ppm) of **1**-d(GpG) adducts. Arrows indicate the protons showing the strong NOE cross-peak.

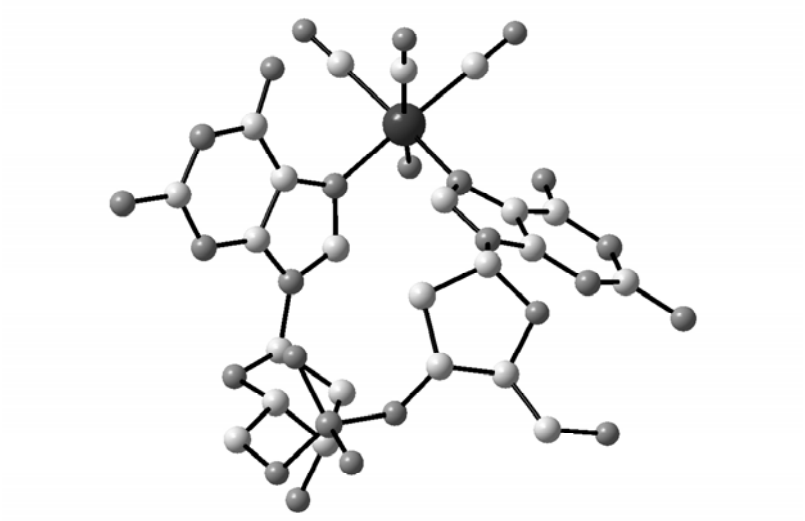

Figure 3.6. MM+ optimized structure of **20a** based on NMR data. The guanine residues are calculated in a HT conformation.

The relative orientation of the ligands in **20a** was further corroborated by ring current shift calculations based on model structure **10HT** and **10HH** (see Chapter 1). In 1977 Abraham and coworkers developed a theoretical model in order to quantify ring current shifts in porphyrin (Ph) and phthalocyanine (Pc) complexes.[28-36] Abraham's model breaks down the porphyrin ring into eight current loops (12 for Pc), each loop with an equivalent dipole placed at its center (Figure 3.7). The magnetic field of each loop is approximated by the equivalent magnetic dipole. The ring current shift at any nucleus H at polar coordinates (r, θ) is obtained by summing the contribution of each equivalent dipole and it is calculated according to Equation 3.1.

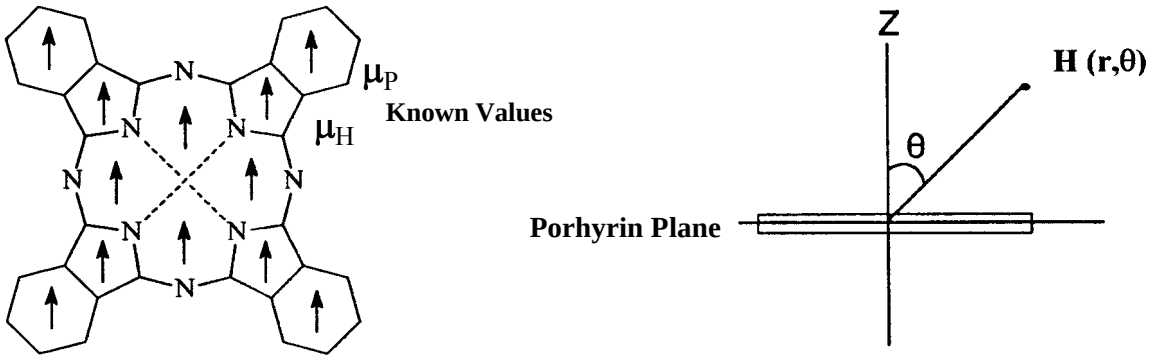

Figure 3.7. The dipole network for Pc (left) and the coordinate axes (right) of Abraham's model.

$$\Delta\delta_H = \sum_{i=1,8}\mu_H (1 - 3 (Z_H \pm 0.64)^2/ r^2_{iH}) / r^3_{iH} + \sum_{j=1,8}\mu_P (1 - 3 (Z_H \pm 0.64)^2/ r^2_{iH}) / r^3_{jH}$$

Equation 3.1. $\Delta\delta_H$ = ppm shift. μ_H and μ_P represent magnetic dipole of pyrrole and benzene rings respectively. $\cos\theta_{iH} = Z_H / r_H$ where r is the distance of H from the dipole μ and θ is the angle that r makes with the z axis.

The μ_H and μ_P were placed at the center of each heterocycle of the guanine ligands in structure **10HT** and **10HH** 0.64 Å above and below the plane of the base as the average position of the π electron cloud as described in the original references. The known pyrrole and benzene dipole values were then assigned to μ_H and μ_P and based on Abraham's equation the average ring current shift that each guanine residue exerts on the H8 proton of the adjacent ligand was calculated. Figure 3.8

shows structures **10HT** and **10HH** and the position of μ_H and μ_P within the ligand system. Table 3.1 summarizes the results of these calculations.

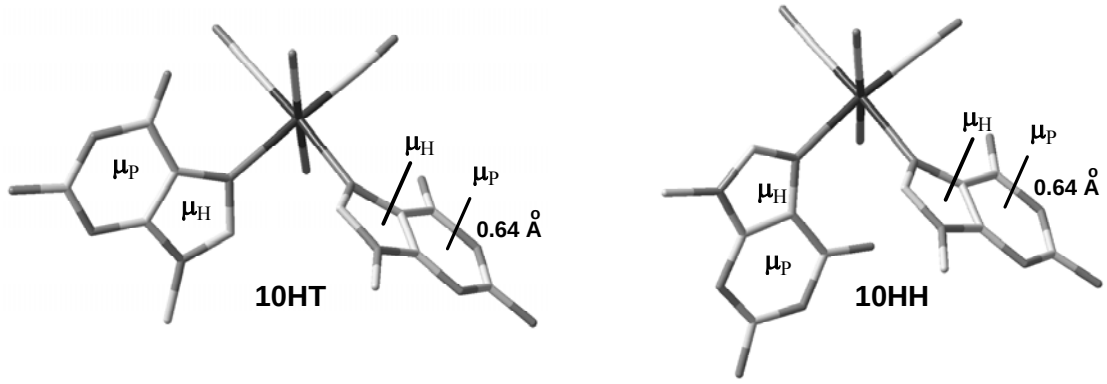

Figure 3.8. Structures **10HT** and **10HH** and the position of μ_H and μ_P within the ligand system.

Table 3.1 Observed and Calculated Δδ (ppm) of 3' and 5'G for **20a** and **20b** with respect to d(GpG).

H8 of base	Observed	Observed	Calculated [a]	Calculated [a]
	20a	**20b**	**10HT**	**10HH**
3'G	-0.03	-0.14	-0.49	-0.83
5'G	-0.18	+0.01	-1.42	+0.32

[a] = Values corrected by +0.55 ppm due to downfield shift caused by Re binding.

Although the calculated values do not exactly agree with the observed values the trend outlined by the calculations is similar to the observed one. One must bear in mind that the calculations are based on rigid crystal structures and that the pyrrole and benzene μ_H and μ_P values certainly do not represent μ values for a guanine base. However, in a HT conformation an upfield shift is predicted for both H8 protons of 3'G and 5'G with H8 5'G shift > H8 3'G shift as observed in the case of **20a**. In a HH orientation an upfield shift is predicted for H8 of 3'G while a downfield shift is expected for H8 of 5'G as observed in the case of **20b**. Based on these considerations **20a** may be assigned as a HT adduct of Re-d(GpG) while **20b** as a HH adduct. These assignments are undoubtedly speculative as a number of different conformations may be suggested. Adducts **20a** and **20b**, for example, might both be HT conformers with the tip of the imidazole ring of 3'G pointing in one case towards a carbonyl ligand and in the other case towards the water molecule *trans* to it. Different HH and HT conformers of d(GpG) bound to a Pt atom are known and they show remarkably different NMR spectra.

The initial approach of **1** to d(GpG) must obviously be monofunctional binding, with metalation occurring either at the 3'G or at the 5'G followed by closure of the macrochelate. The time course of the macrochelate closure (i.e. formation of complexes **20a** and **20b**) in the reaction of **1** with d(GpG) was followed by ^{1}H NMR spectroscopy. Kinetic data reveal that **20a** and **20b** form at the same rate (Figure 3.9). The $t_{½}$'s for the formation of **20a** and **20b** are virtually identical within experimental error and they are about twice the $t_{½}$ value for d(GpG) disappearance. This implies that d(GpG) is consumed twice as fast as **20a** or **20b** are formed, indicating that macrochelate closure is not the rate determining step but a rather fast reaction.

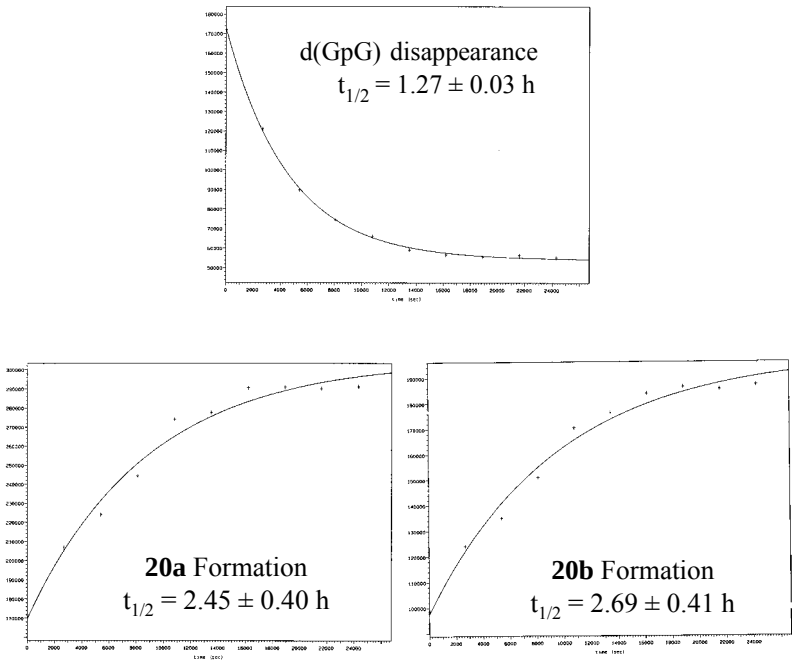

Figure 3.9. The time course of d(GpG) disappearance and formation of complexes **20a** and **20b** in the reaction of **1** with d(GpG) was followed by ^{1}H NMR spectroscopy.

Interaction of 1 with d(CpGpG). The reaction of **1** with 1 eq. of d(CpGpG) in D_2O was also monitored by ^{1}H NMR spectroscopy. As described above for d(GpG), at 37 ^oC the addition of **1** to a solution of d(CpGpG) causes the immediate appearance in the spectrum of four peaks in the 8.4-8.7 ppm region. With time the resonances due to the H8 signals of free d(CpGpG) decrease in intensity, a new set of sharp well separated peaks of the non equivalent H8 protons appear between 7.7 and 8.0 ppm while the original peaks in the 8.5-8.7 ppm region remain relatively constant with respect

to the total H8 signal intensity. Figure 3.10 shows the aromatic region (7.0-9.0 ppm) at the end of the reaction of **1** with d(CpGpG) (1h incubation).

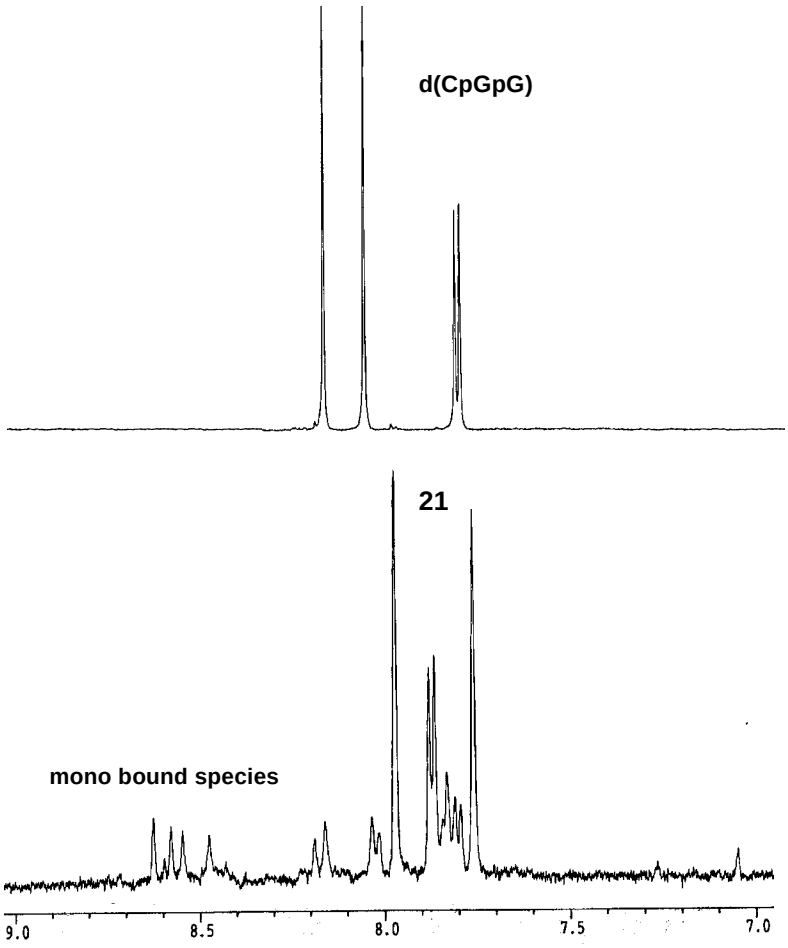

Figure 3.10. ^{1}H NMR spectrum (D_2O, 37 ^{o}C, 7.0-8.0 ppm) of d(CpGpG) (top) and the same sample after 1h incubation with 1eq of **1** (bottom).

In accordance with what has been described in the previous section, the peaks in the 8.4-8.7 ppm are assigned to mono bound Re-d(CpGpG) species. The two peaks of the single major product between 7.7 and 8.0 ppm are consequently assigned to H8 resonances of a bis bound Re-d(CpGpG) species (**21**). While the H8 signals of **21** resonate upfield with respect to free d(CpGpG), the cytosine resonances (the two peaks at 7.6 and 7.7 ppm, top spectrum in Figure 3.10) suffer a downfield shift.

The two guanine bases bind to Re through N7, a fact corroborated by the pH independence of the H8 resonances at pH values near 2 (Figure 3.11). In fact all chemical shifts of the H8 are unaffected by lowering the pH below 4, contrary to what is expected for a free guanine N7. On the other hand resonances assigned to mono bound Re-d(CpGpG) species suffer a progressive downfield shift as the pH is lowered below 4. The cytosine signals also suffer a remarkable downfield shift as the pH is lowered below 6. This suggests that the three most common metal binding sites of N1 blocked cytosine (namely N3, O2 and N4) are not protected by metal coordination and are consequently affected by pH changes. This implies that only the guanine residues are bound to the Re center.

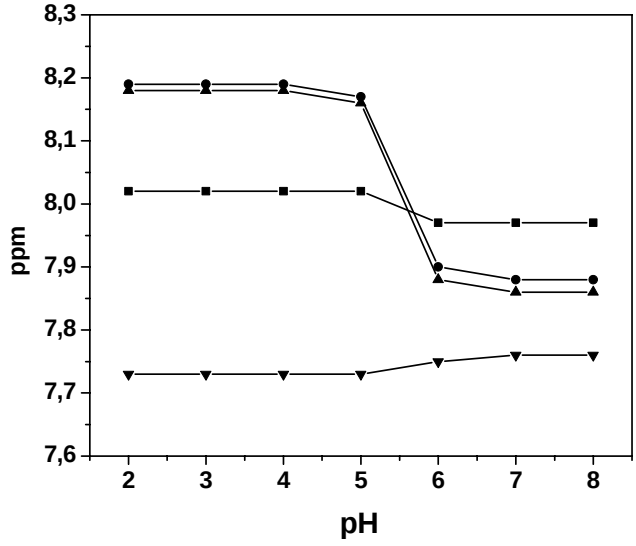

Figure 3.11. pH dependence of the ^{1}H NMR resonances of adduct **21** between 7.6 and 8.3 ppm.

Binding of **1** to d(CpGpG) also causes a downfield shift of the ^{31}P resonances with respect to the free ligand (Figure 3.12). As mentioned above, such a downfield shift of the ^{31}P signal is common for metal macrochelates of similar DNA fragments and it might be indicative of an increase in the unwinding angle characterized by changes in the R-O-P-O-R torsion angles. Since this DNA fragment binds to Re via the guanine residues one might expect that the greater change in the R-O-P-O-R torsion angles concerns the -GpG phosphate while the CpG- phosphate would be relatively less affected. The most downfield signal of the bottom spectrum in Figure 3.12 is therefore assigned to the -GpG phosphate. The other signal, closer to free d(CpGpG) resonances, is assigned to the CpG- phosphate.

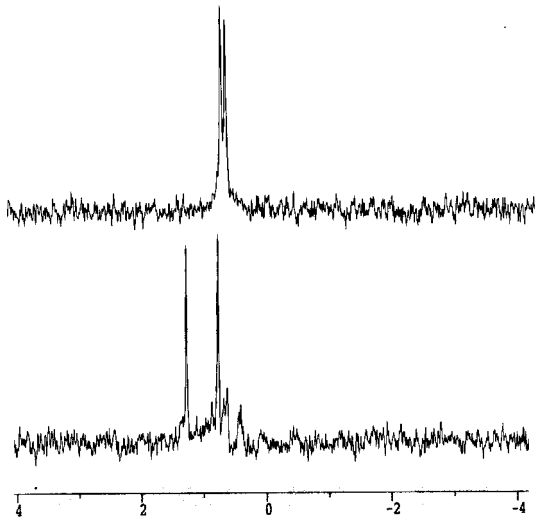

Figure 3.12. ^{31}P NMR spectrum of d(CpGpG) (top) and of a 1:1 mixture of **1** : d(CpGpG) incubated in D_2O, 37 ^{o}C, 1h (bottom).

Addition of **1** to d(CpGpG) alters the CD spectrum of this DNA fragment to a lesser extent than in the case of d(GpG). The CD profile of a solution of d(CpGpG) shows a minimum at 238 and maxima at 259 and 286 nm (Figure 3.13, spectrum a). After the addition of 1 eq. of **1**, in the same profile the minimum shifts to 224 nm while enhanced maxima are detected at 258 and 292 nm (Figure 3.13, spectrum b).

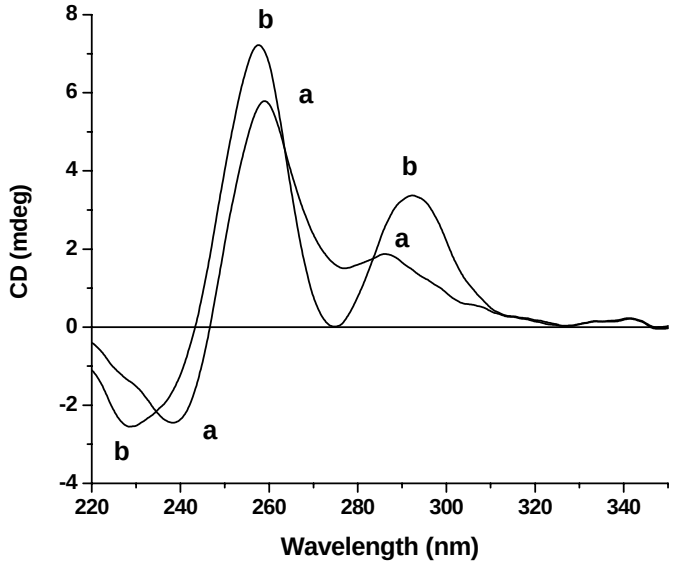

Figure 3.13. CD profile (H_2O, 37 ^{o}C) of a 71 μM solution of d(CpGpG) (a) and of the same solution after the addition of 1 eq. of **1** (b, 24h incubation).

In water, at RT, species **20a**, **20b** and **21** are only slightly soluble. Following the NMR experiments (37 ^{o}C) the complexes precipitate out of solution as white microcrystalline solids as the temperature equilibrates to ambient (~25 ^{o}C). After the reaction of **1** with d(GpG) **20a** and **20b** are obtained as a mixture of products while complex **21** is obtained as a single product with the monobound species and free d(CpGpG) remaining in solution (see Figure 3.10). The IR spectrum of **20a**, **20b** and **21** is shown in Figure 3.14. Both spectra show typical *fac*-[$Re^{I}(CO)_3$] carbonyl vibrations at around 2025 and 1900 cm^{-1} together with vibrations assigned to the olygonucleotide ligands. All attempts to grow single x-ray quality crystals from the isolated solids proved unsuccessful.

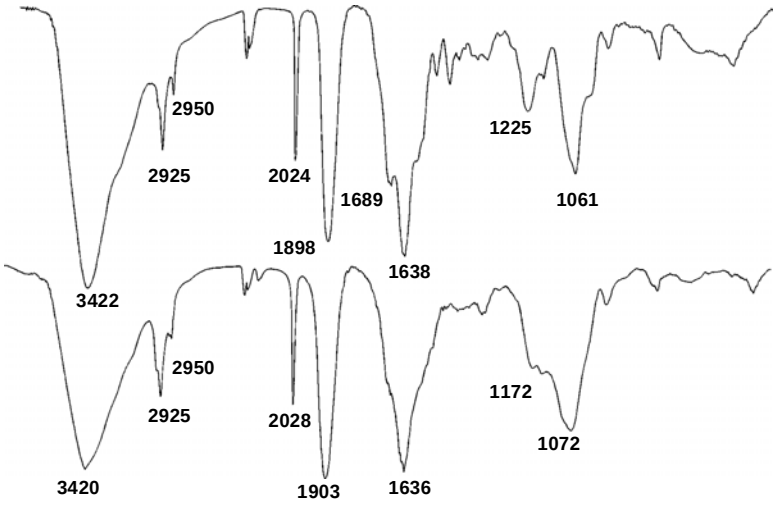

Figure 3.14. IR spectrum (KBr pellet, cm^{-1}) of **21** (top) and of a mixture of **20a** and **20 b** (bottom).

3.2 Conclusion

In this chapter it was shown that Re^{I} forms stable adducts with d(GpG) and d(CpGpG) via coordination of the N7 atom of guanine residues as corroborated by the pH-dependence studies of the H8 resonances at pH values near 2. Reaction of **1** with d(GpG) yields two major adducts. NMR data and ring current shift calculations based Abraham's model, tentatively suggest that these may be HH and HT conformers. Kinetic investigations have revealed that macrochelate closure is not the rate determining step but rather a fast step in the reaction. Interaction of **1** with d(CpGpG) yields a

single major product. NMR investigation has proven that the olygonucleotide binds to the *fac*-$[Re^{I}(CO)_3]$ core via the N7 atom of guanine bases.

3.3 References

(1) Sherman, S. E.; Lippard, S. J. *Chem. Rev.* **1987**, *87*, 1153-1181.

(2) Jamieson, E. R.; Lippard, S. J. *Chem. Rev.* **1999**, *99*, 2467-2498.

(3) Reedijk, J. *Chem. Rev.* **1999**, *99*, 2499-2510.

(4) Sherman, S. E.; Gibson, D.; Wang, A. H. J.; Lippard, S. J. *Science* **1985**, *230*, 412-417.

(5) Sherman, S. E.; Gibson, D.; Wang, A. H. J.; Lippard, S. J. *J. Am. Chem. Soc.* **1988**, *110*, 7368-7381.

(6) Spingler, B.; Whittington, D. A.; Lippard, S. J. *Inorg. Chem.* **2001**, *40*, 5596-5602.

(7) Spingler, B.; Whittington, D. A.; Lippard, S. J. *J. Inorg. Biochem.* **2001**, *86*, 440-440.

(8) Admiraal, G.; Vanderveer, J. L.; Degraaff, R. A. G.; Denhartog, J. H. J.; Reedijk, J. *J. Am. Chem. Soc.* **1987**, *109*, 592-594.

(9) Admiraal, G.; Alink, M.; Altona, C.; Dijt, F. J.; Vangarderen, C. J.; Degraaff, R. A. G.; Reedijk, J. *J. Am. Chem. Soc.* **1992**, *114*, 930-938.

(10) Esposito, G.; Cauci, S.; Fogolari, F.; Alessio, E.; Scocchi, M.; Quadrifoglio, F.; Viglino, P. *Biochem.* **1992**, *31*, 7094-7103.

(11) Chifotides, H. T.; Koshlap, K. M.; Perez, L. M.; Dunbar, K. R. *J. Am. Chem. Soc.* **2003**, *125*, 10703-10713.

(12) Chifotides, H. T.; Koshlap, K. M.; Perez, L. M.; Dunbar, K. R. *J. Am. Chem. Soc.* **2003**, *125*, 10714-10724.

(13) Chifotides, H.; Dunbar, K. R. *Biochem.* **2003**, *42*, 8606-8606.

(14) Cerasino, L.; Williams, K. M.; Intini, F. P.; Cini, R.; Marzilli, L. G.; Natile, G. *Inorg. Chem.* **1997**, *36*, 6070-6079.

(15) Williams, K. M.; Cerasino, L.; Intini, F. P.; Natile, G.; Marzilli, L. G. *Inorg. Chem.* **1998**, *37*, 5260-5268.

(16) Ano, S. O.; Intini, F. P.; Natile, G.; Marzilli, L. G. *J. Am. Chem. Soc.* **1998**, *120*, 12017-12022.

(17) Marzilli, L. G.; Intini, F. P.; Kiser, D.; Wong, H. C.; Ano, S. O.; Marzilli, P. A.; Natile, G. *Inorg. Chem.* **1998**, *37*, 6898-6905.

(18) Wong, H. C.; Intini, F. P.; Natile, G.; Marzilli, L. G. *Inorg. Chem.* **1999**, *38*, 1006-1014.

(19) Ano, S. O.; Intini, F. P.; Natile, G.; Marzilli, L. G. *Inorg. Chem.* **1999**, *38*, 2989-2999.

(20) Marzilli, L. G.; Williams, K.; Sullivan, S.; Villanueva, J.; Ano, S. O.; Marzilli, P.; Saad, J.; Ciccarese, A.; Intini, F.; Fannizi, F.; Natile, G. *J. Inorg. Biochem.* **1999**, *74*, 223-223.

(21) Wong, H. C.; Shinozuka, K.; Natile, G.; Marzilli, L. G. *Inorg. Chim. Acta* **2000**, *297*, 36-46.

(22) Williams, K. M.; Scarcia, T.; Natile, G.; Marzilli, L. G. *Inorg. Chem.* **2001**, *40*, 445-454.

(23) Saad, J. S.; Scarcia, T.; Shinozuka, K.; Natile, G.; Marzilli, L. G. *Inorg. Chem.* **2002**, *41*, 546-557.

(24) Saad, J. S.; Scarcia, T.; Natile, G.; Marzilli, L. G. *Inorg. Chem.* **2002**, *41*, 4923-4935.

(25) Bernersprice, S. J.; Ranford, J. D.; Sadler, P. J. *Inorg. Chem.* **1994**, *33*, 5842-5846.

(26) Dunham, S. U.; Lippard, S. J. *J. Am. Chem. Soc.* **1995**, *117*, 10702-10712.

(27) Dunham, S. U.; Turner, C. J.; Lippard, S. J. *J. Am. Chem. Soc.* **1998**, *120*, 5395-5406.

(28) Abraham, R. J.; Fell, S. C. M.; Smith, K. M. *Org. Mag. Res.* **1977**, *9*, 367-373.

(29) Abraham, R. J.; Rowan, A. E.; Goff, D. A.; Mansfield, K. E.; Smith, K. M. *J. Chem. Soc. Perkin Trans. 2* **1989**, 1633-1641.

(30) Abraham, R. J.; Goff, D. A.; Smith, K. M. *J. Chem. Soc. Perkin Trans. 1* **1988**, 2443-2451.

(31) Abraham, R. J.; Medforth, C. J.; Smith, K. M.; Goff, D. A.; Simpson, D. J. *J. Am. Chem. Soc.* **1987**, *109*, 4786-4791.

(32) Smith, K. M.; Goff, D. A.; Abraham, R. J. *J. Org. Chem.* **1987**, *52*, 176-180.

(33) Smith, K. M.; Bobe, F. W.; Goff, D. A.; Abraham, R. J. *J. Am. Chem. Soc.* **1986**, *108*, 1111-1120.

(34) Smith, K. M.; Goff, D. A.; Abraham, R. J. *Org. Mag. Res.* **1984**, *22*, 779-783.

(35) Smith, K. M.; Goff, D. A.; Abraham, R. J.; Plant, J. E. *Org. Mag. Res.* **1983**, *21*, 505-511.

(36) Abraham, R. J.; Smith, K. M.; Goff, D. A.; Lai, J. J. *J. Am. Chem. Soc.* **1982**, *104*, 4332-4337.

Chapter 4. Vitamin B12 as a Shuttle for Rhenium Complexes

In the previous chapters it was demonstrated that the *fac*-$[Re(CO)_3]^+$ core can bind two guanine bases in a *cis* fashion and that complexes based on this moiety alter the tertiary structure of plasmid DNA by covalently binding to two bases. In Chapter 2 amino acid were introduced as a kind of protecting group for the above mentioned core as in human serum (HS) $[Re(H_2O)_3(CO)_3]^+$ (**1**, see Chapter 2) interacts unspecifically with potential coordination sites in serum proteins and is therefore not available at high concentration. An important aspect, which has not yet been considered in this study, is the problem of targeting our compounds to the biological site of interest (i.e. cancer cells) for using these molecules in chemo- or radiotherapy.

In radiotherapy the common strategy followed by many is to protect the *fac*-$[Re(CO)_3]^+$ core with robust tridentate ligands and to attach the molecule thus obtained to receptor seeking biomolecules (usually peptides) via a chemical spacer. The peptide then "shuttles" the radionucleide to the target tumor site. In this Chapter, a different approach is introduced in as much as a vitamin (namely Vitamin B12) is used as the shuttle for rhenium complexes.

Vitamin B12 is an essential biomolecule, produced by a few bacteria only but fundamental for most living organisms. It plays a key role in enzymatic processes in mitochondria, the cell nucleus, and in the cytoplasm. Its uptake in humans is very complex, comprising at least the three different transport proteins intrinsic factor (IF), transcobalamin, and haptocorrin. The human organism treats vitamin B12 very economically. The daily requirement is only about 10μg. The chemistry, biochemistry, and biology has comprehensively been reviewed.[1-4]

The demand for vitamin B12 (abbreviated as B12) is distinct at places of enhanced proliferation, in particular in cancer cells or at sites of bacterial infections. Its inevitable need makes B12 very attractive as a targeting agent in chemo- or radiotherapy. Corresponding applications of B12 are persistently studied in the delivery of radioisotopes or various cytotoxic agents to cancer cells.[5, 6] Studies from the Mayo Clinic with radiolabelled B12 are in preclinical trials[7, 8] and Grissom and others showed that B12 can be used as a Trojan horse.[9-11] For both strategies, derivatization of B12 is required and the introduction of ligands or receptor binding molecules has been reported.[5, 7, 8, 11] Chelators for radiometals have been conjugated to peripheral acid groups, received by controlled amide hydrolysis, and to the 5'-OH group in the ribose ring of the backloop. Alternatively, Co(III)

was reduced to Co(I) and a molecule introduced by oxidative alkylation.[10, 12] Both approaches require rather tedious synthetic procedures.

The only functionality in B12 that has not received much attention is the Co(III) coordinated cyanide. It is well established that M-CN moieties distinctly tend to bridge two metal centers to form a M-C≡N-M‘ unit. Numerous examples have been described and reviewed in literature[12] but examples with porphyrin like systems are rare[13-15] and, to our knowledge, unknown for B12. The reverse situation in which $[Fe(CN)_6]^{3-}$ or nitroprusside $[Fe(NO)(CN)_5]^{-}$ are coordinated to Co(III) or Co(II) of aqua-cobalamin has been studied in detail.[16-22]

In this brief Chapter the synthesis and characterization of $[Re(DMGly)(CO)_3]$-B12 adducts (DMGly = N,N-dimethylglycine) is described and it is show that B12 acts as the monodentate ligand for rhenium complexes via the Co(III) coordinated cyanide. $[Re(DMGly)(CO)_3]_3$ (**14**, see Chapter 2) was chosen for the reaction because, as demonstrated in Chapter 2, while DMGly protects the metal tricarbonyl core, **14** is able to influence the tertiary structure of ΦX174 plasmid DNA indicating that DMGly is displaced from the rhenium coordination sphere in favor of DNA bases (see Figure 2.2).

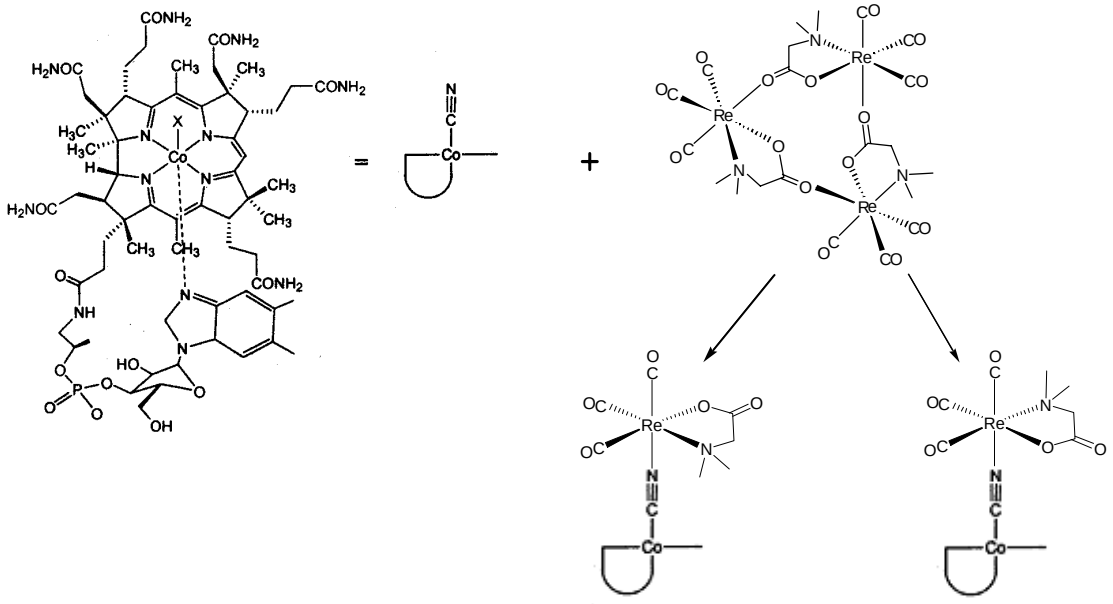

Scheme 4.1. Structure of vitamin B12 and coordination of **14** to the vitamin.

4.1 Results and Discussion

The reaction of **14** with B12 in methanol afforded the formation of [(**14**-B12)] (**22**), in good yield. HPLC analysis of the reaction with Re gave only two well separated peaks in a ratio of about 1:1 (see Figure 4.1). The peaks can be understood by the two possible orientations adopted by the bidentate N,O ligand DMGly relative to the corrin ring (complexes $[M(L^2)(OH_2)(CO)_3]$ where L^2 = bidentate N,O ligand are racemic) and, thus, the presence of two diastereomers. Both peaks, separated by preparative HPLC, showed the same and correct mass [M^{2+}=869.1; M^{+}=1736.9] in ESI-MS and ^{1}H and ^{31}P NMR confirmed the proposed composition.

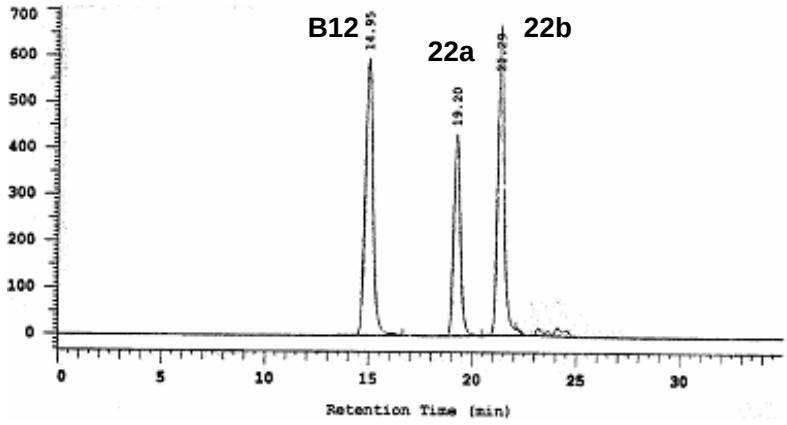

Figure 4.1. HPLC trace (UV/vis at λ= 350 nm) of the reaction between B12 and **14** showing the two diastereomers.

We attempted to determine the orientation of B12 relative to the bidentate ligand by ROESY experiments as recently performed for a B12 derivative in which the CN^- has been replaced by a (methoxycarbonyl)-methyl group.[23] However, no cross peaks could be observed even at low temperature, indicating fast rotation of the complex. Since the equatorial planes of the complexes are relatively far away from the corrin framework, they are not locked in a fixed position. The two isomers of **22** can be separated well by preparative HPLC. X-ray quality crystals for one of isomer **22a** (see Figure 4.1) could be grown and the structure elucidated (see Figure 4.2).

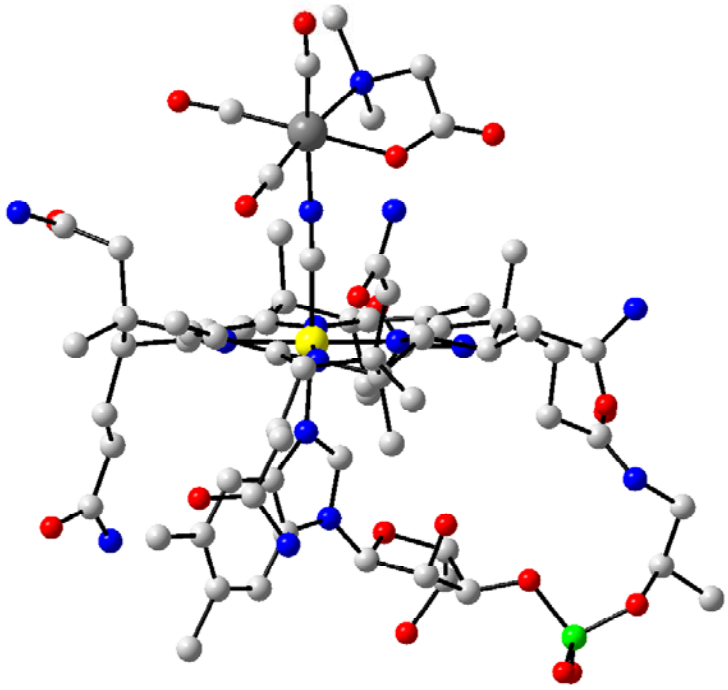

Figure 4.2. X-ray analysis of **22a**. Important bond lengths and angles are: Co-CN: 1.90(1) Å, Co-N(benzimidazole): 2.032(7) Å, C-N(cyanide): 1.180(12) Å, CN-Re: 2.14(1) Å, Co-C-N: 167.7(9)°, C-N-Re: 169.2(9)°.

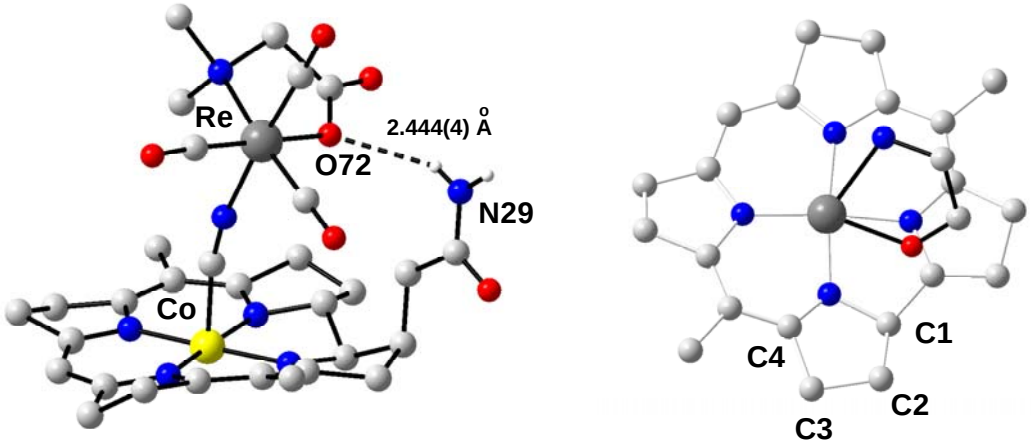

Figure 4.3. Hydrogen bonding in **22a** (left) and orientation of the DMGly ligand relative to the corrin ring (right). C2 represents the carbon to which the a-sidechain is attached.

The relative orientation of the N,O ligands L^2 in **22a** is shown in Figure 4.3. Complex **22a** depicts a hydrogen bridge between the coordinated carbonyl oxygen O72 and the amide nitrogen of the a-side chain in B12 (Figure 4.3). The bridge probably determines the orientation of the Re complex in the crystal. The b-side chain is also bent upwards but does not display any interaction to the complex. We assume that the diastereomers of complex might be represented by different orientations of the DMGly ligand relative to the corrin ring.

We observed that diastereomerically pure complexes $[M(L^2)(L'^1)(CO)_3]$ with one labile ligand (e.g. L-serine (L^2) and guanine L'^1) always return to equilibrium in water within hours, probably through a five-coordinate intermediate by dissociation of the monodentate ligand. The pure diastereomers of **22** do not interconvert into each other even after days in water at r.t. confirming the high kinetic stability of monodentately bound B12. Acetonitrile is a strong ligand for complexes $[Re(L^2)(OH_2)(CO)_3]$. Dissolving **22a** or **22b** in an H_2O/CH_3CN mixture and analyzing the solution for days showed only about 10% cleavage for both species confirming again the stability of the Co-CN-[Re] bond.

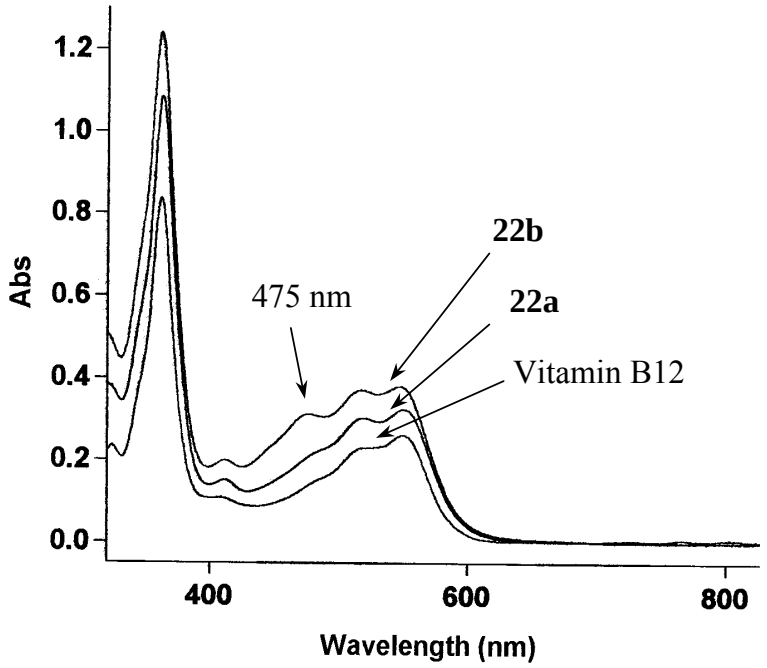

Figure 4.4. Electronic spectra (H_2O/Acetone, 2:1) of the two diastereomers of **22** and of Vitamin B12. Abs (nm) in 360, 410, 560 and 550 region.

Interestingly, the electronic spectra of the two diastereomers of **22** are different (Figure 4.4). Although both have essentially the B12 shape, the weak shoulder at about 482 nm in B12 becomes a distinct peak at 475 nm.

Biological applications of these compounds require stability in serum and affinity for the various B12 binding proteins. It is known that haptocorrin tolerates derivatives of B12 whereas the transcobalamins are more sensitive towards structural changes.[24-26] Derivatizations at the Co(III) center are generally more tolerated by both proteins and a direct labeling of B12 with $[^{99m}Tc(L^2)(OH_2)(CO)_3]$ is feasible. Complexes $[^{99m}Tc(L^2)(OH_2)(CO)_3]$ reacted quantitatively with B12 between 10^{-2} and 10^{-3} M within 60 min at 50°C. The CN^- in B12 is a slow ligand (hence the relatively high concentrations). Once formed and separated by HPLC, the isomers are stable over at least 24 h at 37° C. This opens a convenient way for studying the biological behaviour of labelled native B12 by varying the nature of L^2. The intracellular B12 dependent enzymes might not recognize these derivatives anymore but then the radionuclide has already reached its target. It should be emphasized that the Re center is likely to mediate biologically active molecules and B12 if the ligand L^2 is coupled to a peptide or a cytotoxic agent (e.g. the free COOH in dipic).

4.2 Conclusion

In conclusion, we have shown that CN^- in B12 bridges to Re(I) to yield robust complexes comprising the central structural feature [Co-CN-Re]. This concept allows direct labeling of B12 with complexes $[^{99m}Tc(OH_2)(N\cap O)(CO)_3]$ for radiodiagnosis or with Re as a mediator between B12 and additional biologically active molecules. The observed kinetic stability let us expect coordination of other fragments with d^6 or d^8 configuration as well. B12 as an enantiomerically pure and stereochemically demanding ligand provides water solubility and is potentially useful in enantioselective synthesis in combination with an appropriate catalyst.

4.3 References

(1) Kräutler, B.; Arigoni, D.; Golding, B. T. *in* "*Vitamin B12 and B12-Proteins",* WILEY-VCH, 1st Ed., Weinheim, Germany, **1998**.

(2) Kräutler, B. *B12-Coenzymes, the Central Theme* **1999**, 3.

(3) Banerjee, R. in "*Chemistry and Biochemistry of B12"*, Wiley-Interscience, 1st Ed., New York, **1999**.

(4) Banerjee, R.; Ragsdale, S. W. *Ann. Rev. Biochem.* **2003**, *72*, 209-247.

(5) Wilbur, D. S.; Hamlin, D. K.; Pathare, P. M.; Heusser, S.; Vessella, R. L.; Buhler, K. R.; Stray, J. E.; Daniel, J.; Quadros, E. V.; McLoughlin, P.; Morgan, A. C. *Bioconjugate Chem.* **1996**, *7*, 461-474.

(6) Collins, D. A.; Hogenkamp, H. P. C. *J. Nucl. Med.* **1997**, *38*, 717-723.

(7) Collins, D. A.; Hogenkamp, H. P. C.; Gebhard, M. W. *Mayo Clin. Proc.* **1999**, *74*, 687-691.

(8) Collins, D. A.; Hogenkamp, H. P. C.; O'Connor, M. K.; Naylor, S.; Benson, L. M.; Hardyman, T. J.; Thorson, L. M. *Mayo Clin. Proc.* **2000**, *75*, 568-580.

(9) Cannon, M. J.; Myszka, D. G.; McGreevy, J. M.; Holden, J. A.; West, F. G.; Grissom, C. B. *Faseb Journal* **2001**, *15*, A556.

(10) Smeltzer, C. C.; Cannon, M. J.; Pinson, P. R.; Munger, J. D.; West, F. G.; Grissom, C. B. *Org. Lett.* **2001**, *3*, 799-801.

(11) Hogenkamp, H. P. C.; Collins, D. A.; Live, D.; Benson, L. M.; Naylor, S. *Nucl. Med. Biol.* **2000**, *27*, 89-92.

(12) Pagano, T. G.; Marzilli, L. G.; Flocco, M. M.; Tsai, C.; Carrell, H. L.; Glusker, J. P. *J. Am. Chem. Soc.* **1991**, *113*, 531-542.

(13) Corsi, D. M.; Murthy, N. N.; Young, V. G.; Karlin, K. D. *Inorg. Chem.* **1999**, *38*, 848-858.

(14) Lee, S. C.; Scott, M. J.; Kauffmann, K.; Munck, E.; Holm, R. H. *J. Am. Chem. Soc.* **1994**, *116*, 401-402.

(15) Takano, S.; Naito, T.; Inabe, T. *J. Mat. Chem.* **1998**, *8*, 511-513.

(16) Stochel, G.; Vaneldik, R.; Kunkely, H.; Vogler, A. *Inorg. Chem.* **1989**, *28*, 4314-4322.

(17) Kunkely, H.; Vogler, A. *Z. Naturforsch. B* **1996**, *51*, 245-248.

(18) Butler, A. R.; Glidewell, C.; Mcintosh, A. S.; Reed, D.; Sadler, I. H. *Inorg. Chem.* **1986**, *25*, 970-973.

(19) Butler, A. R.; Glidewell, C. *Chemical Society Reviews* **1987**, *16*, 361-380.

(20) Wolak, M.; Stochel, G.; Hamza, M.; van Eldik, R. *Inorg. Chem.* **2000**, *39*, 2018-2019.

(21) Wolak, M.; Zahl, A.; Schneppensieper, T.; Stochel, G.; van Eldik, R. *J. Am. Chem. Soc.* **2001**, *123*, 9780-9791.

(22) Wolak, M.; Stochel, G.; van Eldik, R. *J. Am. Chem. Soc.* **2003**, *125*, 1334-1351.

(23) Puchberger, M.; Konrat, R.; Krautler, B.; Wagner, U.; Kratky, C. *Helv. Chim. Acta* **2003**, *86*, 1453-1466.

(24) Stupperich, E.; Nexo, E. *Eur. J. Biochem.* **1991**, *199*, 299-303.

(25) Pathare, P. M.; Wilbur, D. S.; Hamlin, D. K.; Heusser, S.; Quadros, E. V.; McLoughlin, P.; Morgan, A. C. *Bioconjugate Chem.* **1997**, *8*, 161-172.

(26) Pathare, P. M.; Wilbur, D. S.; Heusser, S.; Quadros, E. V.; McLoughlin, P.; Morgan, A. C. *Bioconjugate Chem.* **1996**, *7*, 217-232.

Chapter 5. Novel Nucleoside-Mimicking Complexes Based on the *fac*-$[Re(CO)_3]^+$ Moiety: Structure, Reactivity and Solution Behaviour of $[Re(CO)_3(Ser)(7\text{-MeG})]$, $[Re(CO)_3(Ser)(3\text{-pic})]$ and $[Re(CO)_3(Ser)(Ade)]$

In radiopharmaceutical design the quadridentate N_2S_2 and N_3S type ligands have been most often employed in the synthesis of ^{99m}Tc and Re complexes (almost always encompassing a M^V=O core).[1-9] The compounds thus obtained are generally appended to a peptide as the biological vehicle for delivering the radiopharmaceuticals to the target tumor site.[10-14] This strategy results in the design of compounds exclusively suited for radiotherapeutic purposes where the metal core is prevented from further interacting at the target site.

The *fac*-$[M(CO)_3]^+$ core, on the other hand, permits the synthesis of $^{99(m)}Tc$ and Re based complexes that could be used not only as radio- but also as chemotherapeutic agents. In Chapter 1 it was demonstrated that $[M(H_2O)_3(CO)_3]^+$ (**1**, M = Re, **2**, M = ^{99}Tc) forms cis-bis(purine) complexes with guanine, and it was shown that the rate constants for the binding of guanosine to the complex are in the same order of magnitude of one the active forms of cisplatin, namely $[Pt(NH_3)_2(OH_2)_2]^{2+}$.

One can therefore envision that if surrounded by a proper set of ligands, the above mentioned moiety may, upon delivery, actively participate in the biochemistry at the desired target tumor site. In Chapter 2 amino acids were chosen as a kind of protecting group for the rhenium $[Re(CO)_3]^+$ core as in human serum (HS) $[Re(H_2O)_3(CO)_3]^+$ (**1**, see Figure 2.1) interacts unspecifically with potential coordination sites in serum proteins and is therefore not available at high concentration. It is also mentioned in the same chapter that amino acids seem good candidates for protecting groups for the rhenium $[Re(CO)_3]^+$ core for two main reasons. First, depending on the choice of the amino acid, they afford robust bi- or tridentate protecting groups for the metal core. Second, since amino acids are not foreign to biological systems, once displaced from the metal core, which can then be thought as activated, they will not give rise to toxic side effects but they will simply be recycled in the biochemical pathways.

Given the structural features of **15** ($[Re(Pro)(9\text{-MeG})(CO)_3]$ see Chapter 2) a guanosine mimicking complexes could be designed by substituting the amino acid proline with serine and the monodentate base 9-MeG with 7-MeG (Scheme 5.1). Similarly, by varying the monodentate base different nucleoside mimicking complexes may be obtained.

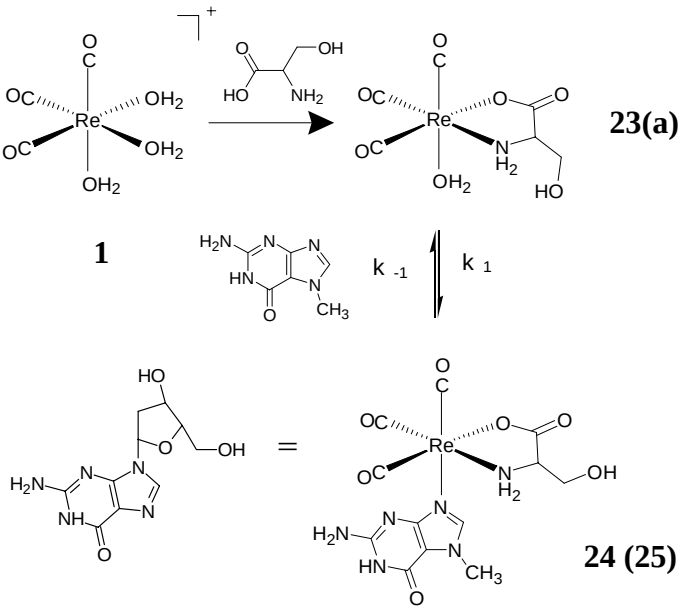

Scheme 5.1. Synthetic scheme for the formation of guanosine mimicking complexes **24** and **25**.

In this chapter the synthesis and characterization of $[Re(CO)_3]^+$-based nucleoside mimicking complexes is described. It will also be shown that these new compounds are remarkably stable in Human Serum (HS) when compared to **10** and **12** (see Chapter 1). Finally the interaction of some of the reported compounds, namely $[Re(CO)_3$(L-Ser)(7-MeG)] (**24**), $[Re(CO)_3$(D-Ser)(7-MeG)] (**25**) and $[Re(CO)_3$(L-Ser)(3-pic)] (**26**), with ΦX174 plasmid DNA and the phosphotransferase Thymidine Kinase Herpes Simplex Virus Type I (HSV1 TK) is described.

5.1 Results and Discussion

Synthetic Aspects. Reaction of **1** with the amino acid L-serine (L-Ser) yields a complex of the type $[Re(L\text{-}Ser)_2(CO)_3]_3$ (**23**) with one amino acid bound in a bidentate and the other in a monodentate fashion (see crystallography and NMR subsections). The reaction goes to completion within a few hours in a methanol/water mixture (9:1) and in the presence of a slight excess of amino acids required to neutralize the proton released upon coordination of the carboxylate group. When dissolved in H_2O, complex **23** is stable for days over a wide pH range ($3 \leq pH \geq 8$). Reaction of **1** with the amino acid D-serine (D-Ser) yields a complex (**23a**) with similar spectroscopic feature as of **23**. Although the compound that formed in this reaction was not isolated we speculate that it is structurally similar to **23**.

Although no evidence of ligand exchange was found in water over 3 weeks, upon addition of a nitrogenous base one of the coordinated amino acids in **23** is displaced in favour of the stronger mono dentate ligand. Addition of 7-methylguanine (7-MeG) to a solution of **23** yields complex $[Re(CO)_3(L\text{-}Ser)(7\text{-}MeG)]$ (**24**) in a few hours. Similarly, after addition of 7-MeG to **23a** complex $[Re(CO)_3(D\text{-}Ser)(7\text{-}MeG)]$ (**25**) could be obtained. Complexes **24** and **25** were isolated as analytically pure white microcrystalline solid although their formation is not complete at a 1:1 stoichiometry (i.e. 1:1 **23(a)**:7-MeG).

Reaction of **23** with 3-picoline (3-pic) yields complex $[Re(CO)_3(L\text{-}Ser)(3\text{-}pic)]$ (**26**) according to Scheme 5.2. It must be mentioned at this point that although **23** is isolated as "bis"-L-Ser complex, in all the schemes **23** is shown as a mono-aquo complex where the H_2O molecule indicates the site of the nitrogenous base coordination. It was found that 3-pic is a weaker ligand for **23** than 7-MeG. To ensure complexation at least 4 eq. of 3-pic were added to a solution of **23** and the pH had to be adjusted to ≈ 6. As mentioned earlier, during formation of **23** coordination of the carboxylate group of the amino acid releases a proton and the pH drops to ≈ 3. While coordination of 7-MeG does not suffer greatly under these conditions and yields (by HPLC analysis) are generally >90%, a close to neutral pH is required for 3-pic coordination. Finally no evidence of coordination of 2,4-dihydroxypyrimidine-5-carboxylic acid (which would afford a much closer thymidine mimicking complex) to **23** was found.

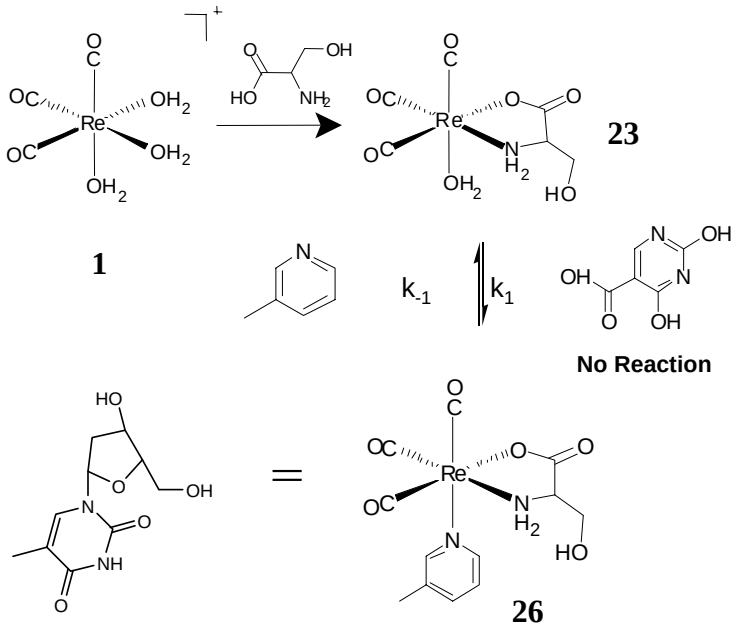

Scheme 5.2. Synthetic scheme for the formation of the thymidine mimicking complex **26**.

Reaction of **23** with adenine (Ade) does not yield a single complex but a mixture of five distinct species (**27a-27e**, see Figure 5.1). As a ligand Ade is a weaker than 3-pic and to ensure complexation an excess of Ade (>12 eq.) must be added to a solution of **23**. Upon addition of Ade to a solution of **23** three species first appear (**27a-27c**) with HPLC R_t of 15.6, 16.6 an 17.2 min respectively. These three species are then followed by two other species with HPLC R_t of 19.6 and 20.9 min (**27d** and **27e**). HPLC-MS analysis revealed that species **27a-27c** have a molecular weight of 509.9 *m/z* (Re_1 pattern) corresponding to $[Re(CO)_3(L\text{-}Ser)(Ade)]$, while species **27d** and **27e** have a molecular weight of 882.5 *m/z* (Re_2 pattern) corresponding to $[Re(CO)_3(L\text{-}Ser)]_2(Ade)$ (see Figure 5.1). Attempts to isolate species **27a** failed, however the bridging nature of Ade in species **27d** was confirmed by x-ray analysis (see Figure 5.2).

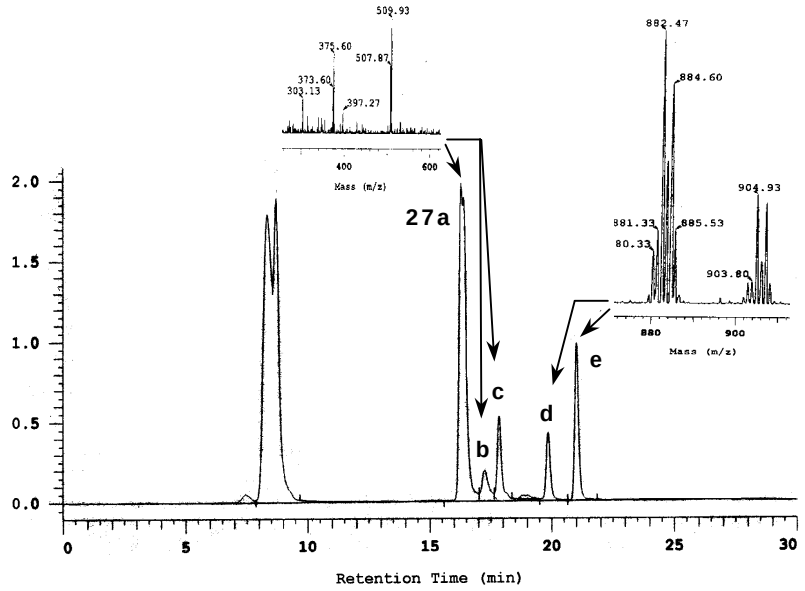

Figure 5.1. HPLC chromatogram of the reaction of **23** with an excess of Ade and MS of species **27a-27e**.

Due to the poor crystal quality no details of structure **27d** can be discussed. It is however interesting to note that the $[Re(L\text{-}Ser)(CO)_3]$ moieties are bridged via the imidazole ring of Ade with one Re bound to N7 and the other Re bound to N9. Possible structures of species **27a-27c** are shown in Scheme 5.3.

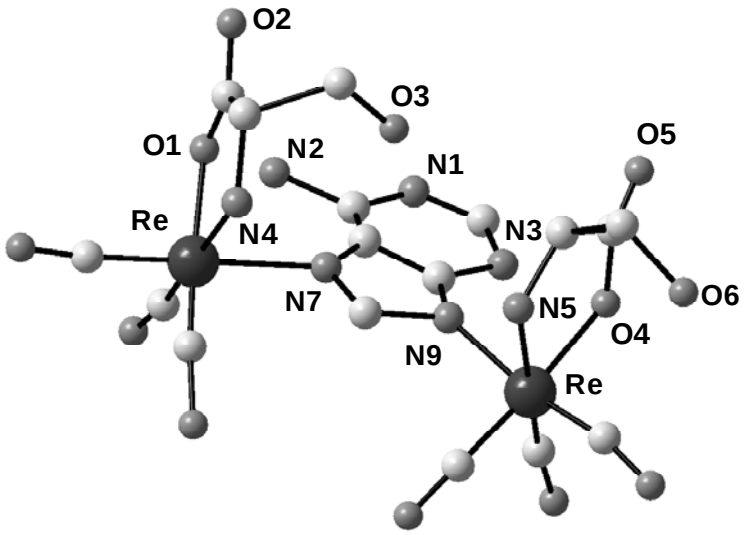

Figure 5.2. Molecular structure of species **27d** obtained from low X-ray quality crystals.

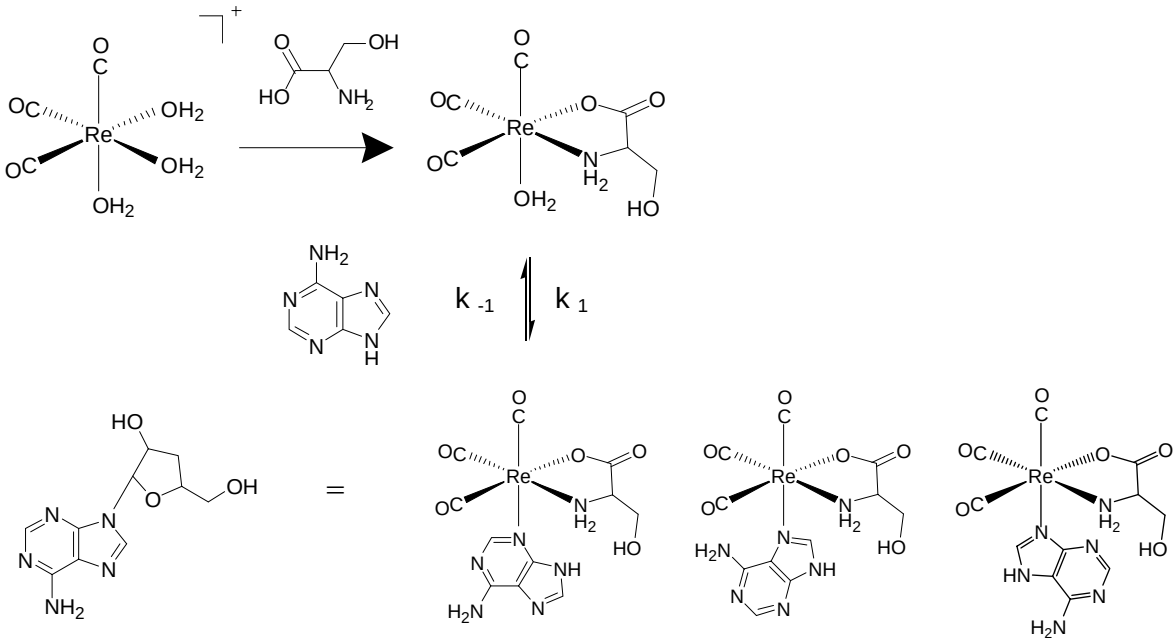

Possible species **27a**, **27b** and **27c**.

Scheme 5.3. Synthetic scheme for the formation of the adenosine mimicking complexes **27a-27c**.

X-ray Crystallography. Crystal data and experiment details are listed in the crystallography section. The crystals structure of compound **23** is shown in Figure 5.3. The molecule crystallizes in the orthorhombic space group $P2_12_12_1$ with no atoms in special position. The geometry around rhenium is octahedral with one face occupied by three carbonyl ligands and the other three coordination sites occupied by two L-Ser. One of the two amino acids is bound in a bidentate fashion with Re-N1 and Re-O1 distances of 2.193(11) and 2.138(8) Å. If compared with structures

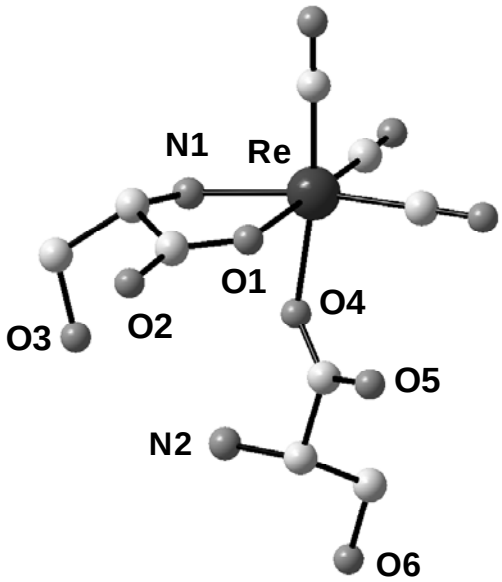

Figure 5.3. Crystal structure of $[Re(L\text{-}Ser)_2(CO)_3]$ (**23**). Selected bond distances (Å) and angles (deg) are the following: Re-N1 2.193(11), Re-O1 2.138(8), Re-O4 2.137(8); N1-Re-O1 77.1(3), N1-Re-O4 76.2(4), O1-Re-O4 81.5(3).

13, **14** and **15** (see Chapter 2) one finds that on average the Re-N1 bond distance is 0.03 Å shorter in **23**, while the Re-O1 bond distance is virtually identical to **13** and again 0.03 Å shorter on average than **14** and **15**. The other amino acid is bound as a zwitter ion in a monodentate fashion via the carbonyl oxygen labelled O4 in Figure 5.3. The Re-O4 bond distance is virtually identical to the Re-O1 distance in the bidentate coordinated L-Ser. Finally, while the OC-Re-CO angles are on average close to 89°, smaller angles are measured between the other atoms bound to the metal center. The O1-Re-O4 angle is 81.5°, the O1-Re-N1 and O4-Re-N1 angles are 77.1° and 76.2° respectively.

Diffraction-quality crystals of **24** were grown from methanol and pentane. Two different conformations of the complex are present in the asymmetric unit and the crystal structures of these are given in Figure 5.4. The difference in the two structures is represented by the orientation of the CH_2OH Ser arm. In structure A the arm projects toward 7-MeG, below the plane defined by the coordinated amino acid and two CO groups, while in structure B the arm is in the plane. The orientation the CH_2OH arms is locked in the solid state by H-bonding interactions involving the hydroxyl proton of O3A (i.e. O3 of structure A) and O6B and the hydroxyl proton of O3B and O2A (please refer to hydrogen bonding subsection). In both structures the 7-MeG ligand bisects the plane defined by the coordinated amino acid and two CO groups with the tip of the imidazole ring pointing in between O1 and the CO group *cis* to it.

Coordination of 7-MeG to **23** causes an elongation of the Re-O1 bond by about 0.02 Å while the Re-N4 bond (Re-N1 bond in **23**, see Figures 5.3 and 5.4) remains virtually unchanged (on average the bond suffers an elongation of < 0.005 Å). The bite angle of the amino acid also decreases by 0.8°. If compared with structures **13** and **15** (see Chapter 2) one finds that the transition from the trimeric structure **13** to the mono-bound 9-MeG derivative **15** causes an elongation of both Re-O1 (+0.03 Å) and Re-N1(4) (+0.01 Å) bonds.

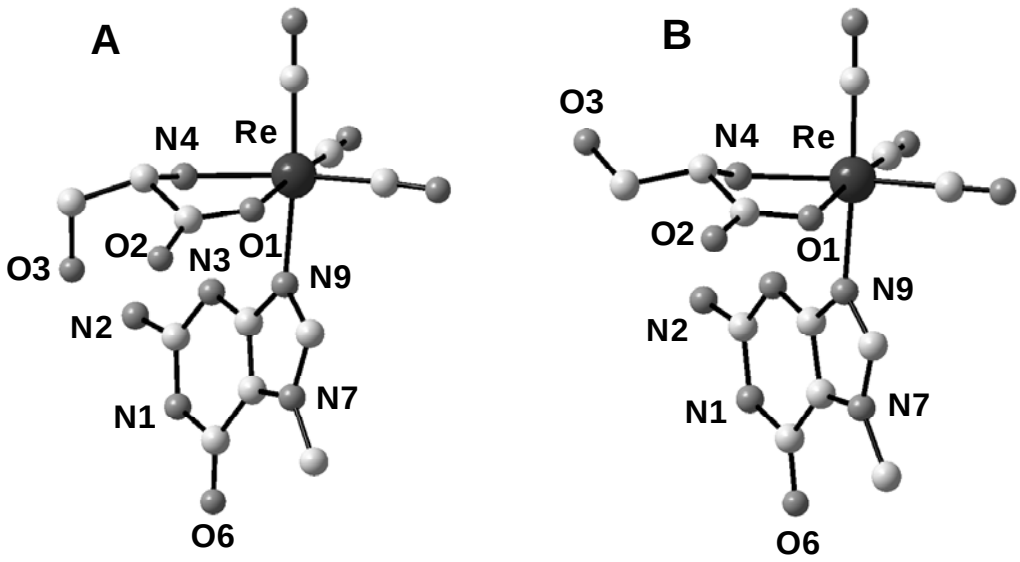

Figure 5.4. Crystal structure of [Re(L-Ser)(7-MeG)$(CO)_3$] (**24**). Selected bond distances (Å) and angles (deg) are the following: A: Re-N9 2.184(9), Re-N4 2.188(9), Re-O1 2.153(7); N9-Re-O1 79.2(3), N9-Re-N4 83.0(3), N4-Re-O1 76.9(3). B: Re-N9 2.197(9), Re-N4 2.206(8), Re-O1 2.152(7); N9-Re-O1 81.1(3), N9-Re-N4 85.6(3), N4-Re-O1 75.9(3).

As a consequence one finds that the bite angle of the amino acid does not decrease but rather increases by 0.3°.

The crystal structure of molecule **25** is shown in Figure 5.5. The structural features of **25** resemble closely those of **24** indeed these two molecules are enantiomers. As with **24** two different conformations of **25** are present in the asymmetric unit. Again the difference in the two structures is represented by the orientation of the CH_2OH Ser arm. Extensive hydrogen bonding interactions lock in position A' and B' (see Figure 5.5) and these will be discussed in more details later on in this chapter.

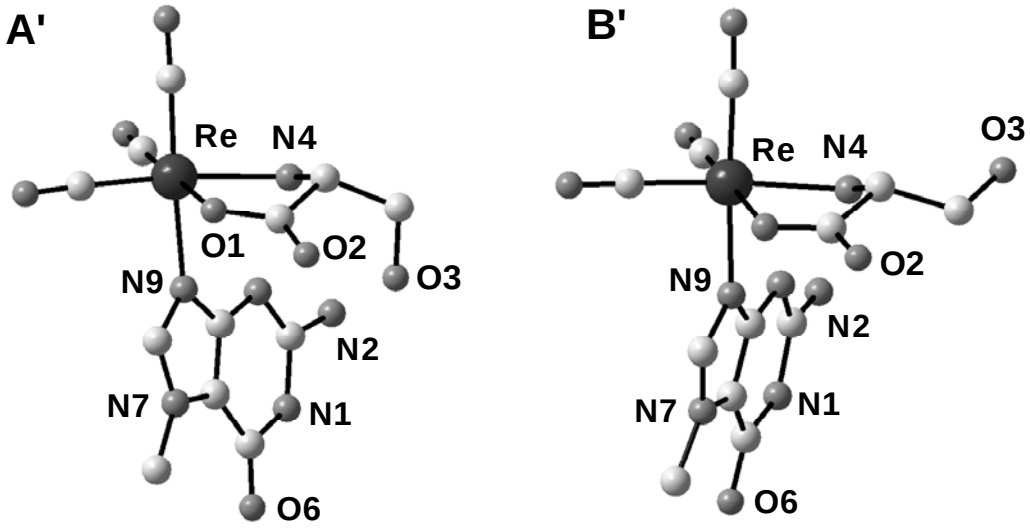

Figure 5.5. Crystal structure of [Re(D-Ser)(7-MeG)$(CO)_3$] (**25**). Selected bond distances (Å) and angles (deg) are the following: A′: Re-N9 2.188(7), Re-N4 2.224(7), Re-O1 2.157(6); N9-Re-O1 80.5(3), N9-Re-N4 83.6(3), N4-Re-O1 76.8(2). B′: Re-N9 2.186(7), Re-N4 2.240(7), Re-O1 2.157(5); N9-Re-O1 80.9(2), N9-Re-N4 84.1(3), N4-Re-O1 75.5(2).

The crystal structure of molecule **26** is shown in Figure 5.6. The molecule crystallizes in the monoclinic space group $P2_1$ with two independent molecules occupying the unit cell. These molecules differ in the coordination geometry of amino acid. In **26A** L-Ser is bound so that the CH_2OH arm projects away from the pyridine base while in **26B** L-Ser is rotated by 180° with respect to its position in **26A** and the CH_2OH arm projects toward the pyridine base. By comparing the two structure one finds that Re-N1 and Re-O1 bond distances are longer in **26B** (by 0.005 and

0.03 Å respectively). This might reflect the need of **26B** to minimize steric repulsion between the CH_2OH arm and the CH_3 group of the pyridine base. Rotation around the Re-N2 bond in **26B** brings the CH_3 group at C9 (see Figure 5.6) in close proximity of O3. Although the molecule might compensate by simply rotating the CH_2OH arm so that O3 projects away from 3-pic, elongated Re-N1 and Re-O1 bonds certainly help **26B** to ease the steric demand imposed by the geometry.

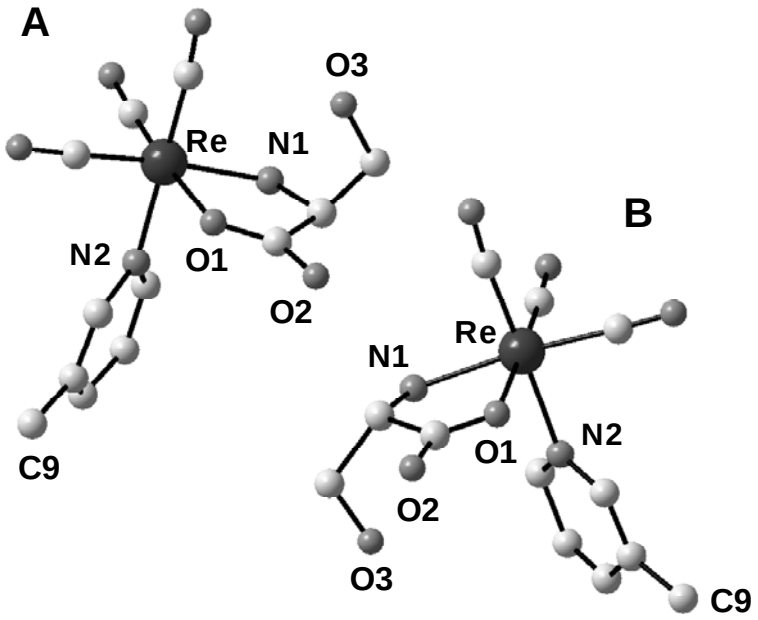

Figure 5.6. Crystal structure of [Re(L-Ser)(3-pic)$(CO)_3$] (**26**). Selected bond distances (Å) and angles (deg) are the following: A: Re-N1 2.21(2), Re-N2 2.12(2), Re-O1 2.101(18); N1-Re-O1 77.4(7), N1-Re-N2 86.6(10), N2-Re-O1 83.2(9). B: Re-N1 2.21(3), Re-N2 2.24(3), Re-O1 2.134(15); N1-Re-O1 76.7(7), N1-Re-N2 76.7(7), N2-Re-O1 83.2(8).

Complexes **23-26** belong to a class of compounds showing typical coordination modes for α-amino acids where the anion is coordinated as a N,O-chelate. The complexes were prepared by classical substitution reactions, a methodology successfully applied especially for compounds in which the organometallic coligands (Cp*, CO, η^6-arene, etc.) function solely as spectator ligands. Numerous octahedral α-aminocarboxylate carbonyl metal complexes have been reported. Among them, complexes of Cr, Mo, W, Mn, Re, Fe, Ru, Os, Rh and Pt are common.[15-21] However, α-aminocarboxylate complexes based on a *fac*-[$M(CO)_3$] core are relatively rare.

Tetracarbonyl [$M(CO)_4$] (M = W, Re) compounds of amino acids N,O-chelates are known,[22, 23] however more common are N,O-chelate complexes of the type [$M(CO)L(PR_3)_2$] (M = Ru, Os)

where L can be either a second CO ligand, or H.[24, 25] Also known are bis carbonyl η^5-cyclopentadienyl (Cp) complexes of the type $[(Cp)M(CO)_2]$ (M = Mo, W) and a number of square planar carbonyl compounds of Rh and Pt in which the amino acid is also found as a N,O-chelate.[16-21, 26, 27] Tricarbonyl complexes of the type *fac*-$[M(CO)_3]$ (M = Cr, Mo, W, Mn, Tc, Re) are generally reported with tridentate ligands such as L-histidine and L-cysteine[14] although examples of tricarbonyl ruthenium chloride complexes of the type *fac*-$[RuCl(CO)_3]$ where the other two coordination sites are occupied by either glycine or proline are known. Compared with the closely related $[Re(His)(CO)_3]$ structure (where His = histidine, **18**, see Chapter 2) one finds that in **23**-**26** while Re-O bonds (O = oxygen of N,O-chelate) are on average virtually identical to the same bond in **18**, Re-N bonds are longer (on average 0.02 Å, but in some cases up to 0.05 Å). This however does not come as a surprise as tridentate ligands are stronger chelators for the above mentioned moiety.

NMR Studies. The ^{1}H NMR spectra of free L-Ser and **23** are given in Figure 5.7. The two spectra show similar features with one set of signals between 3.98 and 3.87 ppm assigned to resonance of the serine CH_2OH arm (the OH group is silent as it exchanges with D_2O) and one signal shifted more up field assigned to resonance of the proton on the α-carbon. Overall the L-Ser resonances shift down field upon coordination to the $[Re(CO)_3]^+$ core. Interestingly, a single set of signal is observed for the crystallografically non-equivalent amino acids in the ^{1}H NMR spectra of **23**. This indicates that the two ligands are in rapid equilibrium and that the resonances observed represent an average of the two conformations.

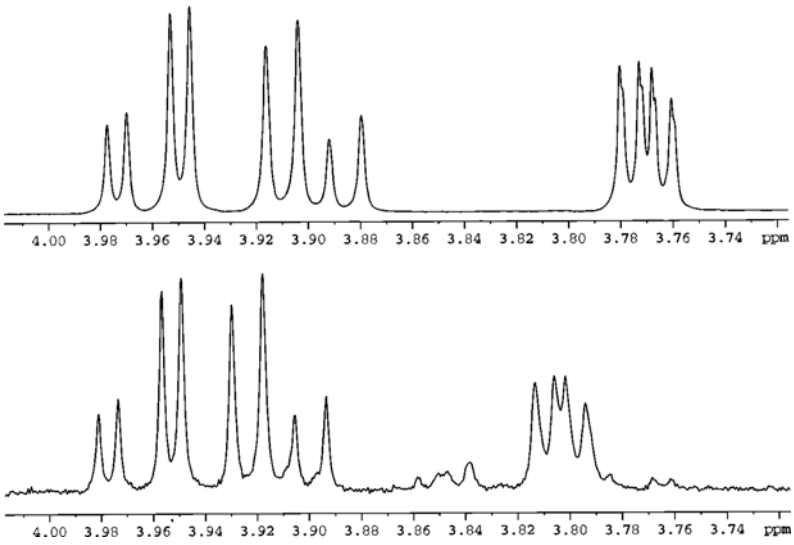

Figure 5.7. ^{1}H NMR spectrum (3.7-4.2 ppm, D_2O:MeOH-d^4, 2:1, 25 ^{o}C) of L-Ser (top) and **23**.

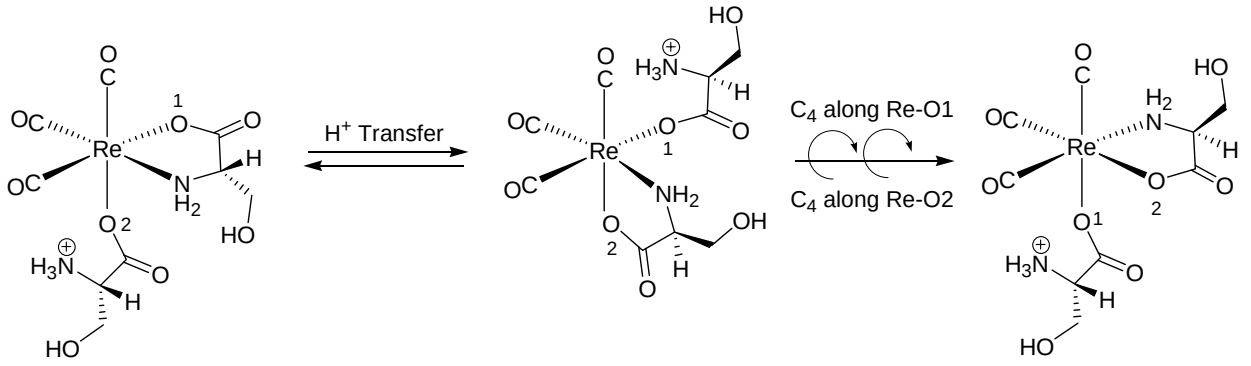

Scheme 5.4. Proposed rearrangement of **23**.

The proposed rearrangement taking place in solution is shown in Scheme 5.4. A fast H^+ transfer between amino groups favors dissociation of the nitrogen atom in the chelate and allows the other NH_2 group to enter the Re-coordination sphere. If at time = 0 one considers structure **23** (see Figure 5.3) where the CH_2OH arm of the chelate serine points toward the other L-Ser ligand, H^+ transfer between amino groups, followed by bond dissociation/formation, gives a complex in which the CH_2OH arm points away from the other L-Ser ligand. In essence one might think as if the net result of the rearrangement is to promote an exchange in position in the Re-coordination sphere between the carboxylate oxygen and the amino group.

Temperature dependent NMR studies (see Figure 5.8) revealed that only at -80 °C do the signals begin to coalescence, indicating that H^+ transfer and intramolecular rearrangement are still fast on the NMR time scale at this low temperature.

The aromatic region of the ^1H NMR spectrum of **24** is shown on the right of Figure 5.9. When crystals of **24** are dissolved in a D_2O/MeOH-d^4 mixture (1:1) a single resonance (8.14 ppm) corresponding to the H8 signal of coordinated 7-MeG is initially present. Within a few minutes however a second and third signals appear at 8.09 and 7.93 ppm. The signal at 7.93 ppm corresponds to the H8 proton of free 7-MeG while the resonance at 8.09 ppm corresponds to the H8 signal of a new species resulting from an intramolecular rearrangement of **24**. The rate constant of this intramolecular rearrangement was measured by NMR and it is $1.36 \times 10^{-2} \pm 0.24\ s^{-1}$. A likely rearrangement is shown to the left of Figure 5.9.

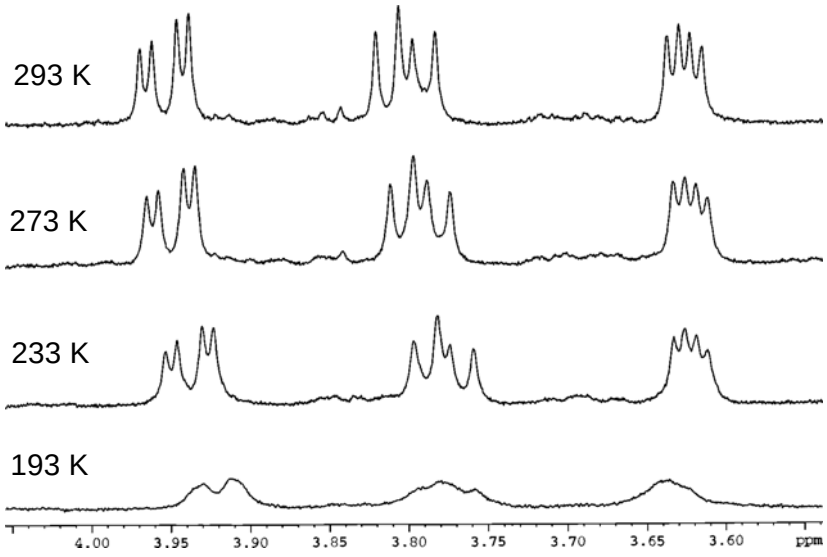

Figure 5.8. Temperature dependent ^{1}H NMR spectrum of **23** (3.5-4.1 ppm, MeOH-d^{4}).

Although the new species formed could not be isolated, indirect evidence supporting the proposed product is provided by: 1, the intramolecular rearrangement of **23**; 2, the crystal structure of **26**; 3, the ^{1}H NMR spectrum of **26**. Further considerations on these intramolecular rearrangements are given later in this section. Finally, when crystals of **25** were dissolved in a D_2O/MeOH-d^{4} mixture (1:1) a similar spectrum and a similar behavior were observed.

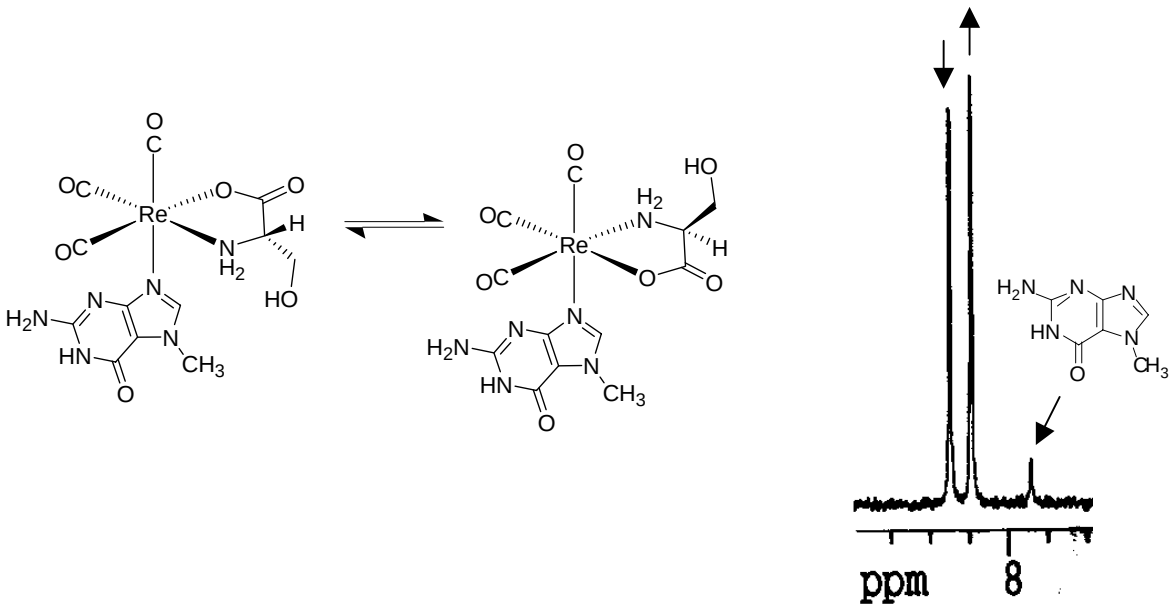

Figure 5.9. ^{1}H NMR spectrum (right, 7.8-8.4 ppm, D_2O:MeOH-d^{4}, 1:1) and proposed intramolecular rearrangement (left) of **24**.

The aromatic region of the ^{1}H NMR spectrum of **26** is shown in Figure 5.10. As mentioned in subsection 5.2.2, crystals of **26** show two independent molecules in the unit cell. When these crystals are dissolved in MeOH-d^4 two sets of resonance are observed for the 3-pic ligand of each conformer of **26**. With time however, a new set of signals corresponding to free 3-pic appears and one of the original sets of signal increases in intensity with respect to the other. It is clear that, as is the case for **24** and **25**, ligand dissociation takes place in **26**. However, since 3-pic is a weaker ligand for **23** than 7-MeG, more free 3-pic is observed. Also, since one of the original sets of resonances increases with respect to the other one of two possibilities must be considered. Either an intramolecular rearrangement is taking place in favor of the more thermodynamically stable conformer of **26**, or 3-pic dissociation refers more predominantly to one of the two conformers.

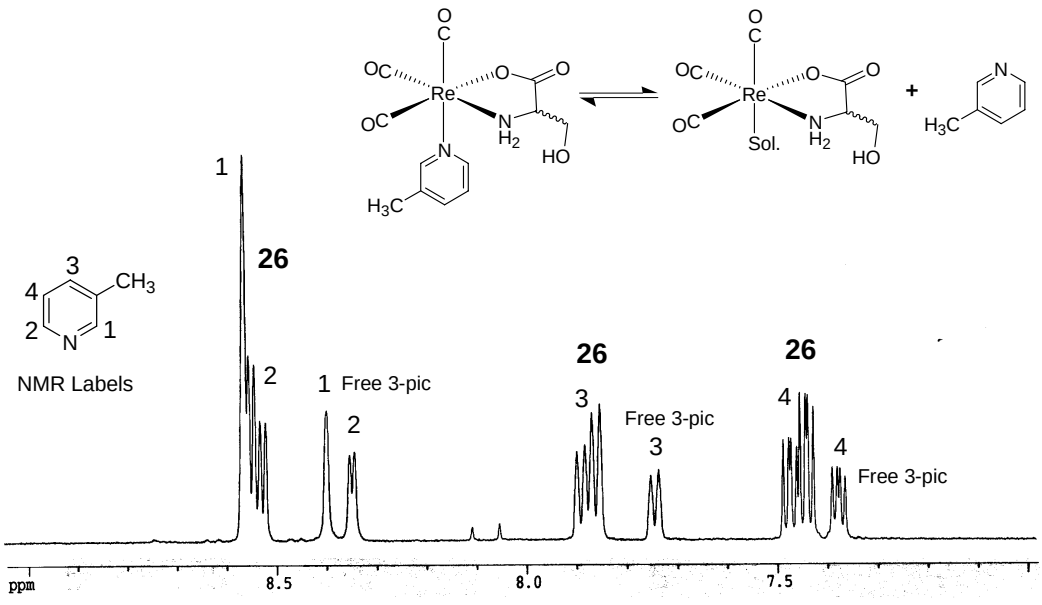

Figure 5.10. ^{1}H NMR spectrum (7.0-9.0 ppm, 1 day, MeOH-d^4) of **26**.

The ^{1}H NMR spectra of **23-26** presented in this section clearly points to an intramolecular rearrangement in the complexes. In the case of **24** and **25** the rearrangement may proceed as shown in Scheme 5.5. Possible protonation of the amino group with 7-MeG dissociation gives Re-N bonds breaking. Deprotonation of the NH_2 group followed by Re-N bonds formation gives the proposed rearrangement product. ^{1}H NMR evidence confirms the presence of free 7-MeG and NH_2-D_2O exchange. Figure 5.11A shows the ^{1}H NMR spectrum (5.3-8.4 ppm) of crystals of **24** taken a few minutes after crystals were dissolved while Figure 5.11B shows the same spectrum taken 24 hours later.

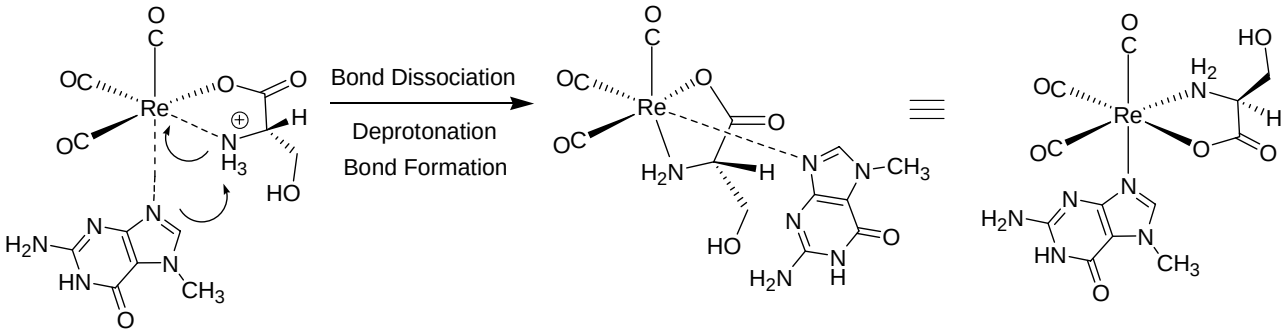

Scheme 5.5. Proposed rearrangement of **24**.

In Figure 5.11A the signals corresponding to the amino group of the coordinated amino acid are visible although rearrangement is already in progress as revealed by the presence of two H8 signals in the aromatic region. After 24h, however, the NH_2 signals disappear indicating that NH_2-D_2O exchange had taken place. Furthermore, the presence of a small H8 signal corresponding to free 7-MeG (of constant relative intensity with respect to the other H8 signals) confirms dissociation of the nitrogenous base. However, if protonation of the NH_2 group does occur this is slower on the NMR time scale than the intramolecular rearrangement as shown in Figure 5.12.

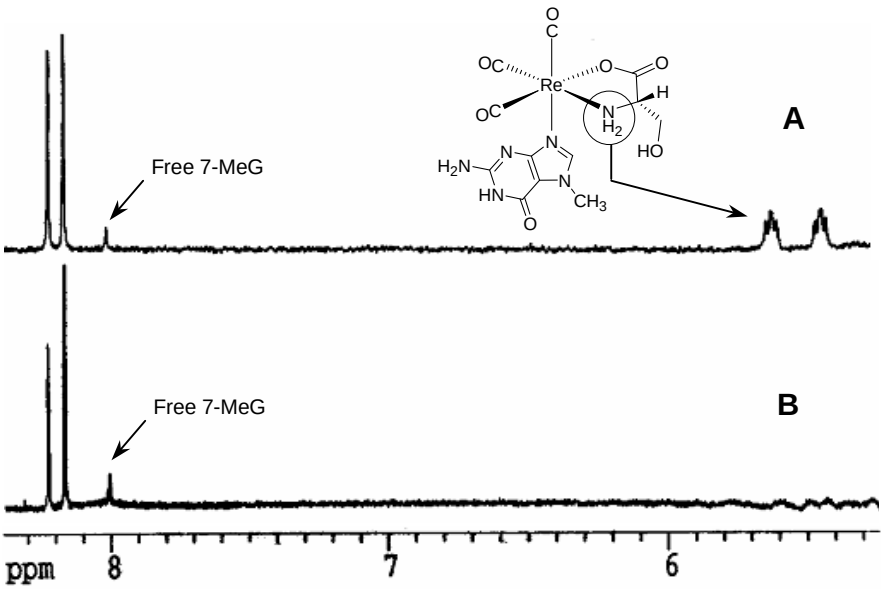

Figure 5.11. A: ^{1}H NMR spectrum (5.3-8.4 ppm, D2O:MeOH-d^4, 1:1) of crystals of **24** taken a few minutes after crystals were dissolved. B: Same ^{1}H NMR spectrum of A taken 24 hours later.

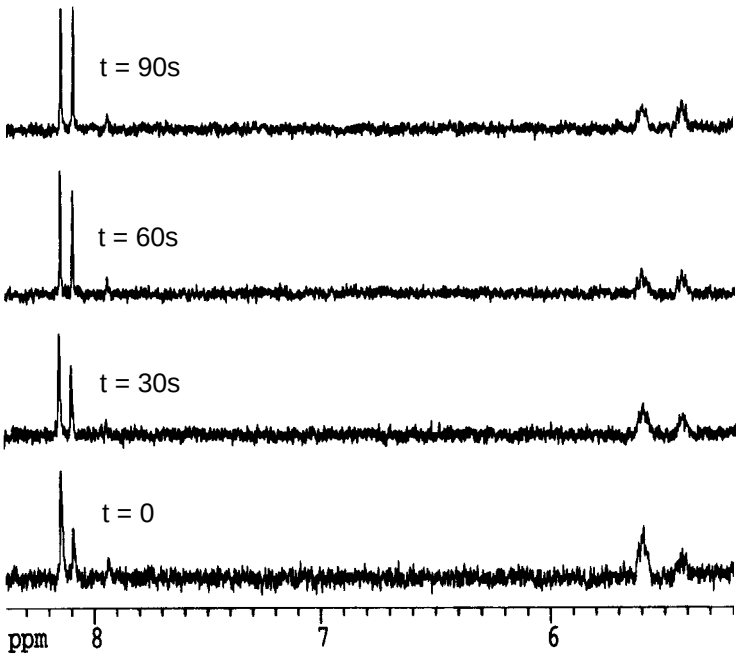

Figure 5.12. ^{1}H NMR spectrum (5.3-8.4 ppm, D2O:MeOH-d^4, 1:1, 30s intervals) of crystals of **24**.

HS Stability of Complexes. The stability of complexes **23-26** in Human Serum (HS) is important to assess the possibility of using the compounds for *in vivo* biological studies. When crystals of **23** are dissolved in HS (final [1mM]) under physiological conditions (37 ^{o}C, O_2) the complex is readily trapped by serum proteins within minutes. The binding of **23** to HS proteins is irreversible as indicated by challenging studies. Once the complex is trapped it is not released when challenged with an excess of imidazole or other rescue agents like sodium diethyldithiocarbamate, over a period of 3 days.

Under the same conditions however, compounds **24** and **25** are stable for hours in HS showing only about 50% decomposition (i.e. reaction with serum proteins) after a 12h incubation period (Figure 5.13B). While in H_2O dissociation of 7-MeG from **24** or **25** establishes the equilibrium depicted in Scheme 5.1 and all species are visible by HPLC (Figure 5.13A), in HS the peak corresponding to the mono bound Re serine species (R_t = 8 min, indicated as **23** in Figure 5.13A) is absent. The absence of the peak corresponding to **23** (see Figure 5.13B and Figure 5.13C) indicates that the Re serine species is trapped by the serum proteins following dissociation of the nitrogenus base.

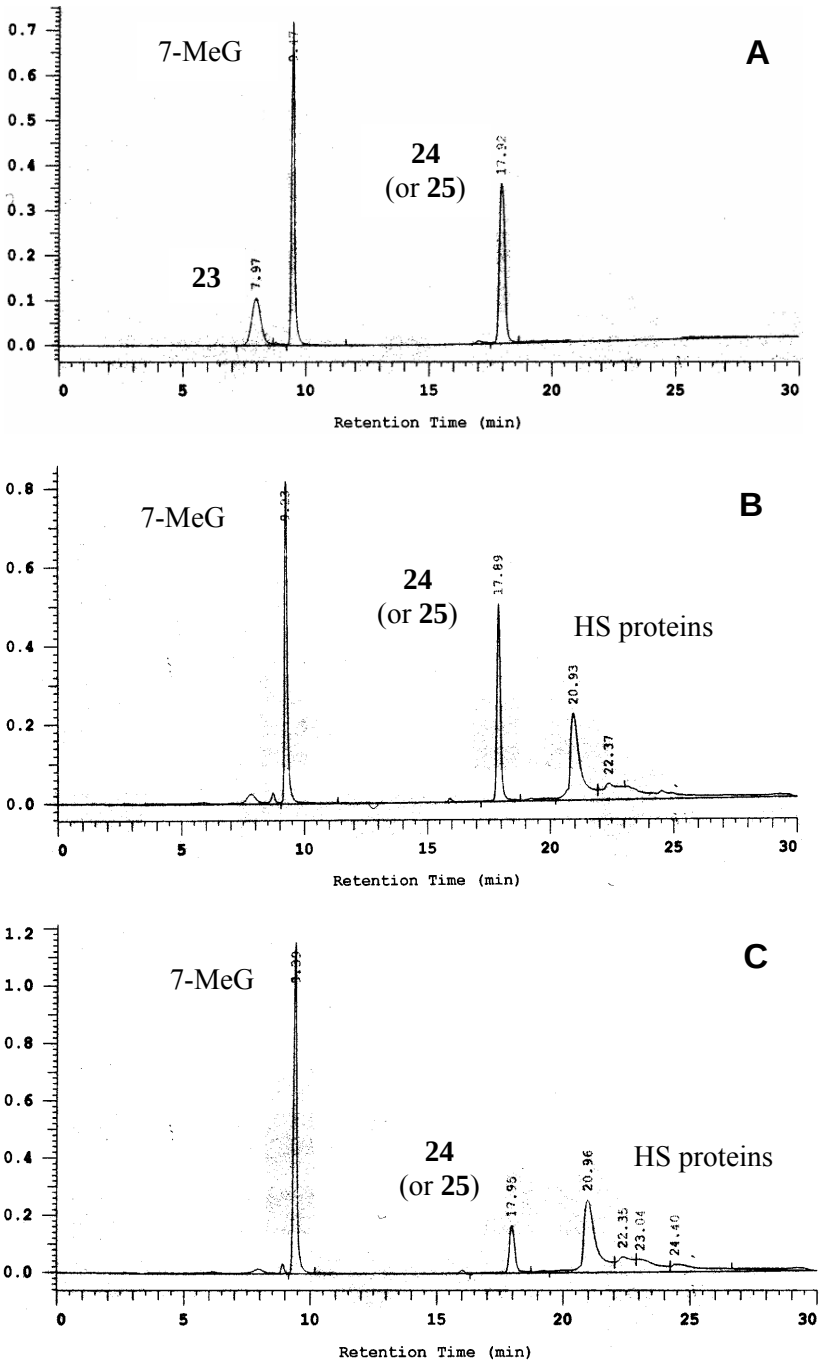

Figure 5.13. A: HPLC chromatogram of a 1mM solution of **24** (or **25**) incubated in H_2O for 24h at 37 ^oC. B: HPLC chromatogram of a 1mM solution of **24** (or **25**) incubated in HS for 12h at 37 ^oC. C: HPLC chromatogram of a 1mM solution of **24** (or **25**) incubated in HS for 24h at 37 ^oC.

Complexes **24** and **25** are however remarkably stable in HS and they are still visible in the HPLC chromatogram after a 24h incubation period (see Figure 5.13C). Compound **26** on the other hand, is completely trapped by the proteins within 12h. Trapping of **26** by HS proteins also follows dissociation of the nitrogenous base as is the case for **24** and **25**.

In order to better appreciate the remarkable HS stability of **24** and **25**, compound **12** ($[Re(H_2O)(7\text{-}MeG)_2(CO)_3](ClO_4)$, see Chapter 1) was subjected to the same study for comparison. Figure 5.14A shows the HPLC chromatogram of a 1mM solution of crystals **12** incubated in H_2O for 1h at 37 ^oC while Figure 5.14B shows the HPLC chromatogram of a 1mM solution of crystals **12** incubated in HS for 1h at 37 ^oC. While in H_2O both the mono bond species $[Re(H_2O)_2(7\text{-}MeG)(CO)_3]^+$ (R_t = 17.3 min) and the bis bound species **12** (R_t = 18 min) are visible, in HS **12** is completely trapped within 1h (Figure 5.14B).

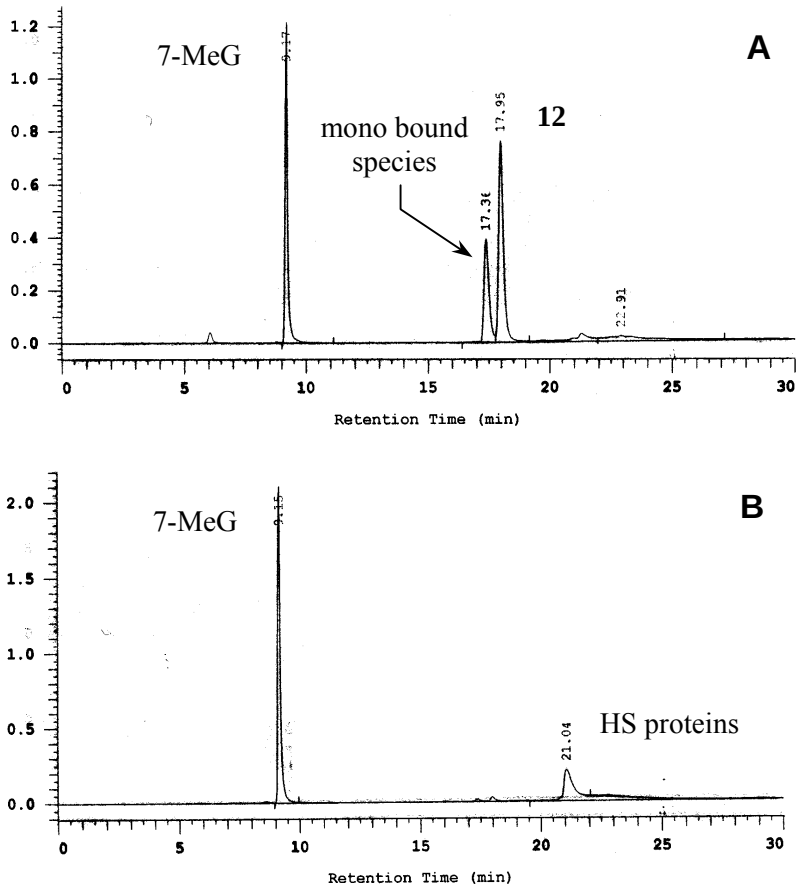

Figure 5.14. A: HPLC chromatogram of a 1mM solution of **12** incubated in H_2O for 1h at 37 ^oC. B: HPLC chromatogram of a 1mM solution of **12** incubated in HS for 1h at 37 ^oC.

Interaction of 24 and 25 with Thymidine Kinase Herpes Simplex Virus Type I (HSV1 TK). Thymidine Kinase Herpes Simplex Virus Type I (HSV1 TK) belongs to a family of viral kinases which phosphorylate thymidine (dT) to thymidine monophosphate (TMP). The protein however also recognizes aciclovir and penciclovir (see Figure 5.15) as substrates for its enzymatic phosphorylation reaction. These molecules are therapeutic compounds that interfere with acute herpes-virus infections by acting as fraudulent substrates of DNA-polymerases blocking viral DNA replication after being activated by HSV1 TK.[29]

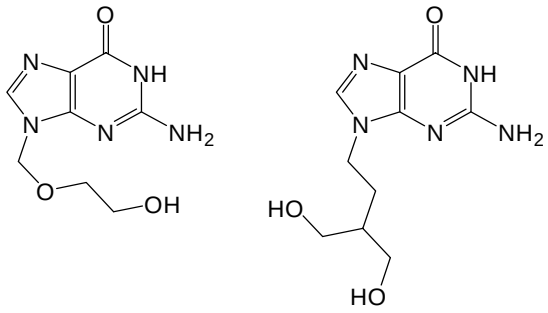

Figure 5.15. Structures of Aciclovir (left) and Penciclovir (right).

Since **24** and **25** were designed as guanosine mimicking complexes, we explored the possibility that HSV1 TK might also recognize these complexes as substrates and catalyze the phosphorylation of the pendent hydroxyl group of the coordinated serine as depicted in Figure 5.16.

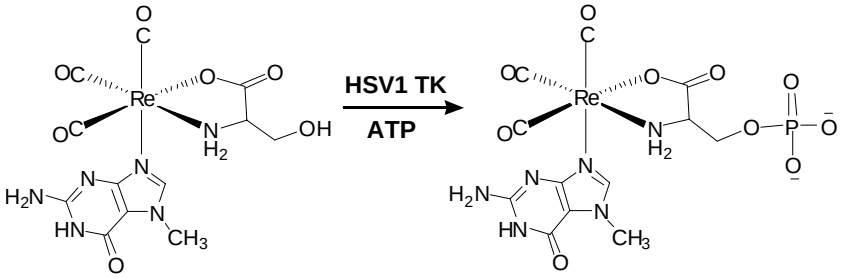

Figure 5.16. Structures of Aciclovir (left) and Penciclovir (right).

Although docking experiments (see Figure 5.17) showed a good fitting of molecules **24** and **25** into the active site of the enzyme, when the compounds were subjected to *in vitro* phosphorylation tests and affinity measurements with HSV1 TK the results showed neither evidence of phosphorylation of **24** or **25** nor inhibition of HSV1 TK activity. Figure 5.18 shows the HPLC

chromatogram of the reaction mixture of the phosphorylation assay. At the end of the reaction the peak corresponding to **24** or **25** (R_t = 2.6 min) remains unchanged indicating that no phosphorylation of the pendent hydroxyl group of the coordinated serine had taken place. Furthermore, the appearance of peaks at 4.6 and 7.2 min points to ADP and TMP production respectively, indicating no inhibition of HSV1 TK activity.

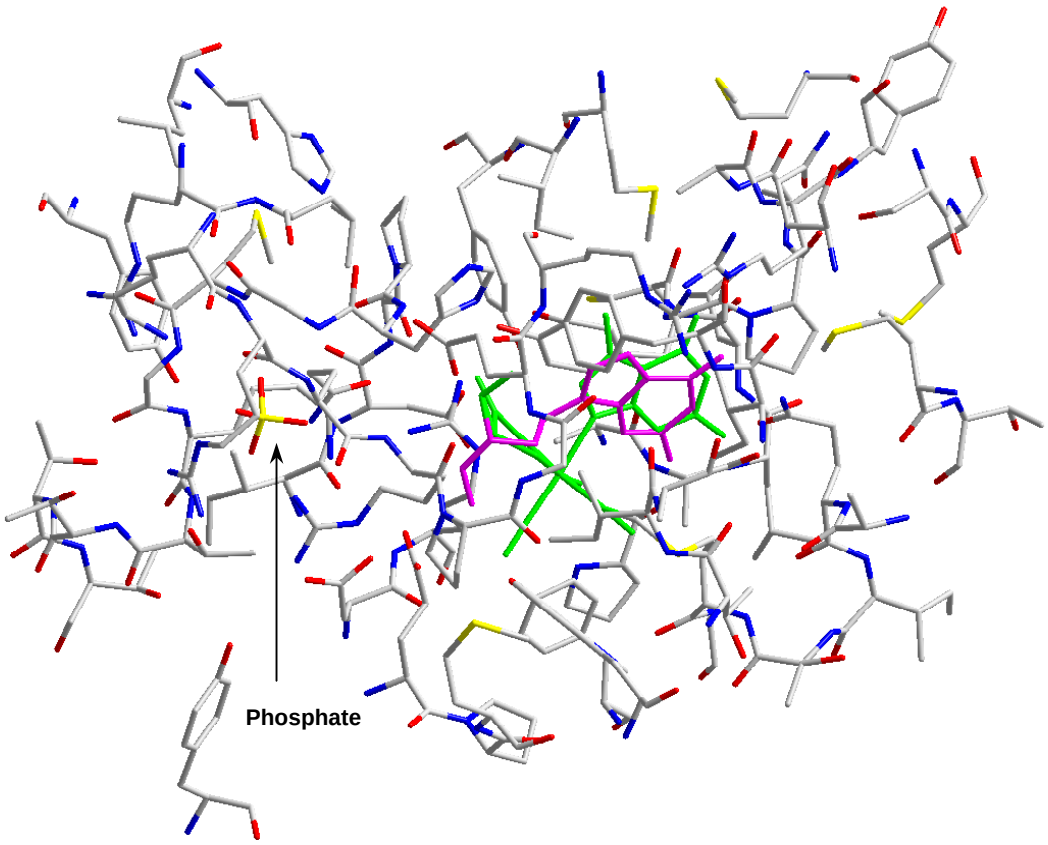

Figure 5.17. Crystal structure of active site of HSV1 TK containing a penciclovir molecule[30] (violet) with the crystal structure of **24** (green) fitted upon it.

While the lack phosphorylation of the pendent hydroxyl group of the coordinated serine might be explained by the fact that in the active site of the enzyme the serine arm is to far away from the phosphate group (about 7.4 Å while the distance of the penciclovir OH group is about 5.3 Å, see Figure 5.19) the lack of inhibition of HSV1 TK activity suggests that **24** and **25** are not substrates for HSV1 TK.

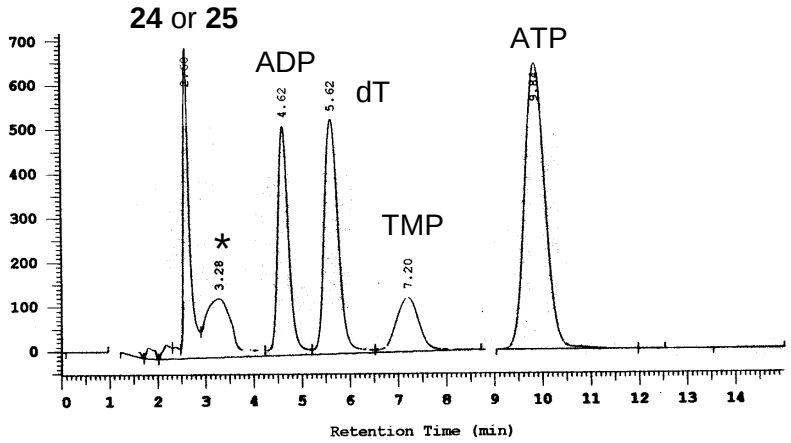

Figure 5.18. HPLC chromatogram of **24** and **25** of *in vitro* phosphorylation assay and affinity measurements with HSV1 TK. * is EDTA.

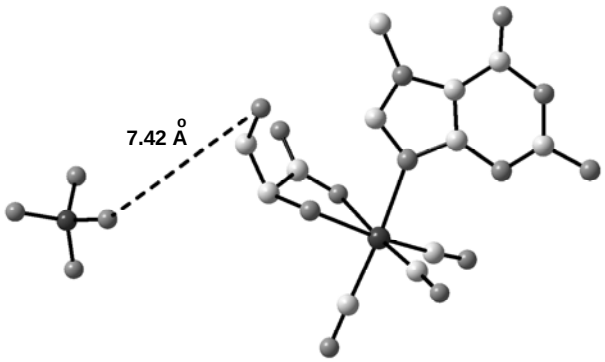

Figure 5.19. Distance of the pendent hydroxyl group of the coordinated serine of **24** from phosphate group in the active site of HSV1 TK. Obtained from docking experiments on the X-ray structure of HSV1 TK.

Interaction of 23, 24 and 25 with ΦX174 Plasmid DNA. The analysis of the binding and of the influence of different Re compounds on the tertiary structure of DNA, determined by their ability to alter the electrophoretic mobility of the open circular and supercoiled form ΦX174 DNA, was described in Chapter 2 (section 2.2.3). Here the results of analogous experiments performed with complexes **23-25** are given. Figure 5.19 shows the mobility of native ΦX174 plasmid DNA and plasmid DNA (abbreviated as pDNA) incubated with compound **23**, **24**, and **25**. None of the

compounds tested induces the increase in mobility of pDNA. In agreement with what described in Chapter 2, these results confirm that two available coordination sites are necessary to induce the DNA shift in mobility.

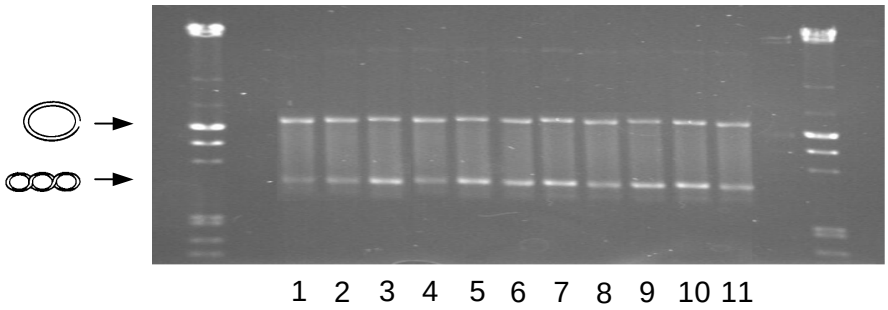

Figure 5.19. Electrophoresis in 0.75% agarose gel of ΦX174 DNA (5 nM) incubated with various concentrations of **23** (lanes 2-4), **24** (lanes 5-7), **25** (lanes 8-10). Lanes 1 and 11 reference ΦX174 DNA. r_b levels for lanes 2-11: (2, 5, 8) 0.018; (3, 6, 9) 0.18; (4, 7, 10) 1.8.

Hydrogen Bonding. Structures **23-26** show extensive hydrogen-bonding interactions in the solid state. In complex **23** the NH_3^+ group of the mono coordinated L-Ser is mainly involved hydrogen-bonding, making four types of unique interactions with four distinct oxygen atoms. The NH_3^+ group forms one hydrogen bond with O1 (oxygen atom of the N,O-chelate) of an adjacent molecule, two bonds with the carboxylate oxygens O2 and O5 of the N,O-chelate and of the mono bound zwitter ion respectively, and one final bond with the pendent hydroxyl group of the bidentate coordinated serine. These interactions are shown in Figure 5.20. Other hydrogen bonds are formed between the oxygen and nitrogen atoms of the N,O-chelate and the OH groups of both coordinated serines but these are not shown for clarity.

Similar atoms are involved in the hydrogen-bonding interactions of complex **26**. Since the pyridine base does not offer any sites to form bonds described in this section, in the crystal structure one finds only intermolecular hydrogen bonds between the amino protons of **26A** and neighbouring carboxylate groups or the pendent CH_2OH arm of **26B**, and a strong interaction between the OH group of the CH_2OH arm of **26A** and the neighbouring carboxylate group of **26B**. These interactions are shown in Figure 5.21. These types of interactions are common for metal carbonyl complexes of amino acids and have been described before.

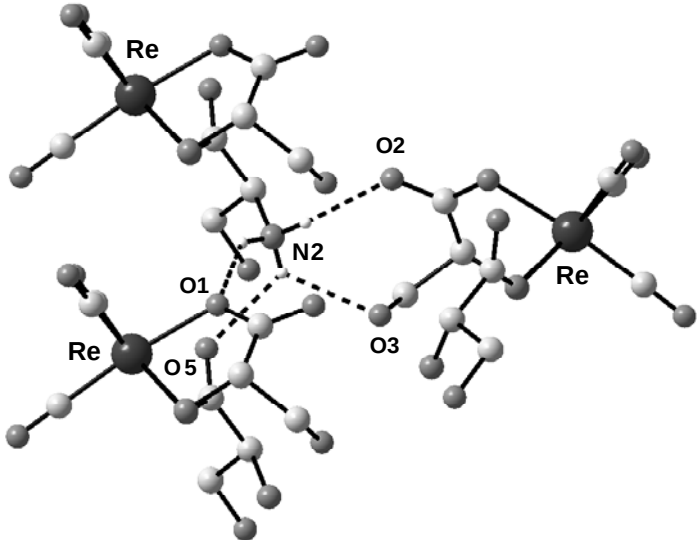

Figure 5.20. Intermolecular hydrogen bonding in complexes **23**. Labels are as in Figure 5.3.

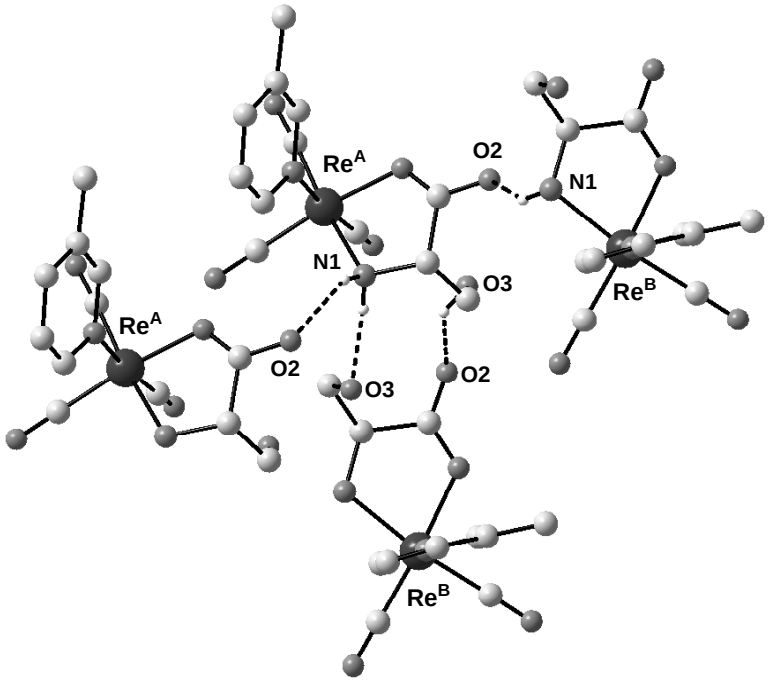

Figure 5.21. Intermolecular hydrogen bonding in complexes **26**. Labels are as in Figure 5.6.

Molecules **24** and **25** also show an extensive network of intermolecular hydrogen-bonding interactions between amino acids residues but also between the guanines and the amino acids. Different types of such interactions for **24** are shown in Figure 5.22. Hydrogen bonds between amino acids residues are comparable to those described for **23** and **26** involving again the amino

protons and neighbouring carboxylate groups or the pendent CH_2OH arm. The proton bound to N1 in **24A** forms a bond with an adjacent **24A** carboxylate O2 while the protons of the extracyclic $N2H_2$ group in **24A** are found bridging the hydroxyl groups of the serine arm of **24A** and **24B**. The average mean distances for these interactions are N1H-O1 = 2.068(6) Å and N2H-O2 = 1.992(3) Å. The same protons in **24B** (i.e. N1 and the protons of the extracyclic NH_2 group) only participate in hydrogen-bonding interactions with solvent molecules which are not shown in Figure 5.22 for clarity.

In the closely related [Re(Pro)(9-MeG)$(CO)_3$] complex (**15**, see Chapter 2) the proton bound to N1 and one of the protons of the extracyclic $N2H_2$ group were always found forming a hydrogen bond with the oxygens O1 and O2, respectively, of the carboxylate group of the coordinated proline. In **24** however, this is not the case. The presence of the CH_2OH arm of the chelate amino acid, which offers further sites to promote these interactions, and the different coordination geometry of 7-MeG compared to 9-MeG create a completely different hydrogen-bonding network.

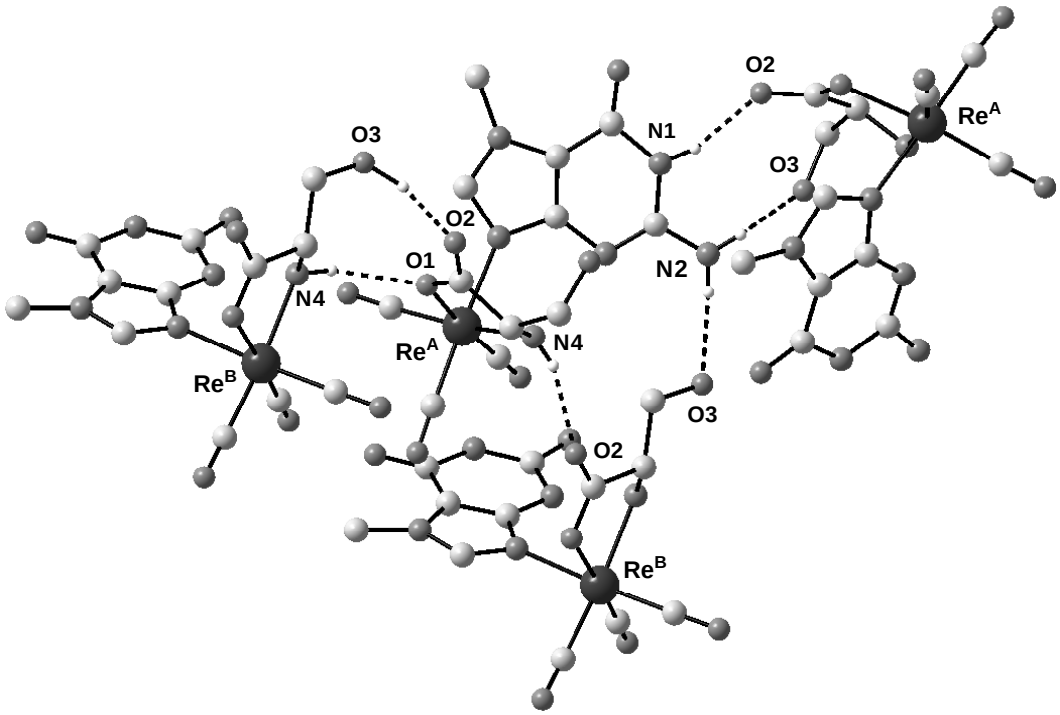

Figure 5.22. Intermolecular hydrogen bonding in complexes **24**. Labels are as in Figure 5.4.

5.2 Conclusion

It was shown in this chapter that $[Re(CO)_3]^+$-based nucleoside mimicking complexes can be obtained from the reaction of the appropriate nitrogenous base with the serine complex of the above mentioned tricarbonyl core. The compounds show an interesting solution behavior displaying an intramolecular rearrangement which, to our knowledge, has never been described for octahedral organometallic complexes in which the α-aminocarboxylate ligand is bound as a N,O-chelate.

Compounds where the nitrogenous base is 7-MeG are remarkably stable in Human Serum (HS) showing only about 50% decomposition (i.e. reaction with serum proteins) after 12h and being still visible in the HPLC chromatogram after a 24h incubation period. When the same compounds were subjected to *in vitro* phosphorylation tests and affinity measurements with HSV1 TK neither evidence of phosphorylation of pendent serine arm nor inhibition of HSV1 TK activity was seen. In agreement with the results presented in Chapter 2, none of the nucleoside mimicking complexes influence the tertiary structure of ΦX174 DNA as determined by their inability to alter the electrophoretic mobility of the open circular and supercoiled form of plasmid DNA.

However, the remarkable HS stability of the guanosine mimicking makes the compounds potentially useful inorganic medicinal drugs. In our vision, they may actively participate in the biochemistry at the desired target tumor site provided that they are able to accumulate to a sufficient extent in the cell and in the nucleus in particular and provided that they are substrates for enzymes involved in DNA synthesis.

5.3 References

(1) Liu, S.; Edwards, D. S. *Chem. Rev.* **1999**, *99*, 2235-2268.

(2) Baidoo, K. E.; Scheffel, U.; Stathis, M.; Finley, P.; Lever, S. Z.; Zhan, Y. G.; Wagner, H. N. *Bioconjugate Chem.* **1998**, *9*, 208-217.

(3) Hnatowich, D. J.; Qu, T.; Chang, F.; Ley, A. C.; Ladner, R. C.; Rusckowski, M. *J. Nucl. Med.* **1998**, *39*, 56-64.

(4) Breitz, H. B.; Weiden, P. L.; Vanderheyden, J. L.; Appelbaum, J. W.; Bjorn, M. J.; Fer, M. F.; Wolf, S. B.; Ratliff, B. A.; Seiler, C. A.; Foisie, D. C.; Fisher, D. R.; Schroff, R. W.; Fritzberg, A. R.; Abrams, P. G. *J. Nucl. Med.* **1992**, *33*, 1099-1112.

(5) Visser, G. W. M.; Gerretsen, M.; Herscheid, J. D. M.; Snow, G. B.; Vandongen, G. *J. Nucl. Med.* **1993**, *34*, 1953-1963.

(6) Edwards, D. S.; Liu, S.; Harris, A. R.; Poirier, M. J.; Ewels, B. A. *Bioconjugate Chem.* **1999**, *10*, 803-807.

(7) Srivastava, S. C.; Mease, R. C. *Nucl. Med. Biol.* **1991**, *18*, 589-603.

(8) Meares, C. F. *Nucl. Med. Biol.* **1986**, *13*, 311-318.

(9) Liu, Y. F.; Wu, C. C. *Pure Appl. Chem.* **1991**, *63*, 427-463.

(10) Dilworth, J. R.; Parrott, S. J. *Chem. Soc. Rev.* **1998**, *27*, 43-55.

(11) Giblin, M. F.; Wang, N.; Hoffman, T. J.; Jurisson, S. S.; Quinn, T. P. *Proc. Natl. Acad. Sci. USA* **1998**, *95*, 12814-12818.

(12) Egli, A.; Alberto, R.; Tannahill, L.; Schibli, R.; Abram, U.; Schaffland, A.; Waibel, R.; Tourwe, D.; Jeannin, L.; Iterbeke, K.; Schubiger, P. A. *J. Nucl. Med.* **1999**, *40*, 1913-1917.

(13) Alberto, R.; Schibli, R.; Egli, A.; Schubiger, A. P.; Abram, U.; Kaden, T. A. *J. Am. Chem. Soc.* **1998**, *120*, 7987-7988.

(14) Alberto, R.; Schibli, R.; Waibel, R.; Abram, U.; Schubiger, A. P. *Coord. Chem. Rev.* **1999**, *192*, 901-919.

(15) Ioganson, A. A. *Russ. Chem. Rev.* **1985**, *54*, 277-292.

(16) Zhou, Y. L.; Wagner, B.; Polborn, K.; Sunkel, K.; Beck, W. *Z. Naturforsch. B* **1994**, *49*, 1193-1202.

(17) Cavoli, P.; Graziani, R.; Casellato, U.; Uguagliati, P. *Inorg. Chim. Acta* **1986**, *111*, L35-L37.

(18) Erickson, L. E.; Brower, D. C. *Inorg. Chem.* **1982**, *21*, 838-840.

(19) Nance, L. E.; Frye, H. G. *J. Inorg. Nucl. Chem.* **1976**, *38*, 637-639.

(20) Carturan, G.; Uguaglia.P; Belluco, U. *Inorg. Chem.* **1974**, *13*, 542-546.

(21) Konya, K.; Fujita, J.; Nakamoto, K. *Inorg. Chem.* **1971**, *10*, 1699-1702.

(22) Darensbourg, D. J.; Draper, J. D.; Reibenspies, J. H. *Inorg. Chem.* **1997**, *36*, 3648-3656.

(23) Darensbourg, D. J.; Atnip, E. V.; Klausmeyer, K. K.; Reibenspies, J. N. *Inorg. Chem.* **1994**, *33*, 5230-5237.

(24) Severin, K.; Sunkel, K.; Beck, W. *Chemische Berichte* **1994**, *127*, 615-620.

(25) Werner, H.; Daniel, T.; Knaup, W.; Nurnberg, O. *J. Organomet. Chem.* **1993**, *462*, 309-318.

(26) Zhou, Y. L.; Beck, W. *J. Organomet. Chem.* **1994**, 479, 217-220.

(27) Meder, H. J.; Beck, W. *Z. Naturforsch. B* **1986**, 41, 1247-1254.

(28) Ru(CO)3 gly pro ref

(29) Pospisil, P.; Pilger, B. D.; Marveggio, S.; Schelling, P.; Wurth, C.; Scapozza, L.; Folkers, G.; Pongracic, M.; Mintas, M.; Malic, S. R. *Helv. Chim. Acta* **2002**, *85*, 3237-3250.

(30) Bennett, M. S.; Wien, F.; Champness, J. N.; Batuwangala, T.; Rutherford, T.; Summers, W. C.; Sun, H. M.; Wright, G.; Sanderson, M. R. *Febs Letters* **1999**, *443*, 121-125.

Chapter 6. Cytotoxicity of Re^{I} Complexes

One of the main structure-activity relationship for antitumor active platinum compounds is the presence of two cis-coordinated leaving groups e.g. chloride ions.[1, 2] In the previous chapters it was demonstrated that the *fac*-$[Re(CO)_3]^+$ moiety displays a principally similar reactivity pattern with plasmid DNA as e.g. cisplatin implying a possible interaction with adjacent guanines in DNA as well. It was also shown that **1** forms stable adducts with d(GpG) and d(CpGpG) via coordination of the N7 atom of guanine residues. If the coordination of rhenium complexes to biologically relevant ligands such as DNA bases is important for its biologically activity, one expects that complexes with two exchangeable cis-coordinated leaving groups would show higher cytotoxicity than complexes lacking this feature.

In this brief chapter, the cytotoxicity of different rhenium complexes toward B16 F1 mouse melanoma cells is presented. A new compound, namely $[Re(L\text{-}Tryp)_2(CO)_3]$ (**27**), obtained from the reaction of **1** with the amino acid L-Tryptophan (L-Tryp) is also introduced. The series of rhenium compounds investigated in this study may be divided in two major categories: molecules with at least two exchangeable cis-coordinated ligands and molecules with one or no exchangeable ligands. Complexes belonging to the first category are **1**, **10**, **14**, **22a** and **22b**; all others belong to the second category. Compounds **1**, **10**, and **14** were shown in Chapter 2 to be ale to alter the tertiary structure of plasmid DNA by covalently binding to two DNA bases while the remaining molecules did not.

6.1 Results and Discussion

Complex **27** was synthesized as a lipophilic analog of $[Re(L\text{-}Ser)_2(CO)_3]_3$ (**23**), described in section 5.2.1. Crystal data and experiment details are listed in the crystallography section. The crystals structure of compound **27** is shown in Figure 6.1. The molecule crystallizes in the triclinic space group P1. The geometry around rhenium is octahedral with one face occupied by three carbonyl ligands and the other three coordination sites occupied by two L-Tryp. One of the two amino acids is bound in a bidentate fashion with Re-N1 and Re-O1 distances of 2.221(13) and 2.085(9) Å. The other amino acid is bound as a zwitter ion in a monodentate fashion via the carbonyl oxygen labelled O3 in Figure 6.1. The Re-O3 bond distance is 2.150 (13) Å longer than the Re-O1 distance in the bidentate coordinated L-Tryp.

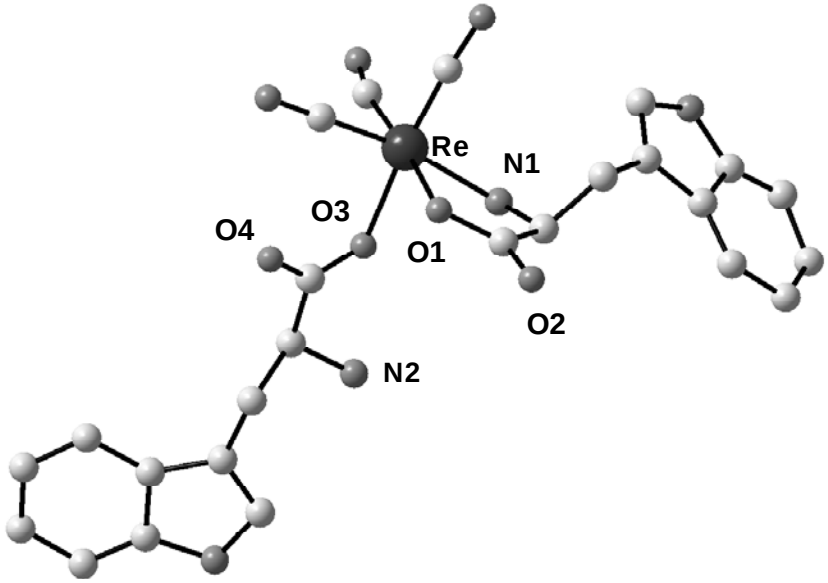

Figure 6.1. Crystal structure of [Re(L-Tryp)$_2$(CO)$_3$] (**27**). Selected bond distances (Å) and angles (deg) are the following: Re-N1 2.220(21), Re-O1 2.088(27); Re-O3 2.151 (19), N1-Re-O1 77.54 (76), N1-Re-O3 76.40 (66), O1-Re-O3 83.48 (71).

Cell proliferation was analyzed by the non-radioactive, colorimetric assay system using XTT, which was first described by Scudiero *et al.*[3, 4] and improved in subsequent years by other investigators.[5, 6] The assay is designed, among other applications, for measurement of cytotoxicity or the assessment of cytotoxic or growth inhibiting agents. The analysis is based on the cleavage of the yellow tetrazolium salt XTT to form an orange formazan dye by metabolic active cells. Therefore, this conversion only occurs in viable cells. The formazan dye is soluble in aqueous solutions and it was directly quantified by a spectrophotometer.

In a typical experiment (Figure 6.2) an average of 2000 cells were grown in microtiter plates (tissue culture grade, 96 wells, flat bottom) in a final volume of 100 µL culture medium per well in a humidified atmosphere (37 ^{o}C, >6.5% CO_2). After 24 h the rhenium complex was added to the wells (final concentrations 200 µM) and the cells were grown for further 24 h under a humidified atmosphere. After the incubation period 50 µL of the XTT labeling mixture were added to each well. The plates were incubated again for 4 h. After the this final incubation period the spectrophotometrical absorbance (optical density OD) of each well was measured at 450 nm.

Control experiments were performed as described above without the addition of the rhenium compounds. Blanks were obtained by adding 50 µL of H_2O instead of the XTT labeling mixture. Experiments were done in double and the results represent the average. The % of cell survival was calculated base on the relative OD of the samples. Maximum control OD was set to 100% cell survival.

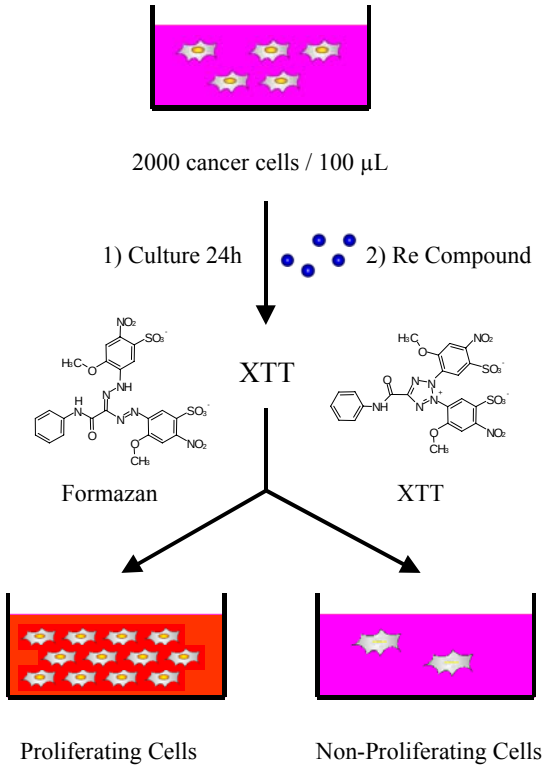

Figure 6.2. Scheme of a typical XTT cell proliferation assay.

Cytotoxicity data of the Re complexes investigated in this study are listed in table 6.1 while Figure 6.3 shows a graphic representation of the same data. With the exception of **1** and **19**, all complexes show low cytotoxicity (i.e. % of cell survival > 50). No structure-activity relationships

Table 6.1. Cytotoxicity of Rhenium complexes, expressed as % of cell survival.[a]

Compound	**1**[b]	**10**[b]	**13**[c]	**14**[c]	**18**[c]	**19**[b]	**22a**[d]	**22b**[d]	**23**[b]	**24**[e]	**25**[e]	**27**[e]
% Cell Survival	25	80	91	71	100	20	83	83	78	91	88	86

[a] $\sigma = \pm 5\%$. [b] in H_2O, 200 µM. [c] in H_2O:MeOH (9:1), 200 µM. [d] in H_2O, 100 µM. [e] in H_2O:MeOH (9:1), 150 µM.

can be extrapolated from the results as both compounds belonging to the first category (i.e. molecules with two exchangeable cis-coordinated ligands) and compounds belonging to the second category (i.e. molecules with one or no exchangeable ligands) show comparable low cytotoxicity. Increased lipophilicity also does not seem to improve the cytotoxic index as both **23** and **27** seem to have very little effect on cell proliferation. The more hydrophilic compound **23** shows a slightly better inhibition of cell growth than **27** although the concentration of the former is higher. For all practical purposes, however, the molecules do not seem to inhibit cancer proliferation.

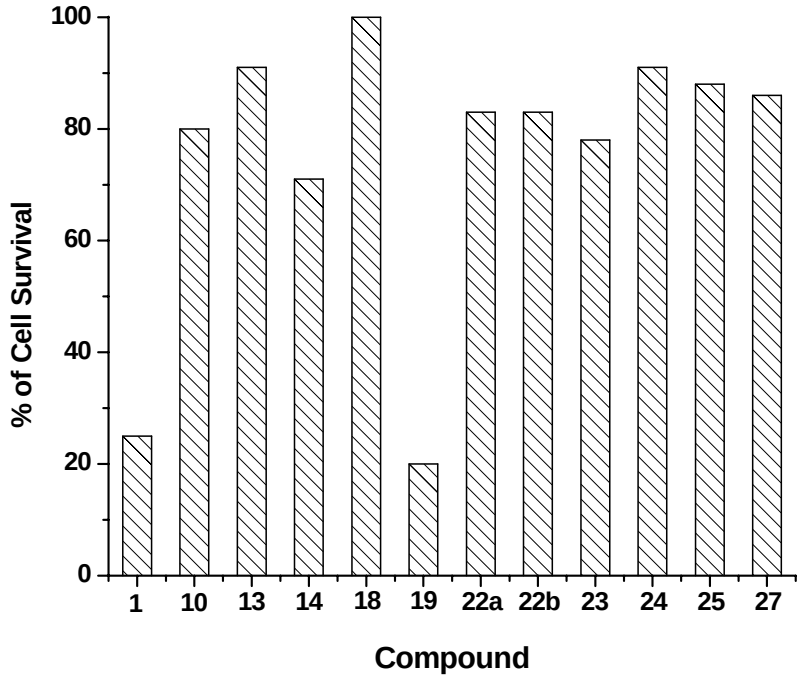

Figure 6.3. Cytotoxicity of Rhenium complexes, expressed as % of cell survival ($\sigma = \pm 5\%$).

Cell proliferation is best inhibited by compounds **1** and **19** which show high cytotoxicity (i.e. % of cell survival < 30) at 200 μM concentration. While it is not possible at the present stage to indicate a mode of action of these molecules, the high kinetic stability of complex **19** rules out possible ligand exchange and inner sphere coordination to biologically relevant ligands such as DNA. While complex **19** might act as an inhibitor in a biochemical pathway, complex **1** might target DNA or peptide residues of proteins.

The cytotoxic effects of **19** came to us as a striking result. Following cisplatin, some of the most promising metal based anticancer agents are [ImH][*trans*-$RuCl_4(Im)_2$], ICR,[7-9] and [ImH][*trans*-$RuCl_4$(DMSO)(Im)], NAMI-A (where Im = Imidazole)[10-12] which both contain imidazole as a

ligand. While structure-function studies have demonstrated, at least for NAMI-A, that the biological activity of the molecule is strictly related to the progressive release of one or more of its chloride ligands, it has also been shown that by replacing Im for thiazole the compounds become virtually noncytotoxic, demonstrating that Im is crucial for the activity of the drug.[13]

These considerations prompted us to study in more details the interaction of Im complexes of rhenium with DNA bases. To this end complex $[Et_4N][ReBr_2(Im)(CO)_3]$ (**28**), synthesized according to reported procedures,[14] was reacted with 9-MeG after precipitation of the halides with

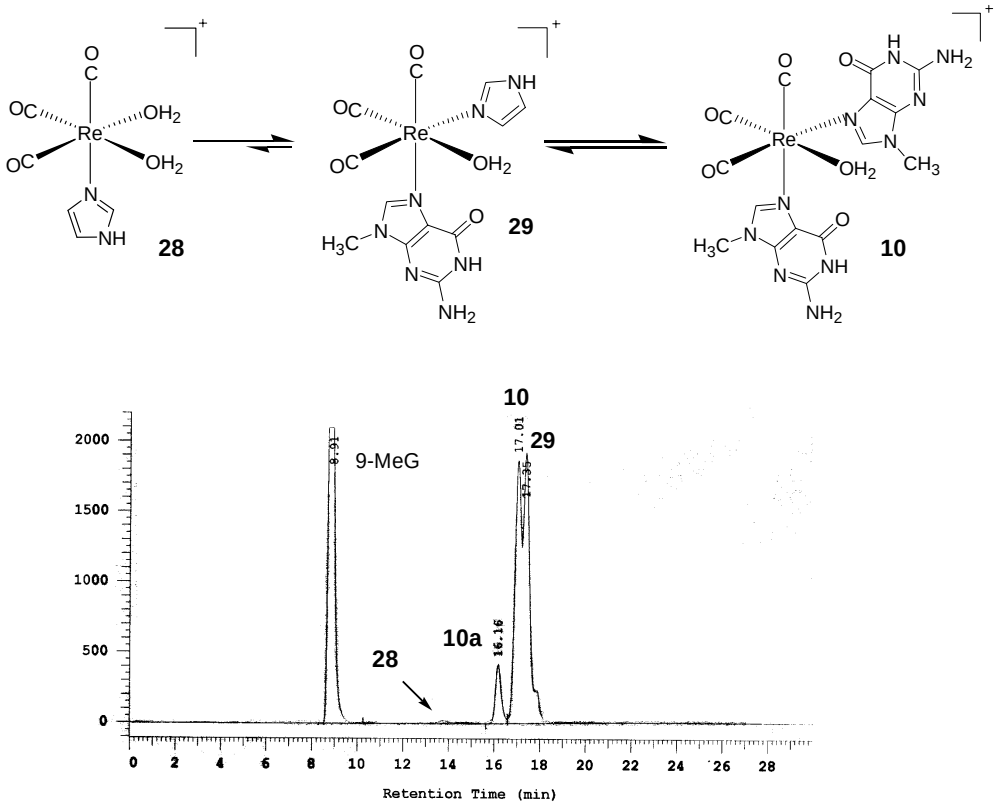

Figure 6.4. Scheme and HPLC chromatogram of reaction of **28** with 2.2 eq. of 9-MeG (24h, 37 °C).

$AgNO_3$. In a water, (37 °C) **28** reacts with 9-MeG stepwise. In our HPLC gradient complex **28** has a retention time (rt) of 13.9 min (see Figure 6.4). After 1h a second peak is observed with rt of 17.4 min. HPLC-MS chromatography indicates that this species is $[Re(Im)(9\text{-MeG})(H_2O)(CO)_3]$ (**29**). After a further 12h a third and a fourth peak appear at 17.0 and 16.2 min which were identified by HPLC-MS chromatography as $[Re(9\text{-MeG})_2(H_2O)(CO)_3]^+$ (**10**) and $[Re(9\text{-MeG})(H_2O)_2(CO)_3]^+$ (**10a**) respectively. The relative height of the peaks, with species **10** and **10a** increasing in

concentration, gave the only other change observed after a further 12h period of incubation. Also observed in the HPLC chromatogram is a shoulder at ~18 min which may be assigned to the intermediate $[Re(Im)(9\text{-}MeG)_2(CO)_3]$ species, however, our data are not conclusive. The results suggest that imidazole also might be a ligand for a model Re pro-drug protecting the $[Re(CO)_3]^+$ core from reacting with coordinating sites in blood proteins.

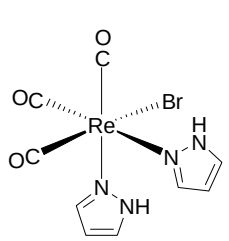

30

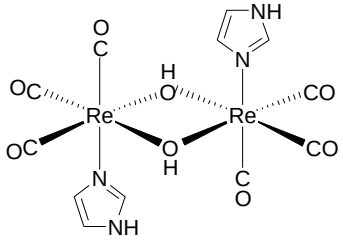

31

Table 6.2. Cytotoxicity of Rhenium complexes, expressed as % of cell survival.[a]

Compound	**cisplatin**[b]	**1**[b]	**19**[b]	**28**[b]	**30**[b]	**31**[b]
% Cell Survival	11	28	25	43	21	20

[a] $\sigma = \pm 10\%$. [b] in H_2O, 200 μM based on Re.

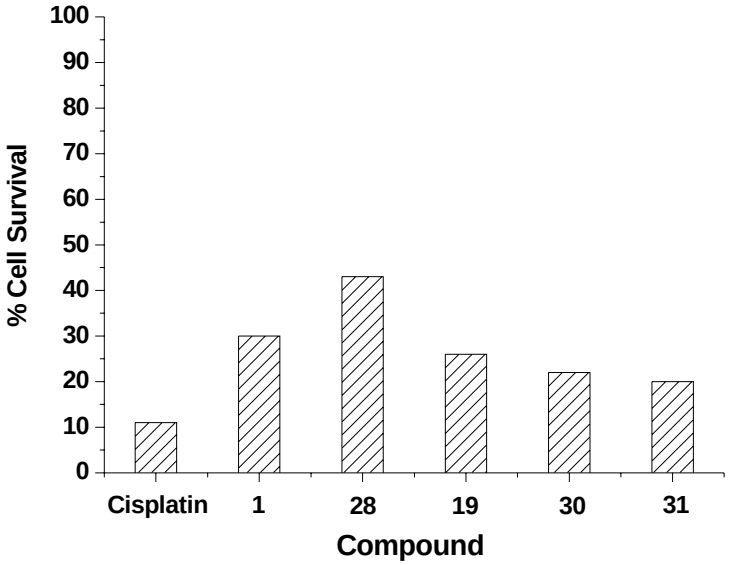

Figure 6.5. Cytotoxicity of Im and HPz Re complexes, expressed as % of cell survival ($\sigma = \pm 10\%$).

Complex **28**, together with complexes $[ReBr(HPz)_2(CO)_3]$ (**30**) and $[Re_2(\mu\text{-}OH)_2(Im)_2(CO)_6]$ (**31**), synthesized according to published procedures,[14, 15] was the subjected to cell proliferation studies. Cytotoxicity data of this second set of Re complexes are listed in table 6.2 while Figure 6.5 shows a graphic representation of the same data. Cell proliferation is inhibited (i.e. % of cell survival < 30) by compounds all compounds bearing at least one Im or HPz ligand but **28**. While it is not possible at the present stage to make any definitive conclusions, the results seem to suggest that, as in the case of Ru-based anticancer agents, five-membered imidazole/pyrazole type rings might also be significant for the antiproliferative activity of Re compounds.

6.2 Conclusion

In this brief chapter the cytotoxicity of a series of Re complexes toward B16 F1 mouse melanoma cells was presented. No structure-activity relationship can be extrapolated from the results as both compounds with two exchangeable cis-coordinated ligands and compounds with one or no exchangeable ligands show comparable activity. However, compounds bearing at least one Im or HPz ligand generally best inhibit cell proliferation. The results suggest that Im or HPz might be ligands for a model Re pro-drug protecting the $[Re(CO)_3]^+$ core from reacting with coordinating sites in blood proteins.

6.3 References.

(1) Lippert, B. *Cisplatin. Chemistry and Biochemistry of a Leading Anticancer Drug*; Verlag Helvetica Chimica Acta, Zurich; Wiley-VCH:Weinheim, **1999**.

(2) Reedijk, J. *Chem. Commun.* **1996**, 801-806.

(3) Paull, K. D.; Shoemaker, R. H.; Boyd, M. R.; Parsons, J. L.; Risbood, P. A.; Barbera, W. A.; Sharma, M. N.; Baker, D. C.; Hand, E.; Scudiero, D. A.; Monks, A.; Alley, M. C.; Grote, M. *J. Heterocyclic Chem.* **1988**, *25*, 911-914.

(4) Scudiero, D. A.; Shoemaker, R. H.; Paull, K. D.; Monks, A.; Tierney, S.; Nofziger, T. H.; Currens, M. J.; Seniff, D.; Boyd, M. R. *Cancer Res.* **1988**, *48*, 4827-4833.

(5) Weislow, O. S.; Kiser, R.; Fine, D. L.; Bader, J.; Shoemaker, R. H.; Boyd, M. R. *J Nat. Cancer Inst.* **1989**, *81*, 577-586.

(6) Roehm, N. W.; Rodgers, G. H.; Hatfield, S. M.; Glasebrook, A. L. *J. Immunol. Met.* **1991**, *142*, 257-265.

(7) Depenbrock, H.; Schmelcher, S.; Peter, R.; Keppler, B. K.; Weirich, G.; Block, T.; Rastetter, J.; Hanauske, A.-R. *Eur. J. Cancer* **1997**, *33*, 2404-2410.

(8) Keppler, B. K.; Lipponer, K. G.; Stenzel, B. in *Metal Complexes in Cancer Chemotherapy*; VCH: Weinheim, Germany, **1993**; p. 187-220.

(9) Galeano, A.; Berger, M. R.; Keppler, B. K.*Arzneim.-Forsch.* **1992**, *42*, 821-824.

(10) Alessio, E.; Balducci, G.; Lutman, A.; Mestroni, G.; Calligaris, M.; Attia, W. M. *Inorg. Chim. Acta* **1993**, *203*, 205-217.

(11) Sava, G.; Clerici, K.; Capozzi, I.; Cocchietto, M.; Gagliardi, R.; Alessio, E.; Mestroni, G.; Perbellini, A. *Anti-Cancer Drugs* **1999**, *10*, 129-138.

(12) Sava, G.; Gagliardi, R.; Bergamo, A.; Alessio, E.; Mestroni, G. *Anticancer Res.* **1999**, *19*, 969.

(13) Mura, P.; Camalli, M.; Messori, L.; Piccioli, F.; Zanello, P.; Corsini, M. *Inorg. Chem.* **2004**, *43*, 3863-3870.

(14) Schibli, R. *Ph. D. Thesis*, P.S.I., Basel, **1996**, p. 136-137.

(15) Ardizzoia, G. A.; LaMonica, G.; Maspero, A.; Moret, M.; Masciocchi, N. *Eur. J. Inorg. Chem.* **1998**, 10, 1503-1511.

Chapter 7. Binding of 9-Methylguanine to [*cis*-Ru(2,2'-bipyridine)$_2$]$^{2+}$

Different ruthenium-based metal complexes are currently being investigated for their antitumor properties. Although the mode of actions of these complexes is not yet well understood, there is evidence that suggests that, similar to the well established platinum drugs, DNA is a likely target for these compounds.[1-11]

Barton and Lolis,[1] and subsequently Thorp and co-workers,[2] have reported the enatiomeric selectivity for the Λ isomer of *cis*-[Ru(phen)$_2$Cl$_2$] and *cis*-[Ru(bpy)$_2$(H$_2$O)$_2$]$^{2+}$ (phen = 1,10-phenanthroline; bpy = 2,2'-bipyridine) type complexes in covalent binding to B-DNA. A direct correlation between cytotoxicity and DNA binding was observed by Clarke and co-workers for the representative *cis*-[Cl$_2$(NH$_3$)$_4$Ru^{III}]Cl$_2$ and *trans*-[(Im)$_2$Cl$_4$Ru^{III}]$^-$ (Im = imidazole) type compounds in cell cultures[3] and it was shown that DNA binding of [(H$_2$O)(NH$_3$)$_5$Ru]$^{2+}$ occurs preferentially at G.[4,5] Brabec and co-workers showed similar results.[6] Furthermore, compounds like *mer*-[Ru(terpy)Cl$_3$] (terpy = 2,2':6', 2''-terpyridine), *mer*-[Cl$_3$(Me$_2$SO)$_3$Ru] and *trans*-[Cl$_4$(Me$_2$SO)$_2$Ru]$^-$ have all been shown to from interstrand cross-links in DNA and to bind guanine derivatives in a *trans* configuration while *trans*-[Cl$_2$(Me$_2$SO)$_4$Ru] forms a stable d(GpG) adduct.[7-10]

To our knowledge, there is no ruthenium complex with two DNA bases covalently bound to the metal center which has been structurally characterized. Reedijk and co-workers have shown that *cis*-[Ru(bpy)$_2$Cl$_2$] only forms a mono adduct with 9-ethylguanine (9-EtG) and 9-methylhypoxanthine and they were able to obtain the crystal structure of the mono 9-EtG adduct.[12] In this brief chapter we present the first example of a structurally characterized *cis*-bis purine complex of ruthenium.

7.1 Results and Discussion

Complex **33** was obtained by refluxing **32** with 2.4 eq. of 9-MeG in aqueous ethanol (Scheme 7.1).[13] Diffraction-quality crystals were grown from ethanol and CH_2Cl_2 and the x-ray structure of Λ-**33** is given in Figure 7.1.[14] The complex crystallizes in the monoclinic P2$_1$/n space group so the Λ and Δ isomers are both present in the unit cell. The guanines coordinate through N7 with the two bases in a head-to-tail (HT) orientation with a base-base dihedral angle of 60.4°. The purine moieties are situated with the keto groups between the pyridyl rings of the bpy ligands. In both

bases the carbonyl groups are slightly bent out of plane with O(6)-C(6)-N(3) and O(16)-C(16)-N(13) angles of 171.2° (4) and 170.8° (5) respectively.

All bond distances and angles are in good agreement with the closely related *cis*-$[Ru(bpy)_2(9\text{-EtG})Cl]^+$ structure[9] although we find that Ru-N(bpy) distances are on average 0.017(2) Å longer in **33**. Furthermore, the bpy ligands are not planar. In the bpy ligand with labels N23 and N24 in Figure 7.1 the two pyridine rings are twisted with respect to each other by an angle of 16.4° while in the other bpy ligand (with labels N21 and N22) the two pyridine rings are twisted by 11.6°. Bond distances and twist angles might be taken together as an indication of the steric hindrance imposed by the need of accommodating two guanines around the metal center.

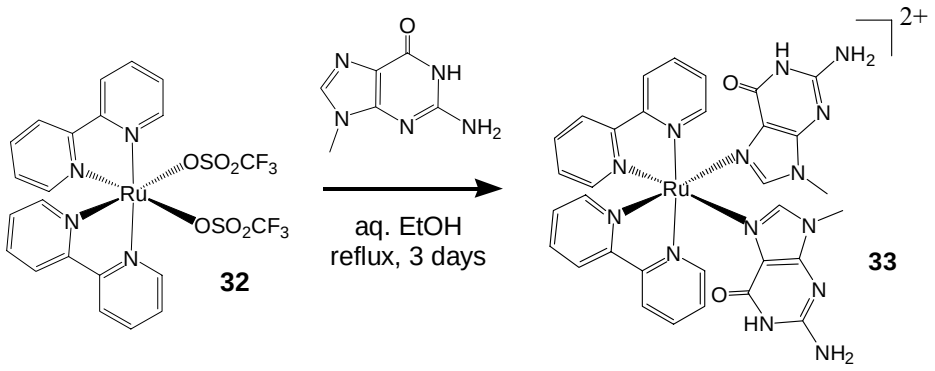

Scheme 7.1.

As previously shown, the guanine ligands can not rotate freely about the Ru-N7/(17) bond.[12] Due to this hindered rotation one might expect the two H8 protons to differ significantly in chemical shift. Indeed, when crystals of **33**$(SO_3CF_3)_2$ are dissolved in water two distinct sharp singlet separated by about 1.2 ppm are observed. The aromatic region of the ^{1}H NMR spectrum of **33** is shown in Figure 7.2. We find no appreciable change in the spectrum during a 4h period at 298K, however, after 3 days the peak of free 9-MeG grows by about 40% indicating that base dissociation takes place. Compared to the *cis*-bis guanine complex of the *fac*-$[Re(CO)_3]^+$ core, which remains the focus of our current research, complex **33** seems more stable as also indicated by the shorter M-N7 distance (on average Re-N7 bond distance = 2.199(9) Å).[15] Although the H8 protons are separated by 2.619(5) Å in the crystal we could not detect a NOESY cross-exchange signal in our 2D NMR experiments.

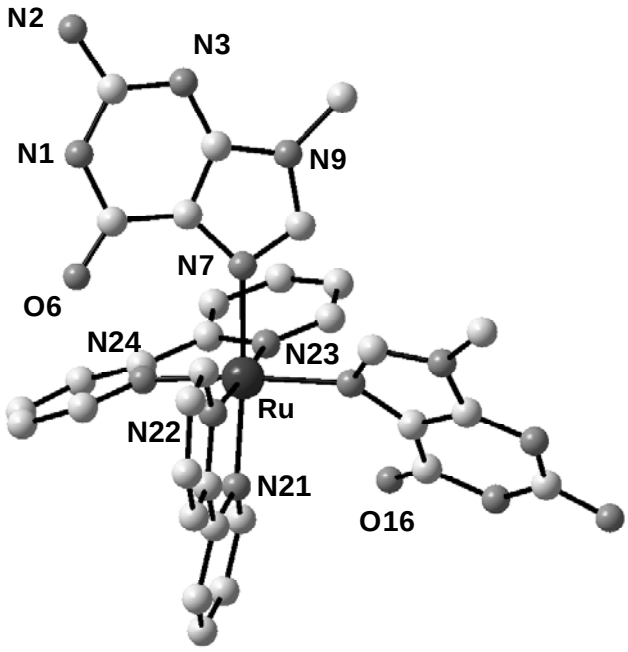

Figure 7.1. Crystal structure of Λ-$[Ru(bpy)_2(9\text{-}MeG)_2]^{2+}$ (**33**). Selected bond distances (Å) and angles (deg) are the following: Ru-N7 2.122(5), Ru-N17 2.131(4), Ru-N21 2.044(5), Ru-N22 2.053(5), Ru-N23 2.047(4), Ru-N24 2.050(4); N7-Ru-N17 89.12(16), N7-Ru-N21 175.26(16), N7-Ru-N22 97.20(19), N7-Ru-N23 83.77(17), N7-Ru-N24 95.74(17), N17-Ru-N21 93.30(16), N17-Ru-N22 86.50(17), N17-Ru-N23 97.36(17), N17-Ru-N24 173.49(17), N21-Ru-N22 78.90(19), N21-Ru-N23 99.95(17), N21-Ru-N24 82.17(18), N22-Ru-N23 176.05(18), N22-Ru-N24 97.17(17), N23-Ru-N24 78.92(17).

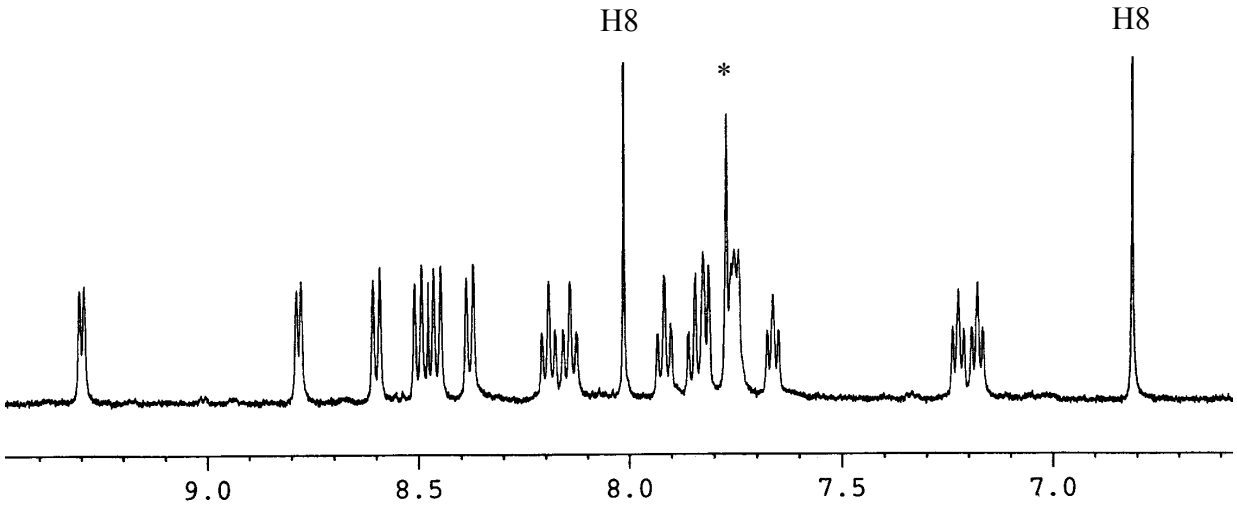

Figure 7.2. Aromatic region (ppm) of the ^1H NMR spectrum of (**33**) in D_2O. The star indicates free 9-MeG.

7.2 Conclusion

In this brief chapter we have presented the first structurally characterized *cis*-bis purine complex of ruthenium. The two guanine bases are in a HT orientation which is the most common solid-state conformation of cis-bis(ligand) complexes of purines with Pt^{II}, Co^{III}, Cu^{II} and Zn^{II}.[16] The complex is stable in water for hours showing a slow off rate of base dissociation. Our results, in agreement with the experimental evidence mentioned above, confirm that DNA is a possible target of ruthenium-based metal drugs.

7.3 References

(16) Barton, J. K.; Lolis, E. *J. Am. Chem. Soc.* **1985**, *107*, 708-709.

(17) Grover, N.; Gupta, N.; Thorp, H. H. *J. Am. Chem. Soc.* **1992**, *114*, 3390-3393.

(18) Frasca, D.; Ciampa, J.; Emerson, J.; Umans, R. S.; Clarke, M. J. *Met.-Based Drugs* **1996**, *3*, 197-209.

(19) Clarke, M. J.; Jansen, B.; Marx, K. A.; Kruger, R. *Inorg. Chim. Acta* **1986**, *124*, 13-28.

(20) McNamara, M.; Clarke, M. J. *Inorg. Chim. Acta* **1992**, *195*, 175-185.

(21) Novakova, O.; Kasparkova, J.; Vrana, O.; van Vliet, P. M.; Reedijk, J.; Brabec, V. *Biochem.* **1995**, *34*, 12369-12378.

(22) van Vliet, P. M.; Toekimin, S. M. S.; Haasnoot, J. G.; Reedijk, J.; Novakova, O.; Vrana, O.; Brabec, V. *Inorg. Chim Acta* **1995**, *231*, 57-64.

(23) Pacor, S.; Sava, G.; Ceschia, V.; Bregant, F.; Mestroni, G.; Alessio, E. *Chem. Biol. Interact.* **1991**, *78*, 223-234.

(24) Cauci, S.; Viglino, P.; Esposito, G.; Quadrifoglio, F. *J. Inorg. Biochem.* **1991**, *43*, 739-751.

(25) Esposito, G.; Cauci, S.; Fogolari, F.; Alessio, E.; Scocchi, M.; Quadrifoglio, F.; Viglino, P. *Biochem.* **1992**, *31*, 7094-7103.

(26) Loseto, F.; Alessio, E.; Mestroni, G.; Lacidogna, G.; Nassi, A.; Giordano, D.; Cosuccia, M. *Anticancer Res.* **1991**, *11*, 1549-15xx.

(27) van Vliet, P. M.; Haasnoot, J. G.; Reedijk, J. *Inorg. Chem.* **1994**, *33*, 1934-1939.

(28) Complex **32** was obtained by reacting $Ru(bpy)_2Cl_2$ (50 mg, 0.1 mmol, prepared by standard methods) with $AgSO_3CF_3$ (55 mg, 0.22 mmol) in aqueous ethanol (10 mL). After filtration of AgCl 9-MeG (40 mg, 0.24 mmol) was added and the solution refluxed for 3 days. The reaction mixture was cooled to room temperature and filtered again. CH_2Cl_2 was then allowed to slowly diffuse into the solution depositing x-ray quality crystals of **33**$(SO_3CF_3)_2$ after 2 days.

(29) Crystals suitable for x-ray diffraction were obtained by vapour diffusion of CH_2Cl_2 into an ethanolic solution of **33**$(SO_3CF_3)_2$. Crystal data: $C_{35}H_{32}Cl_2F_6N_{14}O_8Ru_1S_2$, MW = 1126.84, red block, Monoclinic, $P2_1/n$, a = 12.5159(6) Å, b = 20.0904(13) Å, c = 17.1202(9) Å, β = 98.981(6) deg, V = 4252.1(4) $Å^3$, Z = 4, ρ_{calc} = 1.76 Mg/m^3, μ(Mo Kα) = 4.62 mm^{-1}, Stoe IPDS diffractometer, Mo Kα radiation (λ = 0.71073 Å), 8711 reflections, 3786 with I > 2σ(I) used for refinement: *R* = 0.0502, *wR2* = 0.0846, hydrogens calculated.

(30) Zobi, F.; Spingler, B.; Fox, T.; Alberto, R. *Inorg. Chem.* **2003**, *42*, 2818-2820.

(31) Xu, Y.; Natile, G.; Intini, F. P.; Marzilli, L. G. *J. Am. Chem. Soc.* **1990**, *112*, 8177-8179, and references therein.

Conclusions and Outlook

This study subject of this thesis is focused on the interaction of the metal ions technetium (Tc) and rhenium (Re) with amino acids and DNA bases, in particular with guanine. The purpose and general aims underlying the study reside in the need to understand whether the above mentioned metal ions are capable of interacting with DNA bases in a fashion similar to cisplatin. It was mentioned in the introduction that while Tc is routinely used in hospitals for diagnosis, as β-particle emitters ^{186}Re and ^{188}Re are two promising FDA approved radionuclides that are extensively used for radiopharmaceutical applications as cytotoxic therapeutic agents in human medicine. A careful search of the recent publications that have appeared on PUBMED reveals a growing consensus in the medical community that by combining radiotherapy and chemotherapy, important therapeutic advantages can be obtained to cure cancer. The consensus might not yet be general given the fact that not all types of cancer respond better to a combined regime of radiotherapy and chemotherapy when compared to radiotherapy or chemotherapy alone. However for tumours that do respond the advantages are undeniable. In cancer treatment it is therefore desirable to employ compounds that might function mechanistically as cisplatin derivatives, thus mimicking the best chemotoxic agent known, in combination with an inherent radioactivity of the metal center, thus fulfilling a radiotherapeutic action.

In the preceding chapters it was clearly demonstrated that the *fac*-$[M(CO)_3]^+$ core meets the above mentioned requirements. The core not only accommodates two untethered guanines but it forms stable adducts with longer oligonucleotides such as d(GpG) and d(CpGpG). The adducts formed with DNA bases by Tc and Re are generally less stable than the corresponding cisplatin adducts however the $[Re(CO)_3]^+$ moiety displays a principally similar reactivity pattern with plasmid DNA as cisplatin. Furthermore, several complexes based on the tricarbonyl core are cytotoxic showing high antiproliferative activity toward B16 F1 mouse melanoma cells. As the Ru based anticancer agents [ImH][*trans*-$RuCl_4(Im)_2$], ICR, and [ImH][*trans*-$RuCl_4$(DMSO)(Im)], NAMI-A, Re compounds bearing at least one Im or HPz ligand generally best inhibit cell proliferation. This observation opens interesting possibilities for further studying the role of such five membered aromatic ligands in terms of cytotoxicity of octahedral complexes. In fact, while not yet demonstrated in the case of Re complexes, it has been shown that by replacing Im for thiazole Ru compounds become virtually noncytotoxic. Although some of the complexes investigated in this study are clearly cytotoxic, no structure-activity relationship could be elucidated from the results as both compounds with two exchangeable cis-coordinated ligands and compounds with one or no

exchangeable ligands show comparable activity. Hence it is important to clarify if in the cell Re compounds act at the DNA level or interfere with (bind to) other cellular components.

In practical terms, the challenge facing further research on this subject is the design of a proper set of ligands for the tricarbonyl core. This study has demonstrated the fundamental potential of using the *fac*-$[M(CO)_3]^+$ moiety as a "chemo-radiotherapeutic agents", however the solvated moiety (i.e. $[M(H_2O)_3(CO)_3]^+$) cannot be used as such for any feasible and realistic applications due to its reaction with blood proteins. In the preceding chapters it was shown that the core can be derivatized with coligands such as N,N-dimethylglycine that can be replaced by coordination to N7 of guanine yielding, therefore, Re complexes in the form of pro-drugs. Complexes with other amino acids are too stable in this respect but both complexes do not cross react with human serum. It was also demonstrated that a single imidazole ligand can also be replaced by coordination to N7 of guanine suggesting that a combination of such ligands (i.e. N,N-dimethylglycine and imidazole type ligands) may be a promising start. Solubility issues must of course be addressed and in this respect a combination of the monodentate imidazole (or pyrazole) ligand with a sterically hindered bidentate ligand derivatized so as to confer good water solubility to the complex appears, at the present stage, as the first step to undertake toward the development of useful Re-based "chemo-radiotherapeutic agents".

Experimental Section

Materials and Methods

Unless otherwise specified, materials were purchased from commercial suppliers and used without further purification.

IR , UV/Vis and NMR Spectroscopy

IR spectra were recorded as pellets (KBr) using a Perkin Elmer FT-IR spectrometer. The peaks are reported using the following abbreviations: s (sharp) or b (broad). UV/Vis spectra were taken on a Perkin Elmer Cary 50 spectrometer with a Peltier thermostat. NMR spectra were recorded on a Bruker DRX 500 MHz spectrometer. The reported chemical shifts (δ/ppm) are relative to the residual solvent peak. The coupling constants (J) are given in Hz. Multiplicities are reported using the following abbreviations: s (singlet), d (doublet), t (triplet), q (quartet), m (multiplet), br (broad) or a suitable combination of them.

Mass Spectrometry

Mass spectra were recorded on a Merck M8000 HPLC/MS spectrometer with electrospray ionization (ESI).

X-ray Data Collection and Processing

Suitable crystals were covered with Paratone N oil, mounted on top of a glass fiber, and immediately transferred to a Stoe IPDS diffractometer. Data were collected at 183(2) K using graphite-monochromated Mo Kα radiation (λ = 0.71073 Å). A total of 8000 reflections distributed over the whole limiting sphere were selected by the program SELECT and used for unit cell parameter refinement with the program CELL. Data were corrected for Lorenz and polarization effects as well as for absorption (numerical). Structures were solved with direct method using SHELXS-97 or SIR-97 and were refined by full-matrix least-squares methods on F^2 with SHELXL-97.

Analytical High Performance Liquid Chromatography (HPLC)

High performance liquid chromatography (HPLC) was performed on a Merck L7000 system, using a Macherey-Nagel EC 250/3 Nucleosil 100-5 C18HD column for non-radioactive compounds and a Macherey-Nagel EC 250/3 Nucleosil 100-5 C18 column for radioactive compounds. HPLC solvents were 0.1% Trifluoroacetic acid (solvent A) and Methanol HPLC grade (solvent B). The

HPLC gradient used is as follows: Gradient 1: 0-3 minutes: 100% A; 3.1-9 minutes: 75% A, 25% B; 9.1-20 minutes: linear gradient from 66% A (34% B) to 0% A (100% B); 20-28 minutes: 100% B; 28.1-30: 100% A. The flow rate was 0.5 ml/min. Gradient 2: 0-5 minutes: 75% A, 25% B; 5.1-30 minutes:: linear gradient from 75% A (25% B) to 0% A (100% B); 30-35 minutes: 100% B; 35.1-40: 75% A, 25% B. The flow rate was 0.5 ml/min. Detection was performed at 250 nm. The detection of radioactive ^{99m}Tc complexes was performed with a Berthold LB506 radiodetector equipped with a NaI(Tl) scintillation detector.

Gel Mobility Shift Assay

ΦX174 plasmids were purchased from Promega and used without further purification. ΦX174 RF plasmid DNA (0.1 μg) was mixed with the rhenium complexes in H_2O at [complex]/[bp] 0.018-1.8/1. The mixtures were incubated in water at 37 ^oC for 22 h in the dark before analyzing by gel electrophoresis. The pH of the mixtures remained constant at ≈ 7 in all cases. Experiments performed in 1 mM or 10 mM $NaClO_4$ showed no significant difference in the binding of **1** to ΦX174 RF plasmid DNA. DNA binding was examined by gel electrophoretic mobility shift assays through 9 cm 0.75% agarose slab gels with TAE running buffer. The gels were run at RT, with voltages varying between 50 and 75 V. Running time depended upon the voltage and were usually between 1.5-2 h. The resultant gels were stained with ethidium bromide in the buffer at a concentration of ≈ 0.3 μg/mL. Bands were visualized by software UV transillumination equipped with a digital camera.

XTT Assay for Cell Proliferation

An average of 1000-1500 cells were grown in microtiter plates (tissue culture grade, 96 wells, flat bottom) in a final volume of 100 μL culture medium per well in a humidified atmosphere (37 ^oC, >6.5% CO_2). After 24 h the rhenium complexes were added to the wells (final concentrations 100 and 200 μM) and the cells were grown for further 24 h under a humidified atmosphere. After the incubation period 50 μL of the XTT labeling mixture were added to each well. The plates were incubated again for 4 h. After the this final incubation period the spectrophotometrical absorbance (optical density OD) of each well was measured at 450 nm. Control experiments were performed as described above without the addition of the rhenium compounds. Blanks were obtained by adding the reagents to wells lacking cells. Experiments were done in double and the results represent the average. The % of cell survival was calculated base on the relative OD of the samples. Maximum control OD was set to 100% cell survival.

Synthesis of Compounds

Complexes $[Re(His)(CO)_3]$ (**18**), $[Re(Im)_3(CO)_3](TFA)$ (**19**), $[Et_4N][ReBr_2(Im)(CO)_3]$ (**28**), $[ReBr(HPz)_2(CO)_3]$ (**30**) and $[Re_2(\mu\text{-}OH)_2(Im)_2(CO)_6]$ (**31**) were prepared according to the reported procedures (see references 31 and 32 of Chapter 2 and references 14 and 15 of Chapter 6).

$[ReBr(G)_2(CO)_3]$ (3): $(Et_4N)_2[ReBr_3(CO)_3]$ (101 mg, 0.13 mmol) was dissolved in hot (~40 ^{0}C) methanol (7 mL). Guanosine (75 mg, 0.26 mmol) suspended in hot methanol (8 mL) was slowly added. The mixture was heated to 50 ^{0}C under a slight N_2 pressure. The colorless solution turned light yellow within minutes. The reaction was monitored by HPLC and it was stopped after 3.5 hr when no further change could be observed. The solution mixture was allowed to equilibrate to room temperature and then the solvent was dried under vacuum leaving a gelatinous yellow residue. This residue was washed with Et_2O and CH_2Cl_2, dried under vacuum and finally washed with CH_3OH. This final wash left a white microcrystalline solid which was dissolved in H_2O and purified on a short C18 column. Yield : 46 mg, 29%.

Elemental analysis calculated for **3**, $C_{23}H_{26}BrN_{10}O_{13}Re$ (916.62): C, 30.14; H, 2.86; N, 15.28, found: C, 30.59; H, 2.81; N, 14.89.

3: ^{1}H NMR (200 MHz, DMSO-d^6, δ/ppm): 10.63 (H_A, s, 1H), 10.58 (H_A, s, 1H), 8.33 (H_B, s, 1H), 7.92 (H_B, s, 1H), 6.59 (H_C, s, 1H), 6.55 (H_C, s, 1H), 5.76 (H_D, d, ^3J = 5, 1H), 5.67 (H_D, d, ^3J = 5, 1H), 5.54 (H_E, d, ^3J = 5, 1H), 5.43 (H_E, d, ^3J = 5, 1H), 5.16 (H_F, d, ^3J = 5, 1H), 5.07 (H_F, d, ^3J = 5, 1H), 4.93 (H_G, s, 1H), 4.48 (H_G, s, 1H), 4.35 (H_J, dd, ^3J = 6, 1H), 4.10 (H_J, dd, ^3J = 6, 1H), 4.08-3.50 (H_K, H_L, H_M, m, 8H). FT-IR for **3** (KBr, ν/cm^{-1}): (C≡O) 2025 (s), (C≡O) 1907 (b). ESI-MS for **3** (ESI+, 60V, *m/z*): 836.5 ([M-Br]$^+$). HPLC R_t for **3** (HPLC, Gradient 1, min): 17.9.

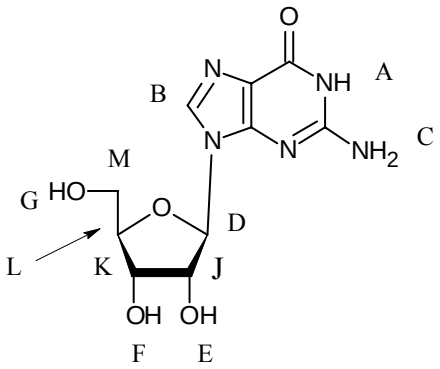

[ReBr(2dG)$_2$(CO)$_3$] (4): $(Et_4N)_2[ReBr_3(CO)_3]$ (101 mg, 0.13 mmol) was dissolved in hot (~40 ^{0}C) methanol (7 mL). 2-deoxyguanosine (70 mg, 0.26 mmol) suspended in hot methanol (8 mL) was slowly added. The mixture was heated to 50 ^{0}C under a slight N_2 pressure. The colorless solution turned light yellow within minutes. The reaction was monitored by HPLC and it was stopped after 3.5 hr. The solution mixture was allowed to equilibrate to room temperature and then the solvent was dried under vacuum leaving a gelatinous yellow residue. This residue was washed with Et_2O and CH_2Cl_2, dried under vacuum and finally washed with CH_3OH. This final wash left a white microcrystalline solid which was dissolved in H_2O and purified on a short C18 column. Yield : 49 mg, 43%.

Elemental analysis calculated for **4**, $C_{23}H_{26}BrN_{10}O_{11}Re$ (884.62): C, 31.23; H, 2.96; N, 15.83, found: C, 32.59; H, 2.21; N, 13.89.

4: ^{1}H NMR (200 MHz, DMSO-d^6, δ/ppm): 10.64 (H_A, s, 1H), 10.57 (H_A, s, 1H), 8.18 (H_B, s, 1H), 7.92 (H_B, s, 1H), 6.57 (H_C, s, 2H), 6.12 (H_D, m, 2H), 5.26 (H_E, d, ^{3}J = 4, 1H), 5.20 (H_E, d, ^{3}J = 4, 1H), 4.80 (H_F, s, 1H), 4.66 (H_F, s, 1H), 4.31-4.22 (H_G, m, 2H), 3.83-3.73 (H_J, m, 2H), 3.44-3.14 (H_K, H_L, H_M, m, 8H). FT-IR for **4** (KBr, ν/cm^{-1}): (C≡O) 2024 (s), (C≡O) 1904 (b). ESI-MS for **4** (ESI+, 60V, *m/z*): 804.9 ([M-Br]$^+$). HPLC R_t for **4** (HPLC, Gradient 1, min): 18.1.

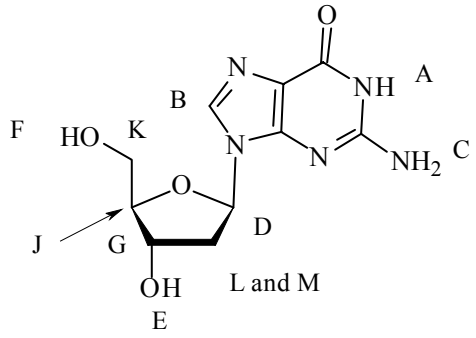

[ReBr(BzIm)$_2$(CO)$_3$] (6): $(Et_4N)_2[ReBr_3(CO)_3]$ (300 mg, 0.39 mmol) of was dissolved in methanol (11 mL). Benzimidazole (93.1 mg, 0.79 mmol) in methanol (4 mL) was added. The reaction was allowed to proceed at 50 ^{0}C under a slight N_2 pressure and it was monitored by HPLC. Complexation was judged complete after 1.5 hr when a single peak was visible in the chromatogram. At this point the reaction was stopped and the solution mixture was allowed to equilibrate to room temperature. The solvent was then dried under vacuum leaving a white residue. The complex was extracted with THF (4.5 mL) and purified on a short C18 column. A white

crystalline solid was obtained. Yield : 131 mg, 22%. Crystals suitable for x-ray diffraction were obtained by slow diffusion of pentane into a dichloromethane solution of the complex.

Elemental analysis calculated for **6**, $C_{17}H_{12}BrN_4O_3Re$ (586.41): C, 34.82; H, 2.06; N, 9.55, found: C, 34.59; H, 2.21; N, 9.89.

6: ^{1}H NMR (200 MHz, DMSO-d^6, δ/ppm): 8.47 (H_A, s, 1H), 7.63 (H_B, d, ^3J = 7, 1H), 7.47 ($H_{B'}$, d, ^3J = 7, 1H), 7.39-7.11 (H_C, m, 2H) FT-IR for **6** (KBr, ν/cm^{-1}): (C≡O) 2017 (s), (C≡O) 1899 (b), (C≡O) 1880 (b). ESI-MS for **6** (ESI+, 40V, *m/z*): 506.0 ([M-Br]$^+$). HPLC R_t for **2** (HPLC, Gradient 1, min): 22.6.

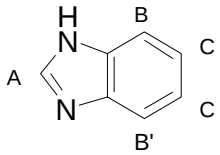

[Re(9-MeG)$_2$(CH$_3$OH)(CO)$_3$](ClO$_4$) • (Et$_4$N)(ClO$_4$) (7): $(Et_4N)_2[ReBr_3(CO)_3]$ (30 mg, 0.04 mmol) was dissolved in hot (~40 ^{0}C) methanol (3 mL). $AgClO_4$ (28 mg, 0.14 mmol) was added and the mixture was stirred for 3 h after which time AgBr was filtered off. 9-methylguanine (16.5 mg, 0.1 mmol) was added and the mixture was heated to 50 ^{0}C under a slight N_2 pressure. The colorless solution turned light yellow within minutes. The reaction was monitored by HPLC and it was stopped after 3.5 hr. The solution mixture was allowed to equilibrate to room temperature and then pentane was allowed to diffuse into it depositing x-ray quality crystals. Yield : quantitative.

Elemental analysis calculated for **7**, $C_{16}H_{18}ClN_{10}O_{10}Re$ (732.04): C, 26.25; H, 2.48; N, 19.13, found: C, 25.86; H, 2.67; N, 18.98.

7: ^{1}H NMR (500 MHz, D_2O, δ/ppm): 8.31 (s, 1H), 3.66 (s, 3H). FT-IR for **7** (KBr, ν/cm^{-1}): (C≡O) 2027 (s), (C≡O) 1918 (b), (C≡O) 1897 (b). ESI-MS for **7** (ESI+, 40V, *m/z*): 600.5 ([M-CH$_3$OH]$^+$). HPLC R_t for **7** (HPLC, Gradient 1, min): 17.1.

[^{99}Tc(9-MeG)$_2$(CH$_3$OH)(CO)$_3$](ClO$_4$) • (Et$_4$N)(ClO$_4$) (8): $(Et_4N)_2[^{99}TcCl_3(CO)_3]$ (30 mg, 0.04 mmol) was dissolved in hot (~40 ^{0}C) methanol (3 mL). $AgClO_4$ (28 mg, 0.14 mmol) was added and the mixture was stirred for 3 h after which time AgBr was filtered off. 9-methylguanine (16.5 mg, 0.1 mmol) was added and the mixture was heated to 50 ^{0}C under a slight N_2 pressure. The reaction was monitored by HPLC and it was stopped after 3.5 hr. The solution mixture was allowed to equilibrate to room temperature and then pentane was allowed to diffuse into it depositing x-ray quality crystals. Yield : quantitative.

[Re(9-MeG)$_2$(H$_2$O)(CO)$_3$](ClO$_4$) (10HT): $(Et_4N)_2[ReBr_3(CO)_3]$ (30 mg, 0.04 mmol) was dissolved in hot (~40 ^{0}C) methanol (3 mL). $AgClO_4$ (28 mg, 0.14 mmol) was added and the mixture was stirred for 3 h after which time AgBr was filtered off. 9-methylguanine (16.5 mg, 0.1 mmol) was added and the mixture was heated to 50 ^{0}C under a slight N_2 pressure. The colourless solution turned light yellow within minutes. The reaction was monitored by HPLC and it was stopped after 3.5 hr when no further change could be observed. The solution mixture was allowed to equilibrate to room temperature, concentrated and then purified on a short C18 column. To the methanol fraction containing the purified complex 3% H_2O (v/v) was added. Pentane was allowed to diffuse into the solution depositing x-ray quality crystals. Yield : quantitative.

Elemental analysis calculated for **10HT**, $C_{15}H_{16}ClN_{10}O_{10}Re$ (718.01): C, 25.09; H, 2.25; N, 19.51, found: C, 25.34; H, 2.70; N, 19.45.

10HT: ^{1}H NMR (500 MHz, D_2O, δ/ppm): 8.31 (s, 1H), 3.66 (s, 3H). FT-IR for **10HT** (KBr, ν/cm^{-1}): (C≡O) 2027 (s), (C≡O) 1918 (b), (C≡O) 1897 (b). ESI-MS for **10HT** (ESI+, 40V, *m/z*): 600.5 ([M-H_2O]$^+$). HPLC R_t for **5** (HPLC, Gradient 1, min): 17.1.

[Re(9-MeG)$_2$(H$_2$O)(CO)$_3$]Br (10HH): $(Et_4N)_2[ReBr_3(CO)_3]$ (30 mg (0.04 mmol) was dissolved in a water/methanol mixture (5 mL, 3:2). 9-methylguanine (16.5 mg, 0.1 mmol) was added and the mixture was heated to 50 ^{0}C under a slight N_2 pressure. The colourless solution turned light yellow within minutes. The reaction was monitored by HPLC and it was stopped after 3.5 hr. The solution mixture was allowed to equilibrate to room temperature and left open to air to allow all the methanol to evaporate. After 1 week white crystals of the title compound were collected. Yield : quantitative.

Elemental analysis calculated for **10HH**, $C_{15}H_{16}BrN_{10}O_6Re$ (698.46): C, 25.79; H, 2.31; N, 20.05, found: C, 25.39; H, 2.54; N, 19.78.

10HH: ^{1}H NMR (500 MHz, D_2O, δ/ppm): 8.31 (s, 1H), 3.66 (s, 3H). FT-IR for **10HH** (KBr, ν/cm^{-1}): (C≡O) 2027 (s), (C≡O) 1915 (b), (C≡O) 1895 (b). ESI-MS for **10HH** (ESI+, 40V, *m/z*): 600.5 ([M-H_2O]$^+$). HPLC R_t for **10HH** (HPLC, Gradient 1, min): 17.1.

[ReBr(7-MeG)$_2$(CO)$_3$] (12HH): $(Et_4N)_2[ReBr_3(CO)_3]$ (30 mg (0.04 mmol) was dissolved in a water/methanol mixture (3 mL, 2:1). 7-methylguanine (16.5 mg, 0.1 mmol) was added and the mixture was heated to 50 ^{0}C under a slight N_2 pressure. The colorless solution turned light yellow within minutes. The reaction was monitored by HPLC and it was stopped after 3.5 hr. The solution was allowed to equilibrate to room temperature concentrated and purified on a short C18 column. A

white crystalline solid was obtained. Yield : 18 mg, 68%. Crystals suitable for x-ray diffraction were obtained by slow diffusion of pentane into a methanolic solution of the complex.

Elemental analysis calculated for **12HH**, $C_{15}H_{14}BrN_{10}O_5Re$ (680.45): C, 26.48; H, 2.07; N, 20.58, found: C, 26.21; H, 2.19; N, 19.97.

12HH: ^{1}H NMR (500 MHz, D_2O, δ/ppm): 8.18 (s, 1H), 3.97 (s, 3H). FT-IR for **12HH** (KBr, ν/cm^{-1}): (C≡O) 2027 (s), (C≡O) 1897 (b). ESI-MS for **12HH** (ESI+, 40V, *m/z*): 600.5 ([M-Br]$^+$). HPLC R_t for **12HH** (HPLC, Gradient 1, min): 17.8.

[Re(7-MeG)$_2$(H$_2$O)(CO)$_3$](ClO$_4$) (12HT): $(Et_4N)_2[ReBr_3(CO)_3]$ (50 mg, 0.065 mmol) was dissolved in methanol/water mixture (2:4, 6 mL). $AgClO_4$ (44.5 mg, 0.22 mmol) was added, the mixture was stirred for 1h and then filtered from AgBr ppt. To the filtrate 7-methylguanine (23.6 mg, 0.143 mmol) was added and the solution was heated to 50 ^{0}C under a slight N_2 pressure. The reaction was monitored by HPLC and it was stopped after 3.5 hr. The solution was cooled to room temperature and then methanol was allowed to evaporate slowly. After 3-4 days x-ray quality crystals of the title compound were obtained. Yield : 23 mg, 49%.

Elemental analysis calculated for **12HT**, $C_{15}H_{16}ClN_{10}O_{10}Re$ (718.01): C, 25.09; H, 2.25; N, 19.51, found: C, 25.12; H, 2.20; N, 19.23.

12HT: ^{1}H NMR (500 MHz, D_2O, δ/ppm): 8.18 (s, 1H), 3.97 (s, 3H). FT-IR for **12HT** (KBr, ν/cm^{-1}): (C≡O) 2030 (s), (C≡O) 1908 (b), (C≡O) 1876 (b). ESI-MS for **12HT** (ESI+, 40V, *m/z*): 600.5 ([M-H_2O]$^+$). HPLC R_t for **12HT** (HPLC, Gradient 1, min): 17.8.

[Re(Pro)(CO)$_3$]$_3$ (13): $(Et_4N)_2[ReBr_3(CO)_3]$ (100 mg, 0.13 mmol) was dissolved in a methanol/water mixture (9:1, 5 mL). L-proline (52 mg, 0.46 mmol) was added and the mixture was stirred for 5 h at 50 ^{0}C under a slight N_2 pressure. The reaction was monitored by HPLC and it was stopped when no further change could be observed (4h). The solution was allowed to equilibrate to room temperature concentrated and purified on a short C18 column. A white crystalline solid was obtained. Yield : 40.1 mg, 60%. Crystals suitable for x-ray diffraction were obtained by slow diffusion of THF into a methanolic solution of the complex.

Elemental analysis calculated for **13**, $C_{24}H_{24}N_3O_{15}Re_3$ (1153.08): C, 25.00; H, 2.10; N, 3.64, found: C, 25.39; H, 2.42; N, 4.00.

FT-IR for **13** (KBr, ν/cm^{-1}): (C≡O) 2027 (s), (C≡O) 1908 (b), (C≡O) 1888 (b). ESI-MS for **13** (ESI-, 40V, *m/z*): 1266.9 ([M+Pro$^-$]$^-$). HPLC R_t for **13** (HPLC, Gradient 1, min): 16.4

[Re(DMGly)(CO)$_3$]$_3$ (14): $(Et_4N)_2[ReBr_3(CO)_3]$ (100 mg, 0.13 mmol) was dissolved in a methanol/water mixture (4:1, 10 mL). N,N-dimethylglycine (70 mg, 0.7 mmol) was added and the mixture was stirred for 12 h at 50 ^{0}C under a slight N_2 pressure. The solution was allowed to equilibrate to room temperature concentrated and purified on a short C18 filter. A white crystalline solid was obtained. Yield : 20 mg, 40%. Crystals suitable for x-ray diffraction were obtained by slow diffusion of ether in a CH_3CN solution of the complex.

Elemental analysis calculated for **14**, $C_{21}H_{24}N_3O_{15}Re_3$ (1117.05): C, 22.58; H, 2.17; N, 3.76, found: C, 23.19; H, 2.78; N, 3.84.

14: ^{1}H NMR (500 MHz, DMSO-d^6, δ/ppm): 4.18 (s, 2H), 3.46 (s, 3H), 3.15 (s, 3H). FT-IR for **14** (KBr, ν/cm^{-1}): (C≡O) 2022 (s), (C≡O) 1911 (b), (C≡O) 1890 (s), (C≡O) 1866 (s). ESI-MS for **14** (ESI+, 40V, *m/z*): 1117.0 ($[M]^+$). HPLC R_t for **14** (HPLC, Gradient 1, min): 15.7.

[Re(Pro)(9-MeG)(CO)$_3$] (15): $(Et_4N)_2[ReBr_3(CO)_3]$ (18 mg, 0.02 mmol) was dissolved in methanol (3 mL). L-proline (8 mg, 0.06 mmol) was added. The solution was stirred and heated to 50 ^{0}C under a slight N_2 pressure until **13** had formed (4h, as revealed by HPLC). 9-methylguanine (5 mg, 0.03 mmol) was added and allowed to react until no further change could be observed in the HPLC (4h). The solution mixture was cooled to room temperature. Then pentane was allowed to diffuse into it depositing x-ray quality crystals. Yield : 10 mg, 78%.

Elemental analysis calculated for **15**, $C_{14}H_{15}N_6O_6Re$ (549.51): C, 30.60; H, 2.75; N, 15.29, found: C, 30.96; H, 2.47; N, 15.70.

15: ^{1}H NMR (500 MHz, D_2O, δ/ppm): 8.01(s, 1H), 5.92 (s, 1H; NH), 3.39 (m, 1H), 3.20 (m, 1H), 2.66 (s, 3H; CH_3), 2.19 (m, 1H), 1.98 (m, 2H), 1.81 (m, 1H), 1.70 (m, 1H). FT-IR for **15** (KBr, ν/cm^{-1}): (C≡O) 2021 (s), (C≡O) 1894 (b). ESI-MS for **15** (ESI-, 40V, *m/z*): 548.5 ($[M-1]^-$). HPLC R_t for **15** (HPLC, Gradient 1, min): 19.1.

[ReBr(NH$_3$)$_2$(CO)$_3$] (16): $[ReBr(CO)_5]$ (75 mg, 0.19 mmol) was dissolved in a NH_3 saturated benzene solution (15 mL) and the mixture was heated to 60 ^{0}C under N_2 pressure. After 2.5 hr a white precipitate appeared, this was filtered, washed with benzene and dried in vacuo. Yield : 35 mg, 49%. Crystals suitable for x-ray diffraction were obtained by slow diffusion of hexane into a THF solution of the complex.

Elemental analysis calculated for **16**, $C_3H_6BrN_2O_3Re$ (384.21): C, 9.38; H, 1.57; N, 7.29, found: C, 10.01; H, 1.79; N, 7.67.

FT-IR for **16** (KBr, ν/cm^{-1}): (C≡O) 2017 (s), (C≡O) 1884 (b). ESI-MS for **16** (ESI+, 40V, *m/z*): 600.5 ($[M-H_2O]^+$). HPLC R_t for **16** (HPLC, Gradient 1, min): 9.6

B12-[Re(DMG)(CO)$_3$] (22): Vitamin B12 (50 mg, 0.04 mmol) was dissolved in methanol (10 mL). [Re(DMG)(CO)$_3$]$_3$ (45 mg, 0.04 mmol) was added and the mixture was stirred for at RT for 12h. Two adducts (clearly distinguishable by HPLC) formed (yield 25% and 36%). These were isolated and purified by preparative HPLC. Yield: 10 mg, 14% (adduct 1), 12 mg, 17% (adduct 2). Crystals of adduct 1 suitable for x-ray analysis were obtained by vapour diffusion of acetone in a H_2O solution of the complex.

Elemental analysis calculated for **22a**, $C_{70}H_{96}CoN_{15}O_{19}PRe$ (1727,71): C, 48.66; H, 5.60; N, 12.16, found: C, 48.42; H, 5.01; N, 12.04 (adduct 1).

FT-IR for **22** (KBr, ν/cm^{-1}): (C≡O) 2033 (s), (C≡O) 1928 (b), (C≡O) 1904 (b).ESI-MS for **22** (ESI+, 30V, *m/z*): 1728.7 ([M]$^+$ + 1). HPLC R_t for **22** (HPLC, Gradient 2, min): 19.2 (adduct 1, **22a**), 21.2 (adduct 2, **22b**).

[Re(L-Ser)$_2$(CO)$_3$] (23): $(Et_4N)_2[ReBr_3(CO)_3]$ (100 mg, 0.13 mmol) was dissolved in a methanol/water mixture (9:1, 5 mL). L-serine (48 mg, 0.46 mmol) was added and the mixture was stirred for 3 h at 50 ^{0}C under a slight N_2 pressure. The reaction was monitored by HPLC and it was stopped when no further change could be observed (3h). The solution was allowed to equilibrate to room temperature and purified by HPLC. A white solid was obtained. Yield : 23 mg, 37%. Crystals suitable for x-ray analysis were obtained by slow evaporation of H_2O.

Elemental analysis calculated for **23**, $C_9H_{13}N_2O_9Re$ (479,41): C, 22.55; H, 2.73; N, 5.84, found: C, 23.17; H, 3.20; N, 5.47.

23: ^{1}H NMR (500 MHz, D_2O : MeOH-d^4 2:1, δ/ppm): 3.98-3.89 (m, 2H), 3.80 (dd, ^{3}J = 3.7, 5.8, 1H). FT-IR for **23** (KBr, ν/cm^{-1}): (C≡O) 2012 (s), (C≡O) 1889 (b), (C≡O) 1874 (b). ESI-MS for **23** (ESI-, 30V, *m/z*): 479.5 ([M]$^+$). HPLC R_t for **23** (HPLC, Gradient 1, min): 7.1.

[Re(L-Ser)(7-MeG)(CO)$_3$] (24): $(Et_4N)_2[ReBr_3(CO)_3]$ (100 mg, 0.13 mmol) was dissolved in methanol/water mixture (9:1, 5 mL). L-serine (48 mg, 0.46 mmol) was added and the mixture was stirred for 3 h at 50 ^{0}C under a slight N_2 pressure. 7-methylguanine (37 mg, 0.20 mmol) was added and the mixture was stirred for 3 h at 50 ^{0}C under a slight N_2 pressure. The solution was allowed to equilibrate to room temperature concentrated and purified on a short C18 filter. A white crystalline solid was obtained. Yield : 45 mg, 58%. Crystals suitable for x-ray diffraction were obtained by slow diffusion of pentane into a methanolic solution of the complex.

Elemental analysis calculated for **24**, $C_{12}H_{13}N_6O_7Re$ (539,47): C, 26.72; H, 2.43; N, 15.58, found: C, 26.66; H, 2.42; N, 15.19.

24: ^{1}H NMR (500 MHz, D_2O : MeOH-d^4 1:1, δ/ppm): Species 1: 8.14 (s, 1H), 5.59 (m, 1H, NH), 4.79 (m, 1H, NH), 3.97 (s, 3H, CH_3), 3.83-3.79 (m, 2H, CH_2), 3.19-3.16 (m, 1H, CH). Species 2: 8.09 (s, 1H), 5.41 (m, 1H, NH), 4.76 (m, 1H, NH), 3.95 (s, 3H, CH_3), 3.72-3.57 (m, 2H, CH_2), 3.44-3.42 (m, 1H, CH). FT-IR for **24** (KBr, ν/cm^{-1}): (C≡O) 2023 (s), (C≡O) 1918 (b), (C≡O) 1890 (b) and (C≡O) 1893 (b), (C≡O) 1873 (b). ESI-MS for **24** (ESI-, 30V, *m/z*): 539.3 ([M]$^-$). HPLC R_t for **24** (HPLC, Gradient 1, min): 17.5.

[Re(D-Ser)(7-MeG)(CO)$_3$] (25): $(Et_4N)_2[ReBr_3(CO)_3]$ (100 mg, 0.13 mmol) was dissolved in methanol/water mixture (9:1, 5 mL). D-serine (48 mg, 0.46 mmol) was added and the mixture was stirred for 3 h at 50 ^{0}C under a slight N_2 pressure. 7-methylguanine (37 mg, 0.20 mmol) was added and the mixture was stirred for 3 h at 50 ^{0}C under a slight N_2 pressure. The solution was allowed to equilibrate to room temperature concentrated and purified on a short C18 filter. A white crystalline solid was obtained. Yield : 40 mg, 52%. Crystals suitable for x-ray diffraction were obtained by slow evaporation of a water/methanol solution (1:1) of the complex.

Elemental analysis calculated for **25**, $C_{12}H_{13}N_6O_7Re$ (539,47): C, 26.72; H, 2.43; N, 15.58, found: C, 25.92; H, 3.00; N, 14.99.

25: ^{1}H NMR (500 MHz, D_2O : MeOH-d^4 1:1, δ/ppm): Species 1: 8.14 (s, 1H), 5.59 (m, 1H, NH), 4.79 (m, 1H, NH), 3.97 (s, 3H, CH_3), 3.83-3.79 (m, 2H, CH_2), 3.19-3.16 (m, 1H, CH). Species 2: 8.09 (s, 1H), 5.41 (m, 1H, NH), 4.76 (m, 1H, NH), 3.95 (s, 3H, CH_3), 3.72-3.57 (m, 2H, CH_2), 3.44-3.42 (m, 1H, CH). FT-IR for **25** (KBr, ν/cm^{-1}): (C≡O) 2023 (s), (C≡O) 1918 (b), (C≡O) 1897 (b) and (C≡O) 1885 (b), (C≡O) 1874 (b). ESI-MS for **25** (ESI+, 30V, *m/z*): 539.3 ([M]$^+$). HPLC R_t for **25** (HPLC, Gradient 1, min): 17.5.

[Re(L-Ser)(3-pic)(CO)$_3$] (26): $(Et_4N)_2[ReBr_3(CO)_3]$ (100 mg, 0.13 mmol) was dissolved in methanol/water mixture (9:1, 5 mL). L-serine (48 mg, 0.46 mmol) was added and the mixture was stirred for 3 h at 50 ^{0}C under a slight N_2 pressure. 3-picoline (50 µL, 0.52 mmol) was added and the mixture was stirred for 1 day at 50 ^{0}C under a slight N_2 pressure. The solution was allowed to equilibrate to room temperature concentrated and purified on a short C18 filter. A white crystalline solid was obtained. Yield : 43 mg, 72%. Crystals suitable for x-ray diffraction were obtained by slow diffusion of pentane into a methanolic solution of the complex.

Elemental analysis calculated for **26**, $C_{12}H_{13}N_2O_6Re$ (467,45): C, 30.83; H, 2.80; N, 5.99, found: C, 31.48; H, 3.19; N, 6.39.

26: ^{1}H NMR (500 MHz, MeOH-d^4, δ/ppm): Species 1: 8.56 (s, 1H), 8.55 (d, ^{3}J = 5.7, 1H), 7.86 (d, ^{3}J = 7.8, 1H), 7.44 (dd, ^{3}J = 5.7, 7.8, 1H), 3.64-3.50 (m, 2H), 3.35 (m, 1H), 2.40 (s, 3H). Species

2: 8.56 (s, 1H), 8.53 (d, ^3J = 5.7, 1H), 7.89 (d, ^3J = 7.8, 1H), 7.47 (dd, ^3J = 5.7, 7.8, 1H), 3.79-3.71 (m, 2H), 2.76 (m, 1H), 2.42 (s, 3H). FT-IR for **26** (KBr, ν/cm^{-1}): (C≡O) 2023 (s), (C≡O) 1907 (b), (C≡O) 1881 (b). ESI-MS for **26** (ESI+, 40V, *m/z*): 468.0 ([M]$^+$). HPLC R_t for **26** (HPLC, Gradient 1, min): 18.2.

[Re(L-Tryp)$_2$(CO)$_3$] (27): This compound was synthesized according to the procedure described for the synthesis of [Re(L-Ser)$_2$(CO)$_3$] (**23**) but using L-Tryptophan instead of L-Serine. Crystals suitable for x-ray diffraction were obtained by slow diffusion of pentane into a methanolic solution of the complex.

FT-IR for **27** (KBr, ν/cm^{-1}): (C≡O) 2016 (s), (C≡O) 1891 (s), (C≡O) 1869 (s). ESI-MS for **27** (ESI+, 40V, *m/z*): 678.1 ([M]$^+$). HPLC R_t for **27** (HPLC, Gradient 1, min): 17.7.

[Ru(bpy)$_2$(9-MeG)$_2$](SO$_3$CF$_3$)$_2$ (33): Ru(bpy)$_2$Cl$_2$ (50 mg, 0.1 mmol, prepared by standard methods) was dissolved in aqueous ethanol (10 mL). AgSO$_3$CF$_3$ (55 mg, 0.22 mmol) was added. After filtration of AgCl, 9-methylguanine (40 mg, 0.24 mmol) was added and the solution refluxed for 3 days. The reaction mixture was cooled to room temperature and filtered again. CH_2Cl_2 was then allowed to slowly diffuse into the solution depositing x-ray quality crystals after 2 days. Yield: quantitative.

Elemental analysis calculated for **33**, $C_{34}H_{30}F_6N_{14}O_8RuS_2$ (1041,88): C, 39.19; H, 2.90; N, 18.82, found: C, 40.04; H, 3.15; N, 19.01.

33: ^{1}H NMR (500 MHz, D_2O, δ/ppm): 9.30, 8.79 (H_A, d, ^3J = 5.7, 2H), 7.81, 7.74 ($H_{A'}$, d, ^3J = 5.7, 2H), 8.60, 8.50 (H_B, d, ^3J = 8, 2H), 8.45, 8.39 ($H_{B'}$, d, ^3J = 8, 2H), 8.19, 8.15 (H_C, t, ^3J = 8, 8, 2H), 7.92, 7.84 ($H_{C'}$, t, ^3J = 8, 8, 2H), 7.73, 7.67 (H_D, t, ^3J = 6, 8, 2H), 7.22, 7.18 ($H_{D'}$, t, ^3J = 6, 8, 2H), 8.02 (H_E, s, 1H), 6.80 ($H_{E'}$, s, 1H), 3.67 (H_F, s, 3H), 3.38 ($H_{F'}$, s, 3H). UV/VIS for **33** (H_2O, nm, (ε, x10^{-4} M^{-1} cm^{-1})): 290 (6.37), 331 (1.04), 475 (1.01). ESI-MS for **33** (ESI+, 40V, *m/2z*): 289.2 ([Ru(bpy)$_2$(9-MeG)]$^{2+}$).

Summary

It was shown in this thesis that two guanine bases can coordinate to a Re^{I} or a Tc^{I} centre yielding reasonably stable complexes with slow on and off rates, the on rates being comparable to an active form of cisplatin. For the first time x-ray structures of a Tc- and Re-complexes with two purine bases bound *cis* to the metal center were presented. Guanine ligands can assume both a HH and a HT conformation in an octahedral complex around the Re^{I} tricarbonyl core and these two forms are present in solution in equilibrium. Theoretical and ^{1}H NMR studies indicate that the two guanines can freely rotate about the Re-N7(9) bond. This implies that the O6 carbonyl oxygen imposes no steric hindrance. The presence of HH and HT conformers in complexes with either 9-MeG or 7-MeG in the solid state and in solution delineates the fact that intramolecular hydrogen bonding and steric hindrance imposed by the carbonyl oxygen of coordinated guanines are not driving forces for the preference of one or the other conformation.

Rhenium forms stable adducts with d(GpG) and d(CpGpG) via coordination of the N7 atom of guanine residues as corroborated by the pH-dependence studies of the H8 resonances at pH values near 2. Reaction of **1** with d(GpG) yields two major adducts. NMR data and ring current shift calculations based Abraham's model, tentatively suggest that these may be HH and HT conformers. Kinetic investigations have revealed that macrochelate closure is not the rate determining step but rather a fast step in the reaction. Interaction of **1** with d(CpGpG) yields a single major product. NMR investigation has proven that the olygonucleotide binds to the *fac*-$[Re^{I}(CO)_3]$ core via the N7 atom of guanine bases.

The $[Re(CO)_3]^{+}$ moiety displays a principally similar reactivity pattern with plasmid DNA as e.g. cisplatin. It binds selectively to two free guanines, implying a possible interaction with adjacent guanines in DNA as well. To protect the Re center in plasma from unwanted coordination (trapping) to serum proteins coligands such as proline or N,N-dimethylglycine were used yielding the Re-complexes in the form of pro-drugs. DMGly in particular can be replaced by coordination to N7 of guanine. The complexes with other amino acids are too stable in this respect but both complexes do not cross react with human serum. If the coligands are labile enough the corresponding complexes such as $[Re(DMGly)(CO)_3]_3$ influence the tertiary structure of ΦX174 DNA by altering the electrophoretic mobility of the open circular and the supercoiled form of plasmid DNA. The induced changes involve most likely covalent binding to two bases as found for cisplatin. Although less potent, the presented model complexes depict the in vitro reactivity

characteristics as required for therapeutic agents. They might therefore serve as future inorganic medicinal drugs provided that they are able to accumulate to a sufficient extent in the cell and in the nucleus in particular.

The *fac*-$[Re(CO)_3]^+$ core can be derivatized with the amino acid serine and the appropriate nitrogenous base to yield nucleoside mimicking complexes. These compounds show an interesting solution behavior displaying an intramolecular rearrangement which, to our knowledge, has never been described for octahedral organometallic complexes in which the α-aminocarboxylate ligand is bound as a N,O-chelate. Nucleoside mimicking compounds where the nitrogenous base is 7-MeG are remarkably stable in Human Serum (HS) showing only about 50% decomposition (i.e. reaction with serum proteins) after 12h and being still visible in the HPLC chromatogram after a 24h incubation period. When the same compounds were subjected to *in vitro* phosphorylation tests and affinity measurements with HSV1 TK neither evidence of phosphorylation of pendent serine arm nor inhibition of HSV1 TK activity could be detected. However, the remarkable HS stability of the guanosine mimicking makes the compounds potentially useful inorganic medicinal drugs. In our vision, they may actively participate in the biochemistry at the desired target tumor site provided that they are able to accumulate to a sufficient extent in the cell and in the nucleus in particular and provided that they are substrates for enzymes involved in DNA synthesis. The amino acid complexes of Re can be bridged by CN^- in B12 to yield robust complexes comprising the central structural feature [Co-CN-Re]. This concept allows direct labeling of B12 with complexes $[^{99m}Tc(OH_2)(N\cap O)(CO)_3]$ for radiodiagnosis or with Re as a mediator between B12 and additional biologically active molecules.

Certain Re complexes show high antiproliferative activity toward B16 F1 mouse melanoma cells. Compounds bearing at least one Im or HPz ligand generally best inhibit cell proliferation. However, no structure-activity relationship can be extrapolated from our results as both compounds with two exchangeable cis-coordinated ligands and compounds with one or no exchangeable ligands show comparable activity. The results suggest that Im or HPz might be ligands for a model Re pro-drug protecting the $[Re(CO)_3]^+$ core from reacting with coordinating sites in blood proteins.

Finally the first structurally characterized *cis*-bis purine complex of ruthenium was presented. The two guanine bases are in a HT orientation which is the most common solid-state conformation of cis-bis(ligand) complexes of purines with Pt^{II}, Co^{III}, Cu^{II} and Zn^{II}. The complex is stable in water for hours showing a slow off rate of base dissociation. Our results, in agreement with the

experimental evidence mentioned above, confirm that DNA is a possible target of ruthenium-based metal drugs.

Crystallography Section.

X-Ray Table 1. $[ReBr(BzIm)_2(CO)_3]$ (**6**)

Empirical formula	C17 H10 Br N4 O3 Re	
Chemical name	Rhenium(I) Dibenzimidazoletricarbonylbromo	
Formula weight	584.40	
Temperature	183(2) K	
Wavelength	0.71073 Å	
Crystal system	Monoclinic	
Space group	P21/n	
Unit cell dimensions	a = 8.3811(6) Å	α= 90°.
	b = 21.4230(14) Å	β= 97.022(8)°.
	c = 10.6260(7) Å	γ = 90°.
Volume	1893.6(2) $Å^3$	
Z	4	
Density (calculated)	2.050 Mg/m^3	
Absorption coefficient	8.551 mm^{-1}	
F(000)	1096	
Crystal size	0.15 x 0.28 x 0.36 mm^3	
Crystal description	colorless plate	
Theta range for data collection	2.63 to 27.98°.	
Index ranges	-11<=h<=11, -28<=k<=28, -13<=l<=13	
Reflections collected	26030	
Independent reflections	4527 [R(int) = 0.1144]	
Reflections observed	3612	
Criterion for observation	>2sigma(I)	
Completeness to theta = 27.98°	99.5 %	
Absorption correction	Numercial	
Max. and min. transmission	0.2911 and 0.0900	
Refinement method	Full-matrix least-squares on F^2	
Data / restraints / parameters	4527 / 0 / 243	
Goodness-of-fit on F^2	0.929	
Final R indices [I>2sigma(I)]	R1 = 0.0361, wR2 = 0.0880	
R indices (all data)	R1 = 0.0459, wR2 = 0.0905	
Largest diff. peak and hole	2.661 and -1.465 e.$Å^{-3}$	

X-Ray Table 2. $[Re(9\text{-}MeG)_2(CH_3OH)(CO)_3](ClO_4) \bullet (Et_4N)(ClO_4)$ (**7HT**)

Empirical formula	C24 H38 Cl2 N11 O14 Re	
Formula weight	961.75	
Temperature	183(2) K	
Wavelength	0.71073 Å	
Crystal system	Monoclinic	
Space group	I2/a	
Unit cell dimensions	a = 28.8620(17) Å	α= 90°.
	b = 8.0097(3) Å	β= 90.923(7)°.
	c = 32.3708(19) Å	γ = 90°.
Volume	7482.4(7) $Å^3$	
Z	8	
Density (calculated)	1.708 Mg/m^3	
Absorption coefficient	3.467 mm^{-1}	
F(000)	3840	
Crystal size	0.33 x 0.17 x 0.11 mm^3	
Theta range for data collection	2.82 to 30.41°.	
Index ranges	-40<=h<=40, -11<=k<=10, -42<=l<=45	
Reflections collected	43462	
Independent reflections	11248 [R(int) = 0.0587]	
Completeness to theta = 30.41°	99.2 %	
Absorption correction	Numerical	
Max. and min. transmission	0.7301 and 0.4539	
Refinement method	Full-matrix least-squares on F^2	
Data / restraints / parameters	11248 / 2 / 472	
Goodness-of-fit on F^2	0.929	
Final R indices [I>2sigma(I)]	R1 = 0.0510, wR2 = 0.1293	
R indices (all data)	R1 = 0.0763, wR2 = 0.1373	
Largest diff. peak and hole	1.800 and -1.430 $e.Å^{-3}$	

X-Ray Table 3. [^{99}Tc(9-MeG)$_2$(CH$_3$OH)(CO)$_3$](ClO$_4$) • (Et$_4$N)(ClO$_4$) (**8HT**)

Empirical formula	C24 H38 Cl2 N11 O14 Tc	
Formula weight	873.55	
Temperature	183(2) K	
Wavelength	0.71073 Å	
Crystal system	monoclinic	
Space group	I2/a	
Unit cell dimensions	a = 28.7533(14) Å	α= 90°.
	b = 8.0631(4) Å	β= 91.543(6)°.
	c = 32.3600(15) Å	γ = 90°.
Volume	7499.6(6) Å^3	
Z	8	
Density (calculated)	1.547 Mg/m^3	
Absorption coefficient	0.602 mm^{-1}	
F(000)	3584	
Crystal size	0.70 x 0.58 x 0.50 mm^3	
Crystal description	colorless block	
Theta range for data collection	2.83 to 30.42°.	
Index ranges	-40<=h<=40, -11<=k<=11, -45<=l<=46	
Reflections collected	41617	
Independent reflections	11284 [R(int) = 0.1011]	
Reflections observed	7224	
Criterion for observation	>2sigma(I)	
Completeness to theta = 30.42°	99.2 %	
Absorption correction	Numerical	
Max. and min. transmission	0.7869 and 0.6777	
Refinement method	Full-matrix least-squares on F^2	
Data / restraints / parameters	11284 / 2 / 494	
Goodness-of-fit on F^2	1.130	
Final R indices [I>2sigma(I)]	R1 = 0.0692, wR2 = 0.1857	
R indices (all data)	R1 = 0.0938, wR2 = 0.1954	
Largest diff. peak and hole	1.414 and -1.254 e.Å^{-3}	

X-Ray Table 4. $[Re(9\text{-}MeG)_2(H_2O)(CO)_3](ClO_4) \cdot 3H_2O$ (**10HT**)

Empirical formula	C15 H22 Cl N10 O13 Re	
Formula weight	772.08	
Temperature	183(2) K	
Wavelength	0.71073 Å	
Crystal system	Monoclinic	
Space group	P21/n	
Unit cell dimensions	a = 12.3307(10) Å	α= 90°.
	b = 16.2620(14) Å	β= 105.525(9)°.
	c = 13.7171(11) Å	γ = 90°.
Volume	2650.2(4) $Å^3$	
Z	4	
Density (calculated)	1.935 Mg/m^3	
Absorption coefficient	4.767 mm^{-1}	
F(000)	1512	
Crystal size	0.39 x 0.26 x 0.13 mm^3	
Crystal description	colorless block	
Theta range for data collection	2.88 to 30.43°.	
Index ranges	-17<=h<=17, -23<=k<=23, -19<=l<=19	
Reflections collected	29286	
Independent reflections	7942 [R(int) = 0.1153]	
Reflections observed	4393	
Criterion for observation	>2sigma(I)	
Completeness to theta = 30.43°	98.7 %	
Absorption correction	Numerical	
Max. and min. transmission	0.4671 and 0.3147	
Refinement method	Full-matrix least-squares on F^2	
Data / restraints / parameters	7942 / 1 / 369	
Goodness-of-fit on F^2	0.798	
Final R indices [I>2sigma(I)]	R1 = 0.0435, wR2 = 0.0999	
R indices (all data)	R1 = 0.0858, wR2 = 0.1105	
Largest diff. peak and hole	1.928 and -2.175 e.$Å^{-3}$	

X-Ray Table 5. $[Re(9\text{-}MeG)_2(H_2O)(CO)_3]Br \bullet H_2O$ (**10HH**)

Empirical formula	C15 H18 Br N10 O7 Re	
Formula weight	716.50	
Temperature	183(2) K	
Wavelength	0.71073 Å	
Crystal system	Monoclinic	
Space group	P21/n	
Unit cell dimensions	a = 15.6260(13) Å	α= 90°.
	b = 9.5269(5) Å	β= 76.951(10)°.
	c = 15.4078(13) Å	γ = 90°.
Volume	2234.5(3) $Å^3$	
Z	4	
Density (calculated)	2.130 Mg/m^3	
Absorption coefficient	7.287 mm^{-1}	
F(000)	1376	
Crystal size	0.171 x 0.030 x 0.025 mm^3	
Crystal description	colorless plate	
Theta range for data collection	2.52 to 28.21°.	
Index ranges	-20<=h<=20, -12<=k<=11, -20<=l<=20	
Reflections collected	17788	
Independent reflections	5430 [R(int) = 0.1347]	
Reflections observed	2746	
Criterion for observation	>2sigma(I)	
Completeness to theta = 28.21°	98.5 %	
Absorption correction	Numerical	
Max. and min. transmission	0.8490 and 0.4576	
Refinement method	Full-matrix least-squares on F^2	
Data / restraints / parameters	5430 / 2 / 317	
Goodness-of-fit on F^2	0.868	
Final R indices [I>2sigma(I)]	R1 = 0.0714, wR2 = 0.1577	
R indices (all data)	R1 = 0.1408, wR2 = 0.1829	
Largest diff. peak and hole	1.830 and -1.128 $e.Å^{-3}$	

X-Ray Table 6. $[ReBr(7\text{-}MeG)_2(CO)_3] \cdot 2.5H_2O$ (**12HH**)

Empirical formula	C15 H19 Br N10 O7.50 Re	
Formula weight	725.51	
Temperature	183(2) K	
Wavelength	0.71073 Å	
Crystal system	Monoclinic	
Space group	P2/c	
Unit cell dimensions	a = 17.5117(9) Å	α= 90°.
	b = 9.8842(5) Å	β= 100.824(7)°.
	c = 15.3539(10) Å	γ = 90°.
Volume	2610.3(3) $Å^3$	
Z	4	
Density (calculated)	1.846 Mg/m^3	
Absorption coefficient	6.240 mm^{-1}	
F(000)	1396	
Crystal size	0.062 x 0.059 x 0.028 mm^3	
Crystal description	colorless plate	
Theta range for data collection	2.70 to 27.00°.	
Index ranges	-22<=h<=22, -12<=k<=12, -19<=l<=19	
Reflections collected	21500	
Independent reflections	5427 [R(int) = 0.1211]	
Reflections observed	3026	
Criterion for observation	>2sigma(I)	
Completeness to theta = 27.00°	95.1 %	
Absorption correction	Numerical	
Max. and min. transmission	0.7673 and 0.6424	
Refinement method	Full-matrix least-squares on F^2	
Data / restraints / parameters	5427 / 12 / 333	
Goodness-of-fit on F^2	0.902	
Final R indices [I>2sigma(I)]	R1 = 0.0641, wR2 = 0.1422	
R indices (all data)	R1 = 0.1161, wR2 = 0.1658	
Largest diff. peak and hole	1.181 and -2.283 e.$Å^{-3}$	

X-Ray Table 7. $[Re(7\text{-}MeG)_2(H_2O)(CO)_3](ClO_4) \bullet H_2O \bullet CH_3OH$ (**12HT**)

Empirical formula	C16 H22 Cl N10 O12 Re	
Formula weight	768.09	
Temperature	183(2) K	
Wavelength	0.71073 Å	
Crystal system	Monoclinic	
Space group	P21/c	
Unit cell dimensions	a = 13.0708(9) Å	α= 90°.
	b = 15.4082(7) Å	β= 117.236(7)°.
	c = 14.3160(9) Å	γ = 90°.
Volume	2563.5(3) $Å^3$	
Z	4	
Density (calculated)	1.990 Mg/m^3	
Absorption coefficient	4.925 mm^{-1}	
F(000)	1504	
Crystal size	0.38 x 0.32 x 0.09 mm^3	
Crystal description	colorless block	
Theta range for data collection	3.09 to 30.38°.	
Index ranges	-18<=h<=18, -21<=k<=21, -20<=l<=20	
Reflections collected	43858	
Independent reflections	7625 [R(int) = 0.1059]	
Reflections observed	5946	
Criterion for observation	>2sigma(I)	
Completeness to theta = 30.38°	98.6 %	
Absorption correction	Numerical	
Max. and min. transmission	0.6573 and 0.2472	
Refinement method	Full-matrix least-squares on F^2	
Data / restraints / parameters	7625 / 0 / 379	
Goodness-of-fit on F^2	0.937	
Final R indices [I>2sigma(I)]	R1 = 0.0416, wR2 = 0.1018	
R indices (all data)	R1 = 0.0516, wR2 = 0.1050	
Largest diff. peak and hole	2.966 and -2.212 e.$Å^{-3}$	

X-Ray Table 8. $[Re(Pro)(CO)_3]_3 \bullet 3THF$ (**13**)

Empirical formula	C12 H16 N O6 Re	
Formula weight	456.46	
Temperature	183(2) K	
Wavelength	0.71073 Å	
Crystal system	Trigonal	
Space group	R3	
Unit cell dimensions	a = 21.6864(11) Å	α= 90°.
	b = 21.6864(11) Å	β= 90°.
	c = 8.1989(3) Å	γ = 120°.
Volume	3339.3(3) $Å^3$	
Z	9	
Density (calculated)	2.043 Mg/m^3	
Absorption coefficient	8.210 mm^{-1}	
F(000)	1962	
Crystal size	0.25 x 0.07 x 0.06 mm^3	
Crystal description	colorless needle	
Theta range for data collection	3.25 to 30.16°.	
Index ranges	-30<=h<=23, -30<=k<=30, -11<=l<=9	
Reflections collected	8254	
Independent reflections	4025 [R(int) = 0.0373]	
Reflections observed	3312	
Criterion for observation	>2sigma(I)	
Completeness to theta = 30.16°	99.9 %	
Absorption correction	Numerical	
Max. and min. transmission	0.6923 and 0.2355	
Refinement method	Full-matrix least-squares on F^2	
Data / restraints / parameters	4025 / 2 / 184	
Goodness-of-fit on F^2	0.874	
Final R indices [I>2sigma(I)]	R1 = 0.0302, wR2 = 0.0596	
R indices (all data)	R1 = 0.0402, wR2 = 0.0615	
Absolute structure parameter	-0.028(12)	
Largest diff. peak and hole	1.417 and -0.587 e.$Å^{-3}$	

X-Ray Table 9. $[Re(DMGly)(CO)_3]_3 \bullet (CH_3CH_2)_2O$ (**14**)

Empirical formula	C25 H34 N3 O16 Re3	
Formula weight	1191.15	
Temperature	183(2) K	
Wavelength	0.71073 Å	
Crystal system	Monoclinic	
Space group	P21/c	
Unit cell dimensions	a = 22.0917(10) Å	α= 90°.
	b = 7.8752(4) Å	β= 92.768(6)°.
	c = 20.2707(12) Å	γ = 90°.
Volume	3522.5(3) $Å^3$	
Z	4	
Density (calculated)	2.246 Mg/m^3	
Absorption coefficient	10.355 mm^{-1}	
F(000)	2232	
Crystal size	0.26 x 0.04 x 0.02 mm^3	
Crystal description	colorless plate	
Theta range for data collection	2.75 to 28.28°.	
Index ranges	-29<=h<=29, -10<=k<=10, -26<=l<=26	
Reflections collected	34342	
Independent reflections	8613 [R(int) = 0.1416]	
Reflections observed	5543	
Criterion for observation	>2sigma(I)	
Completeness to theta = 28.28°	98.6 %	
Absorption correction	Numerical	
Max. and min. transmission	0.8359 and 0.2312	
Refinement method	Full-matrix least-squares on F^2	
Data / restraints / parameters	8613 / 19 / 430	
Goodness-of-fit on F^2	0.966	
Final R indices [I>2sigma(I)]	R1 = 0.0708, wR2 = 0.1259	
R indices (all data)	R1 = 0.1051, wR2 = 0.1381	
Largest diff. peak and hole	2.492 and -1.744 e.$Å^{-3}$	

X-Ray Table 10. [Re(Pro)(9-MeG)$(CO)_3$] • CH_3OH • 1/3pentane (**15**)

Empirical formula	C105 H150 N36 O42 Re6	
Formula weight	3705.81	
Temperature	183(2) K	
Wavelength	0.71073 Å	
Crystal system	Monoclinic	
Space group	P21	
Unit cell dimensions	a = 15.1130(5) Å	α= 90°.
	b = 15.4589(7) Å	β= 90.629(4)°.
	c = 15.4093(5) Å	γ = 90°.
Volume	3599.9(2) $Å^3$	
Z	1	
Density (calculated)	1.709 Mg/m^3	
Absorption coefficient	5.111 mm^{-1}	
F(000)	1818	
Crystal size	0.57 x 0.17 x 0.08 mm^3	
Crystal description	colorless needle	
Theta range for data collection	2.95 to 30.42°.	
Index ranges	-21<=h<=21, -22<=k<=22, -21<=l<=21	
Reflections collected	78907	
Independent reflections	20395 [R(int) = 0.0402]	
Reflections observed	18665	
Criterion for observation	>2sigma(I)	
Completeness to theta = 30.42°	93.1 %	
Absorption correction	Numerical	
Max. and min. transmission	0.7018 and 0.3285	
Refinement method	Full-matrix least-squares on F^2	
Data / restraints / parameters	20395 / 69 / 889	
Goodness-of-fit on F^2	0.996	
Final R indices [I>2sigma(I)]	R1 = 0.0328, wR2 = 0.0821	
R indices (all data)	R1 = 0.0356, wR2 = 0.0831	
Absolute structure parameter	-0.015(6)	
Largest diff. peak and hole	1.857 and -0.550 e.$Å^{-3}$	

X-Ray Table 11. $[ReBr(NH_3)_2(CO)_3]$ (**16**)

Empirical formula	C3 H6 Br N2 O3 Re	
Formula weight	384.21	
Temperature	183(2) K	
Wavelength	0.71073 Å	
Crystal system	Orthorombic	
Space group	Pnma	
Unit cell dimensions	a = 10.8300(6) Å	α= 90°.
	b = 9.8501(7) Å	β= 90°.
	c = 7.2163(8) Å	γ = 90°.
Volume	769.81(11) $Å^3$	
Z	4	
Density (calculated)	3.315 Mg/m^3	
Absorption coefficient	20.927 mm^{-1}	
F(000)	688	
Crystal size	0.15 x 0.12 x 0.08 mm^3	
Crystal description	colorless block	
Theta range for data collection	3.39 to 30.47°.	
Index ranges	-15<=h<=15, -13<=k<=13, -10<=l<=10	
Reflections collected	15621	
Independent reflections	1228 [R(int) = 0.0670]	
Reflections observed	876	
Criterion for observation	>2sigma(I)	
Completeness to theta = 30.47°	99.5 %	
Absorption correction	Numerical	
Max. and min. transmission	0.2764 and 0.1368	
Refinement method	Full-matrix least-squares on F^2	
Data / restraints / parameters	1228 / 0 / 53	
Goodness-of-fit on F^2	1.000	
Final R indices [I>2sigma(I)]	R1 = 0.0407, wR2 = 0.0975	
R indices (all data)	R1 = 0.0540, wR2 = 0.1028	
Largest diff. peak and hole	1.687 and -2.438 $e.Å^{-3}$	

X-Ray Table 12. [B12- Re(DMGly)$(CO)_3$] • nH_3O (**22a**)

Empirical formula	C73 H112.60 Co N15 O27.30 P Re	
Formula weight	1913.28	
Temperature	183(2) K	
Wavelength	0.71073 Å	
Crystal system	Orthorhombic	
Space group	P212121	
Unit cell dimensions	a = 15.8758(7) Å	α= 90°.
	b = 21.8451(10) Å	β= 90°.
	c = 26.3673(14) Å	γ = 90°.
Volume	9144.4(8) $Å^3$	
Z	4	
Density (calculated)	1.390 Mg/m^3	
Absorption coefficient	1.601 mm^{-1}	
F(000)	3964	
Crystal size	0.46 x 0.08 x 0.07 mm^3	
Theta range for data collection	1.86 to 26.00°.	
Index ranges	-19<=h<=19, -26<=k<=26, -32<=l<=32	
Reflections collected	68628	
Independent reflections	17853 [R(int) = 0.1048]	
Completeness to theta = 26.00°	99.5 %	
Absorption correction	Numerical	
Max. and min. transmission	0.9257 and 0.7060	
Refinement method	Full-matrix least-squares on F^2	
Data / restraints / parameters	17853 / 2 / 1071	
Goodness-of-fit on F^2	0.900	
Final R indices [I>2sigma(I)]	R1 = 0.0662, wR2 = 0.1588	
R indices (all data)	R1 = 0.1159, wR2 = 0.1742	
Absolute structure parameter	-0.014(8)	
Largest diff. peak and hole	2.044 and -1.063 e.$Å^{-3}$	

X-Ray Table 13. $[Re(L\text{-}Ser)_2(CO)_3]$ (**23**)

Empirical formula	C9 H13 N2 O9 Re	
Formula weight	479.41	
Temperature	183(2) K	
Wavelength	0.71073 Å	
Crystal system	Orthorhombic	
Space group	P212121	
Unit cell dimensions	a = 5.6071(5) Å	α= 90°.
	b = 13.0977(17) Å	β= 90°.
	c = 18.4664(19) Å	γ = 90°.
Volume	1356.2(3) $Å^3$	
Z	4	
Density (calculated)	2.348 Mg/m^3	
Absorption coefficient	9.009 mm^{-1}	
F(000)	912	
Crystal size	0.18 x 0.03 x 0.02 mm^3	
Theta range for data collection	1.91 to 26.07°.	
Index ranges	-6<=h<=6, -16<=k<=15, -22<=l<=22	
Reflections collected	8330	
Independent reflections	2639 [R(int) = 0.0547]	
Completeness to theta = 26.07°	99.0 %	
Absorption correction	Numerical	
Max. and min. transmission	0.8393 and 0.6899	
Refinement method	Full-matrix least-squares on F^2	
Data / restraints / parameters	2639 / 18 / 191	
Goodness-of-fit on F^2	1.069	
Final R indices [I>2sigma(I)]	R1 = 0.0400, wR2 = 0.0963	
R indices (all data)	R1 = 0.0456, wR2 = 0.0978	
Absolute structure parameter	0.01(2)	
Largest diff. peak and hole	1.387 and -0.915 $e.Å^{-3}$	

X-Ray Table 14. [Re(L-Ser)(7-MeG)$(CO)_3$] (**24**) • 1/2 CH_3OH

Empirical formula	C25 H30 N12 O15 Re2	
Formula weight	1111.01	
Temperature	183(2) K	
Wavelength	0.71073 Å	
Crystal system	Orthorombic	
Space group	P212121	
Unit cell dimensions	a = 10.0312(5) Å	α= 90°.
	b = 14.1639(5) Å	β= 90°.
	c = 24.9026(8) Å	γ = 90°.
Volume	3538.2(2) $Å^3$	
Z	4	
Density (calculated)	2.086 Mg/m^3	
Absorption coefficient	6.922 mm^{-1}	
F(000)	2136	
Crystal size	0.16 x 0.082 x 0.022 mm^3	
Theta range for data collection	2.84 to 30.46°.	
Index ranges	-14<=h<=12, -20<=k<=19, -30<=l<=35	
Reflections collected	25535	
Independent reflections	10699 [R(int) = 0.0840]	
Completeness to theta = 30.46°	99.5 %	
Absorption correction	Numerical	
Max. and min. transmission	0.8101 and 0.3713	
Refinement method	Full-matrix least-squares on F^2	
Data / restraints / parameters	10699 / 4 / 516	
Goodness-of-fit on F^2	0.895	
Final R indices [I>2sigma(I)]	R1 = 0.0493, wR2 = 0.1064	
R indices (all data)	R1 = 0.0812, wR2 = 0.1178	
Absolute structure parameter	-0.007(15)	
Largest diff. peak and hole	1.773 and -2.120 $e.Å^{-3}$	

X-Ray Table 15. [Re(D-Ser)(7-MeG)$(CO)_3$] (**25**) • 1/2 H_2O

Empirical formula	C24 H26 N12 O14 Re2	
Formula weight	1078.97	
Temperature	183(2) K	
Wavelength	0.71073 Å	
Crystal system	Orthorombic	
Space group	P212121	
Unit cell dimensions	a = 10.0219(4) Å	α= 90°.
	b = 12.7847(4) Å	β= 90°.
	c = 26.4572(10) Å	γ = 90°.
Volume	3389.9(2) $Å^3$	
Z	4	
Density (calculated)	2.114 Mg/m^3	
Absorption coefficient	7.219 mm^{-1}	
F(000)	2064	
Crystal size	0.202 x 0.101 x 0.0012 mm^3	
Theta range for data collection	2.81 to 30.47°.	
Index ranges	-14<=h<=14, -17<=k<=18, -37<=l<=37	
Reflections collected	34305	
Independent reflections	10251 [R(int) = 0.1058]	
Completeness to theta = 30.47°	99.5 %	
Absorption correction	Numerical	
Max. and min. transmission	0.9078 and 0.2391	
Refinement method	Full-matrix least-squares on F^2	
Data / restraints / parameters	10251 / 6 / 504	
Goodness-of-fit on F^2	1.041	
Final R indices [I>2sigma(I)]	R1 = 0.0467, wR2 = 0.1115	
R indices (all data)	R1 = 0.0548, wR2 = 0.1155	
Absolute structure parameter	-0.012(12)	
Largest diff. peak and hole	2.221 and -2.039 e.$Å^{-3}$	

X-Ray Table 16. [Re(L-Ser)(3-pic)$(CO)_3$] (**26**)

Empirical formula	C12 H13 N2 O6 Re	
Formula weight	467.44	
Temperature	183(2) K	
Wavelength	0.71073 Å	
Crystal system	Monoclinic	
Space group	P21	
Unit cell dimensions	a = 6.2005(3) Å	α= 90°.
	b = 26.1517(17) Å	β= 92.112(7)°.
	c = 8.7539(5) Å	γ = 90°.
Volume	1418.51(14) $Å^3$	
Z	4	
Density (calculated)	2.189 Mg/m^3	
Absorption coefficient	8.595 mm^{-1}	
F(000)	888	
Crystal size	0.225 x 0.060 x 0.058 mm^3	
Theta range for data collection	3.29 to 30.47°.	
Index ranges	-8<=h<=8, -36<=k<=36, -12<=l<=12	
Reflections collected	13689	
Independent reflections	7224 [R(int) = 0.0922]	
Completeness to theta = 30.47°	87.9 %	
Absorption correction	Numerical	
Max. and min. transmission	0.7042 and 0.3170	
Refinement method	Full-matrix least-squares on F^2	
Data / restraints / parameters	7224 / 159 / 385	
Goodness-of-fit on F^2	1.114	
Final R indices [I>2sigma(I)]	R1 = 0.0867, wR2 = 0.2670	
R indices (all data)	R1 = 0.1218, wR2 = 0.3031	
Absolute structure parameter	-0.03(5)	
Largest diff. peak and hole	4.095 and -4.259 $e.Å^{-3}$	

X-Ray Table 17. $[Ru(bpy)_2(9\text{-}MeG)_2](SO_3CF_3)_2 \bullet CH_2Cl_2$ (**33**)

Empirical formula	C35 H32 Cl2 F6 N14 O8 Ru S2	
Formula weight	1126.84	
Temperature	183(2) K	
Wavelength	0.71073 Å	
Crystal system	Monoclinic	
Space group	P21/n	
Unit cell dimensions	a = 12.5159(6) Å	α= 90°.
	b = 20.0904(13) Å	β= 98.981(6)°.
	c = 17.1202(9) Å	γ = 90°.
Volume	4252.1(4) $Å^3$	
Z	4	
Density (calculated)	1.760 Mg/m^3	
Absorption coefficient	0.689 mm^{-1}	
F(000)	2272	
Crystal size	0.11 x 0.07 x 0.05 mm^3	
Crystal description	red block	
Theta range for data collection	2.36 to 28.10°.	
Index ranges	-16<=h<=16, -25<=k<=26, -20<=l<=22	
Reflections collected	23723	
Independent reflections	10149 [R(int) = 0.1119]	
Reflections observed	3786	
Criterion for observation	>2sigma(I)	
Completeness to theta = 28.10°	97.8 %	
Absorption correction	Numerical	
Max. and min. transmission	0.9766 and 0.9256	
Refinement method	Full-matrix least-squares on F^2	
Data / restraints / parameters	10149 / 0 / 639	
Goodness-of-fit on F^2	0.692	
Final R indices [I>2sigma(I)]	R1 = 0.0502, wR2 = 0.0846	
R indices (all data)	R1 = 0.1535, wR2 = 0.1044	
Largest diff. peak and hole	0.761 and -0.482 e.$Å^{-3}$	

Curriculum Vitae

Name:

Fabio ZOBI

Nationality:

Italian Citizen, born in Napoli 05/04/1976

Education:

2002-2005 University of Zurich, Zurich, Switzerland.

Ph. D. in Radiopharmaceutical Inorganic Chemistry, January 2005.

"The interaction of the *fac*-$[M(CO)_3]^+$ core (M = $^{99/99m}$Tc, Re) with DNA Bases"

1999-2001 York University, Toronto, Ontario, Canada.

Master of Science in Inorganic Chemistry, October 2001.

"Synthesis and Characterization of Novel μ-oxo Bridged Metal Complexes"

1994-1999 York University, Toronto, Ontario, Canada.

Honours B. Sc. Combined in Biology (Biochem. & Molec. Biol.) and Chemistry, May 1999.

"Synthesis and Characterization of Novel μ-oxo Bridged Metal Complexes"

1989-1994 Liceo Scientifico "Ettore Majorana", Pozzuoli, Napoli, Italy.

High School Diploma, July 1994.

Honors and Awards:

2004 Recipient of the "Swiss National Science Fund"

Summary of Publications in Refereed Journals:

2005 **Zobi, F.;** Spingler, B. and Alberto, R. Guanine and Plasmid DNA Binding of Mono- and Trinuclear *fac*-$[Re(CO)_3]^+$ Complexes with Amino Acid Ligands *Chem. BioChem.*, **Accepted**.

2004 Kunze, S.; **Zobi, F.;** Kurz, P.; Spingler, B. and Alberto**,** R. Vitamin B12 as a Ligand for Technetium and Rhenium Complexes**.** *Angew. Chem*.**, 2004**, *43*, 5025-5029.

2004 **Zobi, F.;** Hohl, M.; Zimmermanm, I. and Alberto, R. Binding of 9-Methylguanine to [*cis*-Ru(2,2'-bpy)$_2$]$^{2+}$: First X-ray Structure of a *cis*-Bis Purine Complex of Ruthenium. *Inorg. Chem*.**, 2004**, *43*, 2771-2772.

2004 **Zobi, F.;** Blacque, O.; Schmalle, H. W.; Spingler, B. and Alberto, R. Head-to-Head (HH) and Head-to-Tail (HT) Conformers of *cis*-Bis Guanine Ligands Bound to the [Re(CO)$_3$]$^+$ Core. *Inorg. Chem*.**, 2004**, *43*, 2087-2096.

2003 **Zobi, F.**; Spingler, B.; Fox, T. and Alberto, R. Toward Novel DNA Binding Metal Complexes: Structure and Basic Kinetic Data of [M(9MeG)$_2$(CH$_3$OH)(CO)$_3$]$^+$ (M = ^{99}Tc, Re). *Inorg. Chem*.**, 2003**, *42*, 2818-2820.

2002 **Zobi, F.**; Alberto, R.; Spingler, B. and Fox, T. Rhenium (I) Complexes of Purine Bases. Towards the Development of Cisplatin Analogs. In *Technetium, Rhenium and Other Metals in Chemistry and Nuclear Medicine*. Vol 6, **2002**, Edited by Nicolini M. and Mazzi, U. SGE Editoriali, Italy. 97-100.